UNIVERSITÀ
DEGLI STUDI
DI PADOVA

Sede Amministrativa: Università degli Studi di Padova

Dipartimento di Ingegneria Civile, Edile e Ambientale

_____

CORSO DI DOTTORATO DI RICERCA IN: Scienze dell'Ingegneria Civile ed Ambientale

CICLO XXIX

BEHAVIOR OF RC BEAMS STRENGTHENED IN SHEAR WITH FRCM COMPOSITES

Coordinatore: Ch.mo Prof. Stefano Lanzoni

Supervisore: Ch.mo Prof. Carlo Pellegrino

Co-Supervisore: Ch.ma Prof. Lesley H. Sneed

Dottorando: Jaime Hernan Gonzalez Libreros

ACKNOWLEDGEMENTS

ABSTRACT

Interventions for strengthening, repairing, and upgrading of existing reinforced concrete (RC) structures are aimed to increase/restore their structural capacity to withstand flexural, shear, torsional, and axial loads. Reasons to carry out such interventions vary from the need to upgrade the structure to current guidelines, overcome design and construction mistakes, and allow an increment in load due to a change in use. In addition, unexpected overloading events, such as earthquakes, might damage the structure, reducing its original performance. The same behavior can be expected in the case of fire or lack of adequate maintenance.

In the previous decades the use of fiber reinforced polymer (FRP) composites has gained worldwide popularity to carry out such interventions due to some of their properties such as high strength-to-weight ratio, ease of application, and good corrosion resistance. However, the use of organic resin matrix in FRP composites has been associated with some limitations of their use such as inability to apply onto wet surfaces, low resistance to relatively high temperatures, and difficulty to carry out post-earthquake assessment. For this reason, in recent years, an important research effort has been developed in order to study composites known as fiber reinforced cementitious matrix (FRCM) composites, in which the organic resin is replaced by an inorganic matrix. In this thesis, the behavior of RC beams strengthened in shear with externally bonded FRCM composites is studied.

The first part of this thesis summarizes the state of research on the topic of shear strengthening of RC beams using externally bonded FRCM composites with the goal of serving as a reference point for the development of future research. A detailed bibliographical review of the literature on the shear strengthening of RC beams using FRCM composites is carried out, and the major findings and main aspects that should be addressed in future research are indicated. The collected experimental evidence shows that FRCM composites are able to increase the shear strength of RC beams, modifying in some cases the type of failure from shear to a flexural mode.

Then, the results of an experimental campaign on shear strengthening of RC beams with externally bonded FRP and FRCM composites are presented. FRP and FRCM composites with two different fiber types are examined. Two different stirrup spacings were employed to investigate the internal-external shear reinforcement interaction. Considering the limited experimental evidence on the use of anchors for RC beams strengthened in shear with FRCM composites, the performance of FRCM strengthened beams with and without anchors is also compared. Results show that the effectiveness of the FRCM system depends on the spacing of the

internal shear reinforcement. In addition, internal-external shear reinforcement interaction was witnessed, but the intereaction appears to be less pronounced than in beams strengthened with FRP composites.

Design models proposed to predict the contribution of the FRCM composite to the shear strength of RC beams are assessed using the database of experimental results collected and compiled by the author and the experimental results included in this thesis. Results show that the performance of the models is highly influenced by the type of failure mode attained by the strengthened beams. In addition, the use of the FRCM composite properties instead of the bare fiber mechanical characteristics does not result in an increase in the accuracy of the models.

Strains measured by strain gauges mounted onto the internal (stirrups) and external (FRCM system) transverse reinforcement of the tested beams are used to compute the individual contributions of the concrete, steel, and fibers to the overall shear strength of the FRCM strengthened beams, and to study the possible interaction among them. It was found that the concrete contribution to the shear resistance starts to decrease after first cracking of the concrete is achieved. After this point, the stirrup and fiber contributions start to increase until the peak load is attained.

Lastly, a new analytical model based on the bond behavior of the FRCM composites applied onto concrete substrates is introduced and discussed. Although additional tests are required to calibrate the model, initial results show that the assumptions and hypothesis used during its development are appropriate.

Keywords: FRP, FRCM, RC beams, shear, strengthening, strains, fibers, stirrups

TABLE OF CONTENTS

LIST OF FIGURES

IX

XII

XIII

XIV

LIST OF TABLES

NOMENCLATURE

a	Shear span
d	Effective depth
g	Global slip
h	Beam height
l	Beam length, bonded length
n	Number of fiber layers
N	Number of tests
P	Experimental applied load
s	Internal transverse steel reinforcement spacing
W	Fiber overall area/weight
A_f	Fiber area per unit length
A_s	Longitudinal steel reinforcement area
A_w	Internal transverse steel reinforcement area
b_w	Beam width
b_1	Bonded width
b^*	Nominal width of a single longitudinal fiber bundle
COV_1	Coefficient of variation
d_f	Effective depth of the FRCM jacket
d_{fv}	Effective depth of the shear reinforcement
E_f	Elastic modulus of the bare fibers stirrups
E_{FRCM}	Elastic modulus of the FRCM composite
E_s	Elastic modulus of stirrups
f'_c	Mean cylinder compressive strength of concrete
f_{ck}	Concrete characteristic strength
f_{cm}	Cementitious matrix compressive strength

f_{ctk}	Concrete characteristic tensile strength
f_{ctm}	Mean concrete tensile strength
f_{fdd}	Design debonding strength of the FRCM reinforcement
f_{fm}	Cementitious matrix flexural strength
f_u	Fiber tensile strength
k_b	Geometric coefficient
k_1	Modification factor applied to κ_v to account for concrete strength
k_2	Modification factor applied to κ_v to account for wrapping scheme
k_e	Effectiveness coefficient (0.5)
L_e, l_e, l_{eff}	Effective bond length
n_i	Coefficient that takes into account the contact area between fiber and matrix
P_{deb}	Debonding load
P_f	Friction load
P_{max}	Maximum experimental load
P^*	Peak load
s_f	Spacing of FRCM strips
t_{cm}	Total thickness of the FRCM composite
t_f	Nominal thickness of fiber sheets
t_m	Nominal thickness of a matrix layer
t^*	Average thickness of a single longitudinal fiber bundle
V_c	Concrete contribution to the shear strength
V_{CON}	Shear strength of the control unstrengthened beam
$V_{c,max}$	Concrete compression strut shear strength
V_f	Shear strength provided by the strengthening system
V_{FRCM}	Increase in the shear strength provided by the FRCM system
V_{max}	Maximum experimental shear strength attained by the beam

$V_{max\text{-}CONTROL}$	Maximum experimental shear strength attained by the control beam
V_n	Total shear capacity of the strengthened beam
V_{pred}	Predicted FRCM shear contribution
V_s	Internal transversal steel contribution to the shear strength
V_{test}	Test FRCM shear contribution
w_{eff}	Width of the composite crossed by the shear crack
w_f	Width of FRCM strips
$w(\psi)$	Shear crack width
α	Angle between the FRP fibers and the beam longitudinal axis
γ_{fd}, γ_c	Partial safety factors
Δ_{Pmax}	Displacement at mid-span corresponding to V_{max}
ε_{eff}	Effective fiber strain
ε_f	Fiber strain
$\varepsilon_{f,max}$	Maximum experimental fiber strain
ε_{fu}	Bare fiber ultimate strain
ε_s	Stirrup strain
ε_{si}	Strain recorded in stirrup i
$\varepsilon_{s,max}$	Maximum experimental stirrup strain
ε_y	Stirrup yield strain
θ	Shear crack angle
κ_v	Bond-dependent coefficient for shear
ρ_f	Fiber reinforcement ratio
ρ_{long}	Longitudinal steel reinforcement ratio
ρ_w	Internal transverse steel reinforcement ratio
σ_{deb}	Debonding stress
σ^*	Peak stress

τ_f Frictional shear stress

ψ Coordinate of the shear crack axis

1.   INTRODUCTION

The need for strengthening existing reinforced concrete (RC) structures may arise from their deterioration with age, change in applied loads due to modification of their original use, or upgrading to current design codes. The intervention of these structures requires the use of rehabilitation and/or strengthening techniques that result in adequate behavior of the structure. Traditional techniques such as the increase of concrete section using concrete jackets or the use of externally bonded steel elements, which are common especially in developing countries, can often be considered as structurally acceptable but may not comply with modern requirements in which time- and cost-efficient interventions are usually required. In addition, they have some disadvantages such as increase in self-weight of the structure, undesirable change in stiffness, and the need for handling of heavy steel parts.

For this reason, there is growing interest to develop strengthening techniques that overcome the aforementioned drawbacks. Among these techniques, externally bonded Fiber Reinforced Polymer (FRP) composites have proven to be an effective solution. FRP composites are comprised of continuous reinforcing fibers and an organic matrix, usually epoxy based, that are bonded to the concrete surface to provide additional strength for flexural, shear, torsional, and axial loads. FRP composites have benefits including low invasiveness, high strength-to-weight ratio, and ease of application. However, some drawbacks of the use of FRP composites have been reported, such as poor behavior at elevated temperatures, poor compatibility with the substrate, inability to apply onto wet surfaces or at low temperatures, and difficulty in carrying out post-earthquake assessment of damaged structures [1], which are linked mainly to the use of organic resins used as matrix. This suggests that the use of FRP might not be suitable for all applications, and new techniques that overcome some of these limitations are needed.

Therefore, composites in which an inorganic matrix (mortar) replaces the organic resin matrix have recently raised interest as they overcome some of the limitations associated to the use of FRP composites. Depending on the matrix and fibers employed, different names have been used to designate these types of composite including textile reinforced concrete (TRC), textile reinforced mortar (TRM), mineral based composites (MBC), and fiber reinforced cementitious matrix (FRCM). The term FRCM will be used in this thesis because only a cementitious

matrix was employed in the FRCM composites employed in the experimental campaign carried out in this study. Although research conducted on the topic is still scarce, the effectiveness of this technique for flexural, shear, and torsional strengthening, and for confinement of axially or eccentrically loaded RC elements is confirmed by the available experimental evidence [1–8].

The case of shear is of interest due to the undesirable brittle failure mode associated with shear failure of RC members. In addition, the shear behavior of RC beams is quite complex due to the interaction of different mechanisms. In general, the factors that contribute to the strength of a RC beam without stirrups are the area of uncracked concrete in compression, aggregate interlock, dowel action, arch action, and residual tensile stresses across the crack [9]. For the case of RC beams with stirrups, the contribution of the reinforcement must be considered. For RC beams strengthened in shear with externally bonded composites, either with FRP or FRCM, the effect of the composite on the strength of the beam and its interaction with the aforementioned mechanisms should be taken into account.

1.1 Research scope and objectives

The research presented in this thesis was developed with the aim of investigating the behavior of RC beams strengthened in shear with FRCM composites and comparing it with that of FRP-strengthened RC beams.

The objectives of this research were to:

- Collect a database of experimental data related to the shear strengthening of RC beams with FRCM composites;
- Identify the main variables that influence the behavior of RC beams strengthened in shear with FRCM composites and point out main aspects that need to be addressed by future research;
- Compare the experimental behavior of RC beams strengthened in shear with FRP and FRCM in terms of additional shear strength provided by the strengthening system, failure mode, and level of strain achieved by the internal and external transverse shear reinforcement;
- Investigate the interaction between the internal and external transverse reinforcements;
- Evaluate the performance of available analytical models for predicting the overall shear strength of FRCM-strengthened beams and the contribution of the FRCM composites to the shear capacity of such beams;

- Quantify the contribution of the concrete and the internal and external transverse reinforcement to the shear strength of RC beams strengthened in shear with FRCM composites;
- Develop an analytical design model for determining the contribution of the FRCM composite to the shear strength of RC beams strengthened in shear with FRCM composites.

1.2   Research methodology

This research consists of three distinct phases. The first phase consisted of a deep review of the available literature regarding the shear strengthening of RC beams with FRCM composites. Within this phase, a database of experimental tests on the topic was developed and used to identify the main variables that influence the behavior of the strengthened beams. In addition, the collected information was used to evaluate the performance of analytical models proposed in the literature to predict both the overall shear strength of the strengthened beams and the contribution of the FRCM system to the shear strength of the beams.

In the second phase of the study, the experimental behavior of RC beams strengthened in shear was analyzed. To do so, 14 RC beams were cast, and 12 of them were strengthened in shear with either FRP or FRCM composite. The variables investigated included the type of composite (FRP or FRCM), type of fiber, and the internal shear reinforcement ratio, i.e., stirrup spacing. In addition, the use of anchors for the case of FRCM-strengthened beams was also studied.

The third and final phase consisted of the development of an analytical model for predicting the contribution of the FRCM composite to the shear strength of RC beams.

1.3   Outline of the thesis

This thesis consists of eight sections, including this chapter.

Chapter 2 of this thesis summarizes the state of research on the topic of shear strengthening of RC beams using externally bonded FRCM composites. A detailed bibliographical review of the literature on the shear strengthening of RC beams using FRCM composites is carried out, and the influence of mechanical and geometrical properties of the beams and the strengthening system on the gain in shear strength is analyzed.

In Chapter 3, the results of an experimental campaign carried out to investigate the behavior of reinforced concrete (RC) beams strengthened in shear with externally

bonded composites is presented. The campaign included two different types of composites: Fiber Reinforced Polymer (FRP) and Fiber Reinforced Cementitious Matrix (FRCM) composites. In addition, different types of fiber (carbon and steel) were employed, and the influence of internal transverse steel reinforcement ratio and presence of composite anchors were investigated.

In Chapter 4, a review of the equations proposed by available models to compute the FRCM contribution and the overall strength of FRCM-strengthened beams, is performed. It comprises a brief recall of some expressions proposed by available design guidelines for shear design of FRP strengthened beams, since analytical models proposed for FRCM composites are developed using equations for FRP composites as a starting point. Then, the performance of the models is analyzed using the database of available experimental tests collected in Chapter 2. A comparison between the effective fiber strains predicted by the models and the strains measured on the fibers during the experimental campaign is also carried out.

In Chapter 5, the contributions of the concrete and the internal and external transverse shear reinforcements are evaluated using the stirrup and fiber strains recorded during the experimental campaign described in Chapter 3, in order to verify the possible interaction among these contributions.

In Chapter 6, a new analytical model for predicting the contribution of the FRCM system to the shear strength of strengthened RC beams is introduced. The chapter includes the model governing equations and points out the key aspects that need to be assessed in future research to validate the model.

Chapters 7 and 8 summarize the conclusions of this work and identify future research areas, respectively.

2. STATE OF RESEARCH ON SHEAR STRENGTHENING OF RC BEAMS WITH FRCM COMPOSITES

The state of research on the topic of shear strengthening of RC beams using externally bonded FRCM composites is summarized in this section. A detailed bibliographical review of the literature on the subject is carried out, and a database of experimental tests is developed. This review summarizes the major findings and points out main aspects that should be addressed in future research. Eighteen articles related to shear strengthening of RC beams using FRCM composites were found in the technical literature, which are summarized in Table 2-1. From these articles, a database that includes the characteristics and results of experimental tests on FRCM strengthened beams was developed and is presented in Appendix A. One hundred and four strengthened beams are included in the database.

In Table 2-1, it can be seen that the research on shear strengthening of RC beams with FRCM composites started approximately in 2006. However, only four articles were published in the following four years, and most of the articles are published after 2012 (14 articles out of 18). In fact, 50% of the articles were published in 2015 and 2016, which indicates how the subject is still in development, and researchers are realizing the need to study further the behavior of RC beams strengthened in shear with FRCM composites.

2.1 Evaluation of the database and distribution of data

The evaluation of the information collected in the database is evaluated in this section by means of the distribution of data and the variation of the increase in the shear strength provided by the FRCM system, V_{FRCM}, with respect to the main geometrical and mechanical properties of the strengthened beams and the FRCM system. In this evaluation, V_{FRCM} is calculated by subtracting the shear strength of the strengthened beam from the corresponding control beam (V_{CON}) for each test. The distribution of data is presented in the form of histograms in which the values of a given variable are divided in different ranges, and the percentage of tests that fall in that range are graphed.

The possible relationship between V_{FRCM} and the selected geometrical and mechanical variables of the strengthened beams and the FRCM system are evaluated in terms of the ratio V_{FRCM}/V_{CON}. It is highlighted that tests are subdivided according to the type of failure: flexural or shear. Shear failure is

5

divided according to whether detachment of the FRCM system from the concrete substrate was observed (see Section 2.4). The observations presented herein are based on the number and distribution of tests collected in the database and need to be validated when more test results become available.

Table 2-1. Summary of studies on shear strengthening of RC beams FRCM composites.

Reference	Year	Beam Cross-sectional Shape[a]	Number of Strengthened Beams	Failure Mode		Strengthening Configuration[d]		
				Flexure[b]	Shear[c]	SB	U[(e)]	W
[1]	2006	R	3	2	1			3
[10]	2006	R	2		2			2
[11]	2008	T	9		9		9 (6)	
[7]	2009	R	7		7	7		
[12]	2012	R	8		8	8		
[13]	2013	R	6	2	4	2	4	
[14]	2014	R	6		6	3	3	
[15]	2014	R	2		2		2 (1)	
[16]	2014	T	10		10		10 (6)	
[17]	2015	R	6		6		6	
[18]	2015	R	8		8	2	6	
[19]	2015	R	7	2	5		7	
[20]	2015	R	8	1	7	3	3	2
[21]	2015	R	1		1			1
[22]	2015	R	4		4		4	
[23]	2016	R	6		6	6		1
[24]	2016	T	9		9		9 (5)	1
[6]	2016	R	2		2		2	1
	Total		104	7	97	31	65 (18)	8

[a]R=Rectangular, T-beam.

[b]Yielding of longitudinal reinforcing steel bars followed by concrete crushing

[c]Failure mode related to FRCM debonding, fiber rupture, diagonal tension, and/or yielding of internal stirrups.

[d]SB=Side bonded, U=U-wrapped, W= Fully wrapped.

[e]Numbers in parentheses indicate tests that include anchors

Although experimental specimens aimed to investigate the shear behavior of strengthened specimens are designed to attain shear failure, it is important to

highlight that in some cases (seven tests, see Table 2-1 and Appendix A), the addition of the FRCM system changed the mode of failure from a brittle shear failure to a more ductile flexural failure. Specimens that failed in flexure can be considered as a lower bound of the strengthening capacity, but the behavior of beams that failed in that mode is not further discussed in this section.

2.1.1 Geometrical and mechanical properties of the beam

In this section, the variation of V_{FRCM}/V_{CON} as a function of the geometrical and mechanical properties of the strengthened beams is presented. The data distribution of the selected properties, listed below, is also included:

- d=effective depth;
- a/d=shear span to effective depth ratio;
- f'_c=mean cylinder compressive strength of concrete;
- ρ_{long}=longitudinal steel reinforcement ratio ($A_s/b_w d$, where A_s=longitudinal steel reinforcement area; b_w=beam width);
- ρ_w=internal transverse steel reinforcement ratio, ($A_w/b_w s$, where; A_w=internal transverse steel reinforcement area, and s=internal transverse steel reinforcement spacing).

Figure 2-1 shows the data distribution for the beam effective depth ratio, d.
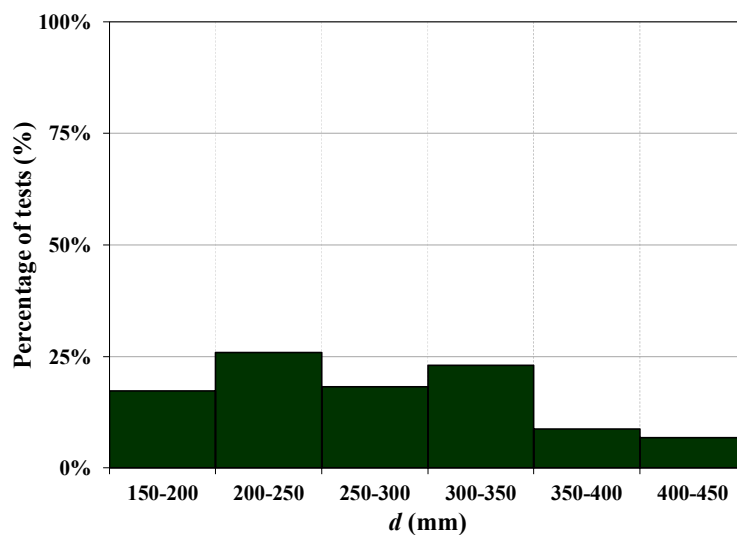
Figure 2-1. Data distribution for d

The beam effective depth has been shown to influence the shear strength of RC beams, mainly in specimens without internal shear reinforcement [25]. According to the experimental available data, the shear strength of the beams reduces as the effective depth increases and is related mainly to the width of the shear cracks that

increases with d, reducing the ability of transmitting crack shear interface stresses [9]. This effect, known as size or scale effect, has also been observed for FRP-strengthened beams [26,27]. For the tests included in the database, d varies from 159 to 419 mm. Most specimens (85%) have values of d between 150-350 with a uniform distribution of the data in that range. Only 15% of test have been carried out in beams with depths higher than 350 mm. Since size effect has been considered as an important factor that influences the shear capacity of RC beams, further research in beams with higher effective depths is required.

The variation of V_{FRCM}/V_{CON} with respect to d is presented in Figure 2-2. The increase in shear strength attributed to the FRCM system varies from 3% to 195% with an average value of 60%. The trend in Figure 2-2 also shows that it appears to be a reduction on V_{FRCM}/V_{CON} with decreasing d. However, considering the limited number of tests carried out with values of d larger than 350 mm, further research is needed to validate the influence of the d on the gain in shear strength provided by the FRCM composite.
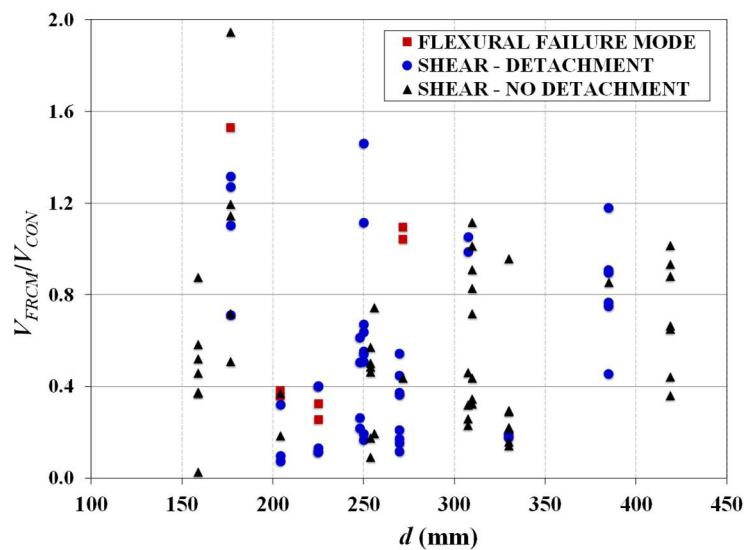
Figure 2-2. Variation of V_{FRCM}/V_{CON} with d

Figure 2-3 shows the data distribution for a/d. For the tests collected in the database, a/d varies from 2.22 to 4.90. Most specimens (58%) have values of a/d between 2.5-3.0, and 81% between 2.5-3.5, which is common for the evaluation of shear strength of RC beams. As shown by Kani [28], the transition point between beam action and arch action corresponds to a/d values ranging from 2.5 to 3.0, which also corresponds to the lowest values of shear strength in terms of average shear stress. Therefore, beams with values of a/d in this range are usually used in research to obtain a lower bound of the shear strength.
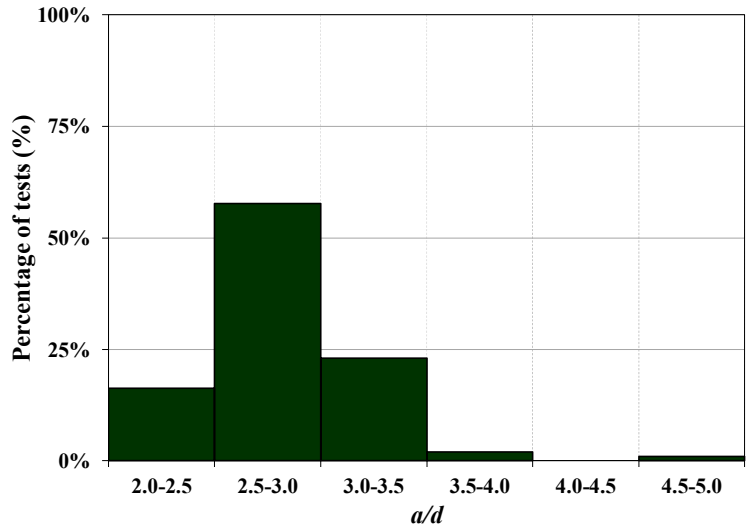
Figure 2-3. Data distribution for *a*/*d*

Figure 2-4 shows the variation V_{FRCM}/V_{CON} with respect to *a*/*d*. For the range of *a*/*d* tested, no clear relation can be observed between V_{FRCM}/V_{CON} and *a*/*d*. This trend is the same no matter the type of failure mode attained by the strengthened beams. However, it is important to note that for the beams that failed in shear, higher values of V_{FRCM}/V_{CON} were observed for values of *a*/*d* around 2.5.
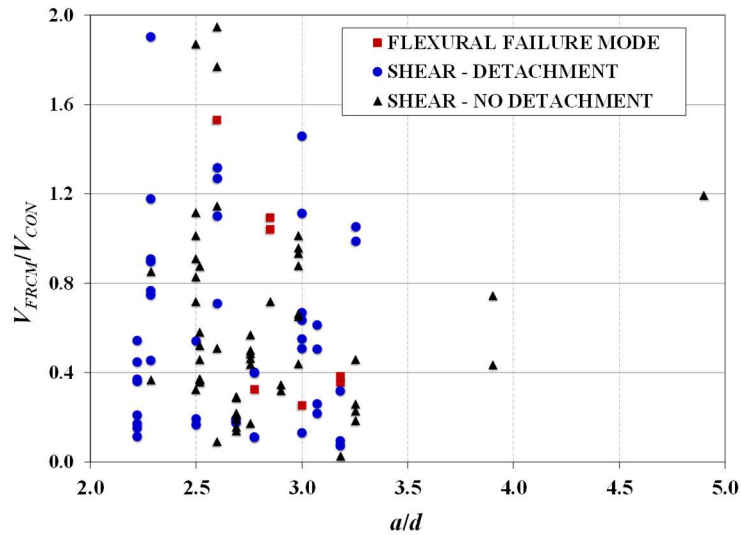
Figure 2-4. Variation of V_{FRCM}/V_{CON} with *a*/*d*

As shown in Figure 2-5, 52% of the tests were performed on beams with f'_c ranging from 20-30 MPa and 71% from 20-40 MPa. These values of f'_c, which are relatively low for new structures, can be considered adequate to represent compressive strengths of many existing structures. It is also worth mentioning how

researchers have also tried to study the behavior of structures with low values of f'_c (10-20 MPa).
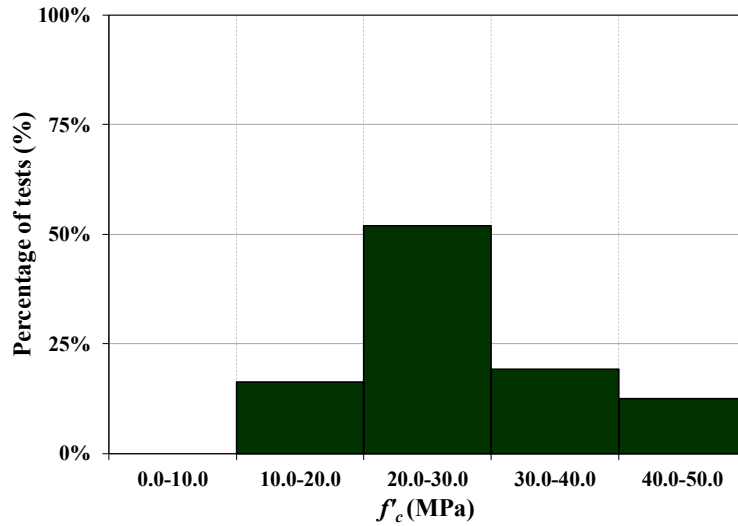
Figure 2-5. Data distribution for f'_c

Although there is not a straightforward relationship between V_{FRCM}/V_{CON} and f'_c, Figure 2-6 shows that the higher values of V_{FRCM}/V_{CON} are obtained for beams with lower values of f'_c, irrespective of the type of shear failure attained, which implies that the efficiency of the system is higher for beams with low value of f'_c.
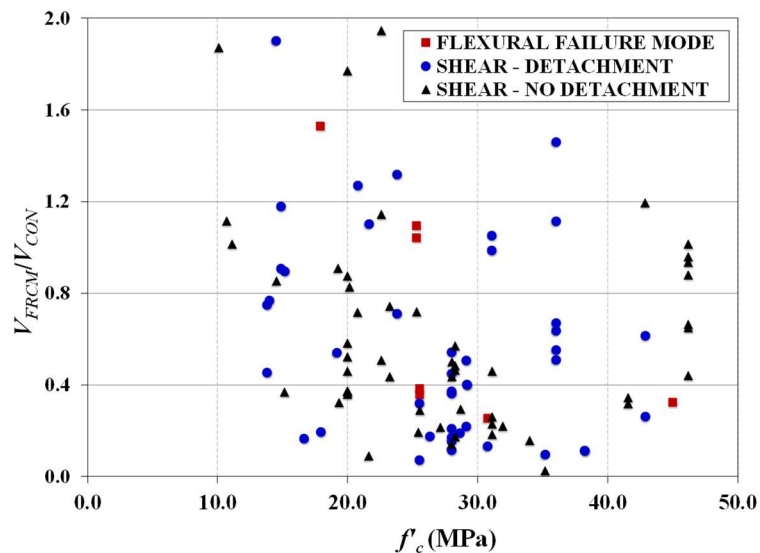
Figure 2-6. Variation of V_{FRCM}/V_{CON} with f'_c

Figure 2-7 shows that 64% of the tests were performed on beams that had a relatively high reinforcement ratio (ρ_{long}>0.02). Although beams with such large values of ρ_{long} are not desirable in real applications, their use is explained by the experimental objective of avoiding failure by bending.

10
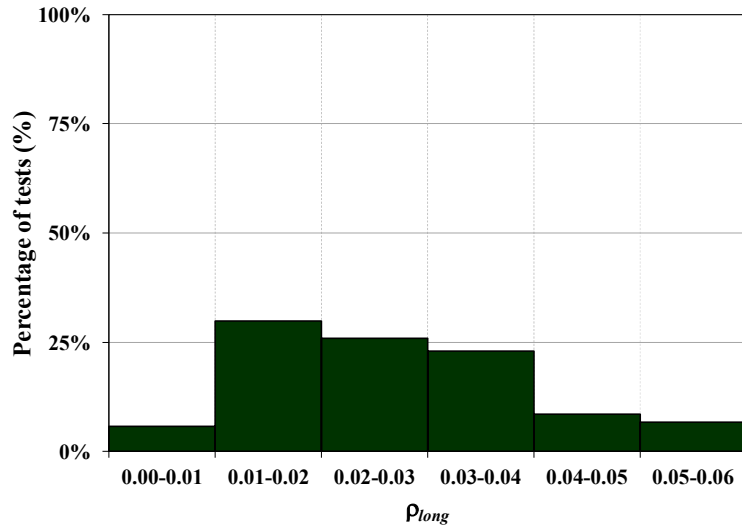
Figure 2-7. Data distribution for ρ_{long}

Figure 2-8 presents the variation of V_{FRCM}/V_{CON} with respect to ρ_{long}. As for the previous variables studied, a direct influence of ρ_{long} on the effectiveness of the FRCM system cannot be identified.
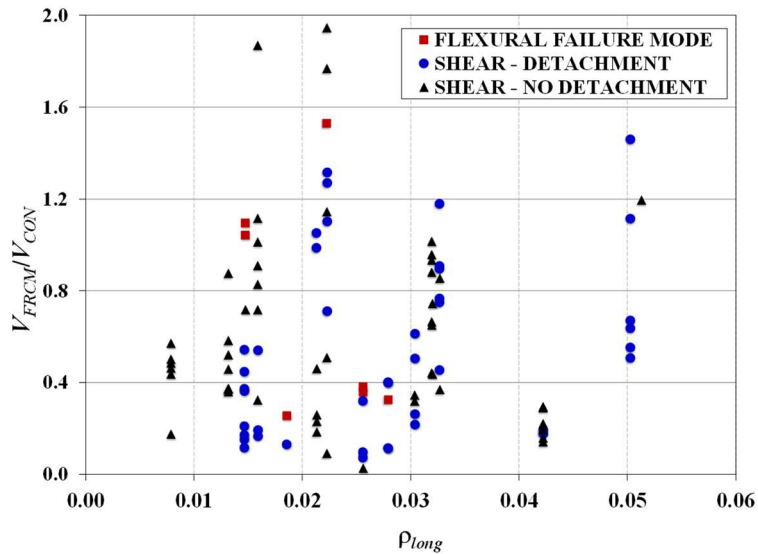
Figure 2-8 Variation of V_{FRCM}/V_{CON} with ρ_{long}

For RC beams, lower shear strengths have been reported for beams with low values of ρ_{long}, due to the reduction of the compression zone caused by wider cracks and the decrease in the dowel action [9]. For the case of the FRCM-strengthened beams collected in the database, this behavior is not observed. However, further discussion on the effect of ρ_{long} on V_{FRCM}/V_{CON} is given in Section 2.2.

11

Only 35% of the tests were performed on beams with transversal steel reinforcement ($\rho_w \neq 0.0$) as seen in Figure 2-9. Unlike the previous variables, and disregarding the beams with $\rho_w = 0.0$, a possible relationship between ρ_w and V_{FRCM}/V_{CON} can be observed (see Figure 2-10).
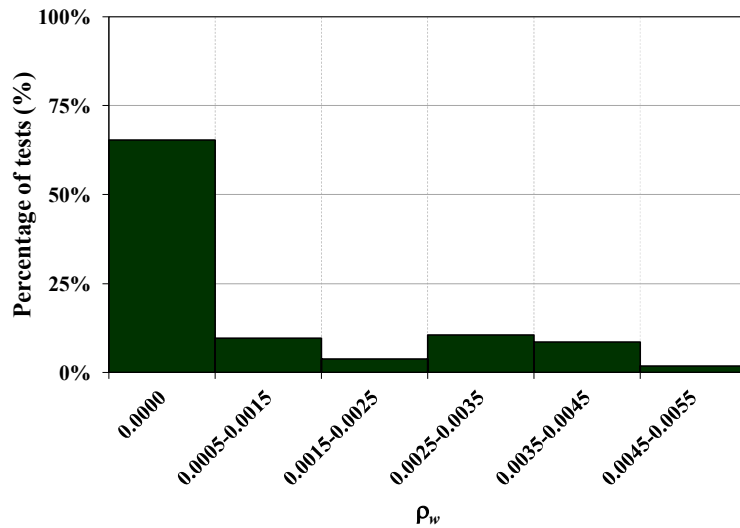
Figure 2-9. Data distribution for ρ_w
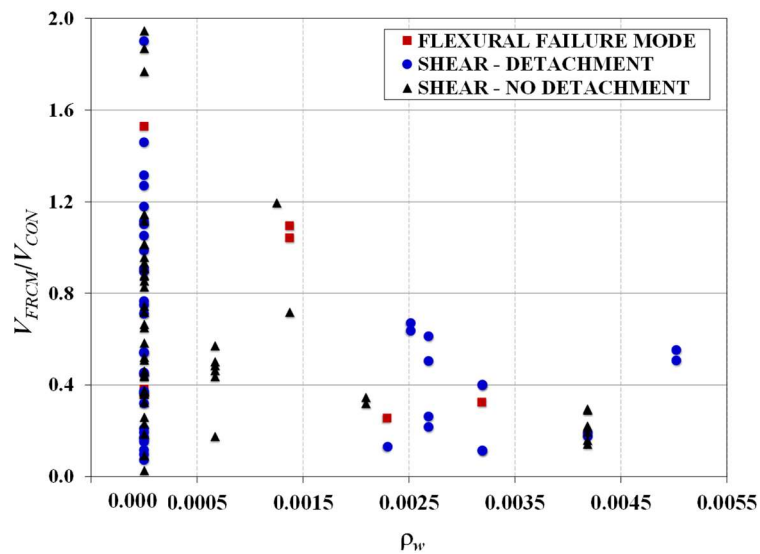
Figure 2-10 Variation of V_{FRCM}/V_{CON} with ρ_w

It appears that presence of a denser distribution of stirrups ($\rho_w > 0.0015$) reduces the effectiveness of the FRCM system. An explanation for this behavior is the possible interaction between the internal transverse steel reinforcement and the external FRCM strengthening, which has been reported for FRP composites [29–31]. A more detailed description of this phenomenon is presented in Section 2.3.

2.1.2 Geometrical properties of the FRCM strengthening system

In this section, the variation of V_{FRCM}/V_{CON} as a function of the geometrical properties of the strengthening system is presented. The data distribution of the properties listed below is also included:

- Strengthening configuration;
- n=number of fiber layers;
- ρ_f=fiber reinforcement ratio, ($2nt_fw_f/b_ws_f$, where t_f=nominal thickness of fiber sheets; w_f=width of FRCM strips; s_f=spacing of FRCM strips);
- ρ_{cm}=FRCM reinforcement ratio, ($2t_{cm}w_f/b_ws_f$, where t_{cm}= total thickness of the FRCM composite $(n+1)*t_m$ with t_m the nominal thickness of a matrix layer).

Most tests have been performed on beams strengthened with continuous side bonded (27%) configurations or continuous U-jackets with (17%) or without anchors (34%) configurations (see Figure 2-11).

Comparing the additional shear strength V_{FRCM} relative to V_{CON} for side bonded and U-wrapped configurations, although slightly higher values of V_{FRCM}/V_{CON} are related to the U-continuous configuration (see Figure 2-12), it is not possible to conclude that using this configuration will result in a better performance of the strengthened beam, which agrees with [14] who concluded that side bonded and U-wrapped configurations showed similar performance in terms of strength. In side bonded configurations detachment of the FRCM composite was less frequently observed, while for U-wrapped configuration most failures were accompanied by composite detachment, either at the composite-substrate interface or within the substrate. Although the experimental evidence is more limited, a similar behavior is also observed in beams strengthened with strips. The use of anchors with the U-wrapped configuration appears to mitigate detachment of the composite. A more detailed analysis regarding the type of failure mode and the influence of anchors is discussed in Sections 2.4 and 2.7, respectively.
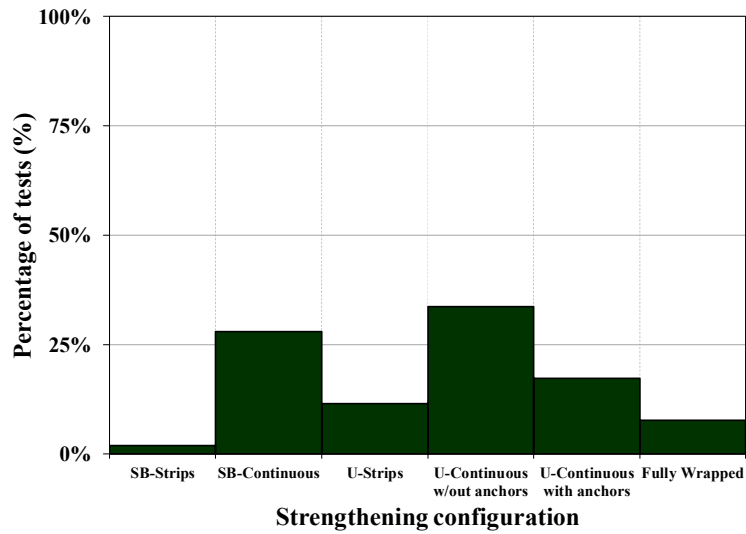
Figure 2-11. Data distribution for the strengthening configuration
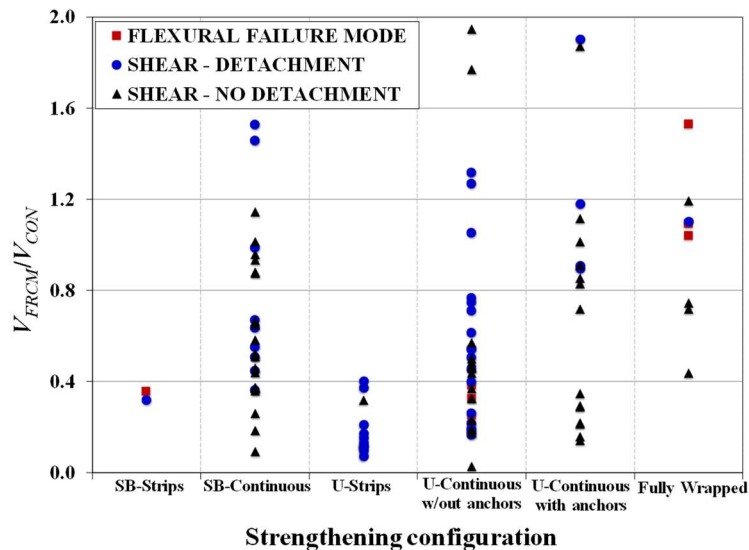
Figure 2-12 Variation of V_{FRCM}/V_{CON} with strengthening configuration

55% of the tests were carried out on beams strengthened with one layer of FRCM composite, while 87% of tests were performed on beams with 3 or less FRCM layers (see Figure 2-13). Although some higher values of V_{FRCM}/V_{CON} can be seen increasing the number of layers from 1 to 2 or 3 as shown in Figure 2-14, the effectiveness of the system appears to be reduced when a larger number of layers are provided, i.e., the gain in shear strength may not be proportional to the number of layers. In fact, higher values average values of V_{FRCM}/V_{CON} are found for beams with 2 or 3 layers of FRCM composite (around 71% gain in shear strength) when compared to those with n equal to 4 or 6. In Figure 2-14, it can also be seen that

most of the beams that failed without detachment of the FRCM jacket were strengthened with just one layer of the composite.
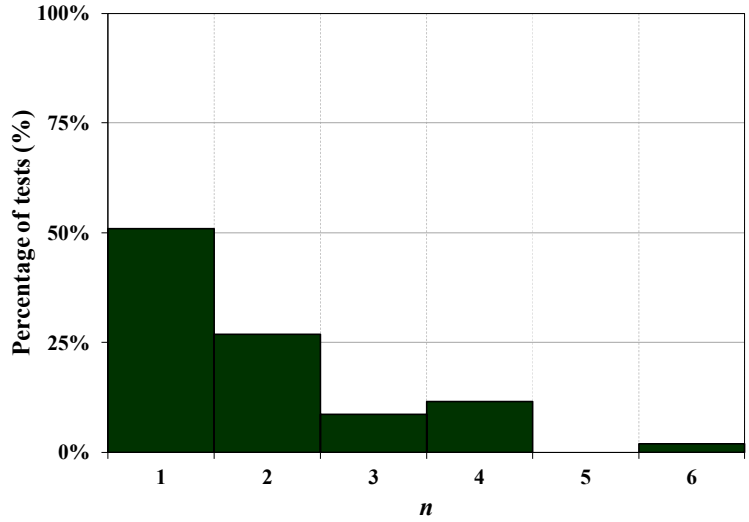
Figure 2-13. Data distribution for *n*
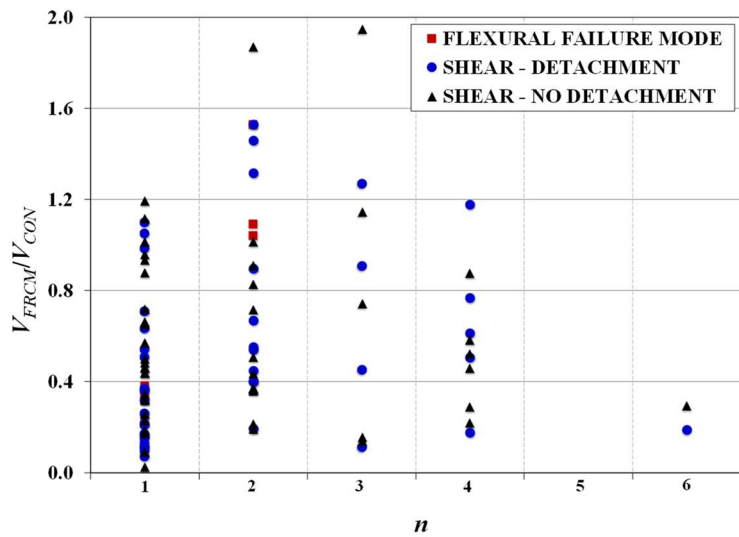
Figure 2-14 Variation of V_{FRCM}/V_{CON} with *n*

Figure 2-15 shows the distribution of data for the fiber reinforcement ratio, ρ_f. It can be seen that this distribution is similar to that observed for *n* (see Figure 2-13), with the larger percentage of tests concentrated for lower values of both *n* and ρ_f. However, it appears that V_{FRCM}/V_{CON} increases with ρ_f (see Figure 2-16), which differs from the behavior seen for *n* in Figure 2-14. This is explained by the fact that although ρ_f is directly proportional to the number of layers, it includes additional parameters such as the nominal thickness of fiber sheets and the strengthening configuration.
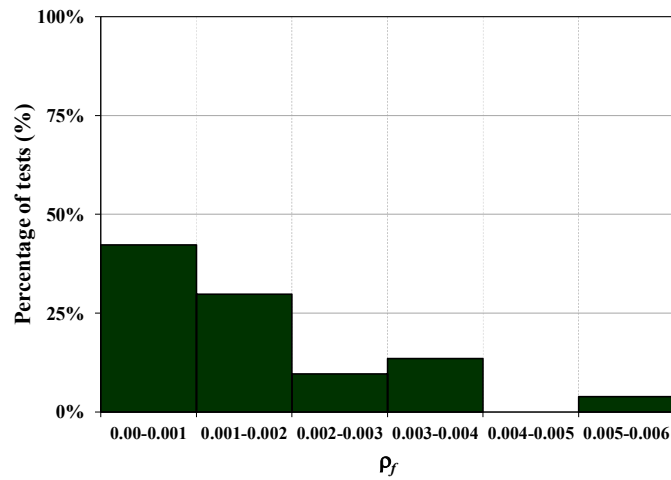
Figure 2-15. Data distribution for ρ_f
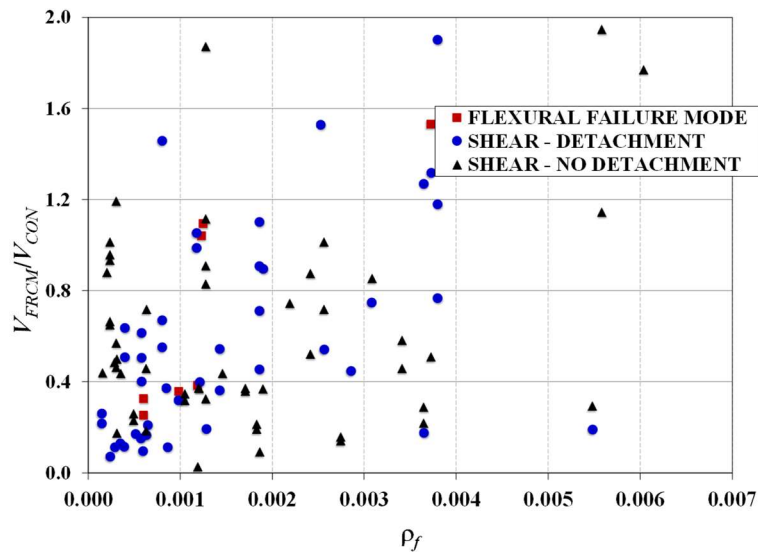
Figure 2-16 Variation of V_{FRCM}/V_{CON} with ρ_f

For the FRCM reinforcement ratio, Figure 2-17 shows that most of the tests were performed on beams with ρ_{cm} ranging from 0.05-0.10 (50% approximately), while a uniform distribution of the data is observed for the remaining categories up to 0.25. In Figure 2-18, an increasing trend is observed with the increase of ρ_{cm} (that can be understood as a relative increase in the width of the concrete cross section) implying that the increase in V_{FRCM}/V_{CON} depends not only on the amount of fibers included but also on the thickness of the cementitious matrix applied. Thicker layers of cementitious matrix, i.e. larger values of ρ_{cm}, imply a larger increase in the concrete section, and therefore an increase in the capacity of the beam would be expected, even if no fibers were included [7]. This trend is clearer for beams that failed by detachment of the composite.

16
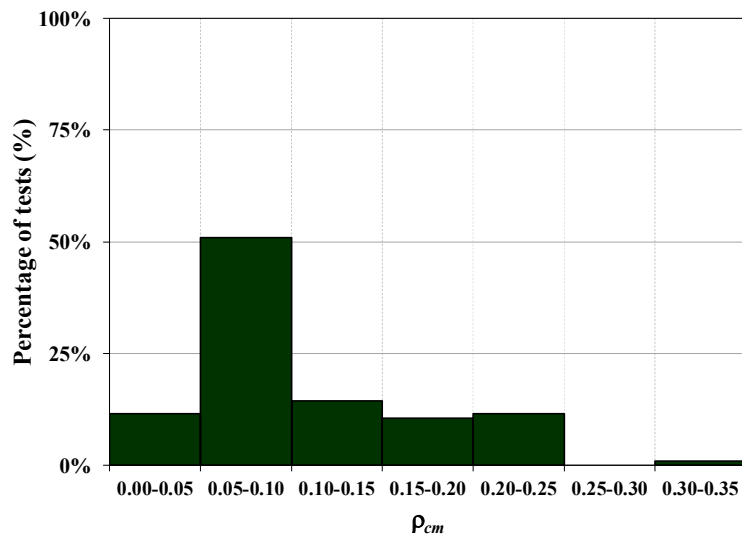
Figure 2-17. Data distribution for ρ_{cm}
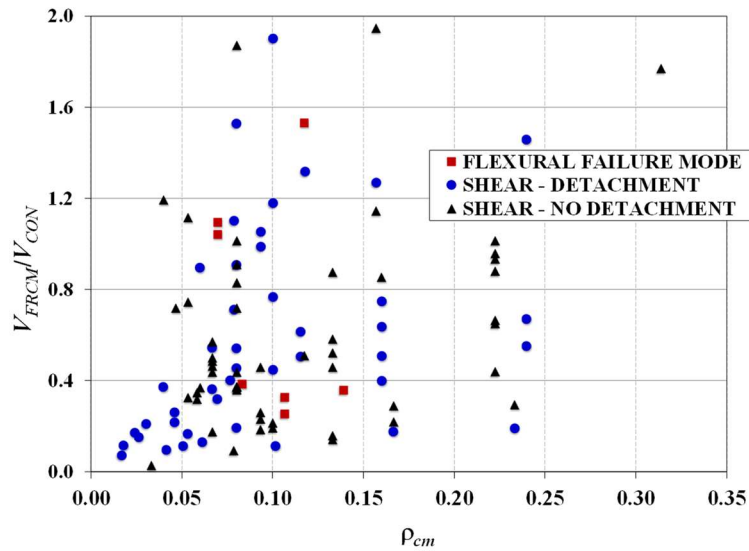
Figure 2-18 Variation of V_{FRCM}/V_{CON} with ρ_{cm}

2.1.3 Mechanical properties of the FRCM strengthening system

In this section, the variation of V_{FRCM}/V_{CON} as a function of the mechanical properties of the strengthening system is presented. The data distribution of the selected properties, listed below, is also included:

- Fiber type;
- Bare fiber ultimate strain (ε_{fu});
- Cementitious matrix compressive strength (f'_{cm});
- Ratio f'_{cm}/f'_c

17

Tests on beams with carbon fiber represent 54% of the available data, followed by glass, polyparaphenylene benzobisoxazole (PBO), and basalt fibers as shown in Figure 2-19. An important observation regarding fiber type is that although beams strengthened with carbon FRCM can achieve larger increases in shear strengths, similar values of V_{FRCM}/V_{CON} were attained with glass and PBO fibers (see Figure 2-20).
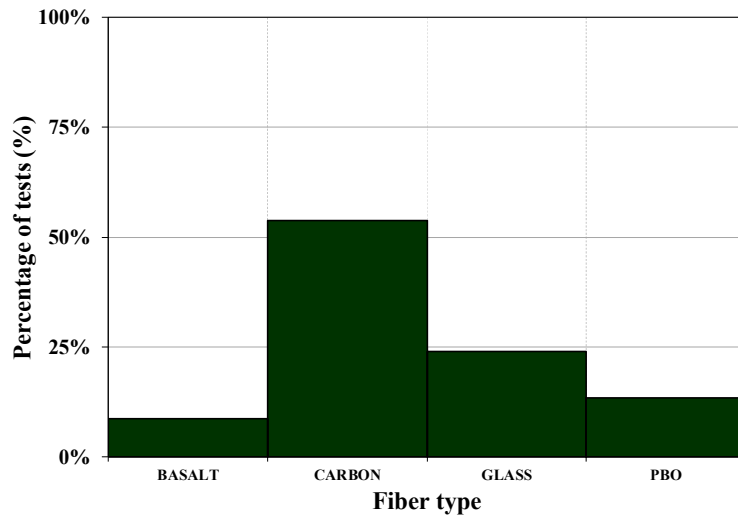
Figure 2-19. Data distribution for fiber type
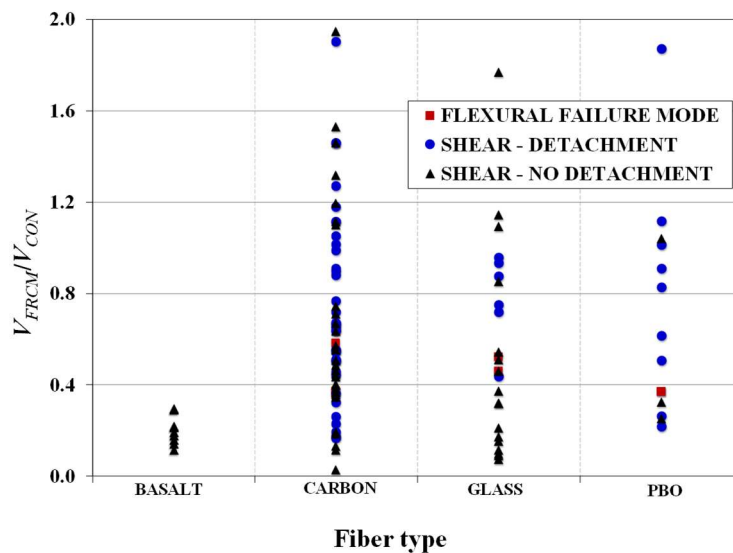
Figure 2-20 Variation of V_{FRCM}/V_{CON} with fiber type

It is also interesting to note that for carbon, and glass fibers, the fiber type did not influence whether detachment of the jacket was attained or not. Detachment of the composite appears to be the more common failure mode for PBO fibers. All beams strengthened with basalt fibers failed without detachment of the FRCM jackets and

showed the lower increase in shear strength with respect to the other fibers. However, tests with this type of fibers only represent 9% of the database, and further experimental evidence is needed to confirm these observations.

In Figure 2-21 and Figure 2-22, the data distribution for the bare fiber ultimate strain (ε_{fu}) and the influence of this variable on V_{FRCM}/V_{CON} are analyzed.
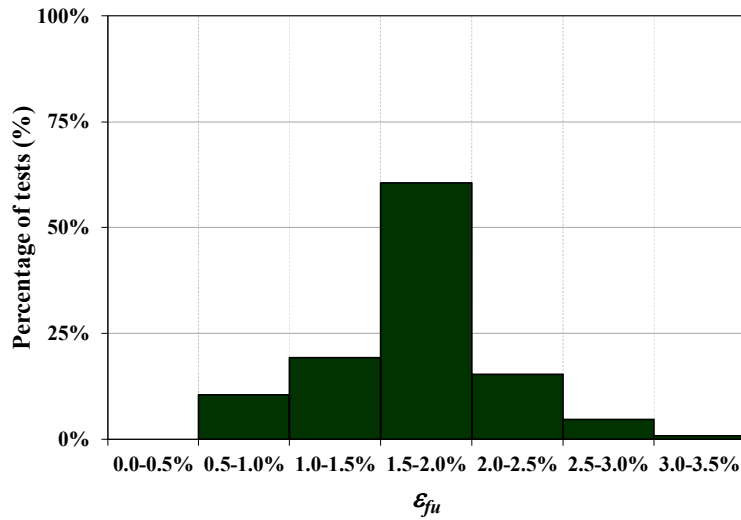
Figure 2-21. Data distribution for ε_{fu}
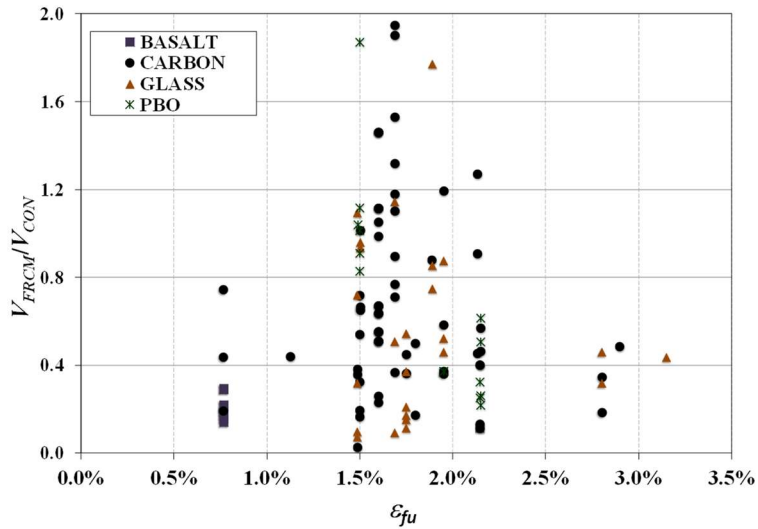
Figure 2-22 Variation of V_{FRCM}/V_{CON} with ε_{fu}

It is interesting to notice that even though there is a large variation for all the fibers, most tests are concentrated in a range from 1.5 to 2.0% (61% of the tests, Figure 2-21). In addition, for carbon, glass, and PBO fibers, the larger values of V_{FRCM}/V_{CON} ratios are also concentrated in the same range as seen in Figure 2-22.

19

In Figure 2-23 and Figure 2-24, the data distribution for the cementitious matrix compressive strength (f'_{cm}) and the influence of this variable on V_{FRCM}/V_{CON} are analyzed. It is worth noting that information regarding how tests for evaluating f'_{cm} were conducted is not usually provided in the papers. Considering that values of f'_{cm} may vary depending on the specimen size, shape, and testing procedure, it is pointed out that a strict analysis of the influence of f'_{cm} on V_{FRCM}/V_{CON} requires normalizing the results to one particular test/specimen size. However, as this information is not available, the analysis presented in this study is based on the values of f'_{cm} as reported in the available literature.
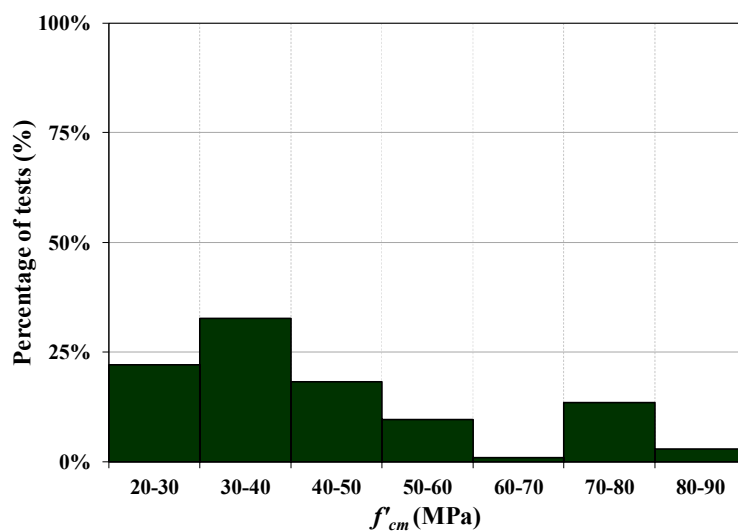
Figure 2-23. Data distribution for f'_{cm}

As shown in Figure 2-23, most of the matrix used have values of f'_{cm} below 50 MPa (73%), with 33% of the tests performed using values of f'_{cm} ranging between 30 and 40 MPa. In Figure 2-24, it can be seen that large values of f'_{cm} appear to be related to a lower effectiveness of the system (i.e., lower V_{FRCM}/V_{CON} values). However, it is worth noting that high strength mortars, i.e., mortars with f'_{cm} higher than 70 MPa, have been used only in 16% of the tests carried out.
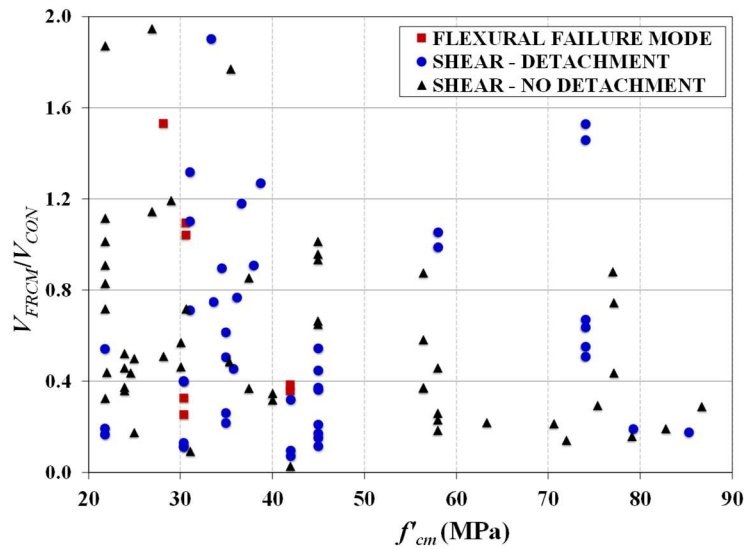
Figure 2-24 Variation of V_{FRCM}/V_{CON} with f'_{cm}

In Figure 2-25 and Figure 2-26, the data distribution for the ratio between the cementitious matrix and beam compressive strengths (f'_{cm}/f'_c) and the influence of this variable on V_{FRCM}/V_{CON} are analyzed. Results show that most of the tests have been performed using cementitious matrices and concrete substrate with similar values of compressive strength. In fact, 61% of the tests were performed with f'_{cm}/f'_c ranging from 0.5 to 1.5.
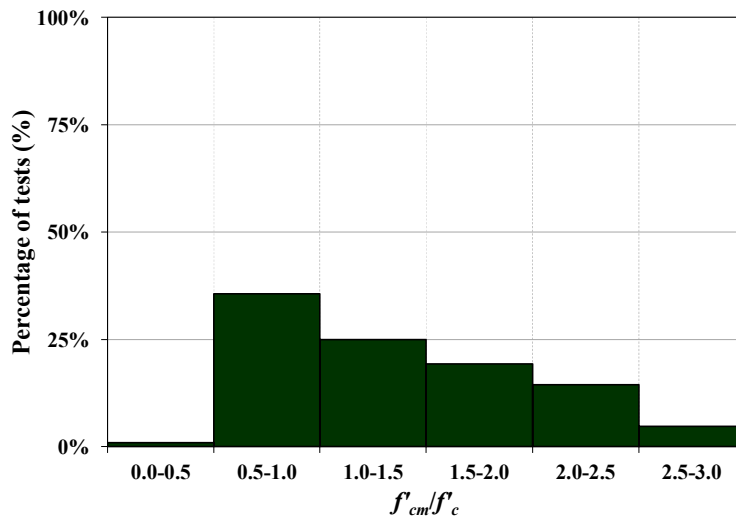
Figure 2-25. Data distribution for f'_{cm}/f'_c

According to Figure 2-26, a better performance of the system is attained when the compressive strengths of the substrate and the cementitious matrix are similar (f'_{cm}/f'_c close to 1.0). This behavior might be related to the better compatibility between the FRCM system and the substrate when they have similar values of compressive strength. However, it is highlighted that the compatibility is not only

21

related to the compressive strength but also to the modulus of elasticity of the materials, among other variables. However, data regarding this parameter for both the cementitious matrix and the concrete substrate are not reported in the available technical literature.
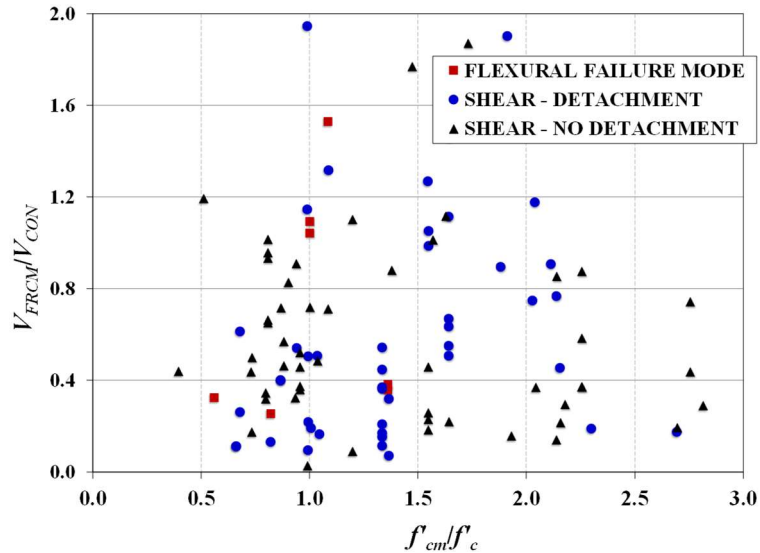
Figure 2-26 Variation of V_{FRCM}/V_{CON} with f'_{cm}/f'_c

2.2 Influence of the longitudinal reinforcement/external transverse shear reinforcement interaction

As discussed in Section 2.1.1, it was not possible to identify the possible influence of the longitudinal steel reinforcement ratio, ρ_{long}, on the gain in shear strength provided by the FRCM-strengthening system (see Figure 2-8). However, for FRP-strengthened beams, an interaction between the ρ_{long} and the strengthening system has been reported [26]. According to the results provided by [26], a higher increase in the shear strength of FRP-strengthened beams can be anticipated for lower values of the ratio of axial stiffness of the longitudinal steel reinforcement to that of the FRP composite ($\rho_{long}E_s/\rho_f E_f$ where E_s=elastic modulus of stirrups, and E_f=elastic modulus of the bare fibers). For the case of FRCM-strengthened beams, a similar trend is observed in Figure 2-27 in which V_{FRCM}/V_{CON} is plotted against $\rho_{long}E_s/\rho_f E_f$. This trend is clearer for values of $\rho_{long}E_s/\rho_f E_f$ lower than 100. However, it is worth noting that 86% of the tests are in this range, i.e., $0<\rho_{long}E_s/\rho_f E_f<100$, which implies that further data are required to understand the behavior of beams with values of $\rho_{long}E_s/\rho_f E_f$ larger than 100.
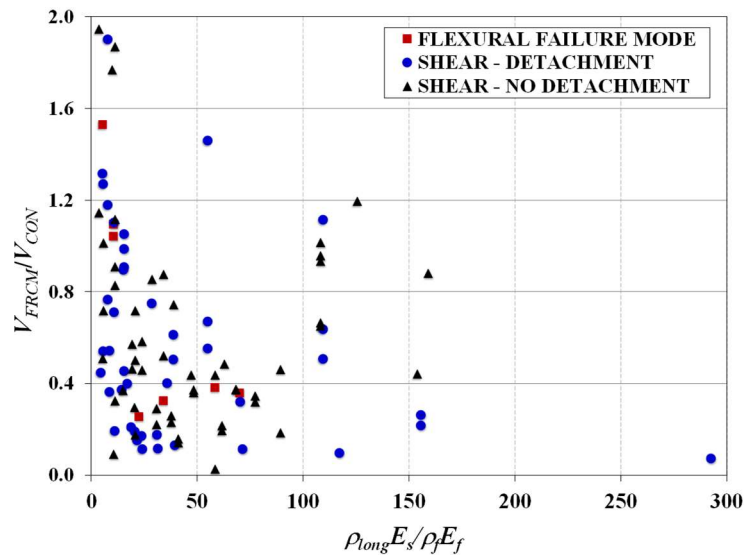
Figure 2-27 Variation of V_{FRCM}/V_{CON} with $\rho_{long} E_s/\rho_f E_s$

2.3 Influence of the internal/external transverse shear reinforcement interaction

It has been noted that the interaction between internal steel reinforcement and external FRP reinforcement should be taken into account to properly predict the overall shear strength of a strengthened beam [26,32]. According to [33], the maximum contributions of steel stirrups and FRP to the shear strength are not reached simultaneously implying that their combined contribution may actually be less than the simple summation of their respective values. The possible interaction between the internal and external shear reinforcement for FRCM systems has also been reported by [7,19], who witnessed a significant reduction in the strain values measured in the stirrups of the strengthened beams when compared with the control beams at the same load levels. In fact, for the beams tested by [19], the presence of the FRCM system precluded yielding of the stirrups, as has also been reported for similar beams strengthened with FRP composites [29].

The ratio of the axial stiffness of the transverse steel reinforcement to that of the FRP composite ($\rho_w E_s/\rho_f E_f$ where E_s=elastic modulus of stirrups, and E_f=elastic modulus of the bare fibers) has been used to evaluate the internal and external shear reinforcement interaction in FRP-strengthened beams. For FRP composites the effectiveness of the strengthening system reduces when the ratio $\rho_w E_s/\rho_f E_f$ increases [29]. The same trend is observed for FRCM composites in Figure 2-28, in which V_{FRCM}/V_{CON} is plotted against $\rho_w E_s/\rho_f E_f$ for strengthened beams with stirrups. Results in Figure 2-28 suggest that, for a given amount of FRCM, increasing the amount of internal reinforcement decreases the contribution of the

23

FRCM (i.e., lower V_{FRCM}/V_{CON} values). Having a larger internal transversal steel reinforcement ratio by providing a smaller stirrup spacing implies that more stirrups will be crossed by the critical shear crack, and they might not yield before failure of the beam. In other words, the internal shear reinforcement may not be able to achieve its design value (based on the assumption of yielding) and provide the same contribution it gives in the unstrengthened element. This implies that subtracting the control beam shear strength from the total shear strength of the strengthened beams to obtain V_{FRCM} may not accurately reflect the contribution of the FRCM system.
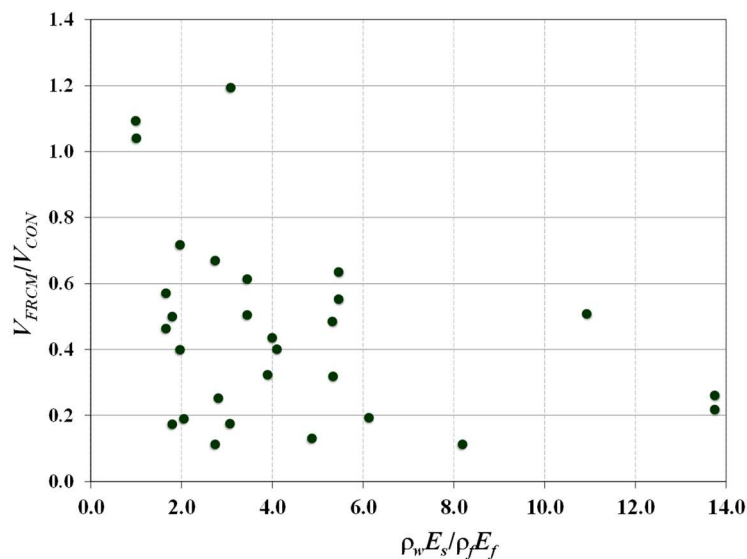
Figure 2-28 Variation of V_{FRCM}/V_{CON} with $\rho_w E_w/\rho_f E_f$ for strengthened beams with stirrups

2.4   Failure modes of FRCM strengthened beams

Regarding fully wrapped beams, [1] reported fiber rupture and observed beam cracking clearly visible on the surface of the FRCM jacket. These findings are corroborated by [10] who reported a similar behavior. This type of failure agrees with the experimental evidence for beams fully wrapped with FRP composites, which tend to fail due to FRP rupture [31]. As noted by [34] for FRP composites, this behavior indicates that the wrapping configuration is able to provide significant anchorage to avoid composite debonding. It is worth mentioning that information on the overlap length and its design is generally not reported in the references but should be related to the effective length of the composite, i.e., the length needed to fully develop the load-carrying capacity of the interface [35].

It is not as straightforward to identify a typical failure mode for side bonded and U-wrap configurations as it is for fully wrapped beams. Composite detachment,

which is described as debonding of the FRCM jacket from the substrate (with or without concrete attached) in this thesis, is reported in some of the references [13,18,19]. In most cases, detachment was located at the matrix-substrate surface without affecting the concrete surface, although peeling off of the concrete cover (i.e., within the substrate) has also been observed [20,23]. However, it is not possible to conclude that failure will be exclusively related to this phenomenon as other failure modes have also been reported in the available literature. Some researchers [12,15,17] described failure caused by diagonal tension. The same behavior, together with rupture of some fibers, was observed by [7]. Azam and Soudki [14] described failure by diagonal tension associated with a large diagonal crack for most of their specimens, although the two beams that reached a higher shear strength experienced composite detachment and shear compression failure. Tetta *et al.* [20] reported slippage of the vertical fibers through the mortar and partial fiber rupture. According to their findings, the type of failure depends on the strengthening configuration with slippage being more pronounced in side bonded configurations and almost eliminated for fully wrapped configurations in which fiber rupture is the dominating failure mechanism. Fiber slippage is another form of debonding that has been observed in some types of FRCM composite-concrete joints [35–37].

Table 2-2 and Figure 2-29 summarize the type of failure mode reported for the different strengthening configurations for beams without anchors. It is interesting to note that the failure mode reported for most of the side bonded configurations was not related to the detachment of the FRCM composite from the substrate. This behavior does not agree with the findings for beams strengthened with FRP composites where two- or three-sided jackets fail mainly by debonding of the composite [34]. In fact, some codes for the design of externally bonded FRP composites do not allow the use of side bonded configurations for shear strengthening of RC beams [38] in order to avoid an early debonding of the system.

For U-wrapped strengthened beams the prevailing failure mode is associated with detachment of the composite, although failure without detachment was reported in 35% of the tests.

Considering that all unstrengthened control beams failed in shear, it is also interesting to note that the ability to transform this type of failure into a flexural failure is not exclusively limited to fully wrapped beams, although it has been rarely reported in side bonded beams.

Table 2-2. Failure modes of beams with different FRCM composite strengthening configurations

Strengthening Configuration	Failure Mode		
	Detachment	No Detachment	Flexure
Side bonded	12	18	1
U-wrapped[a]	29	15	3
Fully wrapped	0	5	3

[a]Beams with anchors are not included
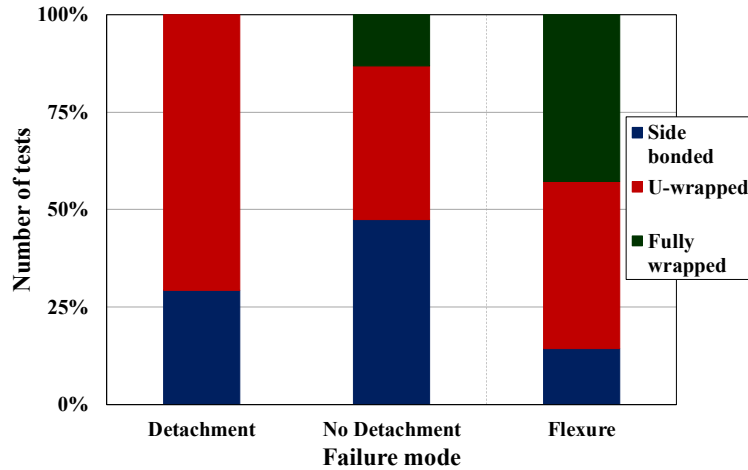
Figure 2-29 Failure modes of beams with different FRCM composite strengthening configurations

2.5 Fiber effective strain

Most available design models compute the contribution of FRP or FRCM composites to the shear strength of RC elements strengthened in shear, V_f, using the well-known truss analogy (e.g. [1,17,39,40]). For the case of FRP or FRCM jackets with fibers perpendicular to the longitudinal axis of the element, V_f can be determined as:

$$V_f = \rho_f E_f \varepsilon_{eff} d_{fv} b_w \cot(\theta)$$

2-1

where ε_{eff} is the effective strain in the fibers, d_{fv} is the effective depth of the shear reinforcement, b_w is the beam width, θ is the shear crack angle, and the other variables were defined previously. It should be noted that, if the truss analogy is employed, d_{fv} should be taken equal to the cross-section inner lever arm [41], whereas, if the format of [39] is employed, d_{fv} should be taken equal to the distance between the top edge of the external shear reinforcement and the centroid of the flexural tension steel reinforcement.

The design models differ mainly in the expression used to determine ε_{eff}, which can be defined as the average strain in the fibers crossing the diagonal shear crack at failure [1], and varies based on the failure mode, type of fiber and wrapping configuration. For U-wrapped or side bonded FRP strengthened beams, the effective strain is usually computed considering the composite-to-concrete bond capacity since failure has been observed to be associated with composite debonding [39].

For the case of the FRCM-strengthened beams collected in the database, Eq. (2-1) can be rearranged to compute the value of ε_{eff} from the contribution of the jacket V_{FRCM} and the mechanical and geometrical properties of the strengthening system and the RC beam:

$$\varepsilon_{eff} = \frac{V_{FRCM}}{\rho_f E_f d_{fv} b_w \cot(\theta)} \qquad 2\text{-}2$$

As a first attempt, d_{fv} in Eq. (2-2) is assumed equal to d, i.e. the method in [39] was adopted. In addition, only beams without anchors and that failed in shear are considered, since Eq. (2-2) does not explicitly include the effect of anchors. Considering the limited data available reporting the actual value of θ, a fixed value of $\theta=45°$ is used to compute values of effective strain. It is also worth noting that in practical design applications, θ is unknown, and a fixed value of $45°$ is usually used. However, further discussion on the shear crack angle is given in Section 2.6. shows the variation of V_{FRCM}/V_{CON} with respect to the effective fiber strain, computed according to Eq. (2-2).

Results in Figure 2-30 show that higher values V_{FRCM}/V_{CON}, i.e., higher gain in shear strength, can be anticipated for beams with higher calculated effective fiber strain. This behavior appears to be clearer for beams that failed without detachment of the FRCM composite.
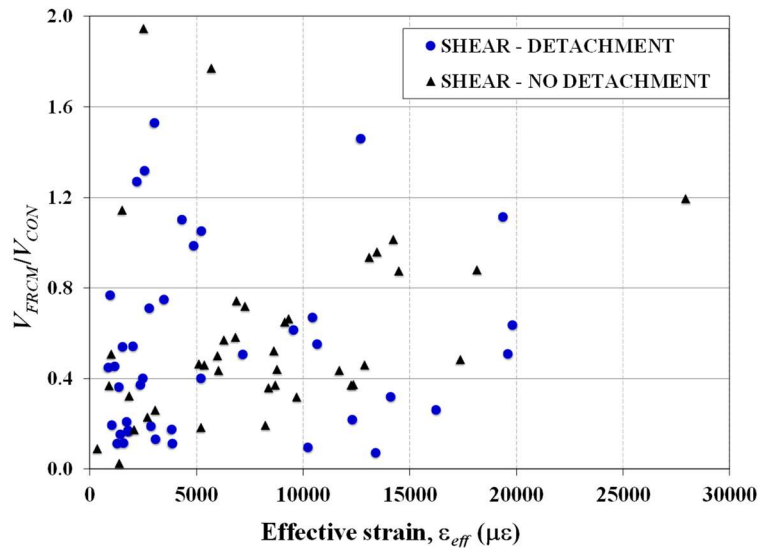
Figure 2-30 Variation of V_{FRCM}/V_{CON} with the effective fiber strain, ε_{eff}

As expressed by [26,42] for FRP-strengthened beams, the effective strain in the fibers depends on the axial rigidity ($E_f\rho_f$) and is inversely proportional to the tensile strength of the substrate expressed as $f'_c{}^{2/3}$. In Figure 2-31, the values of $\varepsilon_{eff}/\varepsilon_{fu}$ are plotted in terms of the ratio $\rho_f E_f/f'_c{}^{2/3}$, where ε_{eff} is calculated using Eq. (2-2), and ε_{fu} is the ultimate bare fiber tensile strain. Figure 2-31 shows that the ratio $\varepsilon_{eff}/\varepsilon_{fu}$ tends to decrease with increasing $\rho_f E_f/f'_c{}^{2/3}$, as has been found for FRP composites. For beams that failed by detachment, ε_{eff} is generally lower than 50% of ε_{fu}, with an average of 0.36 (COV=0.98). For beams that did not show detachment, the average value is 0.47 (COV=0.71). Beams that did not show detachment generally present lower values of $\rho_f E_f/f'_c{}^{2/3}$. In fact, 79% of tests that did not fail by detachment present values of $\rho_f E_f/f'_c{}^{2/3}$ lower than 0.02, while only 39% of beams with detachment fall in that range. For a constant concrete strength, this finding indicates that a less stiff strengthening solution, i.e. lower values of $E_f\rho_f$, might avoid the onset of detachment. For a constant axial rigidity, having higher values of f'_c might as well avoid the onset of detachment. Although both detachment and shear failure can be considered as brittle failures, a better exploitation of the system can be expected with larger values of effective strain, which are associated to beams with no detachment.

It is also interesting to note that in Figure 2-31, that for some limited cases (4), Eq. (2-2) predicts values of values of ε_{eff} larger than $\varepsilon_{eff}/\varepsilon_{fu}$, i.e., $\varepsilon_{eff}/\varepsilon_{fu} >1.0$.
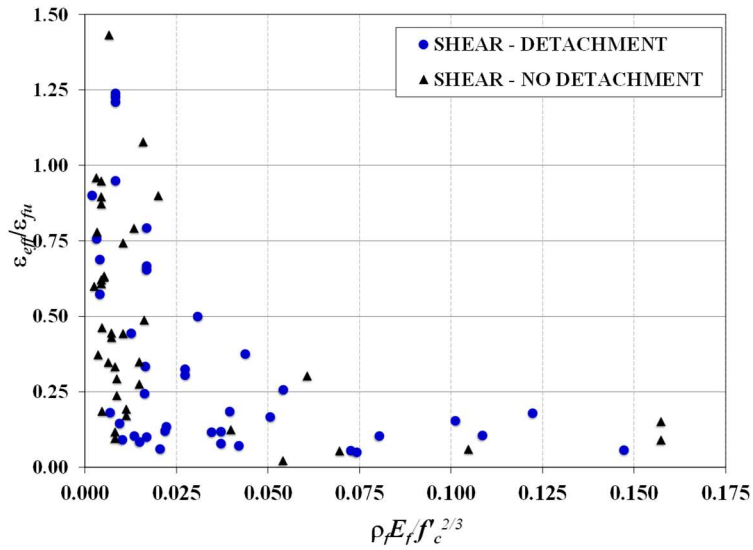
Figure 2-31 Normalized effective fiber strain $\varepsilon_{eff}/\varepsilon_{fu}$ vs. $\rho_f E_f /f'_c{}^{2/3}$

Figure 2-32 presents the values of $\varepsilon_{eff}/\varepsilon_{fu}$ plotted in terms of the ratio $\rho_f E_f /f'_c{}^{2/3}$ for the tests in the database, divided by type of fiber. For basalt fibers (Figure 2-32a), all the tests have values of $\rho_f E_f /f'_c{}^{2/3}$ lower than 0.0150. Considering that all beams strengthened with basalt fibers failed without detachment of the FRCM jackets (see Section 2.4), this behavior is in agreement with the assumption that lower values of $\rho_f E_f /f'_c{}^{2/3}$ can prevent detachment of the FRCM system. In fact, for carbon, glass, and PBO fibers (see Figure 2-32b, c, and d, respectively), it can be also observed that most of the beams that did not attain detachment of the composite present values of $\rho_f E_f /f'_c{}^{2/3}$ lower or around 0.02. For specimens that failed by detachment, there is a larger dispersion of the values of $\rho_f E_f /f'_c{}^{2/3}$, although most of the beams with this type of failure mode have $\rho_f E_f /f'_c{}^{2/3}$ higher than 0.02, as discussed before. This might be related to the fact that the presence of detachment can be associated to additional factors not considered by Eq. (2-2). Among these factors, it is possible to name the substrate preparation before applying the composite or the presence of shrinkage cracks in the cementitious matrix, as pointed out by [43].
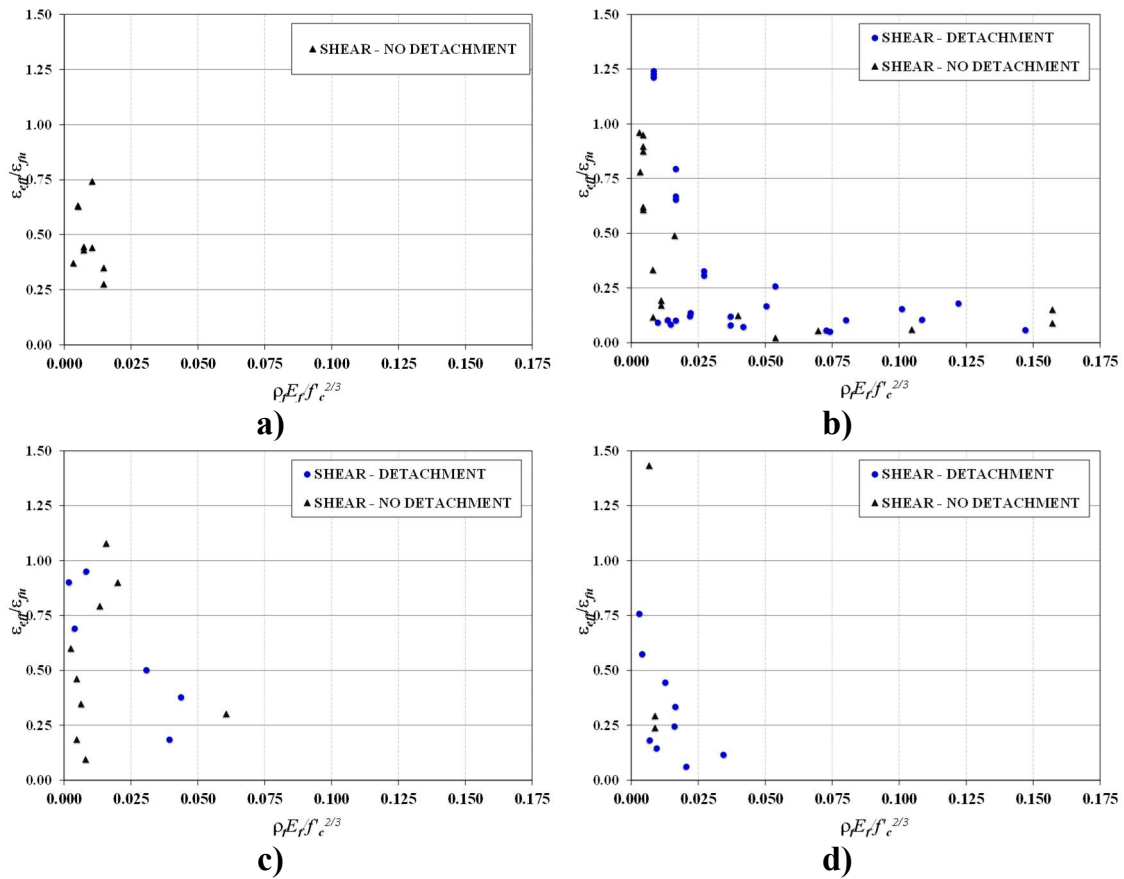
Figure 2-32 Normalized effective fiber strain $\varepsilon_{eff}/\varepsilon_{fu}$ vs. $\rho_f E_f /f'^{2/3}_c$ for: a) basalt fibers; b) carbon fibers; c) glass fibers; d) PBO fibers

2.6   Shear crack angle (θ)

In Eq. (2-1), the contribution of the FRP or FRCM strengthening to the shear strength of RC beams is assumed to be directly proportional to the cotangent of the shear crack angle, θ. American guidelines, such as [39,44], use implicitly a value of θ equal to 45°, as it provides conservative values [26]. However, analytical models developed in Europe allow the use of shear crack angles that can vary between 21.8° and 45° [41].

For FRP-strengthened beams, experimental evidence has shown that the value of θ can be influenced by the amount of internal transverse reinforcement, concrete quality, and FRP reinforcement ratio, among other variables [45]. Values of θ greater than 45° can be anticipated for beams with high values of ρ_w, as a more inclined crack will require less energy to pass through a section with closely spaced stirrups.

To verify the influence of the FRCM-strengthening system on the shear crack angle, i.e., cracking pattern, values of θ from the papers listed in Table 2-1 were collected. These values were either reported directly in the papers or were obtained graphically using photographs or sketches included in the papers. However, this information was not available for all tests, and only values of θ for 16 control beams out of a total of 28 specimens, and for 54 strengthened beams out of a total of 104 specimens were gathered. Information regarding the mechanical and geometrical properties of the control beams collected from the papers included in Table 2-1 are presented in Appendix B.

Figure 2-33 shows the variation of V_{FRCM}/V_{CON} with the angle θ. Although there is not a clear relationship between the gain in shear strength provided by the FRCM system and the shear crack angle, it appears that a lower effectiveness of the strengthening system is achieved as θ increases, which agrees with the behavior predicted by Eq. (2-1), at least for the range of θ considered.
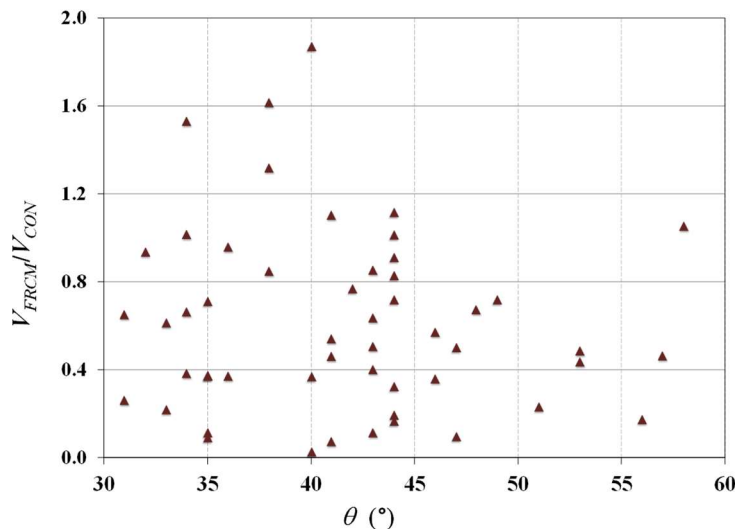
Figure 2-33 Variation of V_{FRCM}/V_{CON} with the shear crack angle, θ

In Figure 2-34, the maximum shear strength attained by the beam (V_{max}) is plotted against the angle θ for control and strengthened beams for which values of θ were available. For control beams, θ varies from 32° and 44°. For the FRCM-strengthened beams, values of θ higher than 45° were observed for 12 beams. This implies that the presence of the FRCM jackets modifies the shear crack angle and, for some cases, the use of θ=45° in Eq. (2-1) might overestimate the contribution of the jacket.
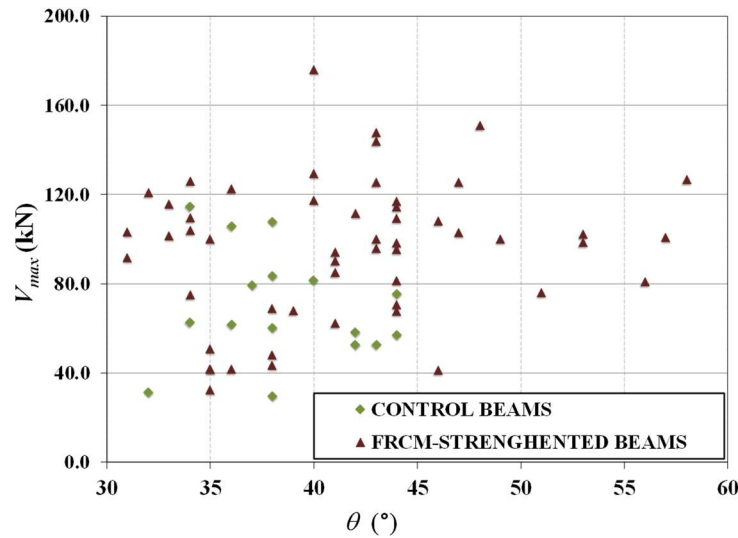
Figure 2-34 Variation of V_{max} with the shear crack angle, θ for control and FRCM-strengthened beams

2.7   Anchorage systems

The few studies that have included anchors for the FRCM composite shear strengthening system have shown mixed results. Baggio *et al.* [15] evaluated the efficiency of FRP spike anchors for rectangular beams strengthened in shear with U-wrapped FRCM composites. The anchors, composed of carbon fibers, were inserted in predrilled holes and then fanned out. The beam with anchors showed an increase of only 3% over the strengthened beam without anchors. Although beams with and without anchors exhibited a diagonal tension shear failure, the presence of the anchors slightly changed the inclination of the shear crack around the anchors. Considering that failure of the strengthened beams by fiber slippage has been reported for certain FRCM composites [35–37], the lack of effectiveness of this type of anchor may be linked to the fact that they are intended to restrain out-of-plane peeling of the composite and do not restrain the in-plane fiber slippage [46].

L-shaped steel sections were used by [11] to anchor the FRCM system for U-wrapped T-beams. One leg of the steel section was glued to the FRCM composite, while the other was anchored to the bottom of the beam flange by means of vertical steel bars installed in pre-drilled holes through the entire thickness of the flange. For beams without anchors, the increase in shear capacity of the beam was approximately 19%, independent of the number of fiber layers. For beams with anchors, the shear increase strength ranged between 14% and 29%, depending on the number of layers. Although higher strengths were achieved for certain beams

32

with anchors, the results were not consistent. However, the presence of the anchors reportedly avoided the FRCM system detachment.

Tzoura and Triantafillou [16] used a 3 mm thick curved steel section fixed to the slab with threaded rods to anchor FRCM U-wrapped T-beams. The steel sections were placed at the corners between the slab and the beam web. The rods were placed inside 45° holes filled with an epoxy adhesive at a fixed spacing. A significant increase in the effectiveness of the FRCM jackets for the beams with anchors was reported. For beams strengthened with low textile density, the increase in strength appeared to be more significant, from approximately 18% for beams without anchors to a maximum of 187% when anchors were present. For beams with high textile density, the increase in shear strength ranged from 32% for beams without anchors to a maximum of 112% for specimens with anchors.

2.8   Effect of high temperatures

The experimental evidence regarding the effect of high temperatures and other different environmental conditions on the performance of RC beams strengthened in shear with FRCM composites is still quite limited, and only specimens tested under normal environmental conditions were discussed in the previous sections. However, results presented by [6] have shown that the strength of FRCM shear strengthened beams subjected to elevated temperatures reduces slightly when compared to specimens tested under normal environmental conditions. The results also show that the reduction in strength is significantly higher for RC beams FRP strengthened beams than for FRCM strengthened beams subjected to similar temperature conditions. These results are in agreement with the findings of [47] for FRCM-confined elements. Under high temperature conditions, [47] observed a significant reduction in the axial strength of FRP-confined members, while for FRCM-confined specimens, the axial strength was marginally affected.

2.9   Conclusions

In this study, experimental results from 18 papers on shear strengthening of RC beams using externally bonded FRCM composites were collected. As result, a database that includes 104 tests was compiled, and the influence of geometrical and mechanical properties of the beams and the strengthening system was assessed. The main conclusions drawn from this analysis are summarized as follows:

- The experimental evidence shows that FRCM composites are able to increase the shear strength of RC beams. For the beams included in the database, an increase of 3% to 195% was reported, with an average of 60%. In addition, the FRCM composite can modify the type of failure from shear to a flexural mode.

- The effectiveness of the FRCM system appears to be related to the compressive strength of the matrix, as lower values of V_{FRCM}/V_{CON} are usually found for matrices with higher values of matrix compressive strength. The influence appears to be related to the compressive strength of the substrate, with larger values of V_{FRCM}/V_{CON} reached when the compressive strengths of the matrix and the substrate are similar.

- As for FRP composites, a possible interaction between the internal transverse steel reinforcement and the FRCM system has been observed. As reported by some researchers, the presence of the FRCM composite can limit the strain in internal stirrups and prevent them from achieving their maximum possible contribution (based on yielding), resulting in lower values of V_{FRCM}/V_{CON}. Based on the experimental tests collected in this work, this effect appears to be more pronounced for higher values of the ratio $\rho_w E_s/\rho_f E_f$.

- For fully wrapped beams, the failure mode has been associated with fracture of the fibers. For side bonded and U-wrapped beams, detachment of the FRCM jackets (with or without concrete attached) has been reported, being the most common failure mode for U-wrapped configurations. However, failure without detachment has also been observed together with diagonal cracking, slippage of the vertical fibers through the mortar, and/or partial fiber rupture.

- According to the available experimental results, strengthening solutions with values of $\rho_f E_f/f'^{2/3}_c$ lower than 0.02 might avoid the onset of composite detachment. It was also observed that having less stiff solutions, i.e., lower values of $\rho_f E_f$, results in a better exploitation of the FRCM system.

3. EXPERIMENTAL BEHAVIOR OF RC BEAMS STRENGTHENED IN SHEAR WITH FRP AND FRCM COMPOSITES

In this chapter, the results of an experimental campaign on shear strengthening of RC beams with externally bonded FRP and FRCM composites are presented. FRP and FRCM composites with two different fiber types, namely carbon and steel, are examined. It is highlighted that FRP and FRCM composites that use steel fibers can be found in the available literature referred to as SRP (Steel Reinforced Polymer) and SRG (Steel Reinforced Grout), respectively [48]. In this chapter, however, SRP and SRG will be referred to as steel FRP and steel FRCM composite.

The additional shear strength provided by each strengthening system, concrete crack pattern, and failure mode are presented and discussed. Strains measured in the internal stirrups and external strengthening system are compared to investigate the internal-external shear reinforcement interaction, which has been reported for beams strengthened in shear with FRP composites [29], as discussed in Section 2.3. Two different stirrup spacings were employed to investigate the internal-external shear reinforcement interaction for different internal shear reinforcement ratios.

Considering the limited experimental evidence on the use of anchors for RC beams strengthened in shear with FRCM composites [15,16] (see Section 2.7), the performance of FRCM strengthened beams with and without anchors is also compared.

3.1 Experimental campaign

A total of 14 RC beams were included in the experimental program. The beams were designated according to the convention: S#-X-F#-UY, where S# corresponds to the center-to-center stirrup spacing in the studied shear span (S1=300 mm, S2=200 mm), X denotes the type of strengthening system (CONTROL, FRP, or FRCM), F# indicates the type of fiber in the composite (F1=carbon sheet, F2=brassed steel sheet, F3=carbon open mesh, and F4=galvanized steel sheet; see Section 3.1.1 for the description of each type of fiber), U identifies the composite wrapping configuration (U-wrapped), and Y is related to the use of composite anchors (N=without anchors, A=with anchors).

The designation of the 14 beams tested is shown in Table 3-1. All strengthened beams were strengthened using one layer of FRP or FRCM composite ($n=1$).

Table 3-1. Experimental test matrix

Series	Beam	Fiber	s (mm)	ρ_w	Anchors	Concrete batch
	S1-CONTROL	-	300	0.0022	-	A
	S1-FRP-F1-UN	F1 (Carbon)	300	0.0022	No	A
	S1-FRP-F2-UN	F2 (Steel)	300	0.0022	No	A
S1	S1-FRCM-F3-UN	F3 (Carbon)	300	0.0022	No	A
	S1-FRCM-F3-UA	F3 (Carbon)	300	0.0022	Yes	A
	S1-FRCM-F4-UN	F4 (Steel)	300	0.0022	No	C
	S1-FRCM-F4-UA	F4 (Steel)	300	0.0022	Yes	C
	S2-CONTROL	-	200	0.0033	-	B
	S2-FRP-F1-UN	F1 (Carbon)	200	0.0033	No	B
	S2-FRP-F2-UN	F2 (Steel)	200	0.0033	No	B
S2	S2-FRCM-F3-UN	F3 (Carbon)	200	0.0033	No	B
	S2-FRCM-F3-UA	F3 (Carbon)	200	0.0033	Yes	B
	S2-FRCM-F4-UN	F4 (Steel)	200	0.0033	No	C
	S2-FRCM-F4-UA	F4 (Steel)	200	0.0033	Yes	C

The beams had a width b=150 mm, height h=300 mm, and total length of 3000 mm. The beams were tested using a four-point bending scheme with a span length l=2700 mm and a shear span a=750 mm, as shown in Figure 3-1. The shear span-to-effective depth ratio a/d was 3.0.
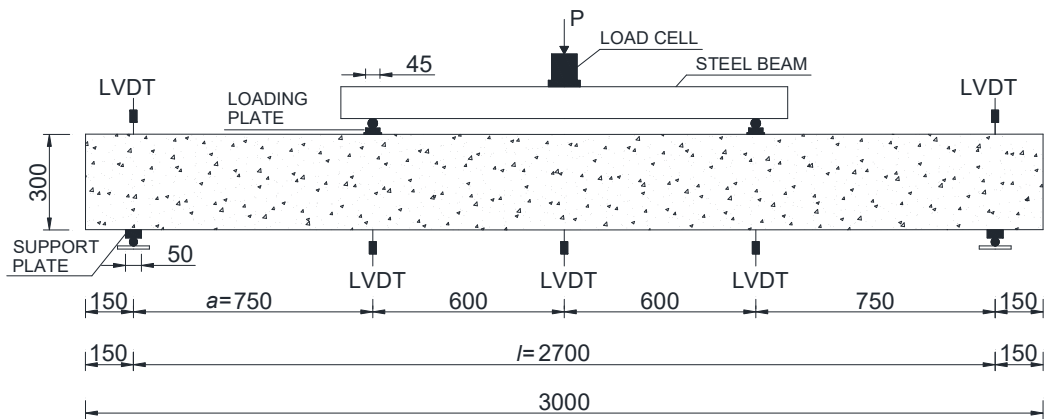
Figure 3-1 Experimental setup: a) scheme (dimensions in mm); b) beam test

3.1.1 Materials

The concrete beams were cast in three batches, named batch A, B, and C (see Table 3-1). Normal weight portland cement concrete with a maximum aggregate size of 12.5 mm was used. After casting, the beams were left in the formwork for at least three days, then they were demolded and remained under environmental conditions. The average concrete compressive strength, determined as the average of three cylinders with dimensions $\phi100\times200$ mm in accordance with EN 12390-3 [49] within four days of the day of testing, was 23.3 MPa (CoV=0.058), 24.7 MPa (CoV=0.088), and 21.3 MPa (CoV=0.057) for batch A, B, and C, respectively.

Deformed (ribbed) steel reinforcing bars of grade B450C were used for the internal longitudinal and transverse reinforcement. Four $\phi26$ mm steel bars were placed as longitudinal tension reinforcement, while two $\phi16$ mm steel bars were placed in

the compression region. All longitudinal bars had 90° hooks at each end. One-piece closed stirrups were placed with a spacing s=300 mm and 200 mm in the studied shear span of beams in series S1 and S2, respectively (Table 3-1). In the other shear span, stirrups were spaced at 75 mm in an attempt to achieve shear failure in the studied shear span. The diameter of the stirrups was ϕ=8 mm. The ϕ8 mm, ϕ16 mm, and ϕ26 mm reinforcing steel bars had a measured yield strength of 527 MPa, 535 MPa, and 545 MPa, respectively. The internal transverse steel reinforcement ratio (ρ_w=A_w/bs, where A_w is the stirrup cross-sectional area) for the series 1 and 2 beams was 0.0022 and 0.0033, respectively (see Table 3-1). The internal longitudinal and transverse reinforcement layout is presented in Figure 3-2).
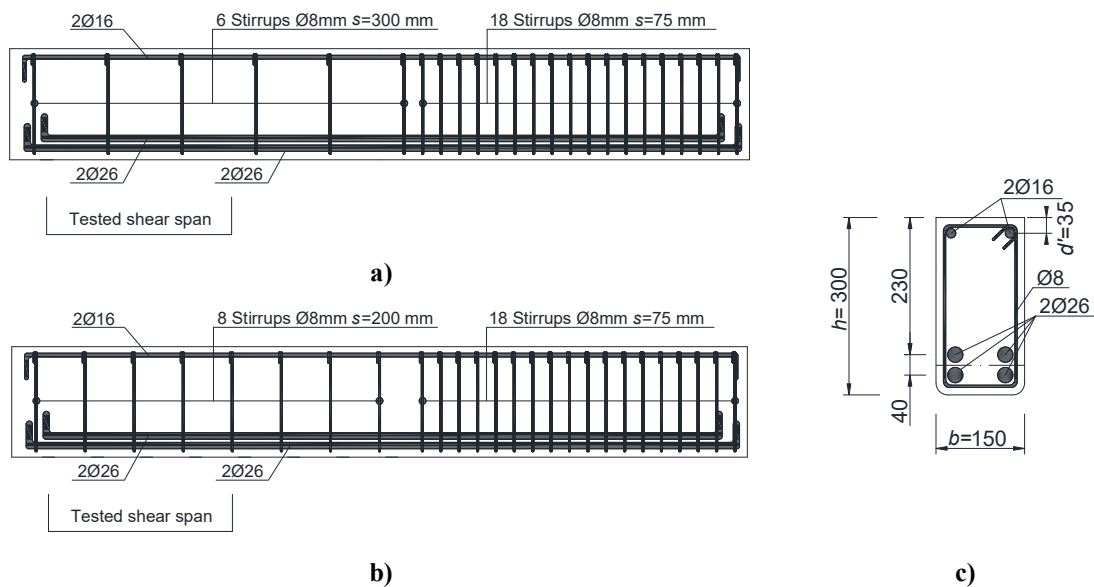
Figure 3-2 Beam longitudinal and transversal reinforcement: a) series S1; b) series S2; c) cross section

FRP and FRCM composites with carbon or steel fibers were used to strengthen the beams. Each composite was commercially available. For the carbon FRP strengthened beams, a unidirectional dry fiber fabric was used, while for the carbon FRCM strengthened beams, a bidirectional, balanced, dry, open mesh textile was employed. Steel FRP and FRCM specimens were strengthened using brassed and galvanized unidirectional sheets, respectively. In both cases, steel fibers consisted of Ultra High Tensile Strength Steel (UHTSS) wires twisted in cords. Figure 3-3 shows the fibers used in this study.
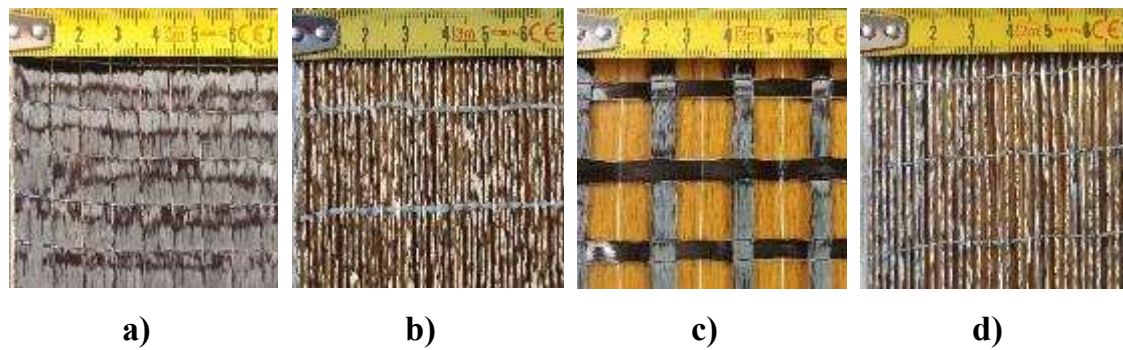
Figure 3-3 Fibers used for beams strengthened with: (a) carbon FRP (F1); (b) steel FRP (F2); (c) carbon FRCM (F3); (d) steel FRCM (F4) composite. Numbers in scale shown are in units of cm.

Table 3-2 summarizes the overall area weight W, elastic modulus E_f, tensile strength f_u, ultimate strain ε_{fu}, and thickness t_f of the fibers, as reported by the manufacturer [50]. It should be noted that for the carbon open mesh (F3) and steel fiber sheets (F2 and F4), t_f corresponds to the equivalent nominal thickness, which is determined considering the fibers as smeared uniformly across the width. For the case of F3 fiber textile, which is bidirectional, the value of t_f reported in Table 3-2 is the equivalent nominal thickness in each direction per unit width (mm/m). Table 3-2 shows that values of E_f for the steel fibers are lower than the values reported for the carbon fibers, but the steel fibers have a higher equivalent nominal thickness.

Table 3-2. Mechanical and geometrical properties of the fibers

| Fiber Type | | W | E_f | f_u | ε_{fu} | t_f | A_f | ρ_f | $A_f E_f$ |
		g/m²	GPa	MPa	%	mm	mm²/mm		(kN)
F1 (carbon)	Unidirectional	300	390	3000	0.8	0.165	0.330	0.0022	128.7
F2 (steel)	Unidirectional	1910	190	3345	2.2	0.240*	0.480	0.0032	91.2
F3 (carbon)	Bidirectional (balanced)	170	240	4700	1.8	0.047*,+	0.094+	0.0006	22.6
F4 (steel)	Unidirectional	2200	190	2400	>1.60	0.270*	0.540	0.0036	102.6

* Equivalent nominal thickness
+ Each direction

Table 3-2 allows for comparing the differences between the strengthening systems in terms of fiber area per unit length applied in the beam transverse direction ($A_f=2nt_f$), fiber reinforcement ratio per unit length ($\rho_f=A_f/b$), and fiber axial rigidity ($E_f A_f$). It should be noted that the definitions of fiber area, fiber reinforcement ratio, and fiber axial rigidity take into account the presence of one composite layer on each lateral size of the beam.

Two-component epoxy resins, free of solvents, thinners, and plasticizers, were used as the matrix for the FRP strengthening systems. Different resins were used for the carbon and steel FRP composites in accordance with the manufacturer's recommendations. For the FRCM composites, a two-component low modulus fiber-reinforced cementitious matrix, consisting of a premixed cement-based mortar to be hydrated with specific synthetic latex, was employed. To obtain the mechanical characteristics of the cementitious matrix, three 40×40×160 mm prisms were cast and tested within four days of testing the strengthened beams. After demolding, the prisms were covered by a wet cloth for at least three days and kept with the beams until testing. The average flexural strength f_{fm} [51] and average compressive strength f_{cm} [49] were 6.3 MPa (CoV=0.150) and 45.2 MPa (CoV=0.039), respectively.

3.1.2 Strengthening procedure

The beams were strengthened with a U-wrapped configuration continuous along the studied shear span. The beams were strengthened using a wet layup procedure. Before installing the FRP or FRCM system, the concrete surface was subjected to mechanical grinding (see Figure 3-4a), the corners of the specimens were rounded to a radius of approximately 20 mm (see Figure 3-4b), and any loose sand grains were removed.

a)   b)

Figure 3-4 Surface preparation: a) mechanical grinding; b) rounding of the corners

For the FRP strengthened beams, a first layer of resin was applied onto the dry concrete surface (see Figure 3-5a), and the fibers were placed using a plastic roller to achieve good impregnation of the resin and avoid possible wrinkles and air bubbles. A second layer of resin was then placed and spread on top of the fibers

using the plastic roller. Figure 3-5b shows the final configuration of a FRP-strengthened beam.

<div align="center">

a)   **b)**

</div>

Figure 3-5 FRP strengthening procedure: a) application of first resin layer; b) FRP-strengthened beam

For the FRCM system, the concrete surface was wetted, and the first layer of cementitious matrix, of approximately 4 mm thickness, was applied. Immediately after, the fibers were placed on top of the matrix, applying a slight pressure. While the first layer of matrix was still fresh, the second layer was applied on top of the fibers. The strengthening procedure for the beams strengthened using FRCM composites is shown in Figure 3-6. F2 and F4 steel fibers used in this study were applied side by side using 300 mm width strips (width of fiber roll provided by the manufacturer), without overlapping, along the longitudinal axis of the beam in the studied shear span. For four FRCM strengthened beams, the FRCM jackets were anchored using 10 mm diameter aramid fiber anchors with E_f=120 GPa and f_u higher than 2900 MPa, as reported by the manufacturer. After being impregnated with an epoxy resin, the anchors were placed in holes drilled 120 mm from the top of the beam, and then they were fanned out on both sides of the beam. The diameter of the fan was approximately 100 mm, and the total length of the anchors was 250 mm. This procedure was carried out two days after the FRCM system was installed so that the cementitious matrix was superficially dry. Figure 3-7 shows the aramid anchors and a photo of beam S1-FRCM-F3-UA.
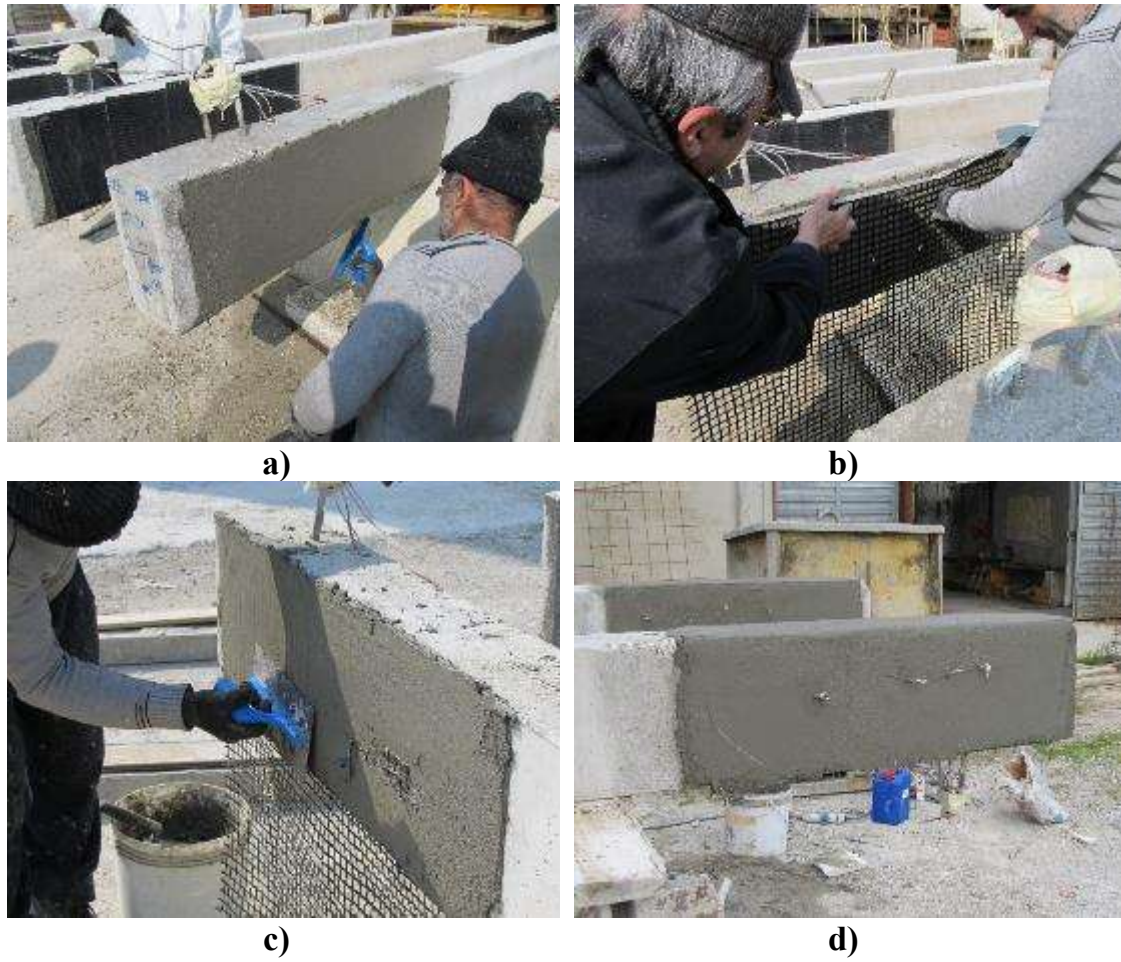
Figure 3-6 FRCM strengthening procedure: a) application of first matrix layer; b) fiber application; c) application of second matrix layer; d) FRCM-strengthened beam.
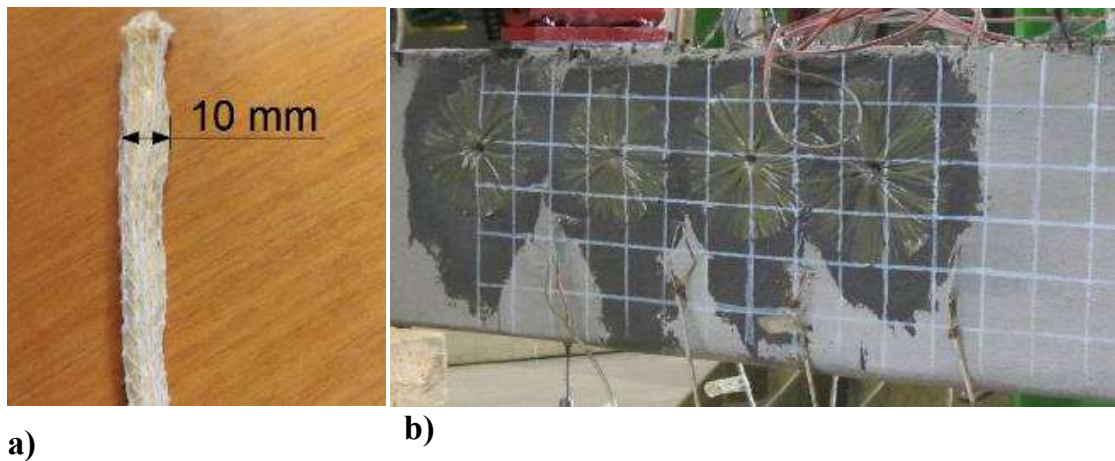
Figure 3-7 Anchorage system: a) aramid fiber anchor; b) strengthened beam with anchors (beam S1-FRCM-F3-UA shown).

3.1.3 Test procedure and instrumentation

The load P was applied to the center of a steel beam positioned on the top of the concrete beam through a servo-hydraulic jack with a total capacity of 500 kN (see Figure 3-1). The steel beam was simply supported creating two symmetrical loading points located at a distance of 600 mm from the concrete beam mid-span. The beams were tested to failure with an average loading rate of 0.25 kN/s. The loading was paused briefly at different load levels to mark cracks on the surface of the beam and take photographs. Three linear variable differential transducers (LVDTs) were located below the beam in order to measure vertical displacements at the locations of the loading points and at mid-span. Two additional LVDTs were located on top of the concrete beam at the support locations. Strains in the stirrups and the composite within the studied shear span were measured with uniaxial electrical resistance strain gauges. For series S1 beams, two stirrups were instrumented, while for series S2 beams, three stirrups were instrumented. Strain gauges were attached to the mid-height of the vertical leg as shown in Figure 3-8.
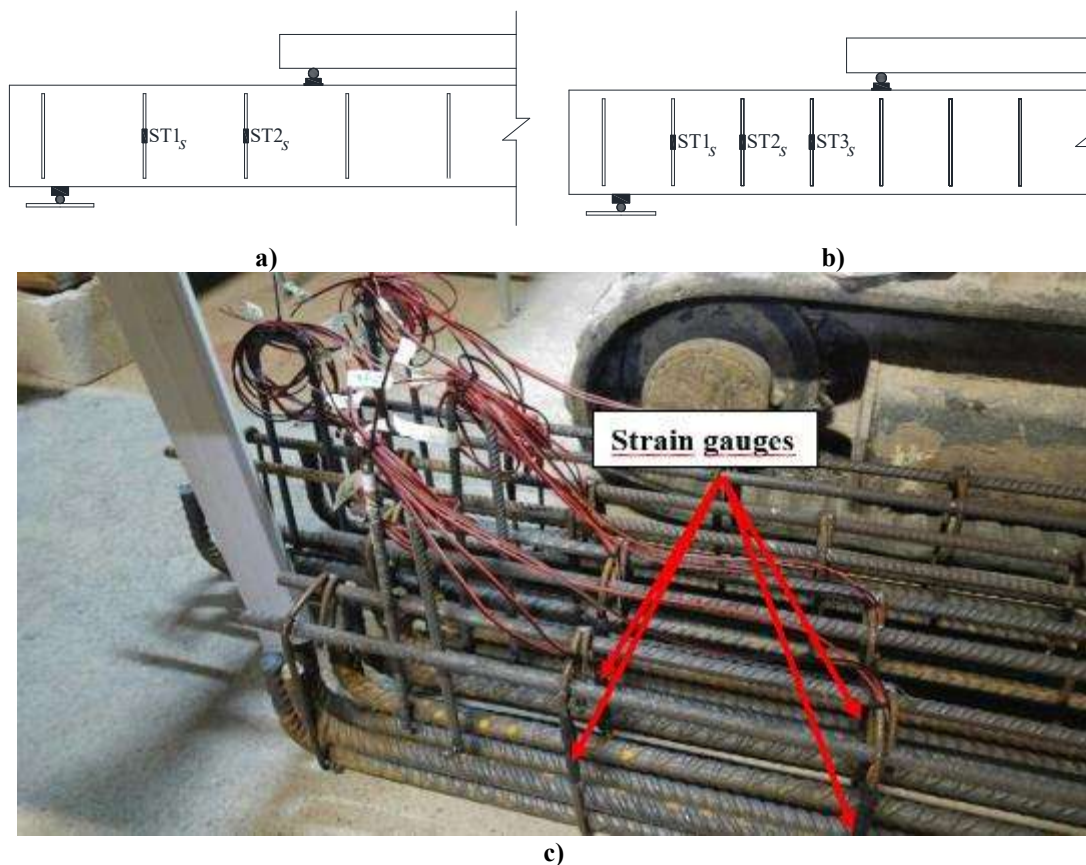
Figure 3-8 Location of strain gauges on: (a) series S1 stirrups; (b) series S2 stirrups; (c) strain gauges on stirrups for beam S2-FRCM-F3-UN

43

For beams strengthened with FRP composite, strain gauges were attached to the surface of the composite after the composite was installed. For beams strengthened with FRCM composites, strain gauges were attached to the fibers that were to be oriented in the beam transversal direction (perpendicular to the beam longitudinal axis) before applying the composite cementitious matrix. For the case of F3 fibers (carbon), the strain gauges were applied directly onto the fiber surface as the width of the fiber bundles was slightly larger than the strain gauge width, as shown in Figure 3-9c. As shown in Figure 3-3d, F4 fibers (steel) are comprised of bundles of twisted wire cords, with a wire diameter that is smaller than the strain gauge width. Therefore, it was not possible to apply the strain gauges directly on the wire surface. Instead, an epoxy resin was used to impregnate approximately three bundles in order to create a flat surface that allowed placing the strain gauges. The location of the strain gauges mounted on the fibers of the series S1 and S2 beams is shown in Figure 3-9. For series S1 beams, four strain gauges were placed (two in the same position as those mounted to the stirrups), while for series S2 beams, three strain gauges were placed in the same position as those mounted to the stirrups. The strain gauges located on the stirrups and the fibers are designated as $ST\#_s$ or $ST\#_f$, respectively. All electronic data were collected with a data acquisition system controlled by a personal computer.
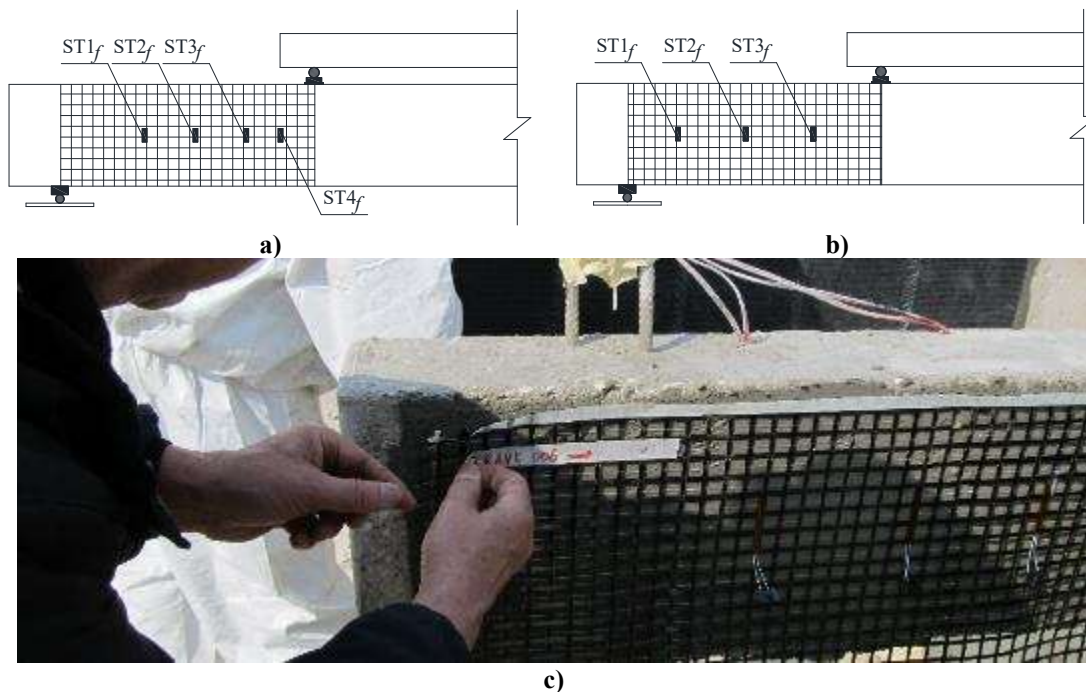
Figure 3-9 Location of strain gauges on: a) series S1 fibers; b) series S2 fibers; (c) strain gauges on fibers for beam S1-FRCM-F3-UN

3.2 Applied load vs. mid-span displacement

Figure 3-10 and Figure 3-11 show the applied load P vs. mid-span displacement Δ curves for the beams in series S1 and S2, respectively. The maximum load P_{max}, the maximum shear V_{max} (where $V_{max}=0.5P_{max}$, assuming perfect symmetry and neglecting the beam self-weight), and the displacement at mid-span corresponding to the maximum load Δ_{Pmax}, of each beam are summarized in Table 3-3. The shear strength provided by the strengthening system V_f, computed as the maximum shear of the strengthened specimen minus the maximum shear of the corresponding control specimen, and the percent increase in maximum shear over the control beam for the strengthened specimens are also included in Table 3-3. It should be noted that V_f is computed neglecting the slight differences in concrete compressive strength between different concrete batches discussed in Section 3.1.

Table 3-3. Summary of tests results

Series	Beam	P_{max} (kN)	V_{max} (kN)	V_f (kN)	Increase over control (%)	Δ_{Pmax} (mm)	Failure mode
	S1-CONTROL	230.5	115.2	-	-	15.4	Shear
	S1-FRP-F1-UN	338.3	169.1	53.9	46.8	26.0	Flexure
	S1-FRP-F2-UN	306.8	153.4	38.2	33.1	16.8	Shear
S1	S1-FRCM-F3-UN	284.8	142.4	27.2	23.6	17.8	Shear
	S1-FRCM-F3-UA	290.3	145.1	29.9	26.0	19.8	Shear
	S1-FRCM-F4-UN	299.5	149.7	34.5	29.9	17.7	Shear
	S1-FRCM-F4-UA	300.3	150.1	34.9	30.3	20.6	Shear
	S2-CONTROL	259.3	129.7	-	-	14.5	Shear
	S2-FRP-F1-UN	338.5	169.2	39.6	30.5	19.7	Flexure
	S2-FRP-F2-UN	347.3	173.7	44.0	33.9	20.8	Flexure
S2	S2-FRCM-F3-UN	307.9	154	24.3	18.7	17.1	Shear
	S2-FRCM-F3-UA	307.9	153.9	24.3	18.7	18.3	Shear
	S2-FRCM-F4-UN	294.4	147.2	17.5	13.5	18.0	Shear
	S2-FRCM-F4-UA	321.9	160.9	31.3	24.1	19.3	Shear

45
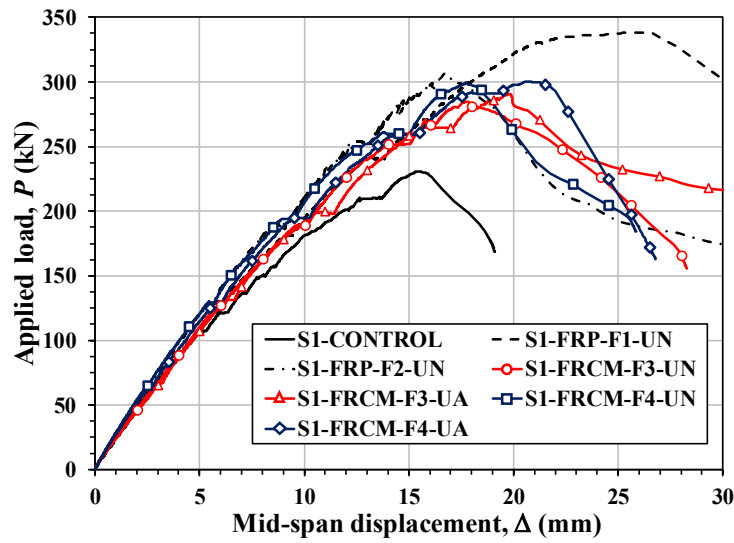
Figure 3-10 Applied load P vs. mid-span displacement Δ curves for series S1 beams
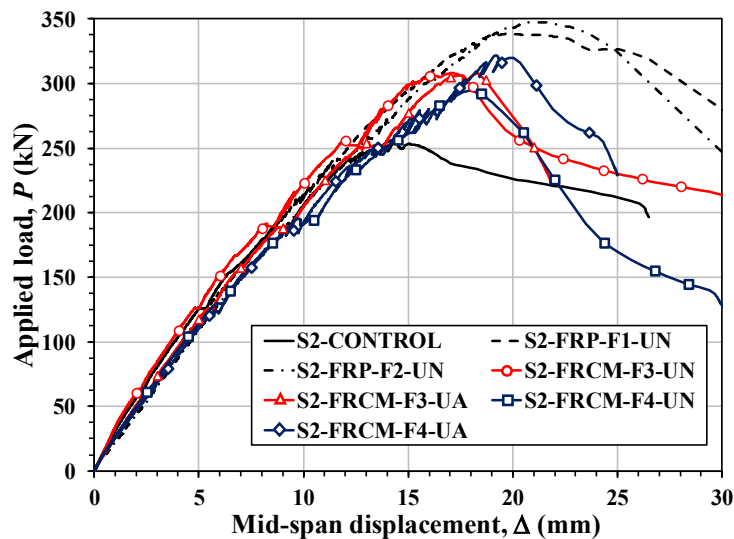
Figure 3-11 Applied load P vs. mid-span displacement Δ curves for series S2 beams

The results in Figure 3-10 and Figure 3-11, and Table 3-3 show that the use of FRP and FRCM composites provides an increase in the shear strength relative to the control beams. Increase in values of Δ_{Pmax} relative to the corresponding control beam were also achieved in all strengthened specimens. However, the increase in stiffness was not significant as shown in Figure 3-10 and Figure 3-11.

3.3   Failure mode

The failure modes of the beams in series S1 and S2 are summarized in Table 3-3.

3.3.1 Control beams

Beams S1-CONTROL and S2-CONTROL presented a typical beam shear failure characterized by the formation of a main diagonal crack in the studied shear span (Figure 3-12 and Figure 3-13). In addition to the main diagonal crack, additional diagonal cracks formed and were distributed along the studied shear span.

a)	b)
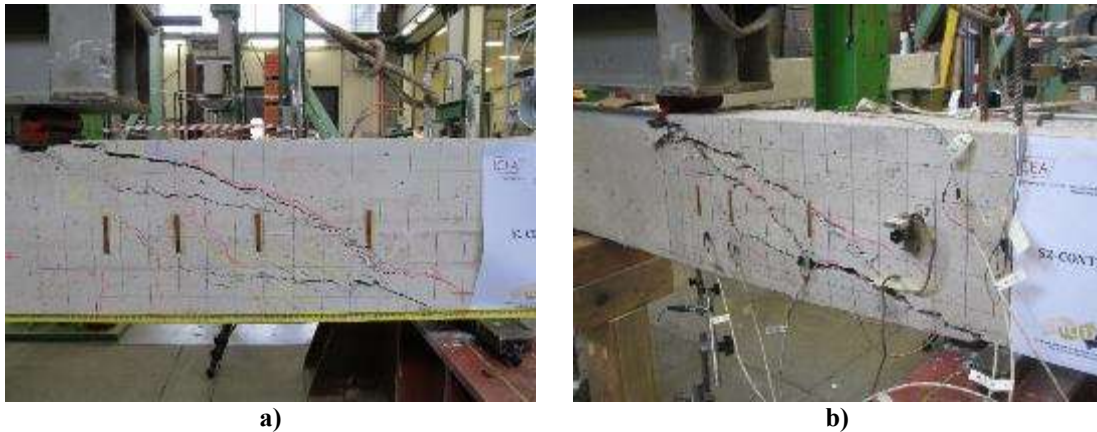
Figure 3-12 Failure mode of beam: a) S1-CONTROL; b) S2-CONTROL

a)	b)
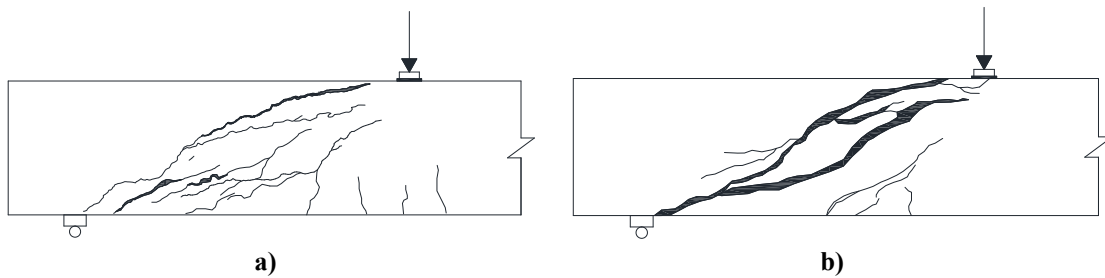
Figure 3-13 Cracking pattern of beam: a) S1-CONTROL; b) S2-CONTROL

3.3.2 FRP-strengthened beams

Regarding beams strengthened with FRP composite, beams S1-FRP-F1-UN, S2-FRP-F1-UN, and S2-FRP-F2-UN exhibited flexural failure caused by concrete crushing (Figure 3-14a). Due to the presence of the FRP jacket, it was not possible to observe cracks on the surface of the beam in the studied shear span. Failure of beam S1-FRP-F2-UN was characterized by debonding of the FRP jacket (Figure 3-14b). A main diagonal crack in the concrete, similar to the one observed for the corresponding control specimen, developed beneath the FRP jacket and was visible after detachment of the FRP composite (see Figure 3-15).

<table>
<tr><td>a)</td><td>b)</td></tr>
</table>
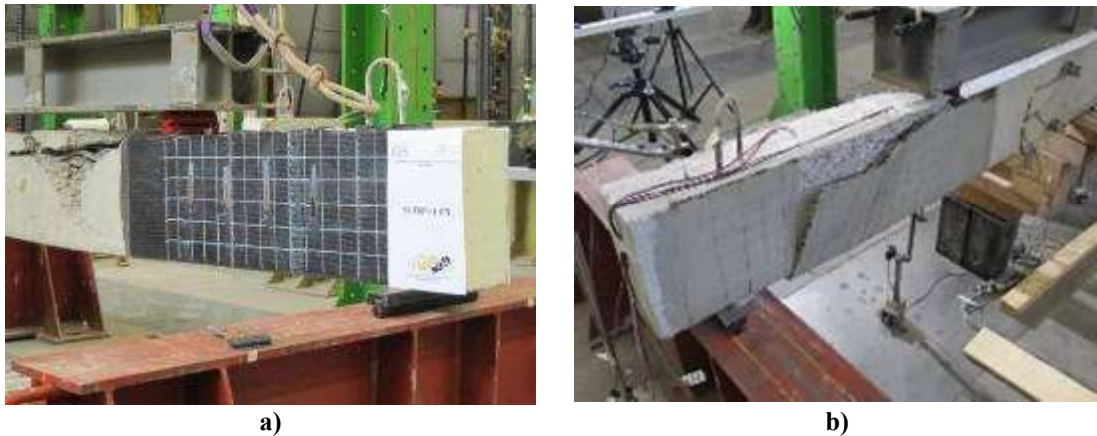
Figure 3-14 Failure mode of beam: a) S1-FRP-F1-UN, S2-FRP-F1-UN, and S2-FRP-F2-UN; b) S1-FRP-F2-UN
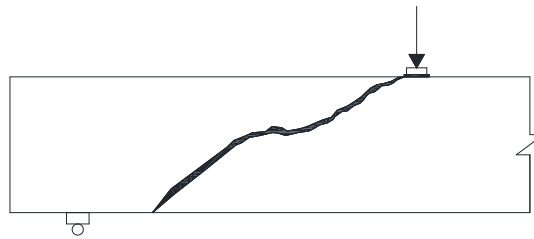
Figure 3-15 Cracking pattern of beam S1-FRP-F2-UN

3.3.3   FRCM-strengthened beams

All beams strengthened with FRCM composite failed in shear. Unlike the FRP strengthened beams, cracking was visible on the surface of the FRCM jackets. This can be considered an advantage of the FRCM system over the FRP system because it allows for immediate and easy inspection of damaged elements [1]. It is worth noting that cracks appeared on the surface of the FRCM jackets from early stages of loading (at an applied load P of approximately 150 kN, see Figure 3-16) and not only close to the failure load.

Figure 3-16 Crack pattern of beam for beam S1-FRCM-F3-UN for load *P*=150 kN

Regarding beams strengthened with carbon FRCM composite without anchors, beam S1-FRCM-F3-UN exhibited a typical shear failure, similar to the control beams, with a main diagonal crack crossing the shear span from the loading point to the support (Figure 3-17a and Figure 3-18a). In addition, local detachment of the entire thickness of the jacket close to the loading point and fiber slippage along the main crack were also observed. A similar behavior was observed for beam S2-FRCM-F3-UN (Figure 3-17b and Figure 3-18b), but local composite detachment was not observed. For beams strengthened with carbon FRCM composite with anchors, beam S1-FRCM-F3-UA exhibited a diagonal crack that formed around the anchors without detachment of the composite (Figure 3-17c and Figure 3-18c). Although there was not a significant increase in the shear strength relative to beam S1-FRCM-F3-UN without anchors (Table 3-3), the crack widths were larger, which explains the larger value of Δ_{Pmax} attained. For beam S2-FRCM-F3-UA, however, the crack did not go around the anchors but instead propagated through the middle of one of the anchors (Figure 3-17d and Figure 3-18d).
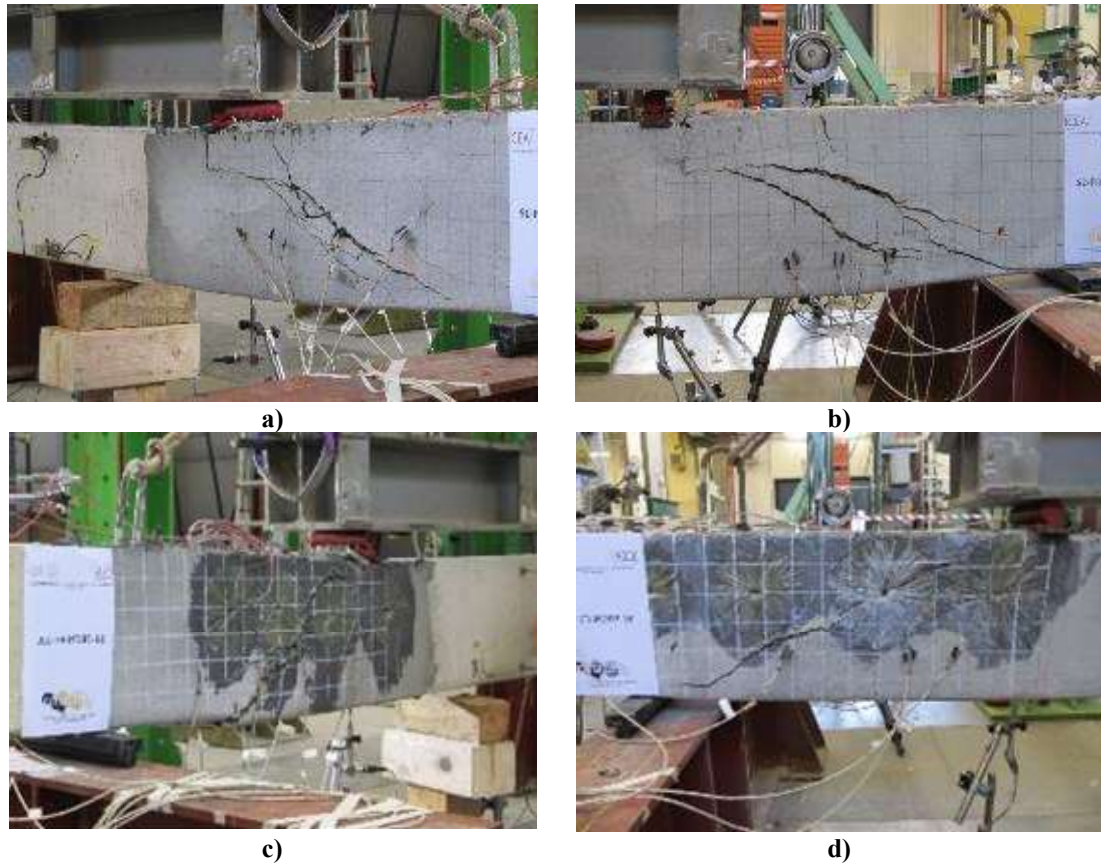
Figure 3-17 Failure mode of beam: a) S1-FRCM-F3-UN; b) S2-FRCM-F3-UN; c) S1-FRCM-F3-UA; d) S2-FRCM-F3-UA
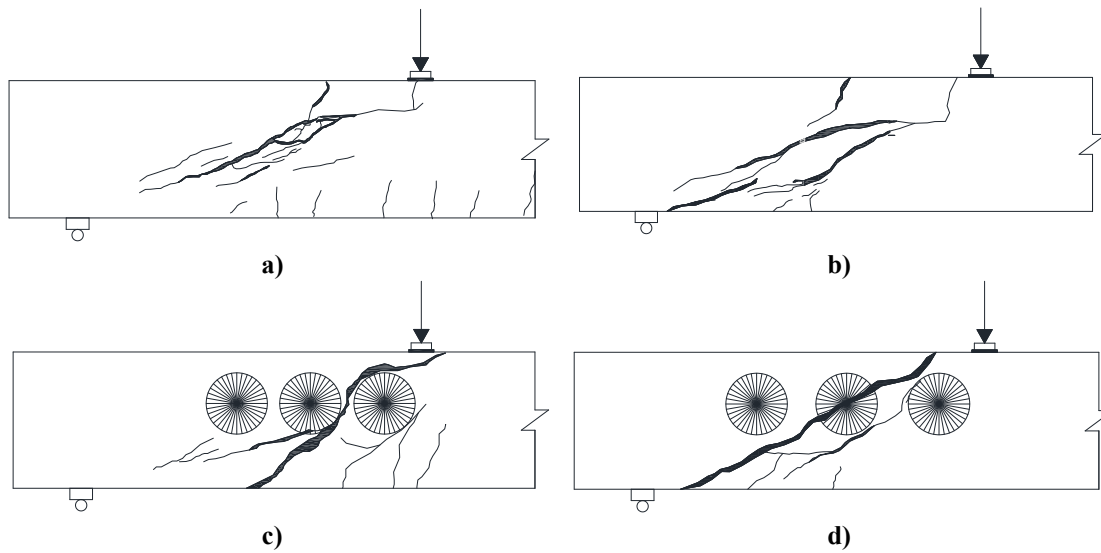
Figure 3-18 Cracking pattern for beam: a) S1-FRCM-F3-UN; b) S2-FRCM-F3-UN; c) S1-FRCM-F3-UA; d) S2-FRCM-F3-UA

50

For beams strengthened with steel FRCM composite without anchors, failure of beams S1-FRCM-F4-UN and S2-FRCM-F4-UN was caused by detachment of the composite system (Figure 3-19a,b) at the interface between the matrix and the concrete without damage to the concrete substrate. It is important to note that the crack pattern reflected on the surface of the jacket for beams strengthened with steel FRCM composites was different than that observed on the control specimens and beams strengthened with carbon FRCM composites. Cracks on the jacket surface, oriented in the fiber direction (beam transverse direction), mostly coincided with the ends of the fiber sheet segments used to form the jacket (discussed in Section 3.1.2). However, after the FRCM jackets were removed, it was observed that diagonal cracks formed in the beam beneath the composite as shown in Figure 3-20a,b and Figure 3-21a,b for beams S1-FRCM-F4-UN and S2-FRCM-F4-UN.

a)   b)

c)   d)
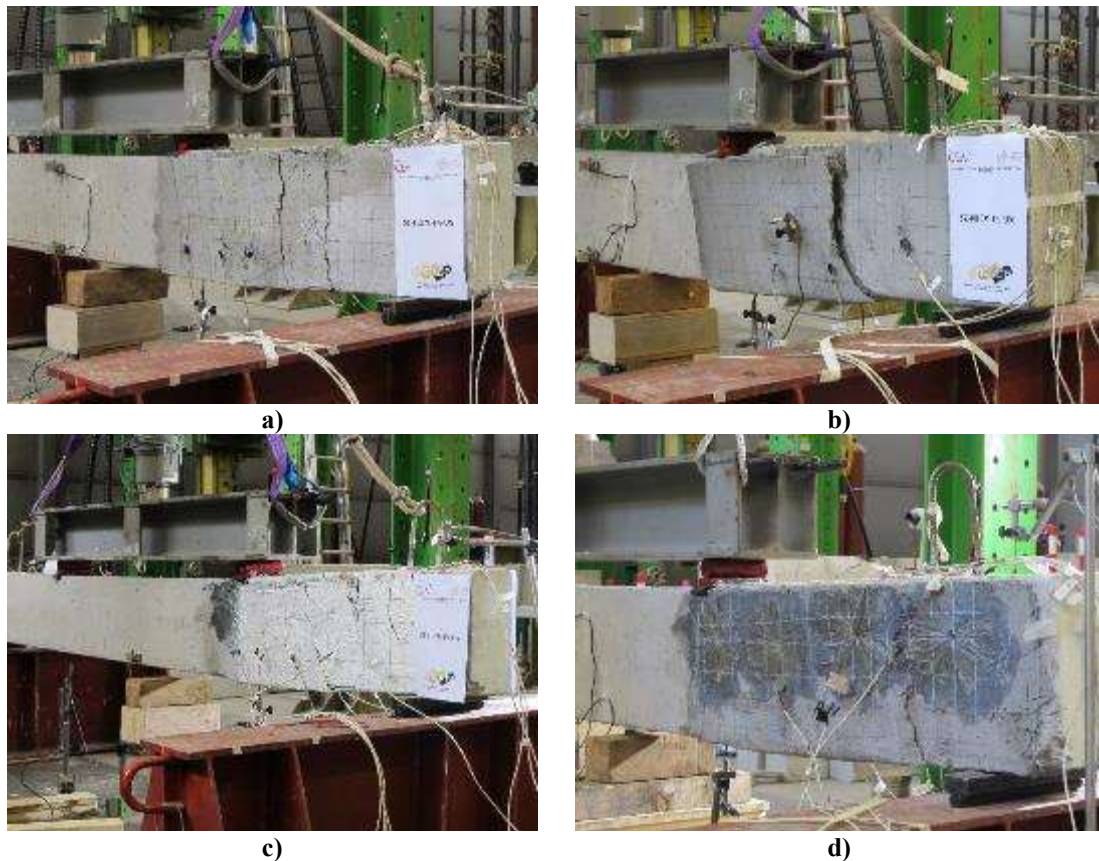
Figure 3-19 Failure mode of beam: a) S1-FRCM-F4-UN; b) S2-FRCM-F4-UN; c) S1-FRCM-F4-UA; d) S2-FRCM-F4-UA

51
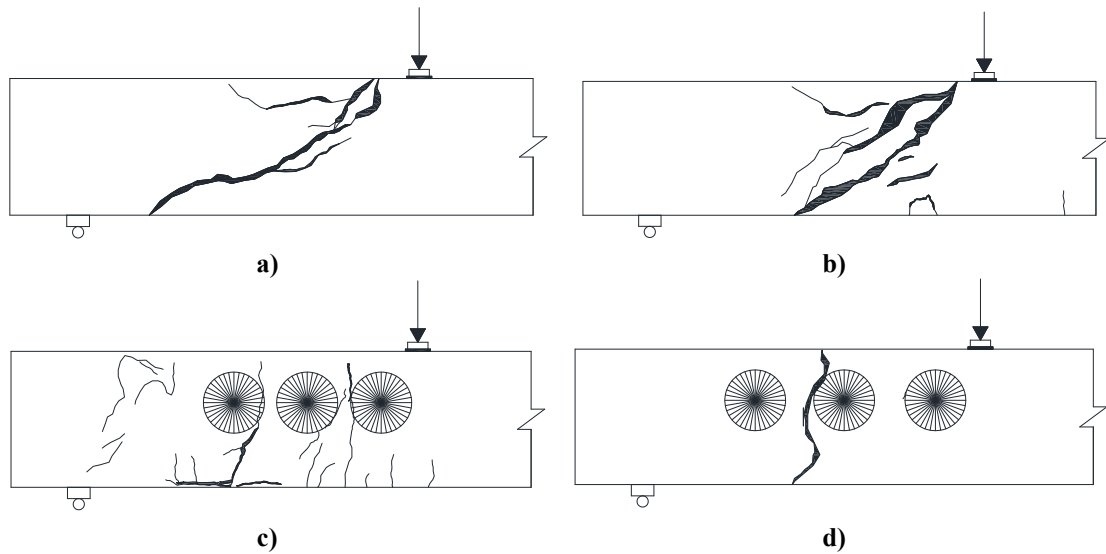
Figure 3-20 Cracking pattern for beam: a) S1-FRCM-F4-UN (underneath the jacket); b) S2-FRCM-F4-UN (underneath the jacket); c) S1-FRCM-F4-UA; d) S2-FRCM-F4-UA

Detachment of the FRCM jackets was prevented by the use of anchors in beams S1-FRCM-F4-UA and S2-FRCM-F4-UA (Figure 3-19c,d). The crack pattern observed was similar to that of the steel FRCM strengthened beams without anchors, i.e., cracks oriented in the beam transverse direction (Figure 3-19c,d and Figure 3-20c,d). Due to the presence of the anchors, it was not possible to remove the jackets after testing to verify the presence of a diagonal crack in the beam.

In Figure 3-21a, it is also observed that, for beam S1-FRCM-F4-UN, the fibers and the external matrix layer detached from the internal matrix layer above the diagonal crack. However, below the diagonal crack, the entire FRCM jacket detached from the concrete substrate. For beam S2-FRCM-F4-UN (see Figure 3-21b), the jacket detached from the substrate in all the affected area. It is important to note that the debonding of the jackets occurred at the matrix-substrate interface and did not affect the concrete cover. This differs from the behavior of beam S1-FRP-F2-UN, in which the debonding occurred within the concrete, which corresponds to the typical failure mode for FRP strengthened beams [31].

Figure 3-21 Crack pattern after removal of FRCM jacket for beams: a) S1-FRCM-F4-UN; b) S2-FRCM-F4-UN.

3.4 Stirrup strain measurements

In this section, the stirrup strains recorded during the tests are discussed. It is worth noting that maximum strains in the stirrups are expected near the diagonal cracks. As the concrete crack pattern is unknown beforehand, strain gauges were located at the same location for all beams in a given series (Section 3.1.3) in an attempt to obtain measurements that are comparable. Therefore, in this section, the comparison of stirrup strains is based on the measurements obtained at the same locations for each beam, although it is highlighted that the strain measured by each gauge is effected by the proximity of the gauge to the diagonal cracks. However, it is noted that for all beams in which the crack pattern was available, at least one of the strain gauges applied on the stirrups was crossed by a diagonal crack.

It is also worth noting that strain gauges were placed on either side of the beams, but in some cases, malfunctioning of the strain gauges made it impossible to obtain readings from all the strain gauges placed on the shear span. Therefore, the analysis shown in the following section and Section 3.5 is based on the readings obtained from a single side in which readings were available for all the strain gauges and where at least one gauge was crossed by the diagonal crack.

3.4.1 Control beams

The applied load P vs. stirrup strain ε_s relationships for the control beams are shown in Figure 3-22. The location of the stirrups and crack pattern at failure are also included in the figures for reference.
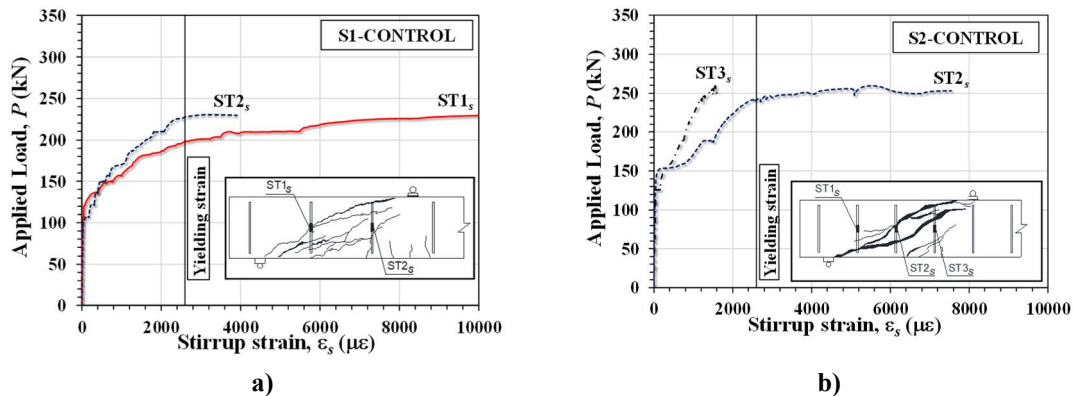
Figure 3-22 Applied load P vs. stirrup strain ε_s for beam: a) S1-CONTROL; b) S2-CONTROL

Figure 3-22a shows that for beam S1-CONTROL, strains larger than the steel yield strain (ε_y=2650 µε) were recorded in both instrumented stirrups, and therefore both contributed to the shear strength. For beam S2-CONTROL, the crack pattern mainly involved two of the three stirrups included within the shear span (Figure 3-22b). In fact, strain gauge ST1$_s$ did not record any significant values of strain, and it is not included in Figure 3-22b. Therefore, it is reasonable to assume that for beam S2-CONTROL one of the three stirrups placed in the shear span (stirrup 1) had a limited contribution to the shear capacity. This explains why the difference in shear strength of beams S1-CONTROL and S2-CONTROL was only 12% even with a 50% increase in internal transverse reinforcement ratio.

3.4.2 FRP-strengthened beams

The applied load P vs. stirrup strain ε_s relationships for FRP-strengthened beams are shown in Figure 3-23. For beams S1-FRP-F1-UN, S2-FRP-F1-UN, and S2-FRP-F2-UN (Figure 3-23a, b, and c, respectively), which failed in flexure, the crack pattern is not shown since it was not possible to observe beneath the FRP jackets.
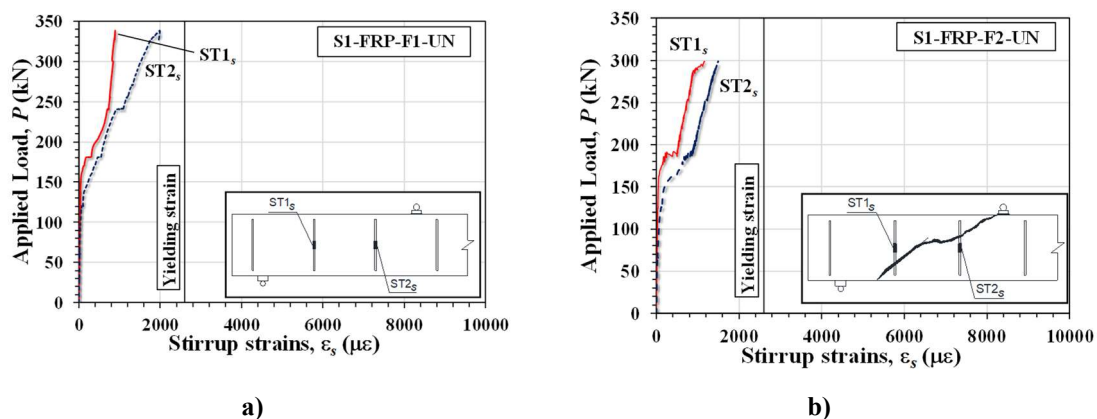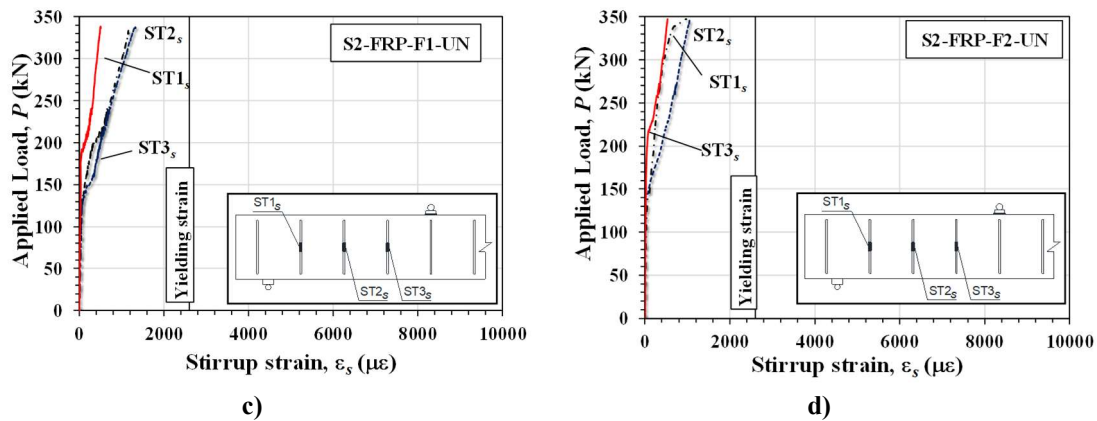
Figure 3-23 Applied load P vs. stirrup strain ε_s for beam: a) S1-FRP-F1-UN; b) S1-FRP-F2-UN; c) S2-FRP-F1-UN; d) S2-FRP-F2-UN

The graphs in Figure 3-23a-d show that for all FRP strengthened beams, strains measured in the stirrups were lower than the yield strain, even though the maximum applied loads were higher than those obtained for the corresponding control beams. In other words, the addition of the FRP jacket resulted in a reduction in strain in the stirrups. It is worth noting that the reduction in the stirrup strain is observed regardless of the type of fiber, stirrup spacing, and failure mode. Further discussion on this behavior can be found in section 3.8.

3.4.3 FRCM-strengthened beams

For the carbon FRCM strengthened beams shown in Figure 3-24, at least one of the stirrups yielded at the maximum applied load. Values of strain recorded at the maximum load were lower than those of the corresponding control beams, even though the maximum applied loads were higher than those obtained for the corresponding control beam. Thus, the addition of the carbon FRCM jacket resulted in a reduction in strain in the stirrups. The reduction in stirrup strain appears to be more significant for beams in series 2, with a higher internal reinforcement ratio ρ_w. For beams in series 1, larger strains were measured in the beam with anchors. This can be explained by the fact that the crack pattern was completely modified by the presence of the anchors, and thus, cracks were located mainly around a single stirrup. For series 2 beams, similar values of strain were obtained in the stirrups for beams with and without anchors.
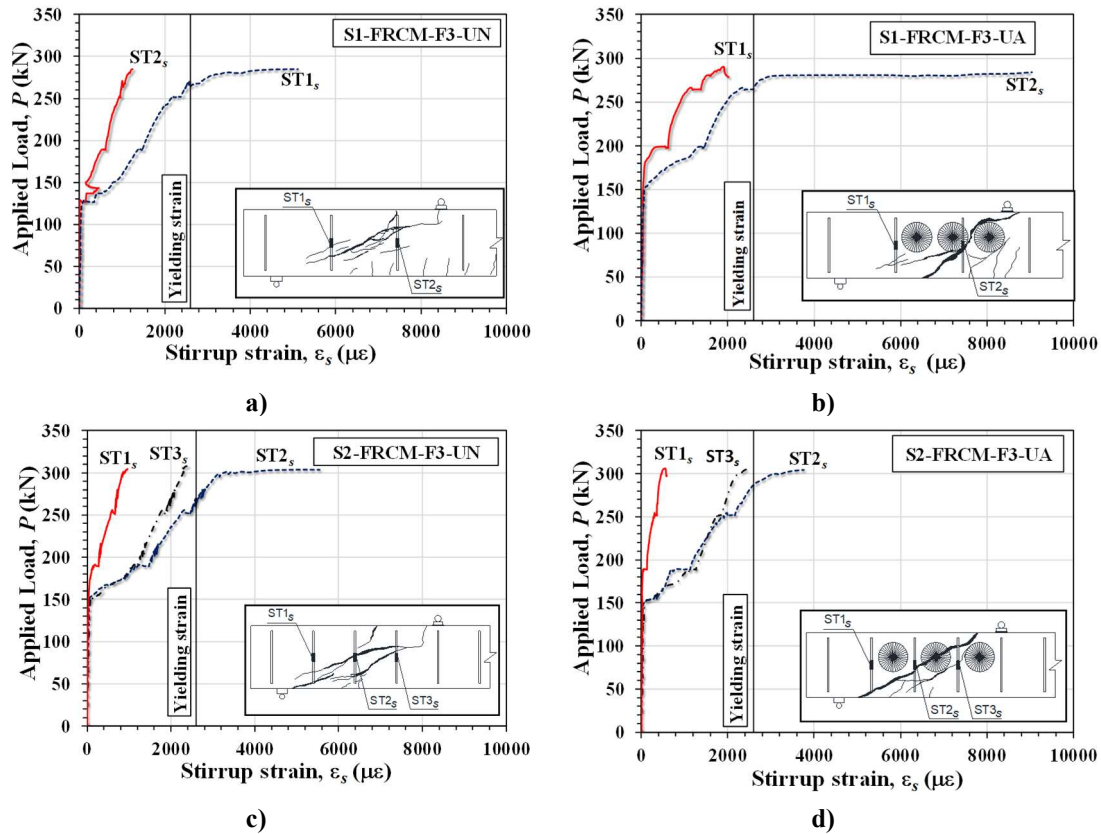
Figure 3-24 Applied load P vs. stirrup strain ε_s for beam: a) S1-FRCM-F3-UN; b) S1-FRCM-F3-UA; c) S2-FRCM-F3-UN; d) S2-FRCM-F3-UA

For steel FRCM strengthened beams shown in Figure 3-25, at least one of the stirrups yielded at the maximum applied load. Again, the reduction of the stirrup strains relative to the control beam is evident. Similar to the carbon FRCM strengthened beams, larger reductions were observed in the series 2 beams with a higher ρ_w. The presence of anchors also had an influence on the measured strains. Beam S1-FRCM-F4-UA shows a reduction of the strain compared to the control beam. However, both stirrups yielded at the maximum load, which implies that their contribution to the shear strength of the strengthened beam is the same as in S1-CONTROL beam.
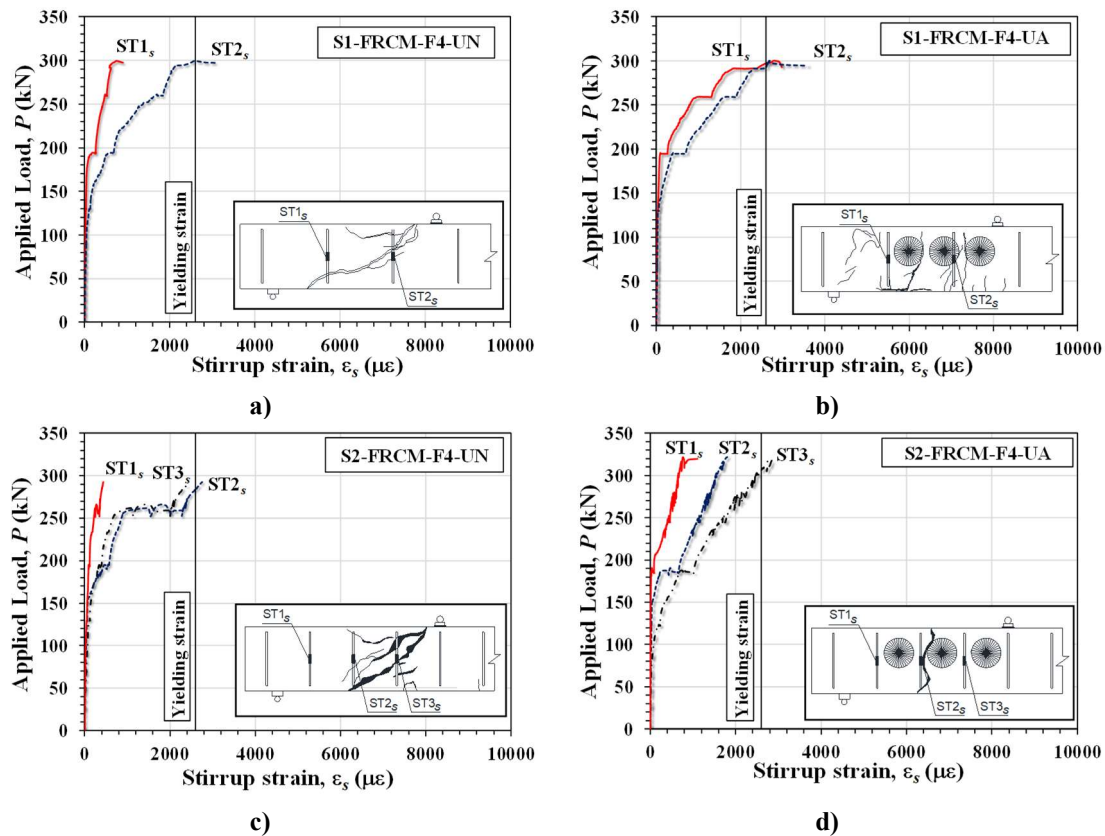
Figure 3-25 Applied load P vs. stirrup strain ε_s for beam: a) S1-FRCM-F4-UN; b) S1-FRCM-F4-UA; c) S2-FRCM-F4-UN; d) S2-FRCM-F4-UA

3.4.4   Additional remarks

When strains at early stages of loading are analyzed, results showed that for all strengthened beams the measurements in the strain gauges start at a similar load level, depending on the value of ρ_w, as shown in Figure 3-26. In Figure 3-26, the P-ε_s relationships for the beams are plotted up to a maximum value of ε_s=1000 µε. It is noted that for each beam only the measurements obtained by the strain gauge that recorded the higher values of strain, i.e., strain gauge crossed by the main crack or closer to it, were included.

For series 1 beams (see Figure 3-26a), stirrup strains start to increase around 125 kN, regardless of the type of strengthening or the presence of anchors. A similar behavior is observed for series 2 beams (see Figure 3-26b), but for this case, the load level at which stirrup strains start to increase is approximately 150 kN, except for beams S2-FRP-F1-UN and S2-FRCM-F4-UA.

These values of load can be associated to the initial cracking of the concrete. For beam S1-CONTROL, the first cracks observed in that beam occurred at a load level of 120 kN, similar to the 125 kN load level discussed before. Assuming that

stirrups start contributing to the shear strength and strains start to develop at higher rate after cracking of concrete, this suggests that the presence of the strengthening system does not delay the occurrence of initial concrete cracking, and contribution of stirrups to the concrete shear capacity of the beam will start at the same load level for strengthened and unstrengthened beams. For FRCM strengthened beams, cracking started to be visible on the surface of the jacket at loads slightly higher than the load at which stirrup strains started to increase.
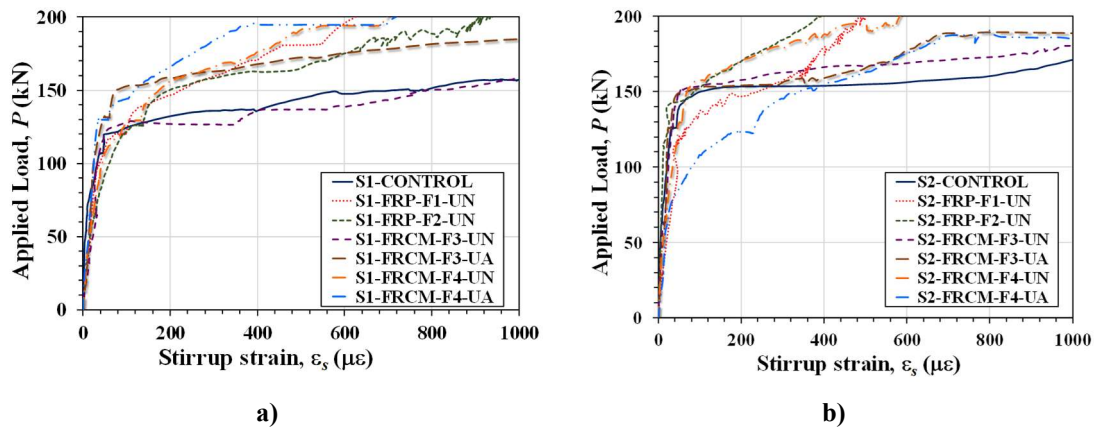
Figure 3-26 Initial applied load P vs. stirrup strain ε_s for: a) series 1 beams; b) series 2 beams

3.5   Fiber strain measurements

In this section, the fiber strains recorded during the tests are discussed. For all strengthened beams in which the crack pattern was available, at least one of the strain gauges applied on the fibers was crossed by the diagonal crack.

3.5.1 FRP-strengthened beams

The applied load P vs. fiber strain ε_f relationships for the FRP-strengthened beams are shown in Figure 3-27. The location of the strain gauges and the concrete crack pattern at failure are included in the figures for reference, with the exception of beams S1-FRP-F1-UN, S2-FRP-F1-UN, and S2-FRP-F2-UN (Figure 3-27a,c, and d, respectively), as discussed in Section 3.4.2. Strain gauge ST4$_f$ of beam S1-FRP-F1-UN and ST3$_f$ of beam S2-FRP-F2-UN malfunctioned at low load levels, and therefore they are not reported in Figure 3-27a and d.
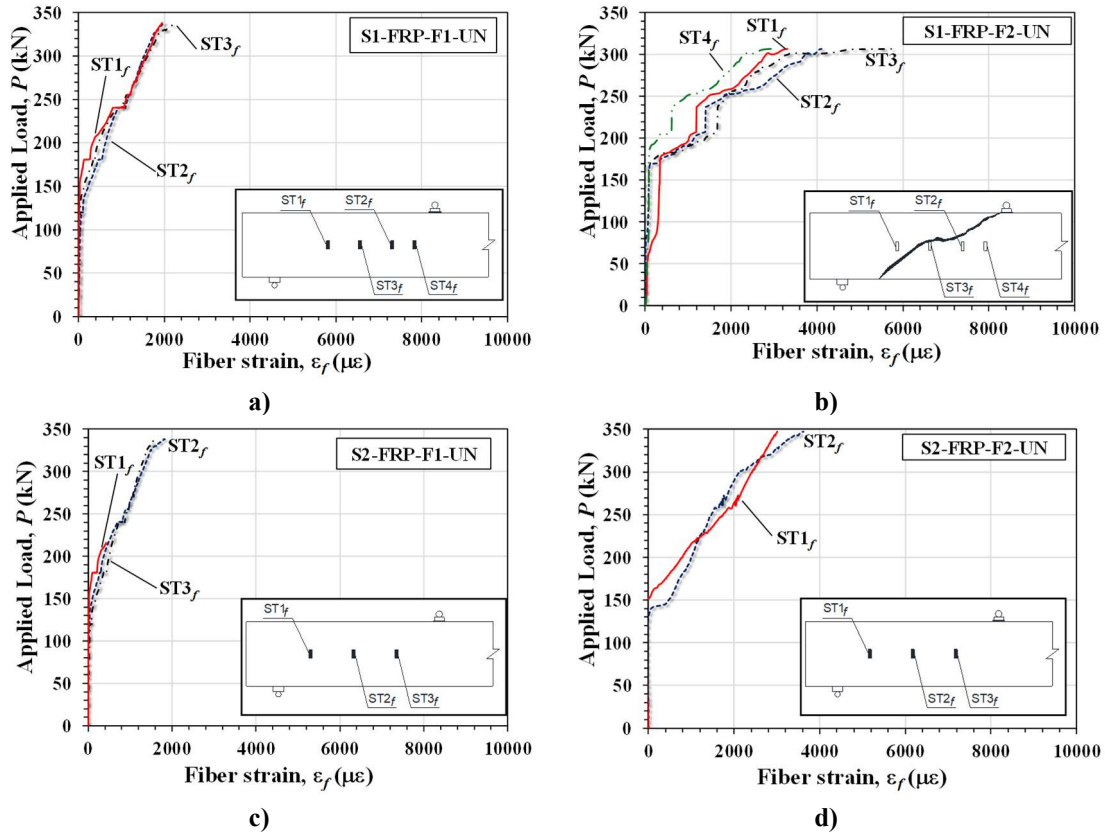
Figure 3-27 Applied load P vs. fiber strain ε_f for beam: a) S1-FRP-F1-UN; b) S1-FRP-F2-UN; c) S2-FRP-F1-UN; d) S2-FRP-F2-UN

For the FRP strengthened beams, lower maximum values of fiber strain were recorded in beams with carbon fibers (Figure 3-27a and c) than those with steel fibers (Figure 3-27b and d). For beams S1-FRP-F1-UN, S2-FRP-F1-UN, and S2-FRP-F2-UN, which failed in flexure, values of strain measured by the different gauges were similar (2-16a,c and d). For beam S1-FRP-F2-UN, which failed in shear, values of fiber strain differed based on the position of the strain gauge within the shear span (Figure 3-27b) with higher values of strains recorded by strain gauge ST3$_f$, which was crossed by the shear diagonal crack. Higher values of fiber strains were observed for beam S1-FRP-F2-UN compared to the other FRP strengthened beams that failed in flexure.

3.5.2 FRCM-strengthened beams

Strains in the fibers for the carbon FRCM strengthened beams are presented in Figure 3-28. Comparing the responses of beams S1-FRCM-F3-UN and S1-FRCM-F3-UA, it is clear that the presence of the anchors allowed for the development of higher fiber strains. For beams S2-FRCM-F3-UN and S2-FRCM-F3-UA, similar values of maximum strains were recorded (around 3000 µε for both specimens).

These values are lower than those recorded for series 1 specimens, which implies that a better exploitation of the system is achieved with larger stirrup spacing.
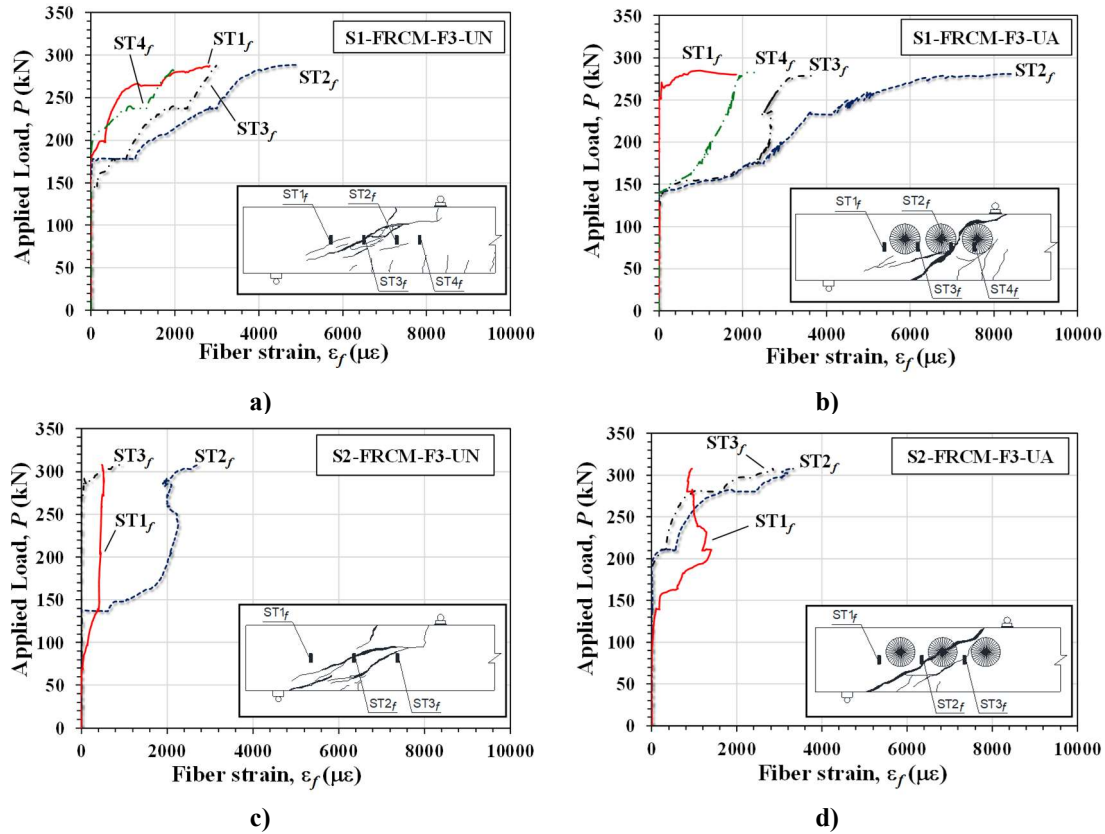
Figure 3-28 Applied load P vs. fiber strain ε_f for beam: a) S1-FRCM-F3-UN; b) S1-FRCM-F3-UA; c) S2-FRCM-F3-UN; d) S2-FRCM-F3-UA

Beams strengthened with steel FRCM jackets exhibited similar values of fiber strains at the maximum load, regardless of the stirrup spacing (Figure 3-29). It is also worth noting that the maximum recorded strains are also lower than those of the beams strengthened with steel FRP composites (Figure 3-27b and c). Considering that F2 and F4 fibers have similar geometrical and mechanical characteristics (Table 3-2), this result suggests that the contribution to the shear strength provided by steel fibers was lower for the case of beams with FRCM jackets than those with FRP jackets. The strain profiles in Figure 3-29a and b show that the steel FRCM jacket of beams S1-FRCM-F4-UN and S2-FRCM-F4-UN experienced local debonding of the composite at load levels less than the maximum load, as discussed in Section 3.3.3.
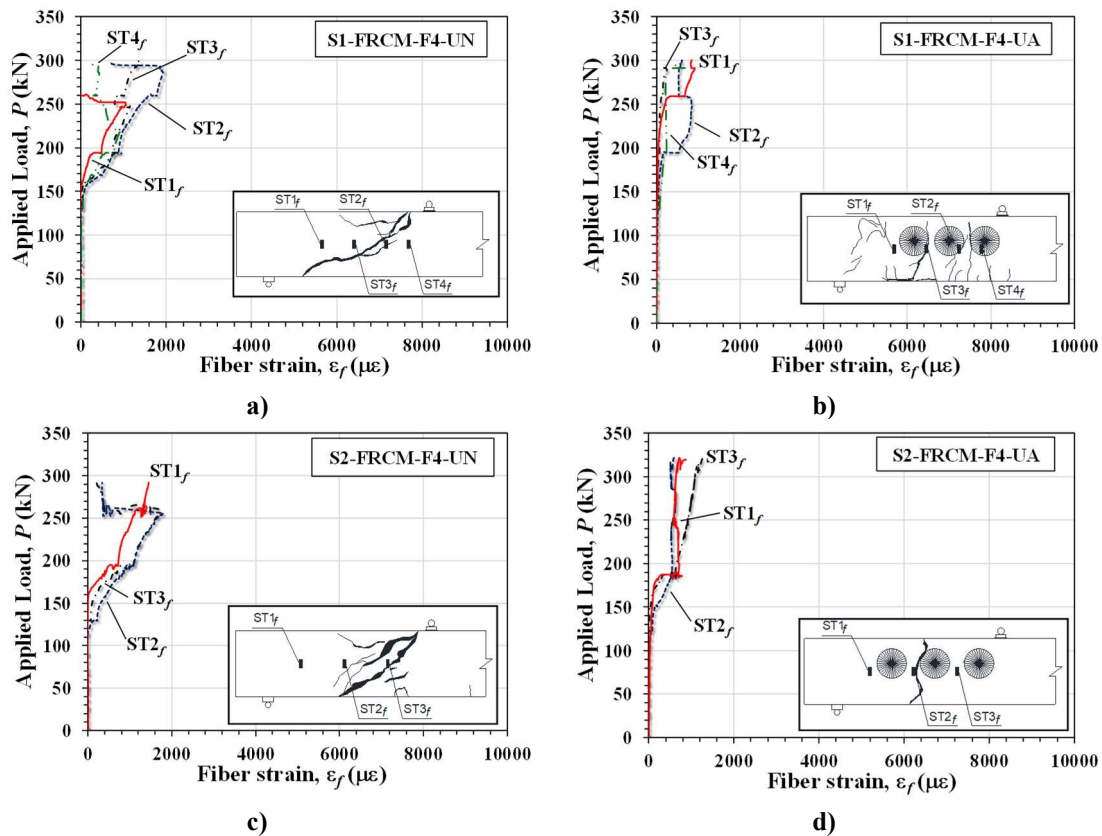
Figure 3-29 Applied load P vs. fiber strain ε_f for beam: a) S1-FRCM-F4-UN; b) S1-FRCM-F4-UA; c) S2-FRCM-F4-UN; d) S2-FRCM-F4-UA

3.6   Effect of composite type

As indicated in Table 3-2, the amount and mechanical properties of the fibers varied according to the composite system used to strengthen the beams. As a first attempt to compare the results of beams strengthened with different types of composite, the axial rigidity of the composite ($A_f E_f$) can be considered. However, it should be noted that comparison based on the axial rigidity does not take into account complex phenomena, such as composite bond behavior, bond length, and effective bond length, that influence the contribution of the composite to the shear strength and failure mode of a strengthened beam. It is highlighted that for fiber type F3, which is bidirectional, only the area of fibers in the beam transverse direction is considered to carry out the comparison.

Figure 3-30 shows the variation of the ratio $V_f/V_{max\text{-}CONTROL}$ vs. $A_f E_f$ for each of the strengthened beams without anchors that failed in shear. The figure shows that the ratio $V_f/V_{max\text{-}CONTROL}$ increases with increasing $A_f E_f$ with the exception of beam S2-FRCM-F4-UN discussed below.

61
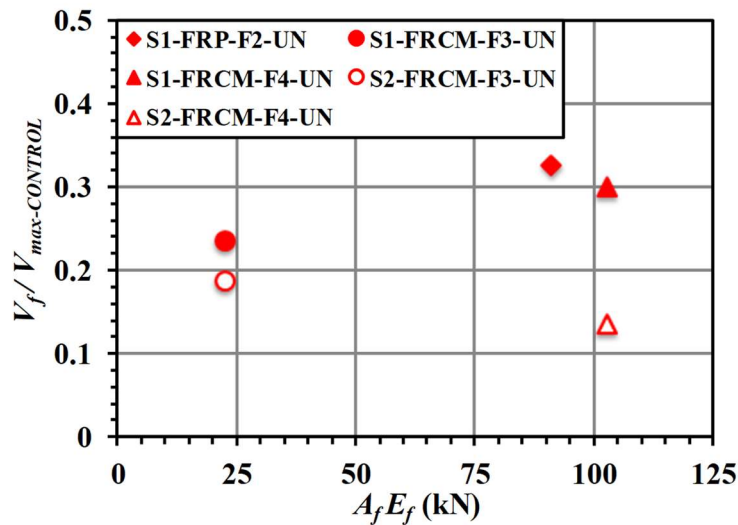
Figure 3-30 Variation of $V_f/V_{max\text{-}CONTROL}$ with A_fE_f

For steel fiber strengthened beams, the values of A_fE_f are similar for both FRP and FRCM composite systems (F2 and F4 fibers, respectively, Table 3-2), and similar values of $V_f/V_{max\text{-}CONTROL}$ were achieved in beams S1-FRP-F2-UN and S1-FRCM-F3-UN, which had the same stirrup spacing. The lower value of $V_f/V_{max\text{-}CONTROL}$ for beam S2-FRCM-F4-UN is attributed to the premature debonding observed for this specimen. In fact, a higher value of $V_f/V_{max\text{-}CONTROL}$, similar to the other steel fiber strengthened beams, was obtained for beam S2-FRCM-F4-UA (24.1% instead of 13.5%, see Table 3-3), in which debonding was prevented by the presence of the anchors.

Strains measured in the fibers at $V_{max\text{-}CONTROL}$ and at V_{max} are shown in Table 3-4, together with the exploitation ratios of the fibers (with respect to the ultimate fiber strain), $\varepsilon_f/\varepsilon_{fu}$. Results in Table 3-4 shows that that exploitation ratios for steel FRCM strengthened beams were significantly lower than those observed for specimens with carbon FRCM for specimens with and without anchors.

Table 3-4. Summary of maximum measured strain in fibers

Beam	Maximum strain measured at maximum shear of corresponding control beam ($V=V_{max-CONTROL}$)	Maximum strain measured at maximum shear ($V=V_{max}$)	
	$\varepsilon_{f,max}$ (µε)	$\varepsilon_{f,max}$ (µε)	$\varepsilon_{f,max}/\varepsilon_{fu}$ (%)
S1-FRP-F1-UN*	833	2274	28.4
S1-FRP-F2-UN	1686	5787	26.3
S1-FRCM-F3-UN	2551	4825	26.8
S1-FRCM-F3-UA	3534	8405	46.7
S1-FRCM-F4-UN	1140	1921**	12
S1-FRCM-F4-UA	817	942	5.9
S2-FRP-F1-UN*	981	1817	22.7
S2-FRP-F2-UN*	1961	3652	16.6
S2-FRCM-F3-UN	2046	2686	14.9
S2-FRCM-F3-UA	1004	3322	18.5
S2-FRCM-F4-UN	1720	1790**	11.2
S2-FRCM-F4-UA	956	1291	8.1

* Failed in flexure

** Maximum recorded value was prior to maximum load due to local debonding of the composite

3.7   Effect of stirrup spacing

Previous research [52–54] has shown that the contribution of the FRP system to the overall shear strength of the strengthened beam is influenced by the internal transverse reinforcement ratio ρ_w, i.e., the spacing and diameter of the stirrups. A lower contribution of the strengthening system to the shear strength is expected for beams with higher values of ρ_w.

Figure 3-31 plots the ratio $V_f/V_{max-CONTROL}$ vs. ρ_w for each of the strengthened beams without anchors that failed in shear. For the FRCM strengthened beams, results in Figure 3-31 show that larger values of $V_f/V_{max-CONTROL}$ were achieved for FRCM strengthened beams in series S1, i.e. beams with lower internal transverse reinforcement ratio, than those in series S2. In other words, a lower contribution of the strengthening system to the shear strength was observed for FRCM strengthened beams with higher values of ρ_w. No conclusions can be made regarding the FRP system since only one beam failed in shear.
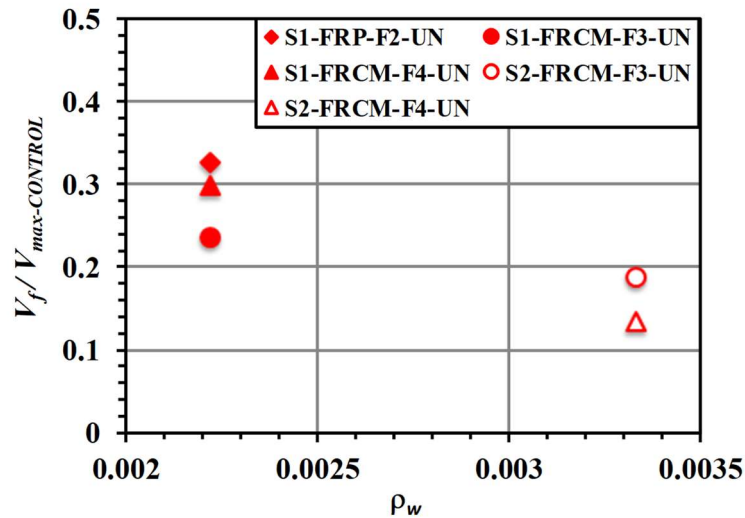
Figure 3-31 Variation of $V_f/V_{max-CONTROL}$ with ρ_w

3.8   Internal-external shear reinforcement interaction

For FRP strengthened beams [32,33,52], and more recently for FRCM strengthened beams [7,19], it has been reported that the presence of the strengthening system influences the contribution of the internal shear reinforcement to the shear strength of the strengthened beam. The strengthening system limits the strain in the internal stirrups because it reduces the width of the critical shear crack and might preclude their yielding. This phenomenon, known as internal-external shear reinforcement interaction, implies that the contributions of steel stirrups and FRP or FRCM jackets to the shear strength may be less than the simple summation of their maximum respective values.

Maximum strains measured in the stirrups at the maximum shear of the corresponding control beam ($V=V_{max-CONTROL}$) and at the maximum shear ($V=V_{max}$) are summarized for each beam in Table 3-5. As noted in Section 3.5, in each of the strengthened beams, at least one strain gauge mounted to the stirrups was crossed by a diagonal crack, and therefore the measured values in that strain gauge can be considered representative of the maximum strains achieved on the stirrups crossed by the diagonal cracks. At the load level corresponding to $V_{max-CONTROL}$, results in Table 3-5 show that the maximum strain measured in the stirrups of the strengthened beams are significantly lower than those measured in the corresponding control beam, which confirms the presence of the internal-external shear reinforcement interaction for both the FRP and FRCM strengthened beams in this study. In fact, at this load level, the maximum stirrup strain measured in each strengthened beam is lower than the yield strain of the stirrups ($\varepsilon_y=2650$ $\mu\varepsilon$).

Table 3-5. Summary of maximum measured strain in stirrups

Beam	Maximum strain measured at maximum shear of corresponding control beam ($V=V_{max\text{-}CONTROL}$)	Maximum strain measured at maximum shear ($V=V_{max}$)
	$\varepsilon_{s,max}$ ($\mu\varepsilon$)	$\varepsilon_{s,max}$ ($\mu\varepsilon$)
S1-CONTROL	9965	9965
S1-FRP-F1-UN*	830	1986
S1-FRP-F2-UN	1034	1497
S1-FRCM-F3-UN	1852	5115
S1-FRCM-F3-UA	1733	5781
S1-FRCM-F4-UN	1025	3219
S1-FRCM-F4-UA	1137	3587
S2-CONTROL	7544	7544
S2-FRP-F1-UN*	828	1330
S2-FRP-F2-UN*	688	1057
S2-FRCM-F3-UN	2513	5547
S2-FRCM-F3-UA	2221	3763
S2-FRCM-F4-UN	2295	2740
S2-FRCM-F4-UA	1968	2912

* Failed in flexure

In Figure 3-32, the P-ε_s relationships for the series 1 and 2 are plotted, including only the measurements obtained by the strain gauge that recorded the higher values of strain. Results in Figure 3-32 and Table 3-5 show that for beams strengthened with FRP, the maximum strains measured in the stirrups were less than the yield strain even at the load level corresponding to V_{max}. These results indicate that the internal-external shear reinforcement interaction is significant in the FRP strengthened beams in this study, where yielding of the stirrups was completely precluded, although it is highlighted that three of the FRP strengthened beams failed in flexure, not reaching their total shear strength. For the FRCM strengthened beams, all of which failed in shear, the maximum measured stirrup strains at the load level corresponding to V_{max} were less than those of the corresponding control beam at its maximum load, however stirrup yielding occurred in each beam. This delayed yielding indicates that the internal-external transversal interaction was present for the FRCM strengthened beams in this study, but it appears to be less significant than for the FRP strengthened beams.
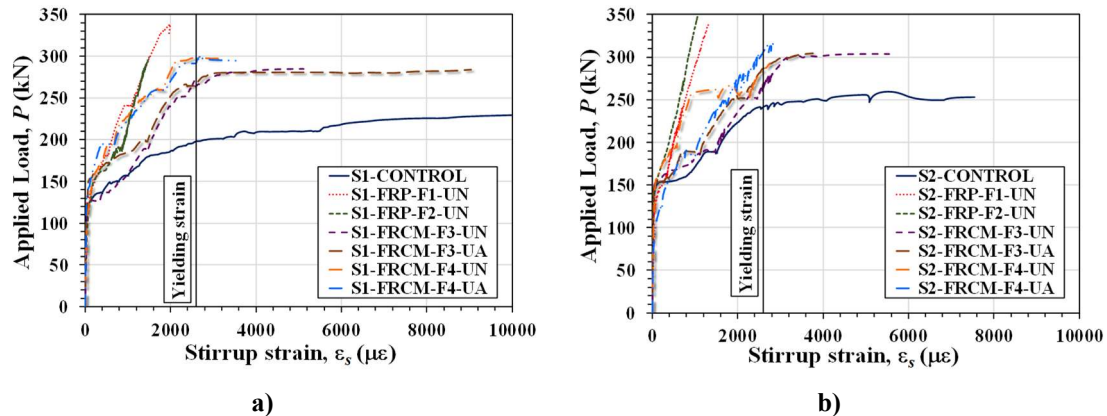
Figure 3-32 Applied load *P* vs. stirrup strain ε_s for: a) series 1 beams; b) series 2 beams

These results suggest that the FRP system is more effective in bridging the critical shear crack, i.e., limiting its width, and therefore, lower values of strain in the stirrups are measured. This observation should be further confirmed for the case of multi-layered strengthening systems and different composite materials.

3.9   Effect of anchors

The results in Table 3-3 show that use of anchors did not result in a significant increase in the shear strength of the FRCM strengthened beams relative to the comparable strengthened beam without anchors, except for beam S2-FRCM-F4-UA with steel fibers (see Figure 3-11, and Figure 3-33). For this beam, the presence of the anchors help avoid the premature debonding observed for beam S2-FRCM-F4-UN, and the contribution of the FRCM composite increased from 13.5% to 24.1%. These findings are in agreement with those by [24], who found that the use of FRP fiber anchors installed into the flange of RC T-beams strengthened in shear with FRCM jackets resulted in a significant increase in shear strength by precluding premature composite debonding. In Figure 3-33, it is also important to note that the behavior of beams S2-FRCM-F4-UN and S2-FRCM-F4-UA was practically the same until beam S2-FRCM-F4-UN reached *Vmax*. This implies that the effect of the anchor is mainly related to the avoid of debonding as expressed before.
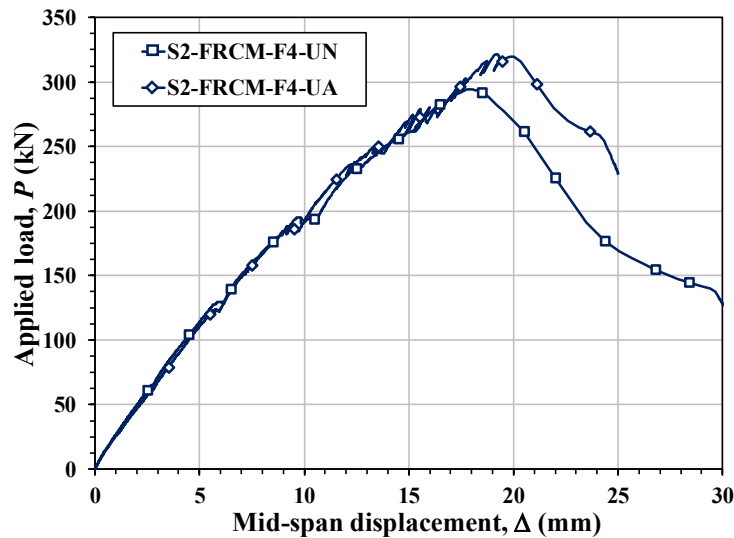
Figure 3-33 Applied load P vs. mid-span displacement Δ curves for beams S2-FRCM-F4-UN and S2-FRCM-F4-UA

For beams strengthened with carbon fibers, in which debonding was not observed, the negligible increase in shear strength indicates that the anchorage system was not effective in preventing additional typical failure mechanisms of the FRCM composite, such as slippage of the fibers within the matrix. In other words, the anchorage system used in this work, which has proven to be efficient for FRP applications [46,55], is not adequate for FRCM composites for which failure does not occur due to debonding from the substrate. As for beams S2-FRCM-F4-UN and S2-FRCM-F4-UA, the presence of the anchors did not have an important influence on the applied load P vs. mid-span displacement Δ curves for beams strengthened with anchor fibers, as shown in Figure 3-34 for beams S1-FRCM-F3-UN and S1-FRCM-F3-UA.
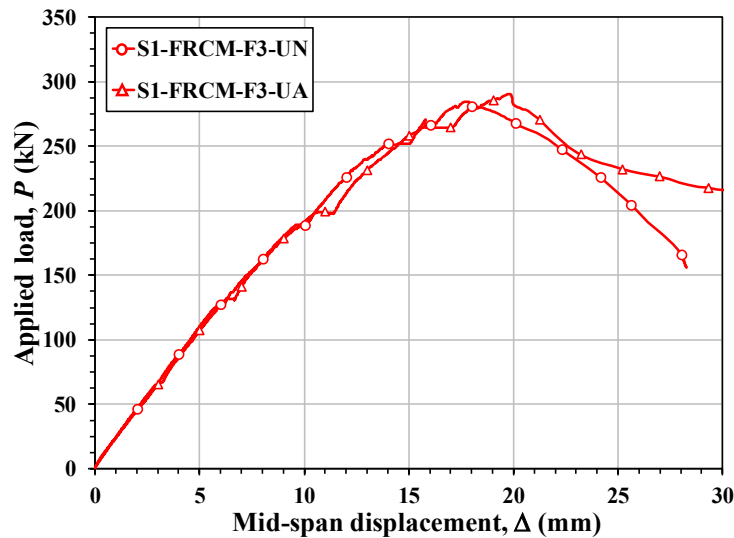
Figure 3-34 Applied load P vs. mid-span displacement Δ curves for beams S1-FRCM-F3-UN and S1-FRCM-F3-UA

The use of anchors did influence the strains measured in the fibers at V_{max}, as shown in Table 3-4. For carbon FRCM (F3) strengthened beams, higher exploitation ratios were achieved for beams with anchors than for those without. For steel FRCM (F4) strengthened beams, on the other hand, there was not a significant variation in the values of fiber strains recorded at the maximum load for beams with or without anchors. However, it is worth noting that the maximum strain values in beams with and without anchors were recorded by strain gauges located in various positions within the shear span, which is explained by the modification of the crack pattern caused by the presence of the anchors.

3.10   Conclusions

This section presented the results of an experimental campaign carried out to study the behavior of RC beams strengthened in shear with externally bonded FRP and FRCM composites. Variables investigated included the type of fiber, internal shear reinforcement ratio, and the use of anchors. The main conclusions drawn from this study can be summarized as follows:

- Results show that the gain in the shear strength of strengthened beams increases with increasing axial stiffness of the composite, $A_f E_f$. For the steel FRP and FRCM strengthened beams that had similar values of $A_f E_f$, the increase in shear strength was similar, i.e., it did not vary depending on the type of matrix.

- The effectiveness of the FRCM composite is related to the spacing of the internal reinforcement. Larger increases in the shear strength were observed for strengthened beams with larger stirrup spacing, i.e., lower internal shear reinforcement ratio.

- All FRCM strengthened beams without anchors failed in shear. For carbon FRCM strengthened beams, local detachment of the entire composite and fiber slippage along the main crack were observed. For steel FRCM strengthened beams, failure was caused by detachment of the composite system, without damage to the concrete substrate. In both cases, cracks on the surface of the FRCM composite were observed for load levels lower than the maximum load.

- Internal-external shear reinforcement interaction was observed for both FRP and FRCM strengthened beams. However, this interaction appears to be less pronounced for beams with FRCM composites.

- The anchors used in this study modified the failure mode, concrete crack pattern, and mid-span displacement of beams strengthened with FRCM composite. However, the use of anchors did not significantly increase the shear strength, with exception of beam S2-FRCM-F4-UA, in which the anchors were able to avoid premature debonding of the FRCM jacket.

- Fiber exploitation ratios for the carbon FRCM strengthened beams were higher than those for the steel FRCM strengthened beams. For the case of carbon FRCM, the exploitation ratio increased with increased stirrups spacing or when anchors were used.

70

4. ASSESMENT OF AVAILABLE MODELS FOR PREDICTING THE SHEAR STRENGTH OF FRCM STRENGTHENED RC BEAMS

In this section, a detailed review of the available models to compute the contribution of the FRCM system to the shear strength of RC beams is performed. Considering that models developed for the case of FRP-strengthened beams serve as a starting point for analytical models proposed for shear strengthening with FRCM, a description of the behavior of RC beams strengthened in shear with externally bonded FRP is included as well in this section. This description is carried out in terms of expected failure mode, including a brief recall of some expressions proposed by design guidelines for shear strengthening with FRP (see Section 4.1).

Next, four models proposed to determine the contribution of the FRCM composite to the shear strength of RC beams are evaluated: Model 1 by Triantafillou and Papanicolaou [1], Model 2 by Escrig *et al.*[17], Model 3 by ACI 549.4R [44], and Model 4 by Ombres [19]. The evaluation of the models is made based on the prediction of the additional shear strength provided by the FRCM system (see Section 4.2) and on the overall shear strength attained by the beams after the strengthening (see Section 4.5). The database collected by the author (see Chapter 2 and Appendixes A and B) is used to carry out the assessment of the models.

Models 1 and 2 are based on the properties of the FRCM composite fibers, and Models 3 and 4 are based on properties of the composite, as discussed in Section 4.2. For the case of Model 3, which is the only guide available at this time for the design and construction of FRCM composites, the contribution to the shear strength provided by the strengthening system V_{FRCM} is considered to be additive to the strength of the unstrengthened (control) beam ($V_{CON}=V_c+V_s$), as discussed in Sections 4.4 and 4.5) and shown in Eq. (4-1), in order to determine the total shear capacity of the strengthened beam V_n:

$$V_n = V_c + V_s + V_{FRCM}$$

4-1

where V_c and V_s are the contributions to the shear strength provided by the concrete and internal transversal steel reinforcement, respectively.

Currently there are no European standards for the evaluation of V_{FRCM}. However, it is worth noting that in European-based approaches for FRP-strengthened beams (see Section 4.1), V_n is computed including only V_s and the contribution of the FRP system, V_f, and its value is limited by the shear strength of the concrete compression strut, $V_{c,max}$, as specified by [56] and shown in Eq. (4-2):

$$V_n = min\{V_s + V_f, V_{c,max}\} \qquad\qquad \text{4-2}$$

Values of V_c, V_s, and $V_{c,max}$ in Eqs. (4-1) and (4-2) are calculated using the equations in current design provisions for unstrengthened RC beams and discussed in Section 4.4.

In Section 4.2 of this work, the evaluation of the models is carried out considering the strength provided by the FRCM system (i.e. V_{FRCM}). In Section 4.5, the evaluation of the models is performed considering the overall shear strength attained by the beams after the strengthening.

Although the four models present different formulations, they are each based on the well-known truss analogy and differ mainly in the expression used to evaluate the stress (or strain) in the FRCM system along the critical shear crack, as discussed in section 2.5. Models 1 and 3 are based on a fixed angle of the diagonal shear crack relative to the longitudinal axis (θ). Models 2 and 4 allow the use of variable angles, however only Model 2 was developed using angles different from 45° when this information was provided in the articles used to calibrate the model; otherwise the value of θ was set to 45° [17]. Therefore, and considering the limited data available reporting the actual value of θ (see Section 2.6), a fixed value of $\theta=45°$ is used to evaluate and compare the different models in terms of additional shear strength provided by the FRCM. However, for the evaluation of the overall shear strength of the beams, the analysis includes as well the variable angle methodology proposed by [56].

For each model, average (AVG) values of test-to-predicted ratios of the FRCM shear contribution (V_{FRCM}) or the total shear strength (V_n), denoted as V_{test}/V_{pred}, are reported. Values of standard deviation (STD) and coefficient of variation (COV$_1$) computed with respect to a mean value of 1, which implies a perfect match between V_{test} and V_{pred}, as shown in Eq. (4-3), are also included:

$$COV_1 = \sqrt{\frac{\Sigma_1^N \left(\frac{V_{test,i}}{V_{pred,i}} - 1\right)^2}{N}} \qquad \text{4-3}$$

where N is the number of tests.

4.1 Design guidelines for RC beams strengthened in shear with FRP composites

The shear behavior of RC beams is quite complex due to the interaction of different mechanisms. In general, the factors that contribute to the strength of a RC beam without internal shear reinforcement, e.g., steel stirrups, are the area of uncracked concrete in compression, aggregate interlock, dowel action, arch action, and residual tensile stress across the crack [9]. For the case of RC beams with internal shear reinforcement, e.g., stirrups, the contribution of the reinforcement must be considered. In this case, it is usually assumed that stirrups crossed by the shear crack will yield before failure [57]. Additional factors such as concrete strength, shear span-to-depth ratio (a/d), flexural reinforcement ratio, shear reinforcement ratio, bond between the stirrups and the concrete, beam size, and aggregate size influence the response of RC beams subjected to shear stresses [9].

For the case of RC beams strengthened in shear with externally bonded FRP composite, the effect of the composite on the shear strength of the beam and its interaction with the aforementioned mechanisms should be taken into account. However, most design guidelines [38–40] compute the contribution of the FRP composite independent of the strength of the unstrengthened RC beam to facilitate the assessment of the total shear strength. These guidelines follow a similar approach to that used for the internal shear reinforcement, despite the fact that the FRP strengthening system is externally bonded [30]. The contribution to the beam overall shear strength provided by the FRP, V_f, is generally computed using the truss analogy and depends mainly on the FRP fiber orientation, crack pattern, amount of FRP fibers, and stress in the composite as shown in Eq. (4-4):

$$V_f = \varepsilon_{fe} E_f \rho_f b d_{fv} (cot\theta + cot\alpha) sin\alpha \qquad \text{4-4}$$

where α is the angle between the FRP fibers and the beam longitudinal axis, and the other variables were defined previously.

The main difference between design guidelines is the way they evaluate the stress level in the FRP composite, i.e., the equation for computing the effective strain (see definition in Section 2.5), ε_{fe}. Additionally, values of d_{fv} and θ adopted vary

among the different guidelines. In ACI 440.2R [39], for instance, d_{fv} is taken as the effective depth of the beam, d, while θ is a constant value of 45°. Models developed in Europe assume that θ can vary from 21.8° to 45°, as in the case of internal shear reinforcement, whereas d_{fv} is taken equal to $0.9d$ in guidelines by CNR DT-200 and *fib* [38,40].

4.1.1 Failure modes

The following sections present an overview of the approaches proposed by different design guidelines to evaluate the effective strain in the FRP composites, depending on the expected failure mode.

- **Concrete integrity and aggregate interlock action**

As diagonal shear cracks develop and increase in width, the concrete integrity, and hence the beam strength, is compromised due to the loss of aggregate interlock action. This failure mechanism is more important for beams without stirrups and for FRP strengthened beams that are fully wrapped and, to a lesser extent, for anchored U-wrapped configurations, in which debonding of the composite is not expected. For beams in which failure is due to debonding of the composite, the strain level reached in the composite are expected to be lower than in the cases mentioned above, and therefore the concrete integrity might not be compromised. For the case of beams with stirrups, although there will be a reduction of the concrete contribution to the shear strength due to the loss of the aggregate interlock, the concrete integrity is maintained due to the presence of the internal transverse shear reinforcement. Considering that the strain in the FRP composite increases with the increase of the crack width, available guidelines impose a maximum value of effective strain in the composite in order to ensure that the concrete integrity is maintained. Based on the recommendations by Khalifa et al [34], guidelines such as ACI 440.2R [39] and TR55 [58] propose a maximum value of effective strain based on a fixed value of 4000 $\mu\varepsilon$. However, based on limited experimental research, some authors [59] have shown that the maximum value of strain reached by the composite before the concrete integrity is compromised is slightly larger than 4000 $\mu\varepsilon$. Nevertheless, as expressed by Denton et al [60], this limit might not be able to prevent the development of wide cracks and might become unsafe as the beam depth increases.

- **Fiber rupture**

Fiber rupture has been observed for fully wrapped and for some U-wrapped beams [53,61]. In order to avoid this phenomenon, ACI 440.2R [39] proposes a limit on the strain in the composite of $0.75\varepsilon_{fu}$, where ε_{fu} is the ultimate strain of the composite. Chen and Teng [61] used a linear crack configuration assuming rigid body movement of the member regions on either side of the shear crack. Considering that the fiber effective strain is proportional to the crack width, they proposed the value of $0.50\ \varepsilon_{fu}$ as the average value of strain from zero at the crack tip to ε_{fu} at the crack end, i.e., where the fibers will rupture. This recommendation is taken by TR55 [58].

The model proposed by *fib* [40] is an empirical design method based on the results presented by Triantafillou and Antonopoulos [42]. Their model was calibrated using a database of 76 FRP-strengthened beams including fully wrapped, U-wrapped, and side bonded configurations. To compute the value of effective strain for failure due to fiber rupture, the proposed equations are based on regression of the data in their database, using Eq. 1 and rearranging it to compute the value of effective strain. According to their results, they proposed best-fit power law expressions for the effective strain depending on the strengthening configuration, type of fiber, and for the case of side bonded and U-wrapped strengthened beams, on the type of expected failure mode, i.e., fiber rupture or peel off. For the case of fiber rupture, the equation proposed for carbon-FRP strengthened elements is:

$$\varepsilon_{fe} = 0.17 \left(\frac{f_{cm}^{2/3}}{E_f \rho_f} \right)^{0.30} \varepsilon_{fu} \qquad \text{4-5}$$

where f_{cm} corresponds to the mean value of the concrete compressive strength.

- **FRP debonding**

Peel-off of the FRP composite from the concrete substrate, which usually occurs within a few millimeters inside the concrete cover, is the most typical failure mode for FRP-strengthened beams with U-wrapped and side bonded configurations. This type of failure is brittle in nature and leads to a sudden collapse. In fact, some available guidelines do not allow the use of side bonded configurations [38] as the occurrence of debonding can occur for relatively low values of load. As shown by [62], the early debonding observed for side bonded FRP strengthened beams with transverse internal shear reinforcement might occur before stirrups yield, which

implies that the shear strength of the beam is the same, or even lower, than that of the unstrengthened beam .

The equations to evaluate the value of effective strain reached at debonding proposed by the ACI 440.2R [39] guidelines are based on the empirical work carried out by Khalifa et al [34]. The equations proposed by Khalifa et al [34] were calibrated using a database comprising 49 tests of RC beams strengthened with FRP composites, most of which with carbon fibers, available at the time of publication of their paper. In their formulation, the value of the effective strain depends on the ultimate fiber strain and on a reduction factor, κ_v, as shown in Eq. (4-19).

$$\varepsilon_{fe} = k_v \varepsilon_{fu} \leq 0.004$$
<div style="text-align:right">4-6</div>

The reduction factor κ_v is a function of the "active" bonded length, L_e, referred to as effective bond length in other guidelines, and of the modification factors k_1 and k_2:

$$k_v = \frac{k_1 k_2 L_e}{11900 \varepsilon_{fu}}$$
<div style="text-align:right">4-7</div>

L_e is defined by ACI 440.2R [39] as the length over which most of the bond stress is maintained. Maeda et al [63] was one of the first studies to identify the presence of an effective bond length based on the results of lap shear tests and proposed an exponential relationship for L_e, which in turn is used by Khalifa et al. [34]. ACI 440.2R [39] uses a modified version of that equation:

$$L_e = \frac{23300}{\left(n_f t_f E_f\right)^{0.58}}$$
<div style="text-align:right">4-8</div>

In Eq. (4-8), L_e is inversely proportional to the FRP axial rigidity, $E_f t_f$. However, as pointed out by several researchers, L_e should be actually proportional to $E_f t_f$ [64,65]. As noted by [65], the different trend predicted by Eq. (4-8) might be due to the fact that the model proposed by [63] was developed using a limited set of experimental tests and does not take into account the cohesive nature of the concrete substrate

The influence of the concrete strength is considered by means of the reduction factor k_1:

$$k_1 = \left(\frac{f_c'}{27}\right)^{2/3}$$
<div style="text-align:right">4-9</div>

where f'_c is the concrete compressive strength. It is worth noting that in the original work by Khalifa et al [34], the denominator in Eq. (4-9) was equal to 42 MPa in order to consider that the work performed by Maeda et al [63] was carried out using a fixed f'_c equal to 42 MPa. The type of wrapping scheme is considered by means of the reduction factor k_2:

$$k_2 = \frac{d_{fv} - L_e}{d_{fv}} \rightarrow for \; U - wrapped \; configurations \qquad 4\text{-}10$$

$$k_2 = \frac{d_{fv} - 2L_e}{d_{fv}} \rightarrow for \; side \; bonded \; configurations \qquad 4\text{-}11$$

For the case of peel-off, the model presented in *fib* [40], which is based on the model by Triantafillou and Antonopoulos [42], proposes the following expression for RC beams strengthened with carbon FRP composites using U-wrapped or side bonded configurations:

$$\varepsilon_{fe} = 0.65 \left(\frac{f_{cm}^{2/3}}{E_f \rho_f} \right)^{0.56} \varepsilon_{fu} \qquad 4\text{-}12$$

It is worth noting that according to *fib* [40], the minimum value of ε_{fe} determined using Eq. (4-5) (rupture) and Eq. 4-12 (peel-off) should be used in design. Unlike the model proposed by Khalifa et al [34], Eq. 4-12 does not explicitly consider L_e, but the equations are similar as the main properties of the FRP and the substrate are included, but with different coefficients.

- **Fracture mechanics approach**

In addition to the empirical approaches described above, early works have pointed out the importance of a fracture mechanics approach to gain a better understanding of the debonding process of the FRP composites from the substrate [66,67]. These approaches are based on the evaluation of the effective bonded length and on the fracture energy. Examples of models that use this approach are those by Chen and Teng [68], TR55 [58], EN-1998-3 [69], and CNR DT-200 [38]. In some cases, the equations proposed are similar but vary in some coefficients that are calibrated experimentally.

One of the simplest approaches is the one presented in TR55 [58]. In addition to the requirements for concrete integrity and fiber rupture, the following limit is proposed to avoid peel-off, based on the recommendations given by Neubauer and Rostasy [70]:

$$\varepsilon_{fe} = 0.5 \left(\frac{f_{ctk}}{E_f t_f} \right)^{0.5} \qquad \text{4-13}$$

where f_{ctk} is the characteristic tensile strength of the concrete.

However more complex equations, based on fracture mechanics, have emerged recently in an attempt to improve the accuracy of previous models such as the one presented in CNR DT-200 [38].

4.1.2   Additional remarks

Although significant research efforts have been carried out to develop safe and accurate design models to evaluate the shear contribution of FRP composites externally bonded to RC beams, it is difficult to say that this goal has been accomplished. As pointed out by D'Antino and Triantafillou [41], available models tend to underestimate the contribution of the FRP, especially for fully wrapped configurations. In addition, significant variations in accuracy can be found for the same model for different strengthening configurations [41].

In general, development, calibration, and/or validation of available design models are based on the assumption that the experimental contribution of the composite ($V_{f,exp}$) can be computed by subtracting the unstrengthened (control) beam shear strength ($V_{control}$) from the total shear strength of the strengthened element (V_{str}) as shown in Eq. (4-14):

$$V_{f,exp} = V_{str} - V_{control} \qquad \text{4-14}$$

The effective strain in the composite can therefore be computed rearranging Eq. 4-1 into Eq. 4-15, as done in Section 2.5:

$$\varepsilon_{fe} = \frac{V_{f,exp}}{E_f \rho_f b d_{fv} (\cot\theta + \cot\alpha) \sin\alpha} \qquad \text{4-15}$$

Values of effective strain determined using Eq. 4-15 are then compared to values determined analytically with equations derived following a mechanics approach or are used to develop empirical equations that best fit the trend of the experimental values.

 Eq. (4-14), however, does not consider the interaction among the different mechanisms activated when a member is subjected to shear forces. As pointed out by several researchers, the contributions of the concrete and, in the case of beams with internal transverse reinforcement, of the steel vary when an FRP jacket is applied to the beam [53,59,71]. In fact, when concrete cracks are wide enough,

research performed by Jirawattanasomkul et al. [71] has shown that degradation of the concrete contribution to the total shear strength can start before the maximum strength of the beam is reached, depending on factors such as the amount of FRP, beam depth, and shear span-to-depth ratio. However, even after the concrete contribution degrades, the beam may be able to carry higher loads by means of an increase in the contribution provided by the FRP composite. For the case of RC beams that include stirrups, the strengthening system might limit the deformation of the internal stirrups and might preclude their yielding as discussed in Section 3.8 and [32,33,52].

Although measurement of the strains in the composite by means of strains gauges, or more recently by full-field measurement techniques such as digital image correlation (DIC) systems, help to gain a better picture of the strain distribution in the composite, the experimental contribution of the strengthening is still computed using Eq. (4-14). This is mainly due to the fact that measuring the actual contributions of the concrete and the reinforcing steel are challenging. To measure the contribution of the stirrups, for instance, it is required to measure the strain in the steel reinforcement at the crack location, but this measurement is difficult to acquire with strain gauges as the shear crack location is not known a priori [33].

Another critical issue has to do with the shape of the cracking pattern, i.e., the angle and crack distribution. Regarding the angle, using a fixed angle θ=45° leads to more conservative predictions when compared to lower values of θ. The use of variable values of θ are allowed by some design models, mainly European guidelines, as the shear crack angle is typically less than 45° [72]. However, there is little information regarding how the presence of the FRP composites affects the inclination of the shear cracks and how this issue could be incorporated in design guidelines. In addition, as noted by Pellegrino and Modena [54], for beams without stirrups, a single shear crack is expected, while for beams with stirrups, multiple parallel cracks distributed in a cracked area are typically observed. The distribution of the cracks influences the performance of the FRP jacket, as debonding of the FRP jacket can be initiated sooner due to the presence of more cracks [73]. This is explained by the concentration of stresses around the crack [74], which also implies that there is not an uniform distribution of the stresses along the shear crack. In addition, the presence of more cracks also implies that the fibers will have smaller available anchorage lengths when compared to a beam with a single shear crack [73]. However, available guidelines assume a single shear crack, which might not be appropriate.

Finally, it is worth mentioning that the use of fracture mechanics based models does not necessarily provide more accurate results than empirical models. For instance, as shown by [41], a simple model as that proposed by [39] produces more accurate results than the EN-1998-3 [69] for U-wrapped configurations.

4.2 Contribution of the FRCM system to the shear strength of RC beams

The development of guidelines for the evaluation of the contribution of externally bonded FRCM systems to the strength of RC beams has relied on the previous work carried out with FRP composites. For the case of shear, this means that most of the assumptions and methodologies described in Section 4.1 have been used in the development of the design models.

The main limitation of the available models for FRCM-strengthened RC beams is that they compute the shear strength of the strengthened beam as the summation of the unstrengthened beam shear strength and the contribution of the FRCM system. However, as discussed in Sections 2.3 and 3.8, similar to the case of FRP systems, interaction between the internal and external shear reinforcement has been reported, which implies that this assumption may not be appropriate.

In addition, for the case of FRCM strengthened beams, evaluation of the strains in the fibers using full-field surface measurement techniques, such as DIC systems, is not totally effective since measurements on the surface of the external matrix layer are not representative of the response of the fibers [75]. Although fiber strains can be measured using traditional methods such as strain gauges, discrete measurements have certain limitations as discussed in Section 4.1.2.

In this section, as per Section 2.1, in the evaluation of the FRCM contribution to the shear strength V_{FRCM}, the value V_{test} is calculated by subtracting the shear strength of the corresponding control beam strength (V_{CON}) from the total shear strength for each test, whereas the value of V_{pred} is computed by the model. In the assessment of the models, strengthened beams that included anchors and/or those that failed in flexure were not considered.

Different subsets of the complete database needed to be used in the assessment of the different models due to the limitations of each model and the parameters included. As mentioned earlier in this section, Models 1 and 2 use the properties of the bare fibers, and all references included in Table 2-1 reported the required properties. The assessment of Model 1 is therefore made using all tests, except those with anchors or that failed in flexure as discussed above, and the resulting

database is referred to as Database 1 ("DB1"), which includes 79 tests. Model 2, on the other hand, was formulated based on tests in which detachment of the FRCM system from the substrate was prevented. For this reason, its evaluation is carried out using a subset of DB1, referred to as Database 2, ("DB2"), which includes only those tests that did not exhibit composite detachment (39 tests). The performance of Models 1 and 2 is then compared using DB2 (Section 4.2.3), since it is common to both.

Models 3 and 4 evaluate the additional shear strength provided by the FRCM system based on the mechanical properties of the FRCM system as a composite and are presented in Section 4.2.2. This approach presents a drawback as most of the experimental studies reported in the literature on the subject do not provide the mechanical properties of the composite, which makes it difficult to validate the model. In addition, as pointed out by D'Antino and Papanicolaou [76], test results to characterize the FRCM composite are highly affected by aspects such as handling, curing, setting up of the specimens, and gripping system employed. Only five of the references [13,17–19,22] reported the required properties of the FRCM composite. Unfortunately, the tests presented by [13] had to be disregarded because the value reported for the elastic modulus of the FRCM composite (E_{FRCM}=2.72 GPa) was approximately 50 times lower than values reported for this variable in the available literature, which resulted in values of V_{pred} that were clearly anomalous with respect to the other tests. Thus, a subset of DB1, referred to as Database 3 ("DB3") that includes 21 available tests from references that reported the mechanical properties of the composite was used to evaluate Models 3 and 4. Comparison of Models 1, 3, and 4 is carried out using DB3 (Section 4.2.3), since it is common to all three models. Model 2 is not included in this comparison because most tests in DB3 failed due to composite detachment of the FRCM system.

In order to facilitate the analysis, the formulations of the models are presented in this work with a uniform notation.

4.2.1 Models based on the properties of the fibers

- **Model 1 (Triantafillou e Papanicolaou [1])**

Model 1 [1] corresponds to the first attempt to evaluate the additional shear strength provided by the FRCM system. It is calibrated using the value of shear strength provided by the FRCM system for a fully wrapped rectangular beam that failed in shear. Considering that the model was developed using a single test, the

authors expressed that Model 1 needs to be validated when further experimental evidence is available but that the methodology used is quite general. In fact, additional authors such as [16] have used similar methodologies to evaluate the shear strength provided by the FRCM system. However, in this section, only the expression proposed by is [1] evaluated.

Assuming that the fiber is comprised of perpendicular rovings aligned perpendicular and parallel to the beam longitudinal axis, Model 1 computes V_{FRCM} using Eq. (4-16):

$$V_{FRCM} = \rho_f \sigma_{eff} b_w d_f \qquad \text{4-16}$$

where d_f is the effective depth of the jacket taken as $0.9d$ (d=effective depth) for rectangular beams or the height of the web for T-beams. The effective stress in the FRCM system (σ_{eff}) is computed based on the average strain reached across the shear crack. Based on limited experimental evidence, [1] indicated that this strain is aproximately 50% of the ultimate strain of the bare fibers ε_{fu}, although they highlighted that further research is needed to validate this approximation. Therefore, σ_{eff} can computed by Eq. (4-17):

$$\sigma_{eff} = 0.5 E_f \varepsilon_{fu} d_f \qquad \text{4-17}$$

Figure 4-2 compares the V_{test} vs. V_{pred} values provided by the FRCM system. The solid line V_{test}/V_{pred}=1.0 (straight line starting from the origin and oriented at a 45° angle) divides safe (points above the line) and unsafe (points below the line) values.

Figure 4-1 V_{test} vs. V_{pred} for Model 1: DB1

a)   b)
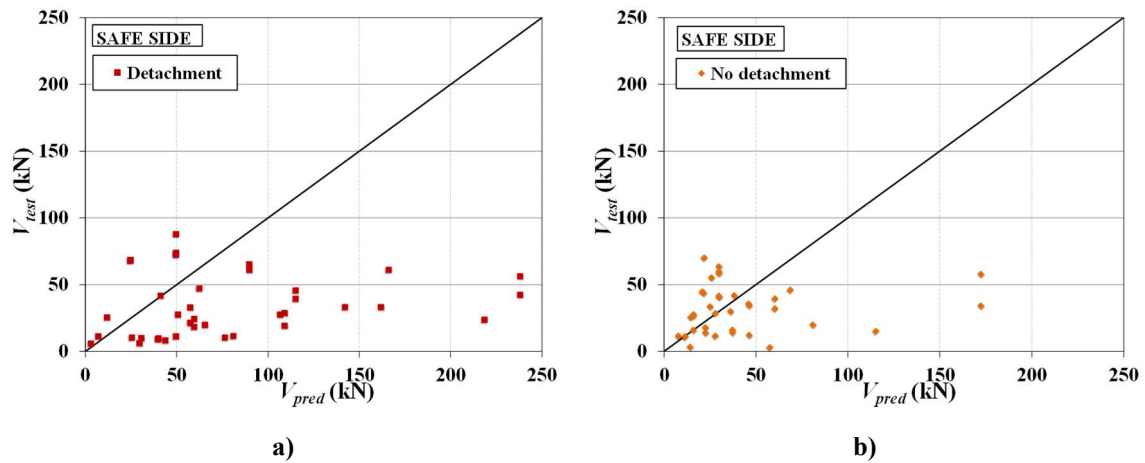
Figure 4-2 V_{test} vs. V_{pred} for Model 1: a) DB1-Detachment; b) DB1-No detachment

For beams that failed by detachment of the strengthening system, Figure 4-2a shows that Model 1 tends to overstimate (unsafe) the contribution of the FRCM composite, with AVG=0.66 (Table 4-1). This overestimation indicates that actual strain in the fibers might be lower than 50% of the ultimate strain assumed by the model. For beams with no detachment (Figure 4-2b), the concentration of points around the solid line indicates a better agreement between predicted and test values. The AVG value for beams with no detachment is 1.05, which indicates a slight understimation (safe) of the FRCM composite contribution. Regarding the accuracy of the model, a larger value of COV_1 is associated with beams that failed by FRCM detachment, although a similar value of COV_1 was attained by beams that failed without detachment of the composite.

Table 4-1. V_{test}/V_{pred} for Model 1 with DB1

PARAMETER	SPECIMENS	N	AVG	STD	COV_1
Failure mode	Detachment	40	0.66	0.74	0.79
	No Detachment	39	1.05	0.80	0.73
Strengthening configuration	Side bonded	29	1.24	0.79	0.81
	U-wrapped	44	0.51	0.47	0.68
	Fully wrapped	6	1.50	1.04	1.07
All		79	0.85	0.75	0.76

Figure 4-3a presents values of V_{test} vs. V_{pred} for FRCM strengthened beams using side bonded configuration. Figure 4-3b includes this information for U-wrapped and fully wrapped beams. In Table 4-1, values of AVG, STD and COV1 for

V_{test}/V_{pred} for Model 1, using DB1 divided according to the strengthening configuration, are included.
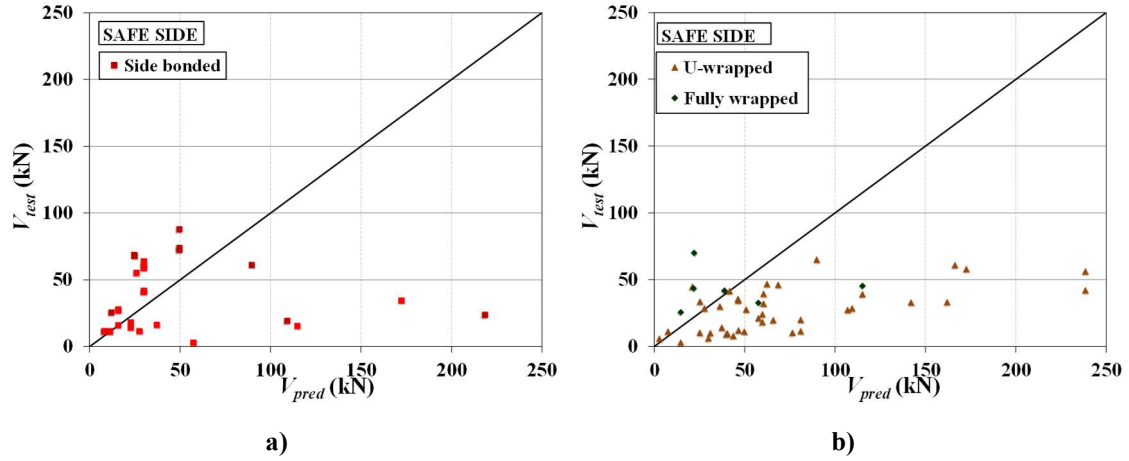
Figure 4-3 V_{test} vs. V_{pred} for Model 1: a) Side bonded configuration; b) U-wrapped and fully wrapped configurations

Results in Figure 4-3 and Table 4-1 show that for side bonded and fully wrapped beams, Model 1 tends to overstimate (safe) the contribution of the FRCM system to the shear strength, which is reflected in values of AVG larger than 1.0 (1.24 and 1.50 for side bonded and fully wrapped configurations, respectevely). On the other hand, the model understimates the contribution for U-wrapped strengthened beams. These results imply that the type of strengthening configuration has a high influence on the performance of the model. It is also worth noting that a the lower value of COV_1, i.e., higher accuracy, is found when the model is applied to U-wrapped strengthened beams.

Considering the limited experimental evidence used by [1] to define the value of σ_{eff}, Eq. (4-18) is used to determine the effective strain in the fibers ε_{eff} for the tests included in DB1. Rearranging Eq. (4-16), ε_{eff} can be calculated from the value of V_{test} as:

$$\varepsilon_{eff} = \frac{V_{test}}{\rho_f E_f b_w d_f} \qquad 4\text{-}18$$

As expressed in Section 2.5, the effective strain in the fibers depends on the axial rigidity ($E_f\rho_f$) and is inversely proportional to the tensile strength of the substrate expressed as $f'_c{}^{2/3}$. Values of $\varepsilon_{eff}/\varepsilon_{fu}$ are plotted in terms of the ratio $\rho_f E_f/f'_c{}^{2/3}$ for all points in DB1 (Figure 4-4), divided according to failure mode (Figure 4-5) and strengthening configuration (Figure 4-6), where ε_{eff} is calculated using Eq. (4-18). The constant value suggested by the model ($\varepsilon_{eff}/\varepsilon_{fu}$=0.5) is also indicated in the

graphs. Figure 4-4 shows that for a few specimens, the value of the ratio $\varepsilon_{eff}/\varepsilon_{fu}$ is slightly larger than 1.0, implying that the effective strain is larger than the rupture strain. It should be noted that the value of ε_{eff} is not measured but rather determined by the model, and in some cases the value of the ε_{fu} is given by the manufacturer as a minimum value. The average value of ε_{eff} normalized by ε_{fu} (i.e., $\varepsilon_{eff}/\varepsilon_{fu}$) for all the points in DB1, without including values of $\varepsilon_{eff}/\varepsilon_{fu}>1.0$, is 0.34 (COV=0.83), which is lower than the factor 0.50 proposed by the model.
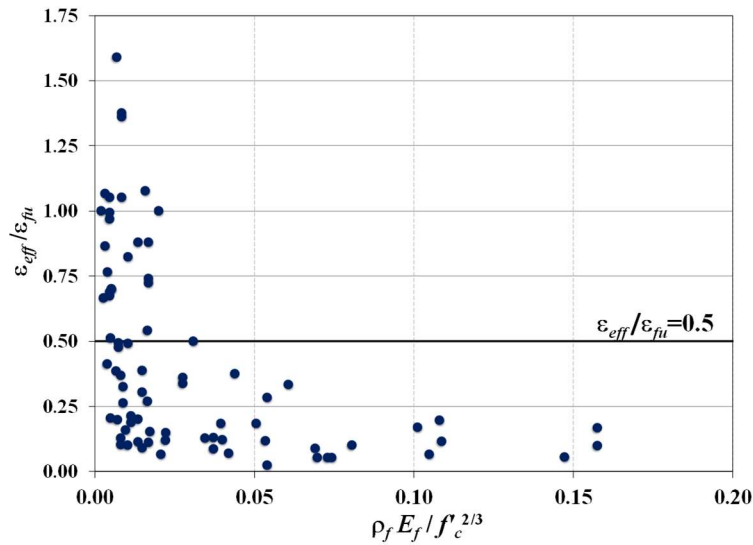
Figure 4-4 Normalized fiber strain $\varepsilon_{eff}/\varepsilon_{fu}$ vs. $\rho_f E_f/f'_c{}^{2/3}$ for Model 1: DB1

For beams that failed by detachment, Figure 4-5a shows that the ratio $\varepsilon_{eff}/\varepsilon_{fu}$ tends to decrease with the increase of $\rho_f E_f/f'_c{}^{2/3}$. For these beams, ε_{eff} is generally lower than 50% of ε_{fu}, with an average of 0.26 (COV=0.98). For beams that did not show detachment (Figure 4-5b), the average value is 0.50 (COV=0.65), which is the value proposed by the model, although the relationship of $\varepsilon_{eff}/\varepsilon_{fu}$ and $\rho_f E_f/f'_c{}^{2/3}$ is not as clear as for beams that failed by detachment.
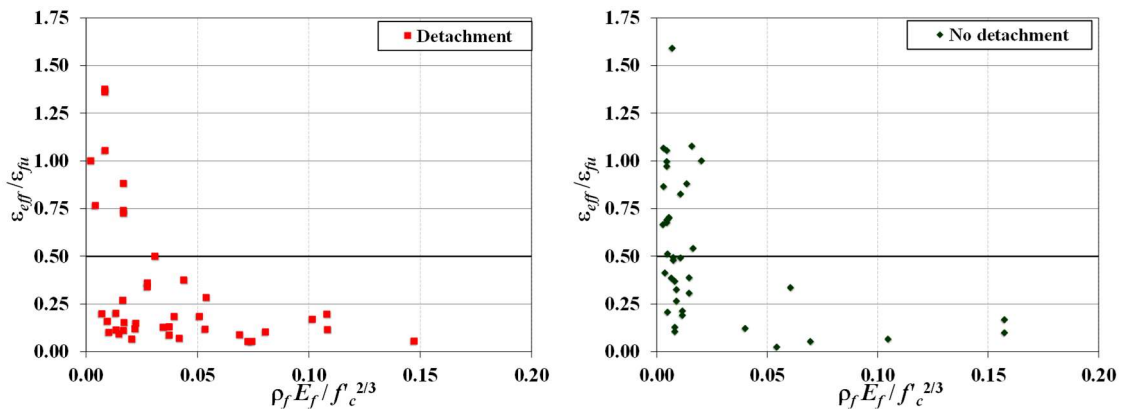
Figure 4-5 Normalized fiber strain $\varepsilon_{eff}/\varepsilon_{fu}$ vs. $\rho_f E_f/f'_c{}^{2/3}$ for Model 1: a) DB1-Detachment; b) DB1-No detachment

For beams strengthened with side bonded configuration, Figure 4-6a shows that the ratio $\varepsilon_{eff}/\varepsilon_{fu}$ tends to decrease with the increase of $\rho_f E_f/f'_c{}^{2/3}$. However, it is worth noting that most of the points have low values of $\rho_f E_f/f'_c{}^{2/3}$, i.e., $\rho_f E_f/f'_c{}^{2/3}<0.025$. For these beams, an average of $\varepsilon_{eff}/\varepsilon_{fu}=0.50$ (COV=0.63). A similar value of $\varepsilon_{eff}/\varepsilon_{fu}$ was found also for fully wrapped strengthened beams ($\varepsilon_{eff}/\varepsilon_{fu}=0.47$, COV=0.82). For U-wrapped beams, the average value of $\varepsilon_{eff}/\varepsilon_{fu}$ is 0.23 (COV=0.85), which is lower than the 0.50 value proposed by the model (see (Figure 4-6b).

a)   b)
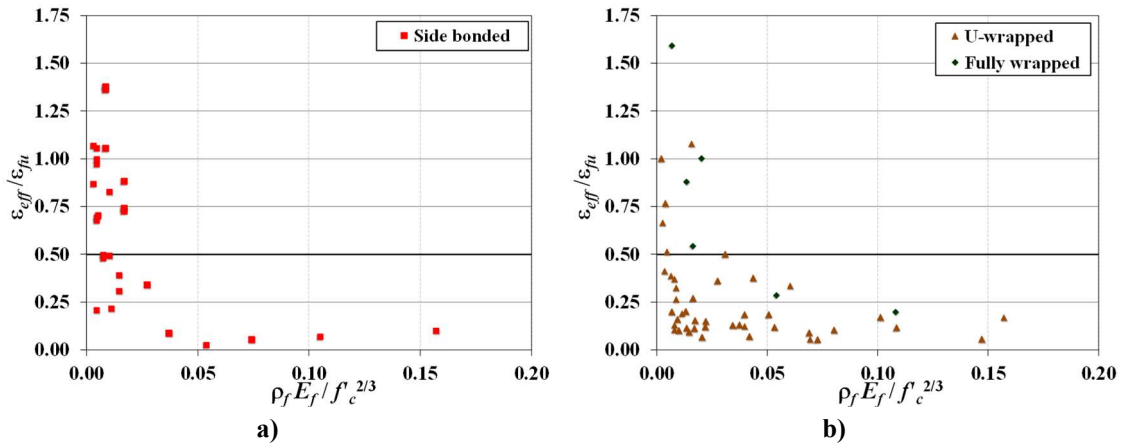
Figure 4-6 Normalized fiber strain $\varepsilon_{eff}/\varepsilon_{fu}$ vs. $\rho_f E_f/f'_c{}^{2/3}$ for Model 1: a) Side bonded configuration; b) U-wrapped and fully wrapped configurations

- **Model 2 (Escrig *et al.* [17])**

Model 2 computes V_{FRCM} according to Eq. (4-19):

$$V_{FRCM} = 2n\varepsilon_{eff}E_f t_f d_f (cot\alpha + cot\theta)sin^2\alpha \qquad \text{4-19}$$

where α is the fiber inclination angle with respect to the longitudinal axis of the beam, and the other variables were defined previously. Based on the research by [42] and using data collected from the literature (18 strengthened beams) and their own research (6 strengthened beams) for FRCM strengthened specimens without anchors that avoided composite detachment, [17] proposed the following equations for computing the effective strain in the fibers ε_{eff}:

- For fully wrapped specimens:

$$\varepsilon_{eff} = 0.035(\frac{f'_c{}^{2/3}}{E_f \rho_f})^{0.65}\varepsilon_{fu} \qquad \text{4-20}$$

- Side bonded or U-wrapped specimens:

$$\varepsilon_{eff} = 0.020(\frac{f'^{2/3}_c}{E_f \rho_f})^{0.55} \varepsilon_{fu} \qquad \text{4-21}$$

In Eqs. (4-20) and (4-21), E_f and f'_c are expressed in units of GPa and MPa, respectively.

Values of V_{test} are plotted vs. V_{pred} using Model 2 for the all the tests included in DB2 (Figure 4-7) and divided according to the strengthening configuration (Figure 4-8). It is noted that all the specimens in DB2 failed without detachment of the composite, and therefore, a plot of V_{test} vs. V_{pred} with DB2 divided according to the failure mode is not included. Table 4-2 sumarizes values of AVG, STD, and COV₁.
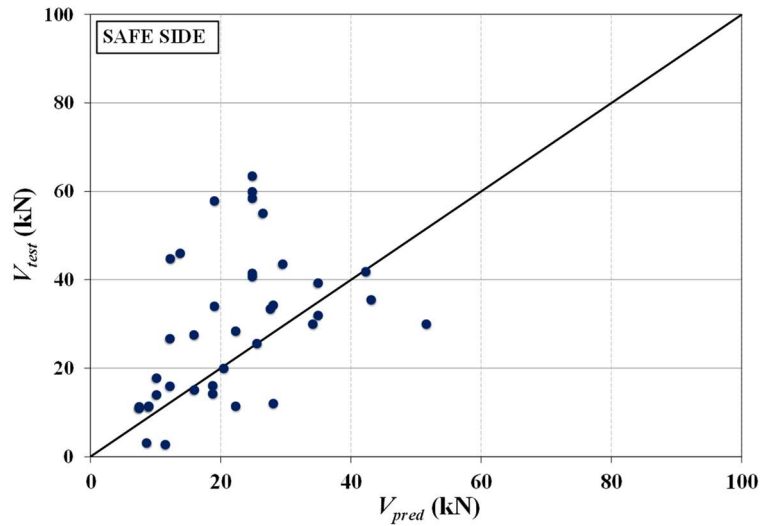
Figure 4-7 V_{test} vs. V_{pred} for Model 2: DB2
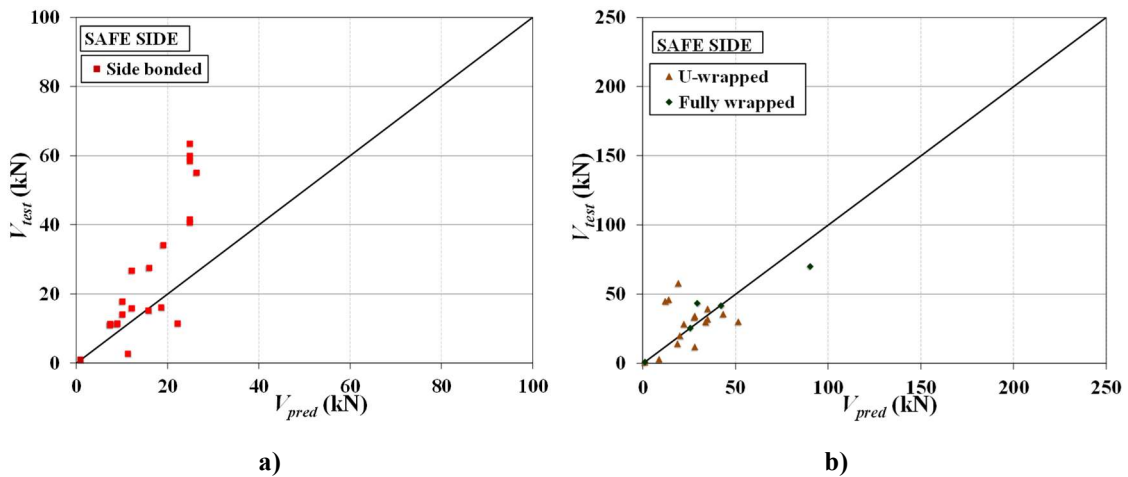
Figure 4-8 V_{test} vs. V_{pred} for Model 2: a) Side bonded configuration; b) U-wrapped and fully wrapped configurations

87

Table 4-2. V_{test}/V_{pred} for Model 2 with DB2

PARAMETER	SPECIMENS	N	AVG	STD	COV$_1$
	Side bonded	20	1.55	0.61	1.24
Strengthening configuration	U-wrapped	15	1.37	1.06	1.17
	Fully wrapped	4	1.06	0.30	1.03
All		39	1.43	0.79	0.89

Results show that Model 2 tends to underestimate (safe) the contribution of the FRCM system to the shear strength, as demonstrated by values of AVG higher than one (see Table 4-2). The model is more conservative for beams strengthened using a side bonded configuration. For the case of fully wrapped beams, the average V_{test}/V_{pred} is slightly higher than 1.0, which implies a good agreement between predicted and experimental values. However, it is worth noting that only four fully wrapped specimens are included in DB2.

For Model 2, the effective strain in the fibers can be computed from the value of V_{test} by rearranging Eq. (4-19) in the form of Eq. (4-22):

$$\varepsilon_{eff} = \frac{V_{test}}{2nE_f t_f d_f (cot\alpha + cot\theta)sin^2\alpha} \qquad 4\text{-}22$$

In Figure 4-9, values of the ratio $\varepsilon_{eff}/\varepsilon_{fu}$ are plotted against $\rho_f E_f/f'^{2/3}_c$, where ε_{eff} is calculated using Eq. (4-22), and are shown as "calculated" in the graph. Figure 4-9 also includes the curves for the normalized values of ε_{eff} computed using Eqs. (4-20) and (4-21). The same information is presented in Figure 4-10, but DB2 has been divided according to the strengthening configuration. Eqs. (4-20) and (4-21) have a better agreement with the experimental results for the case of U-wrapped and fully wrapped strengthening configurations than for side bonded configuration.
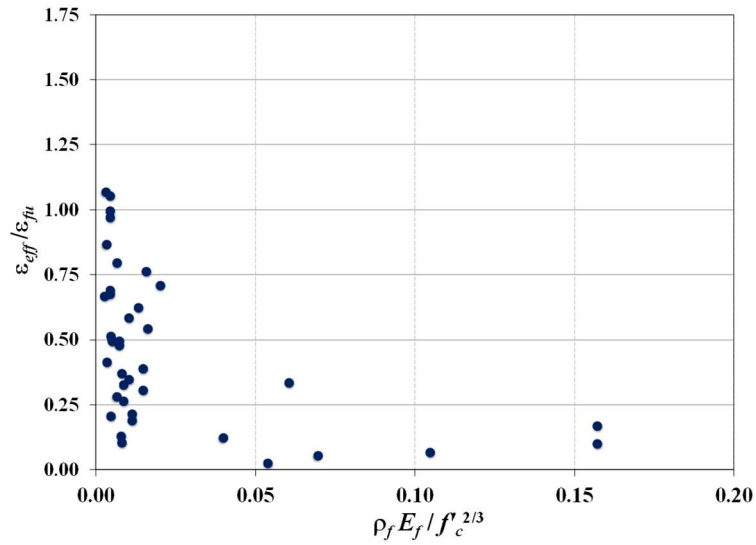
Figure 4-9 Normalized fiber strain $\varepsilon_{eff}/\varepsilon_{fu}$ vs. $\rho_f E_f/f'^{2/3}_c$ for Model 2: DB2
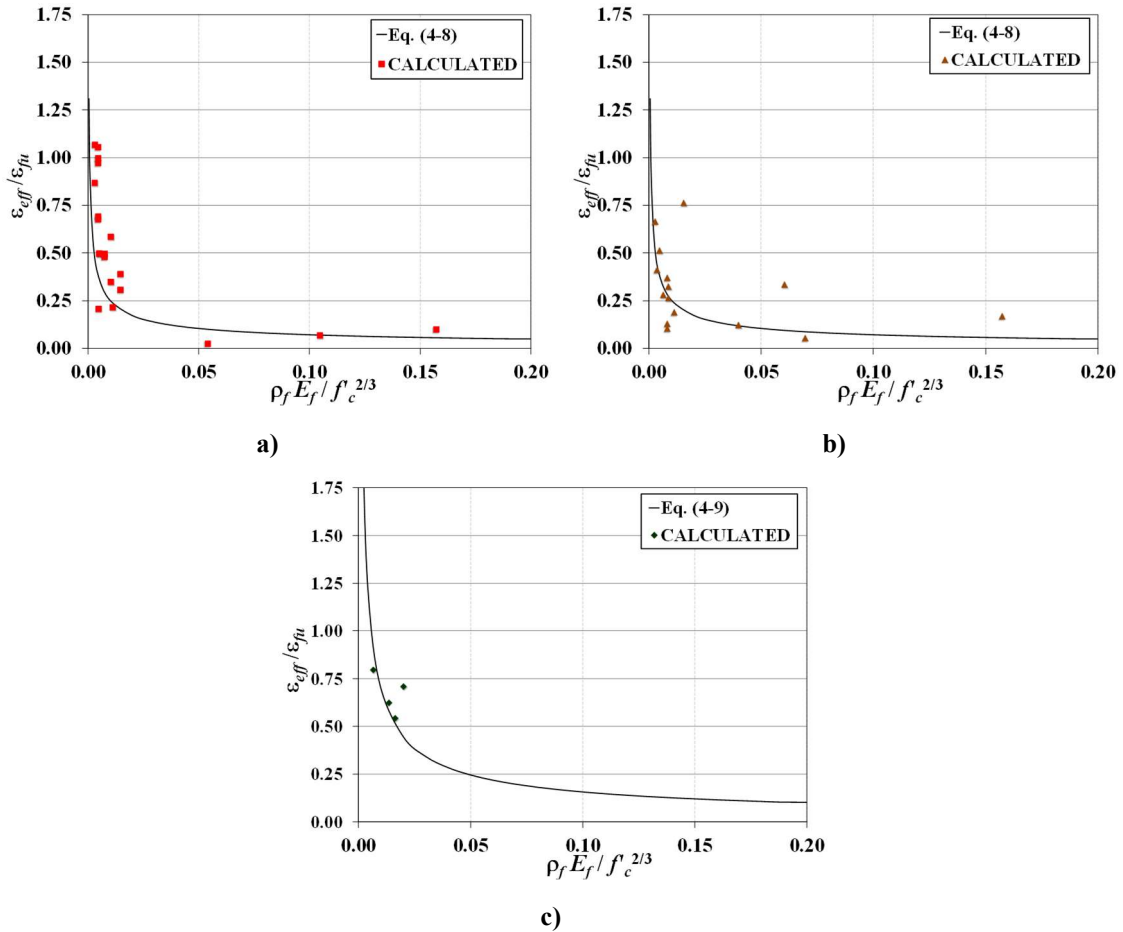
Figure 4-10 Normalized fiber strain $\varepsilon_{eff}/\varepsilon_{fu}$ vs. $\rho_f E_f/f'^{2/3}_c$ for Model 2: a) Side bonded configuration; b) U-wrapped configuration; c) Fully wrapped configuration

4.2.2 Models based on the properties of the FRCM composite

- **Model 3 (ACI 549.4R** [44]**)**

The ACI 549.4R guideline [44] is currently the only guide for design and construction of FRCM systems. However, it is based on few experimental tests, and the guidelines note that the equations require further validation.

According to Model 3, the contribution to the shear strength of RC beams by continuous FRCM U-wrapped or continuous fully wrapped composite is computed using Eq. (4-23):

$$V_{FRCM} = nA_f\sigma_{eff}d \qquad\qquad \text{4-23}$$

In Eq. (4-23), A_f is the area of mesh reinforcement per unit width effective in shear, and the other variables were defined previously. The so-called design tensile strength of the FRCM shear reinforcement σ_{eff} depends on the so-called design tensile strain of the reinforcement ε_{eff} and the tensile modulus of elasticity of the cracked FRCM composite material E_{FRCM}, and is computed using Eqs. (4-24) and (4-25):

$$\varepsilon_{eff} = \varepsilon_{FRCM,u} \leq 0.004 \qquad\qquad \text{4-24}$$

$$\sigma_{eff} = E_{FRCM}\varepsilon_{eff} \qquad\qquad \text{4-25}$$

Eq. (4-24) limits the maximum strain to the lesser of the ultimate tensile strain of FRCM composite $\varepsilon_{FRCM,u}$ and 0.004. Unfortunately, the guideline does not discuss evidence behind the 0.004 limit and/or the type of failure that is intended to be prevented by imposing this limitation. However, it is worth noting that the ACI 440.2R guide [39] imposes the same limitation for FRP composite strengthening systems to preclude the loss of aggregate interlock or delamination of FRP from the substrate for completely wrapped and two- or three-sided wrapping configurations.

Figure 4-11 plots V_{test} vs. V_{pred} using Model 3 for the tests included in DB3, while in Figure 4-12 the database is divided according to the failure mode attained by the RC beams. It is noted that all specimens in DB3 were strengthened using a U-wrapped configuration, and therefore, a plot of V_{test} vs. V_{pred} with DB3 divided according to the strengthening configuration is not included. Table 4-3 summarizes

values of AVG, STD, and COV_1. For beams that failed by detachment of the strengthening system, points are almost equally divided above and below the V_{test}/V_{pred}=1.0 line, although an AVG=1.22 is obtained (Table 4-3). For beams that did not show detachment of the FRCM composite from the substrate, all points plot above the V_{test}/V_{pred} =1.0 line with AVG= 3.70. Regarding the accuracy of the model, results in Figure 4-12 and Table 4-3 show that it is highly affected by the failure mode. The COV_1 for beams with detachment is considerbly lower (0.68) than that of beams with no detachment (3.02). However, it is important to highlight that the six tests that comprise the no detachment subgroup are from a single reference [17], which might influence the performance of the model for this subgroup, for both AVG and COV_1 parameters.
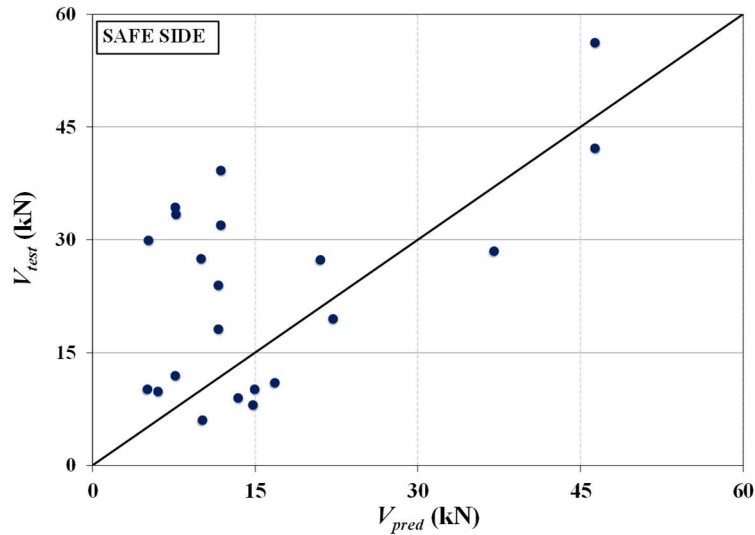
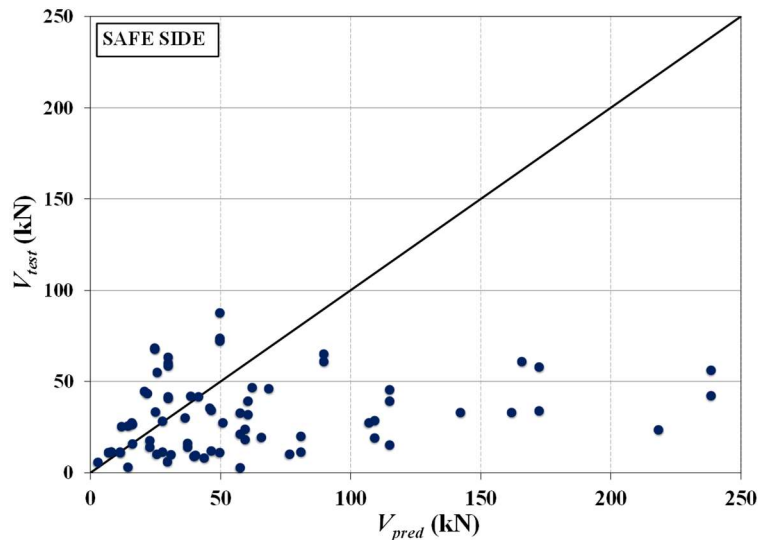

Figure 4-11 V_{test} vs. V_{pred} for Model 3: DB3

a)   b)
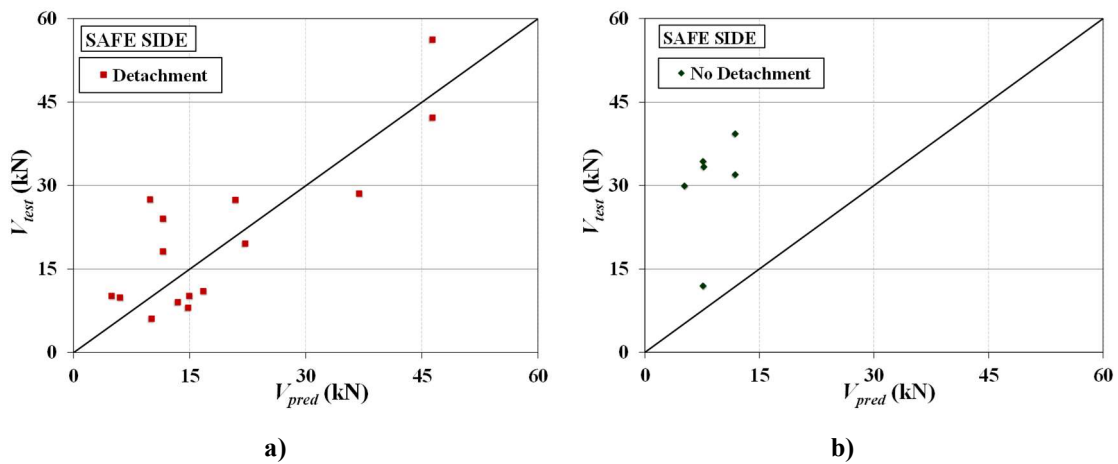
**Figure 4-12** V_{test} vs. V_{pred} for Model 3: a) Detachment; b) No detachment

91

Table 4-3. V_{test}/V_{pred} for Model 3 with DB3

PARAMETER	SPECIMENS	N	AVG	STD	COV_1
Failure mode	Detachment	15	1.22	0.67	0.68
	No Detachment	6	3.70	1.49	3.02
	All	21	1.93	1.48	1.71

A possible explanation of performance of the model could be related to the limitation of design strain imposed by the model. In fact, when Eq. (4-24) is applied to the 21 tests in DB3, the limiting value of 0.004 controls the value of ε_{eff} for each beam, i.e., $\varepsilon_{FRCM,u}$ is always higher than the limit imposed by the model.

Rearranging Eq. (4-23), Eq. (4-26) can be used to determine the effective strain in the FRCM composite from the value of V_{test}:

$$\varepsilon_{eff} = \frac{V_{test}}{nA_f E_{FRCM} d} \qquad 4\text{-}26$$

It is worth noting that in Eq. 4-26, ε_{eff} corresponds to the effective strain in the FRCM composite and not in the fiber. Values of $\varepsilon_{eff}/\varepsilon_{fu}$ are plotted against $\rho_f E_{FRCM}/f'_c{}^{2/3}$ for all tests in DB3 in Figure 4-13 and divided according to the failure mode in Figure 4-14. In Figure 4-13 and Figure 4-14, values of ε_{eff} are calculated using Eq. (4-26), and are shown as "calculated" in the graphs. Figure 4-13 and Figure 4-14 also include the strains used to compute V_{pred}, normalized by the ultimate strain of the FRCM composite, shown as "Model 3" in the graphs.
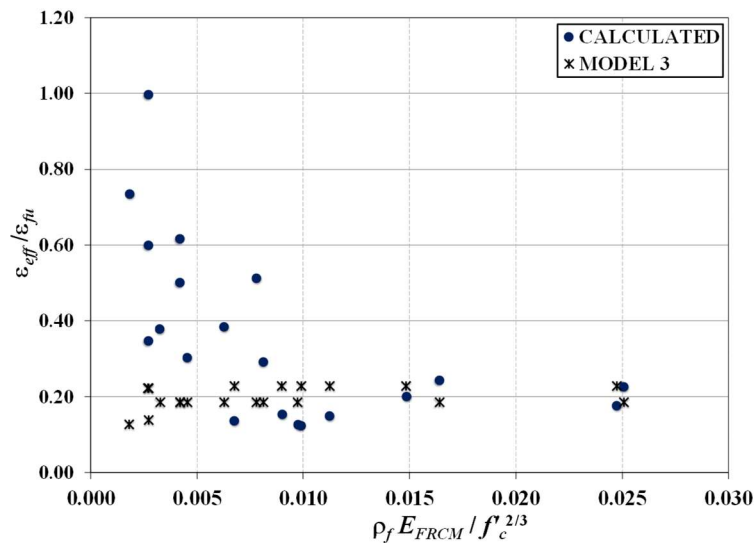
Figure 4-13 Normalized fiber strain $\varepsilon_{eff}/\varepsilon_{fu}$ vs. $\rho_f E_f/f'_c{}^{2/3}$ for Model 3: DB3
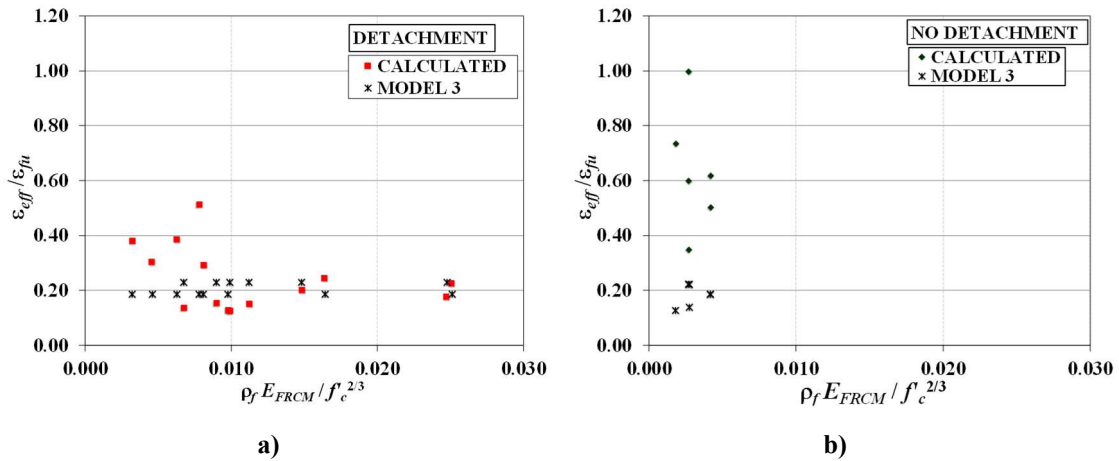
Figure 4-14 Normalized fiber strain $\varepsilon_{eff}/\varepsilon_{fu}$ vs. $\rho_f E_f/f'_c{}^{2/3}$ for Model 3: a) DB3-Detachment; b) DB3-No detachment

Figure 4-13 shows that strains calculated by the model are always lower than 25% of the ultimate strain of the fibers. However, while these values appear to agree with the calculated ε_{eff} for larger values of $\rho_f E_{FRCM}/f'_c{}^{2/3}$, they do not agree for small values of $\rho_f E_{FRCM}/f'_c{}^{2/3}$. The agreement between the calculated and predicted strains is clearer for beams that failed due to detachment of the FRCM system. All beams that failed by detachment have values of $\rho_f E_{FRCM}/f'_c{}^{2/3}$ larger than 0.003, while 66% of the remaining tests (i.e., tests that showed no detachment) present lower values. This suggests that $\rho_f E_{FRCM}/f'_c{}^{2/3}$ influences the failure mode.

- **Model 4 (Ombres** [19]**)**

Model 4 is developed based on the experimental response of seven U-wrapped beams tested by [19]. According to Model 4, V_{FRCM} is computed as:

$$V_{FRCM} = k_e \varepsilon_{eff} E_{FRCM} \rho_f b d_f (cot\alpha + cot\theta)sin\alpha \qquad 4\text{-}27$$

where k_e is an "effectiveness coefficient" taken as 0.5 based on the results by [1,77], and the other variables were defined previously.

The effective strain ε_{eff} is computed based on the formulation adopted by the 2004 Italian CNR-DT 200 Guidelines [78] shown in Eqs. (4-28) and (4-29):

$$\varepsilon_{eff} = \frac{f_{fdd}}{E_{FRCM}}\left[1 - \frac{1}{3}\frac{l_e sin\alpha}{min(0.9d; h_w)}\right] \qquad 4\text{-}28$$

$$f_{fdd} = \frac{0.24}{\gamma_{fd}\sqrt{\gamma_c}}\sqrt{\frac{E_{FRCM}k_b\sqrt{f_{ck}f_{ctm}}}{t_f}} \qquad 4\text{-}29$$

93

where f_{ck} is the concrete characteristic strength, and f_{ctm} is the mean value of concrete tensile strength computed as:

$$f_{fdd} = 0.30 f_{ck}^{2/3}$$

4-30

The partial safety factors, γ_{fd} and γ_c, are set to 1.0 in this analysis. The geometric coefficient k_b is calculated with Eq. (4-30):

$$k_b = \left[\frac{2 - {w_f}/{b}}{1 + {w_f}/{400}} \right]^{0.5}$$

4-31

where b is equal to s_f for discontinuous strips or $0.9d\sin(\theta+\alpha)/\sin\alpha$ for continuous configuration. The ratio w_f/b should be larger than 0.33, otherwise the value of k_b with w_f/b equal to 0.33 shall be adopted. Model 4 uses the expression in the 2004 Italian CNR-DT 200 Guidelines [78] for FRP systems to evaluate l_e and applies it to FRCM systems:

$$l_e = \left[\frac{E_{FRCM} t_f}{2 f_{ctm}} \right]^{0.5}$$

4-32

It should be noted that the term l_e has not yet been clearly defined for the case of FRCM composites. Results have shown that debonding of the FRCM-concrete interface can occur within the composite itself at the fiber-matrix interface, as opposed to the composite-concrete interface with FRP [36]. In fact, for the case of some FRCM composites where debonding is associated with slippage of the fibers relative to the embedding matrix [37], the force transferred between the concrete and the FRCM composite has been shown to increase even after the stress transfer zone (STZ) is fully established because of friction (interlocking) between fibers and the matrix in the portion of the composite where the fibers have debonded [35]. Other work suggests that the concrete strength may not significantly influence the load-carrying capacity of the interface [43]. Therefore, the use of Eq. (4-32) for the case of FRCM composites may not be appropriate and requires further study.

In Figure 4-15, V_{test} is plotted against V_{pred} for Model 4. For beams that failed by detachment, most points fall close to the line $V_{test} / V_{pred} = 1.0$. Figure 4-16a. Figure 4-16b, on the other hand, shows that the model highly underestimates the contribution of the FRCM system in the overall shear strength of beams with no detachment.
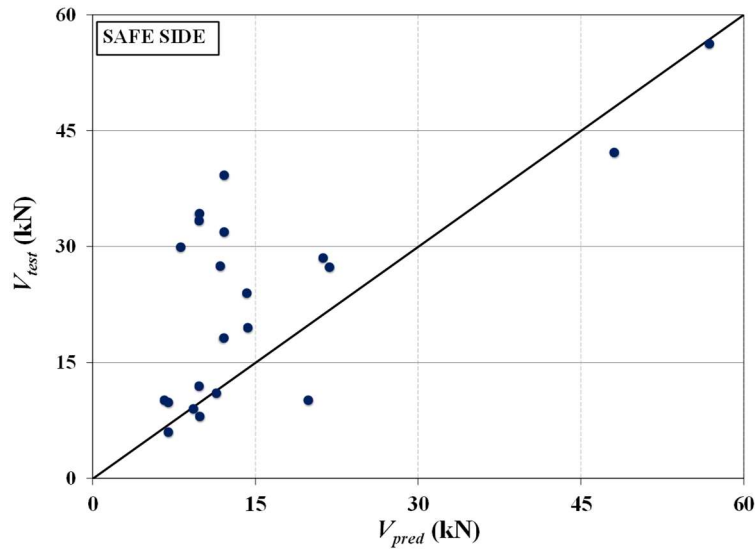
Figure 4-15 V_{test} vs. V_{pred} for Model 4: DB3
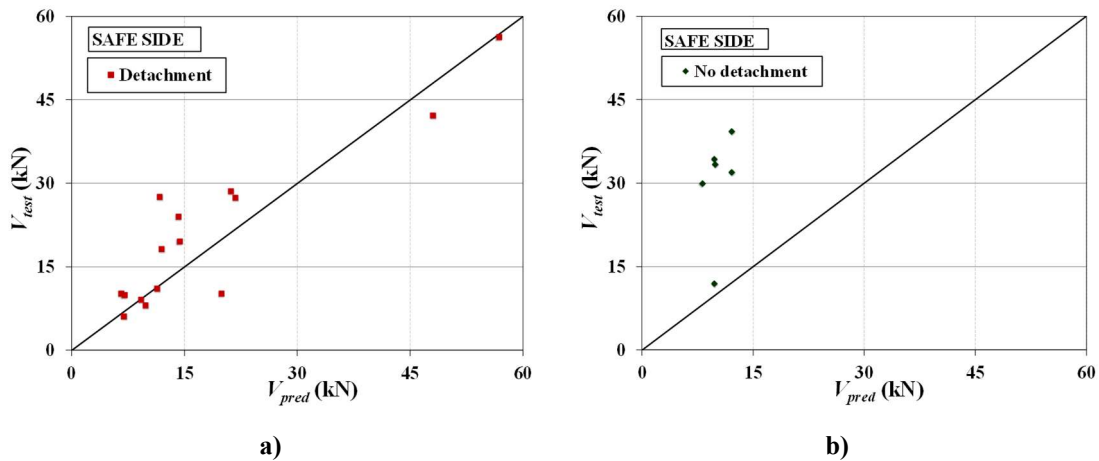
Figure 4-16 V_{test} vs. V_{pred} for Model 4: a) DB3-Detachment; b) DB3-No detachment

Table 4-4 presents the values of AVG, STD, and COV$_1$ determined for Model 4 and the tests in DB3. For beams that failed by composite detachment, the model predicts V_{FRCM} with good accuracy with AVG=1.23 and COV$_1$=0.49. It is worth pointing out that five out of the 15 tests available are from [19] and therefore were used to calibrate Model 4. For beams with no detachment, the model tends to highly understimate the contribution of the FRCM system, and the accuracy is relatively low. The poorer performance of the model for beams with no detachment negatively affects the performance of the model when all 21 available tests are evaluated, as infered by the values of AVG and STD.

Table 4-4. V_{test}/V_{pred} for Model 4 with DB3

PARAMETER	SPECIMENS	N	AVG	STD	COV$_1$
Failure mode	Detachment	15	1.23	0.45	0.49
	No Detachment	6	2.94	0.92	2.11
All		21	1.72	0.99	1.20

Rearranging Eq. (4-27), the effective strain can be computed from the value of V_{test} using Eq. (4-35):

$$\varepsilon_{eff} = \frac{V_{FRCM}}{k_e \varepsilon_{eff} E_{FRCM} \rho_f b d_f (cot\alpha + cot\theta) sin\alpha} \qquad 4\text{-}33$$

In Figure 4-17 and Figure 4-18, $\varepsilon_{eff}/\varepsilon_{fu}$ ratios are plotted against $\rho_f E_{FRCM}/f'^{2/3}_c$, where ε_{eff} is calculated using Eq. (4-33), and are shown as "calculated" in the graphs. Figure 4-17 and Figure 4-18 also include the normalized values of ε_{eff} computed using Eq. (4-28), shown as "Model 4" in the graph. The behavior of Model 4 follows the same trend as Model 3 discussed above.
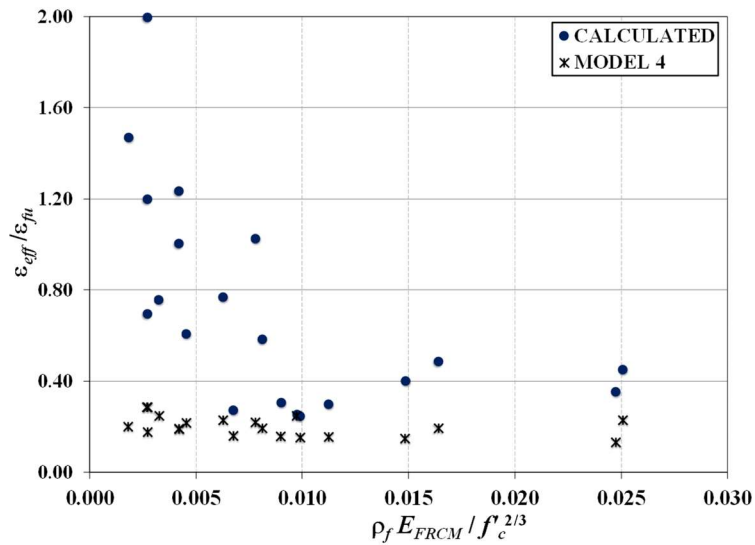
Figure 4-17 Normalized fiber strain $\varepsilon_{eff}/\varepsilon_{fu}$ vs. $\rho_f E_f/f'^{2/3}_c$ for Model 4: DB3
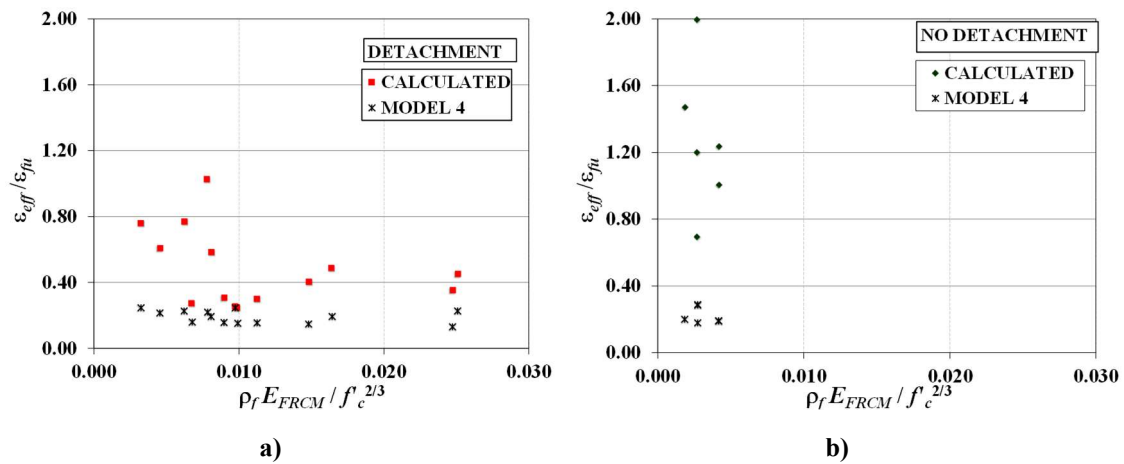
Figure 4-18 Normalized fiber strain $\varepsilon_{eff}/\varepsilon_{fu}$ vs. $\rho_f E_f/f'^{2/3}_c$ for Model 4: a) DB3-Detachment; b) DB3-No detachment

4.2.3   Comparison of the performance for Models 1, 2, 3, and 4

Table 4-5 summarizes values of AVG, STD, and COV_1 determined for the four models studied, divided according to the failure mode attained by the strengthened RC beams. Since different subsets of the entire database were used in the assessment of each model, Table 4-5 includes the database and number of points considered for each analysis. As discussed in Section 4.2 the performance of Models 1 and 2 can be compared using DB2, since specimens in DB2 are common to both models. The performance of Models 1, 3, and 4 can be compared using DB3, since specimens in DB3 are common to all three models.

Table 4-5. V_{test}/V_{pred} for all models with different databases: Failure mode

DB	MODEL	FAILURE MODE	N	AVG	STD	COV1
		Detachment	40	0.66	0.74	0.79
1	1	No detachment	39	1.05	0.80	0.73
		All	79	0.85	0.75	0.76
2	1	Detachment	39	1.05	0.80	0.73
	2			1.43	0.79	0.89
	1			0.28	0.11	0.73
	3	Detachment	15	1.22	0.67	0.68
	4			1.23	0.45	0.49
	1			0.72	0.36	0.43
3	3	No detachment	6	3.70	1.49	3.02
	4			2.94	0.92	2.11
	1			0.40	0.29	0.64
	3	All	21	1.93	1.48	1.71
	4			1.72	0.99	1.20

97

In general, although based on limited experimental evidence, Model 1 presents a more consistent behavior in terms of COV_1 for both failure modes within all the databases. In addition, for the cases of beams that did not fail by detachment of the FRCM composite, it has the value of AVG closest to 1.0 for all the analyzed subsets of the databases.

Although it was calibrated using a larger database, the AVG value obtained by Model 2 (1.43) is larger than the value obtained by Model 1 (1.05) when the common dataset DB2 is considered. The fact that Model 2 is only recommended for beams in which composite detachment is prevented limits its applicability.

When DB3 is analyzed, Models 3 and 4 have values of AVG closest to 1.0 considering only beams that failed due to detachment (1.22, and 1.23, respectively). However, these models were not capable of accurately predicting the FRCM composite shear contribution for beams that did not show detachment as large values of AVG and COV_1 are obtained for the database subset comprised of those beams. In fact, the largest AVG is found for Model 3 (3.70) for beams that did not show detachment. Model 1 tends to highly overestimate the contribution of the FRCM system for beams that showed detachment with AVG values as low as 0.28 (DB3). Considering tests with both failure modes, Model 3 has an AVG of 1.87, which is somewhat misleading since its performance is highly affected by failure mode.

Table 4-6 summarizes values of AVG, STD, and COV_1 determined for the four models studied, divided according to the strengthening configuration of the RC beams. As expressed above, all points in DB3 correspond to U-wrapped beams, and therefore it is only possible to evaluate the performance of Models 3 and 4 for this type of strengthening configuration.

For the side bonded strengthened beams included in DB2, results in Table 4-6 show that Model 1 presents a better performance than Model 2 in terms of AVG and COV_1. This result was not anticipated considering that Model 1 was calibrated using the results of a single fully wrapped beam, while Model 2 included values obtained of beams strengthened using a side bonded configuration.

For U-wrapped beams, Model 1 consistently overestimates the contribution of the FRCM jacket for all the three considered databases. Models 2, 3, and 4, on the other hand, underestimate the FRCM contribution for configuration-wrapped beams. When the models are compared in terms of COV_1, lower values of this parameter are found for Model 1, for both DB2 and DB3.

For fully wrapped beams, the best performance is achieved by Model 2, both in terms of AVG and COV_1. However, it is worth noting that only four fully wrapped beams are included in DB2, and therefore, further experimental evidence is required to validate the model.

Table 4-6. V_{test}/V_{pred} for all models with different databases: Strengthening configuration

DB	MODEL	STRENGTHENING CONFIGURATION	N	AVG	STD	COV_1
1	1	Side bonded	29	1.24	0.79	0.81
		U-wrapped	44	0.51	0.47	0.68
		Fully wrapped	6	1.50	1.04	1.07
		All	79	0.85	0.75	0.76
2	1	Side bonded	20	1.13	0.68	0.67
	2			1.55	0.61	0.81
	1	U-wrapped	15	0.68	0.53	0.60
	2			1.37	1.06	1.09
	1	Fully wrapped	4	2.01	0.87	1.26
	2			1.06	0.30	0.26
	1	All	39	1.05	0.80	0.73
	2			1.43	0.79	0.89
3	1	U-wrapped	21	0.40	0.29	0.64
	3			1.93	1.48	1.71
	4			1.72	0.99	1.20

4.3   Comparison of predicted and measured fiber strains

In this section, values of predicted and measured fiber strains are compared. In order to do so, Eq. (4-34) is used to compute the value of ε_{fe} from the contribution of the jacket V_f (see Table 3-3), and the diagonal crack angle θ for the beams without anchors and that failed in shear presented in Section 3 since Eq. (1) does not explicitly include the effect of anchors.

$$\varepsilon_{fe} = \frac{V_f}{\rho_f E_f d_{fv} b_w \cot(\theta)} \qquad \text{4-34}$$

In Eq. (4-34), V_f is the experimental hear strength provided by the strengthening system, computed as the maximum shear of the strengthened specimen minus the maximum shear of the corresponding control specimen, as discussed in Section 3.2. In Eq. (4-34), d_{fv} is assumed equal to $0.9d$, i.e. the method in [56] is adopted.

Table 4-7 summarizes the values of ε_{fe} calculated for the strengthened beams in this study considering the experimental values of V_f and θ, and considering only those fibers oriented perpendicular to the longitudinal axis of the beam. Table 4 includes also experimental values for θ, the maximum strain recorded in the fibers $\varepsilon_{f,max}$, and the ratios $\varepsilon_{fe}/\varepsilon_{f,max}$, $\varepsilon_{fe}/\varepsilon_{fu}$, and $\varepsilon_{f,max}/\varepsilon_{fu}$

Table 4-7. Comparison of predicted and measured fiber strains

BEAM	θ (°)	V_f(kN)	ε_{fe} (με)	$\varepsilon_{f,max}$ (με)	$\varepsilon_{fe}/\varepsilon_{f,max}$	$\varepsilon_{fe}/\varepsilon_{fu}$ (%)	$\varepsilon_{f,max}/\varepsilon_{fu}$ (%)
S1-FRP-F2-UN	35	38.2	1304	5787	0.23	5.9	26.3
S1-FRCM-F3-UN	25	27.2	2499	4825	0.52	13.9	26.8
S1-FRCM-F4-UN	29	34.5	828	1921*	0.43	5.2	12.0
S2-FRCM-F3-UN	23	24.3	2032	2686	0.76	11.3	14.9
S2-FRCM-F4-UN	39	17.5	614	1721*	0.36	3.8	10.8

*Maximum recorded value was prior to maximum load due to local debonding of the composite

Results in Table 4-7 show that values of ε_{fe} calculated using Eq. (4-34) with the aforementioned assumptions are considerably lower than the maximum measured fiber strains. This can be explained, in part, by the fact that Eq. (4-34) assumes a constant value of strain in the fibers along the shear crack, whereas measured values are determined at discrete locations. Additionally, the experimental value of V_f is computed as the shear strength of the strengthened beam minus the shear strength of the control beam. However, as discussed previously in Section 3.8, due to the internal-external shear reinforcement interaction, the contribution of the stirrups to the shear strength is lower in strengthened beams in which the steel shear reinforcement did not yield as compared to control beams in which the steel shear reinforcement yielded, which implies a higher force in the external shear strengthening than that computed in this manner. In fact, the largest difference between the calculated and measured strains occurs for beam S1-FRP-F2-UN in which the stirrups did not yield.

For FRCM strengthened beams, information on determining the effective strain in the composite is currently limited, especially for beams strengthened with a U-wrapped or side bonded configuration. Furthermore, information on the FRCM composite-to-concrete bond capacity is also limited in the technical literature. Thus, expressions to determine ε_{fe} for FRCM composites are in need of development. For the carbon FRCM strengthened beams in this study (S1-FRCM-F3-UN and S2-FRCM-F3-UN), Table 4-7 shows that ε_{fe} computed using the procedure described above range from approximately 2000 με to 2500 με, with a

corresponding fiber exploitation ratio $\varepsilon_{fe}/\varepsilon_{fu}$ of 11.3-13.9%. Values of ε_{fe} from this study are in general agreement with those in [36], who reported values of ε_{fe}, determined in an analogous manner, of 1200 $\mu\varepsilon$ to 2200 $\mu\varepsilon$ ($\varepsilon_{fe}/\varepsilon_{fu}$ of approximately 7%) for U-wrapped carbon FRCM strengthened beams.

Compared to the carbon FRCM strengthened beams, lower values of effective strain (ε_{fe}=614 $\mu\varepsilon$ to 828 $\mu\varepsilon$) and fiber exploitation ratio ($\varepsilon_{fe}/\varepsilon_{fu}$=3.8-5.2%) were determined for the steel FRCM strengthened beams (S1-FRCM-F4-UN and S2-FRCM-F4-UN).

In Table 4-8, values of strain predicted by Models 1 and 2 (named $\varepsilon_{fe,M1}$ and $\varepsilon_{fe,M2}$, respectively) are compared to the fiber strains measured for FRCM-strengthened beams tested in this work.

Table 4-8. Comparison of Model 1 and Model 2 predicted strains and measured strains

BEAM	$\varepsilon_{f,max}$ ($\mu\varepsilon$)	Model 1		Model 2	
		$\varepsilon_{fe,M1}$ ($\mu\varepsilon$)	$\varepsilon_{f,max}/\varepsilon_{fe,M1}$	$\varepsilon_{fe,M2}$ ($\mu\varepsilon$)	$\varepsilon_{f,max}/\varepsilon_{fe,M2}$
S1-FRCM-F3-UN	4825	9000	0.54	3237	1.49
S1-FRCM-F4-UN	1921*	8000	0.24	1210	1.59
S2-FRCM-F3-UN	2686	9000	0.30	3307	0.81
S2-FRCM-F4-UN	1721*	8000	0.22	1210	1.42

*Maximum recorded value was prior to maximum load due to local debonding of the composite

For U-wrapped strengthened beams, results in Table 4-6 had shown that Model 1 tends to overestimate the contribution of the FRCM system to the shear strength, i.e., values of AVG lower than one for all the databases subsets studied. These results are confirmed by the values of $\varepsilon_{f,max}/\varepsilon_{fe,M1}$ in Table 4-8, which indicate that effective strains predicted by Model 1 are considerably higher than those measured in the fibers by the strain gauges. It can be observed that for the case of carbon-FRCM strengthened beams S1-FRCM-F3-UN and S2-FRCM-F3-UN, values of $\varepsilon_{f,max}/\varepsilon_{fe,M1}$ vary depending on the beam series, i.e., internal reinforcement ratio. For steel-FRCM strengthened beams S1-FRCM-F4-UN and S2-FRCM-F4-UN, on the other hand, values of $\varepsilon_{f,max}/\varepsilon_{fe,M1}$ do not show a significant variation among the two series, although marginally higher values were observed for the S1 beam.

Unlike Model 1, Model 2 predicted values of ε_{fe} that are lower than $\varepsilon_{f,max}$, with the exception of beam S2-FRCM-F3-UN. These results agree with the value of AVG reported for Model 2 for U-wrapped configurations in Table 4-6, which indicate that the model underestimates the contribution of the FRCM system. Similar to Model 1, for carbon-FRCM strengthened beams, values of $\varepsilon_{f,max}/\varepsilon_{fe,M2}$ vary

depending on the internal reinforcement ratio, while for steel-FRCM strengthened beams, the influence of this parameter is negligible. It is worth noting that for both steel-FRCM strengthened RC beams, detachment of the composite at the composite-concrete interface was observed, and a different variation of $\varepsilon_{f,max}/\varepsilon_{fe,M2}$ might be expected if detachment had been avoided.

Values of $\varepsilon_{f,max}/\varepsilon_{fe,M2}$ determined using Model 2 are closer to unity than those determined using Model 2. This result was expected as Model 2 was developed considering a larger experimental set of data and U-wrapped strengthened beams. However, the results of the analysis show that additional parameters, such as the internal reinforcement ratio, need to be considered to developed more accurate and reliable design models.

4.4   Predicted shear strength of the unstrengthened beams

To evaluate the overall shear strength of the FRCM-strengthened beams, it is necessary to compute the shear strength of the unstrengthened (control) specimens as the additional strength given by the FRCM system is added to that of the unstrengthened specimens. As expressed before, the shear behavior of reinforced concrete structures is quite complex, and several efforts has been carried out in the past in order to obtain expressions that can predict the shear behavior of RC beams with accuracy. These efforts have allowed the development of different models for predicting the shear strength of RC beams such as truss models with concrete contribution, shear/compression theories, truss models with variable angle of inclination, and compression field [79]. Some of these models, such as the modified compression field theory (MCFT) [80], provide a rational method of analysis and design, but are too complex for regular use in the shear design of beams [81] and have been simplified in order to be implemented in design standards [82]. In some cases, such simplifications might imply that the models neglect important key variables, which results in a reduction of their accuracy [79]. In addition, some of the proposed models need further validation before they can be used safely and confidently by design engineers.

In this section, two available codes used for the design of concrete structures were chosen to compute the shear strength of the unstrengthened beams: ACI 318-14 [83] and Eurocode 2 [56]. The assessment of these codes is carried out with a database of control specimens (DB4) collected from the journal papers included in Table 2-1 and presented in Annex 2.

4.4.1 ACI 318-14

According to the ACI 318-14 code [83], the nominal one-way shear strength, V_n, shall be computed as:

$$V_n = V_c + V_s \tag{4-35}$$

In Eq. (4-35), the concrete (V_c) and internal steel (V_s) contributions are computed as follows:

$$V_c = 0.17\sqrt{f_c'}b_w d \tag{4-36}$$

$$V_s = \frac{A_w f_{yw} d}{s} \tag{4-37}$$

It is noted that for beams without stirrups, V_n is taken equal to V_c. Figure 4-19 compares the test (V_{test}) vs. predicted (V_{pred}) values for the control beams in the database. In Figure 4-19, beams are divided depending on beams with or without stirrups. Values of AVG, STD, and COV$_1$ are presented in Table 4-9.
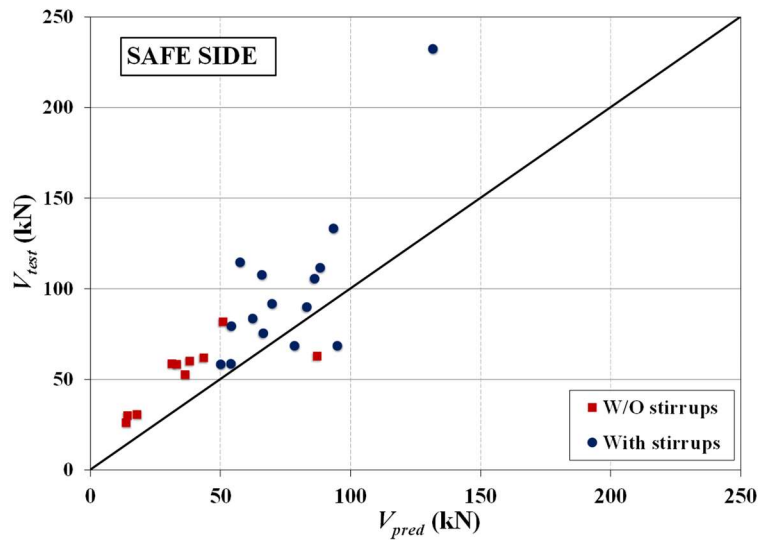
Figure 4-19 V_{test} vs. V_{pred} for ACI 318-14

Table 4-9. Values of AVG, STD, and COV$_1$ for ACI 318-14 model

MODEL	SPECIMENS	N	AVG	STD	COV$_1$
	W/O stirrups	10	1.60	0.37	0.69
ACI 318-14	With stirrups	15	1.30	0.33	0.43
	All	25	1.42	0.37	0.55

Figure 4-19 shows that the equations given in the ACI 318-14 code mainly predict safe results for beams with and without stirrups included in the database, as most points fall above the $V_{test}/V_{pred}=1.0$. These results are corroborated by the values of AVG included in Table 4-9 that are higher than 1.0 for all the three cases considered. However, it is worth noting that higher values of AVG are obtained for beams without stirrups. It is also interesting to note that a higher value of COV_1, which indicates a lower accuracy, is also found for beams without stirrups.

4.4.2 Eurocode 2

For beams without stirrups, the value of shear strength ($V_{Rd,c}$) is computed using the following expression in the Eurocode 2 model [56] for members not requiring design shear reinforcement without acting axial forces:

$$V_{Rd,c} = C_{Rd,c}k(100\rho_l f_{ck})^{1/3}b_w d \qquad \text{4-38}$$

with a minimum of:

$$V_{Rd,c} = 0.035k^{3/2}f_{ck}^{1/2}b_w d \qquad \text{4-39}$$

where $C_{RD,c}$ is taken equal to 0.18, k is given by Eq. (4-40), f_{ck} is the characteristic concrete cylinder compressive strength, and the other variables were defined previously.

$$k = 1 + \sqrt{\frac{200}{d}} \leq 2.0 \; with \; d \; in \; mm \qquad \text{4-40}$$

For members with stirrups, the shear strength, V_{Rd}, is the smaller value of:

$$V_{Rd,s} = \frac{A_w f_{yw} z}{s} cot\theta \qquad \text{4-41}$$

and,

$$V_{Rd,max} = \frac{\alpha_{cw} b_w z v_1 f_{cd}}{cot\theta + tan\theta} \qquad \text{4-42}$$

where α_{cw} is taken equal to 1.0, v_1 is equal to 0.6 for values of f_{ck} lower than 60 MPa (all specimens in the database), θ may vary between 21.8° and 45°, and the other variables were defined previously.

The assessment of the expressions given by [56] is made using two different approaches. In the first one, named EC2-FA, a fixed value of the angle θ equal to

45° is used. In the second approach, named EC2-VA, the angle varies between the limits recommended by the code and defined above. For the latter case, the value of θ is computed using Eq. (4-43), which is found assuming that $V_{Rd,s}$ is equal to $V_{Rd,max}$ which gives the following expression for θ:

$$\theta = arcsin\left[\left(\frac{A_w f_{yw}}{b_w s v_1 f_{cd}}\right)^{1/2}\right] \qquad 4\text{-}43$$

If a value of θ lower than 21.8° is obtained, θ equal to 21.8° should be used. It is worth noting that assuming either a fixed or variable value of θ will affect only results of beams with stirrups, as the variable θ is not included in the expression for members without internal shear transverse reinforcement, as indicated in Eq. (4-38). It is worth noting that for all beams in DB4, Eq. (4-43) predicts values of θ lower than 21.8°. However, according to the experimental evidence collected, values of θ for control specimens varied between 32° and 44°, as shown in Figure 2-34 (see Section 2.6).

In Figure 4-20 values of V_{test} are plotted against V_{pred} for EC2-FA. Values of AVG, STD, and COV_1 for this model are given in Table 4-10. Results show that the values of shear strength predicted by the EC2 model for beams without stirrups are in good agreement with the experimental values as demonstrated by the values of AVG and COV_1 (see Table 4-10). However, the EC2-FA approach is not able to predict adequately the tests values for beams with stirrups as the model highly underestimates the member shear strength, as demonstrated by the higher value of AVG (3.03). In addition, the model presents a low accuracy as confirmed by the value of COV_1 (2.16).
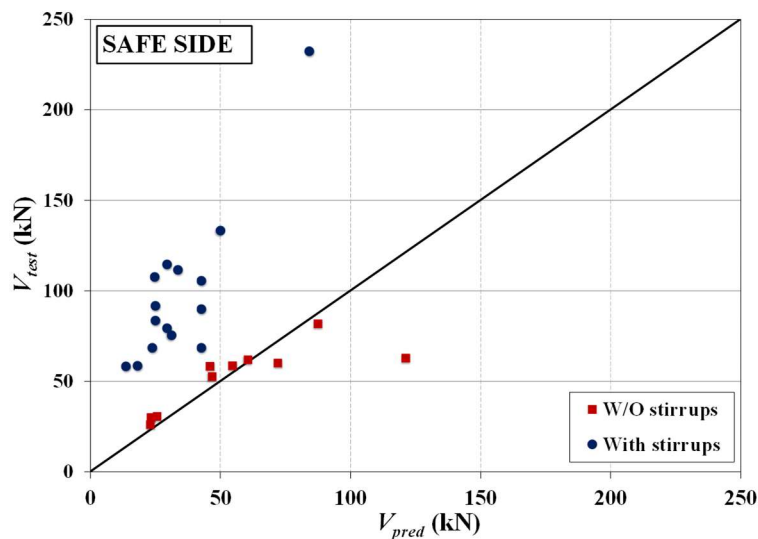
Figure 4-20 V_{test} vs. V_{pred} for EC2-FA

Table 4-10. Values of AVG, STD, and COV_1 for EC2-FA model

MODEL	SPECIMENS	N	AVG	STD	COV_1
	W/O stirrups	10	1.03	0.23	0.22
EC2-FA	With stirrups	15	3.03	0.77	2.16
	All	25	2.23	1.17	1.68

An improvement of the behavior of the EC2 model for beams with stirrups is achieved using variable truss angles, as shown in Figure 4-21 and Table 4-11. In Figure 4-21, the points for beams with stirrups fall closer to the 45° line than for EC2-FA, which corroborates the computed values of AVG included in Table 4-11. In addition, the model also presents relatively low value of COV_1, for both beams with and without stirrups.
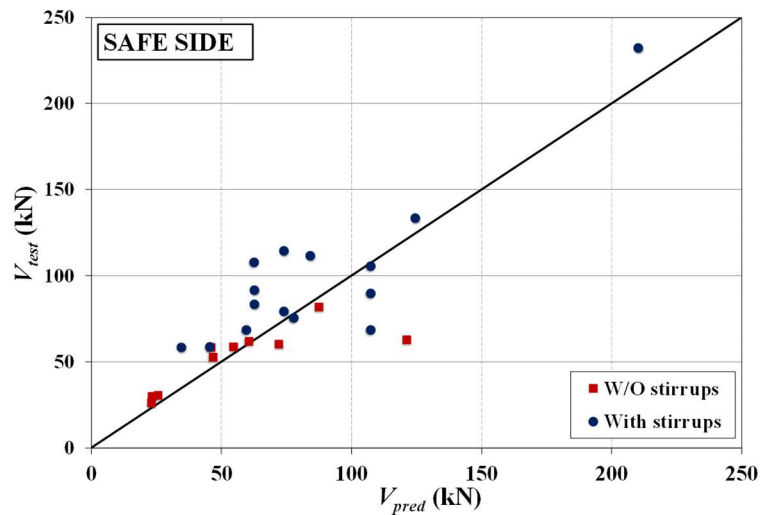
Figure 4-21 V_{test} vs. V_{pred} for EC2-VA

Table 4-11. Values of AVG, STD, and COV_1 for EC2-VA model

MODEL	SPECIMENS	N	AVG	STD	COV_1
	W/O stirrups	10	1.03	0.23	0.22
EC2-VA	With stirrups	15	1.21	0.31	0.36
	All	25	1.14	0.29	0.31

4.4.3   Comparison of the performance for ACI 318-14, EC2-FA, and EC2-VA models

Table 4-12 presents the values of AVG, STD, and COV_1 determined for the three models evaluated in this section. For members without stirrups, the EC2 model shows a better performance than the ACI 318-14 model, both in terms of AVG and COV_1. For the case of beams with stirrups, values of AVG and COV_1 for ACI 318-14 and EC2-VA are similar, although the latter model shows a slightly better performance. When a fixed value of the angle θ equal to 45° is used, highly conservative results are obtained together with a COV_1 value that is significantly higher than those obtained for the other two models. When all control (unstrengthened) specimens of the included in DB4 are studied, the EC2-VA model presents the best performance in terms of AVG and accuracy, followed by the ACI 318-14.

Table 4-12. Values of AVG, STD, and COV_1 for all the models

MODEL	SPECIMENS	N	AVG	STD	COV_1
ACI 318-14			1.60	0.37	0.69
EC2-FA	W/O stirrups	10	1.03	0.23	0.22
EC2-VA			1.03	0.23	0.22
ACI 318-14			1.30	0.33	0.43
EC2-FA	With stirrups	15	3.03	0.77	2.16
EC2-VA			1.21	0.31	0.36
ACI 318-14			1.42	0.37	0.55
EC2-FA	All	25	2.23	1.17	1.68
EC2-VA			1.14	0.29	0.31

4.5   Predicted overall shear strength of FRCM strengthened beams

In this section the performance of the available models for predicting the contribution of the FRCM composites to the shear strength of RC beams is made based on the overall shear strength attained by the members after the strengthening. In order to do so, the predicted shear strength of the control beams, computed according to ACI 318-14 (see Section 4.4.1) and the Eurocode 2 (see Section 4.4.2), is added to the shear contribution of the FRCM jackets predicted by Models 1, 2, 3, and 4 (see Sections 4.2.1 and 4.2.2).

Considering that Models 1, 2, and 4, were developed following the format employed by the Eurocode 2, the overall shear strength of these models will be computed only in combination with this code. On the other hand, the FRCM contribution to the shear strength of the beams computed by Model 3 will be added only to the shear strength of the unstrengthened specimens predicted by the ACI 318-14 code, as they follow the same format. Thus, the following combinations of models will be assessed in this section:

- Model 1 + EC2-FA (or EC2-VA)
- Model 2 + EC2-FA (or EC2-VA)
- Model 3 + ACI 318-14
- Model 4 + EC2-FA (or EC2-VA)

4.5.1   Model 1 + EC2

In Figure 4-22a, V_{test} is plotted against V_{pred} for Model 1 + EC2-FA, while in Figure 4-22b, this information is presented for Model 1 + EC2-FA. Table 4-13 summarizes values of AVG, STD, and COV_1 determined for these cases.

a)

b)
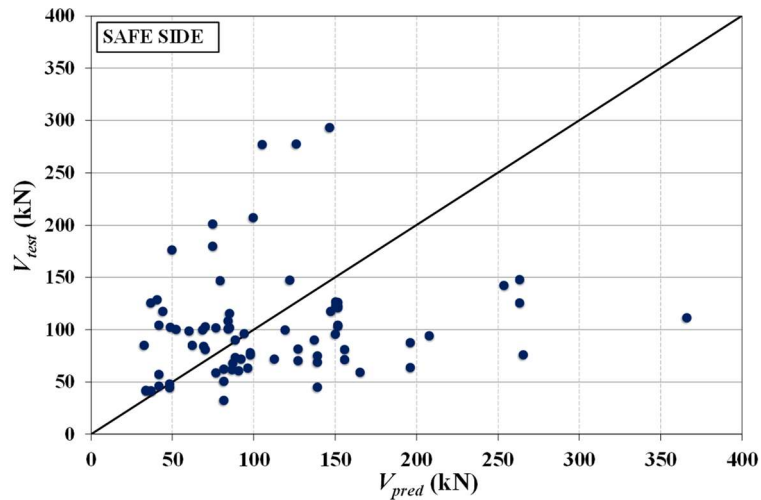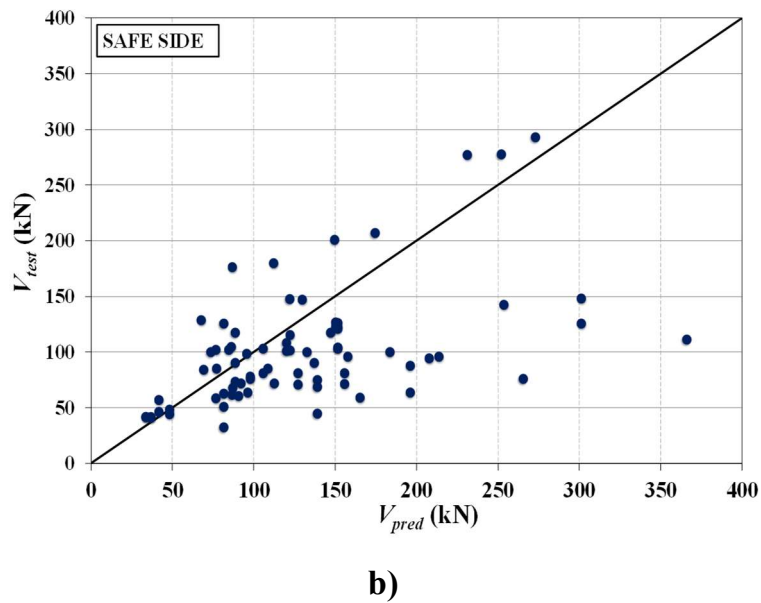
Figure 4-22 V_{test} vs. V_{pred} for: a) Model 1 + EC2-FA; 2) Model 1 + EC2-VA

Table 4-13. Values of AVG, STD, and COV_1 for Model 1+ EC2

MODEL	DB	N	AVG	STD	COV_1
Model 1 + EC2-FA	1	79	1.14	0.77	0.78
Model 1 + EC2-VA			0.85	0.37	0.40

Results show that using Model 1 in combination with EC2-FA slightly overestimates the overall shear strength of the strengthened beams. However, it is worth noting that for the tests including in DB1, Model 1 tends to underestimate the FRCM contribution when the FRCM contribution is determined by subtracting the shear strength of the corresponding control beam from that of the strengthened beam, as shown in Table 4-1. This implies that adding the shear strength of the unstrengthened beam changes the performance of Model 1 from unsafe to safe.

When Model 1 is used in combination with EC2-VA, the overall shear strength is underestimated (AVG=0.85, see Table 4-11). The same is true for Model 1 and the FRCM contribution alone (AVG=0.85, see Table 4-1), but the accuracy of the model increases when Model 1 is used in combination with EC2-VA (COV_1=0.40 for Model 1 + EC2-VA, COV_1=0.76 for Model 1).

4.5.2 Model 2 + EC2

Figure 4-23 presents values of V_{test} vs. V_{pred} for FRCM strengthened beams using Model 2 together with EC2. Table 4-14 summarizes values of AVG, STD, and COV_1 for V_{test}/V_{pred} for Model 2 + EC2-FA and Model 2 + EC2-VA.

Results in Figure 4-23 and Table 4-14 show that both Model 2 + EC2-FA and Model 2 + EC2-VA tend to underestimate (safe) the overall shear strength of the strengthened beams, although a value of AVG closer to 1.0 is found for the latter model combination. A better performance in terms of COV_1 is also observed for Model 2 + EC2-VA. When the performance of Model 2 with or without the control (unstrengthened) beam strength is compared, values in Table 4-14 and Table 4-2 show that a better performance is attained when EC2-FA and EC2-VA predicted strengths are added to Model 2, both in terms of AVG and COV_1.
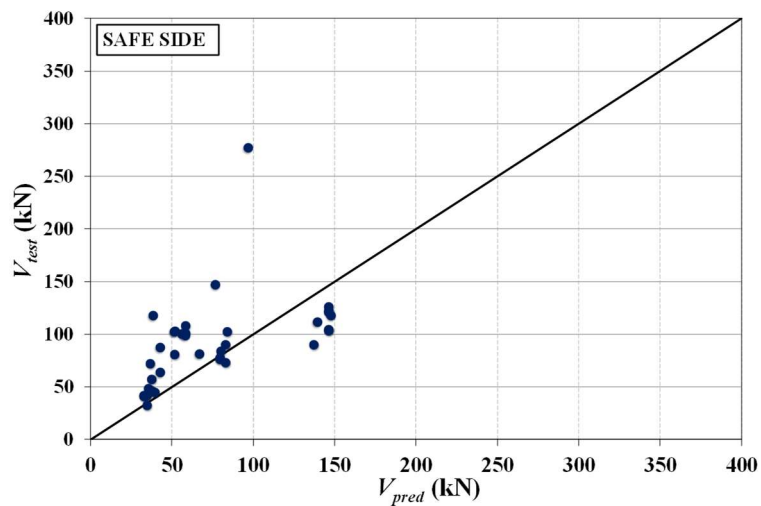
a)
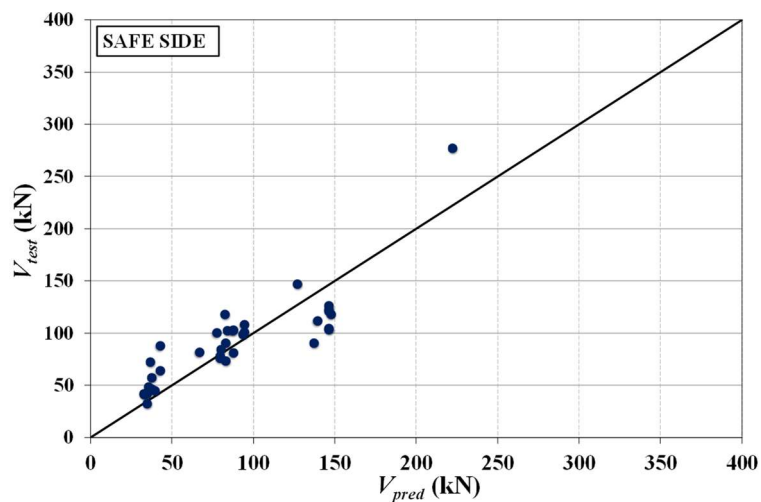
b)

Figure 4-23 V_{test} vs. V_{pred} for: a) Model 2 + EC2-FA; 2) Model 2 + EC2-VA

Table 4-14. Values of AVG, STD, and COV_1 for Model 2+ EC2

MODEL	DB	N	AVG	STD	COV_1
Model 2 + EC2-FA	2	39	1.36	0.56	0.66
Model 2 + EC2-VA			1.13	0.30	0.32

4.5.3 Model 3 + ACI 318-14

Figure 4-24 plots V_{test} vs. V_{pred} using Model 3 in combination with ACI 318-14. In Figure 4-24, the points are mainly distributed above the V_{test}/V_{pred}=1.0 line, with a value of AVG=1.12 (see Table 4-15). When results in Table 4-15 and Table 4-3 are compared, it can be seen that adding the shear strength predicted by ACI 318-14 to the FRCM contribution calculated by Model 3 improves the performance of the Model 3, both in terms of AVG and COV_1.
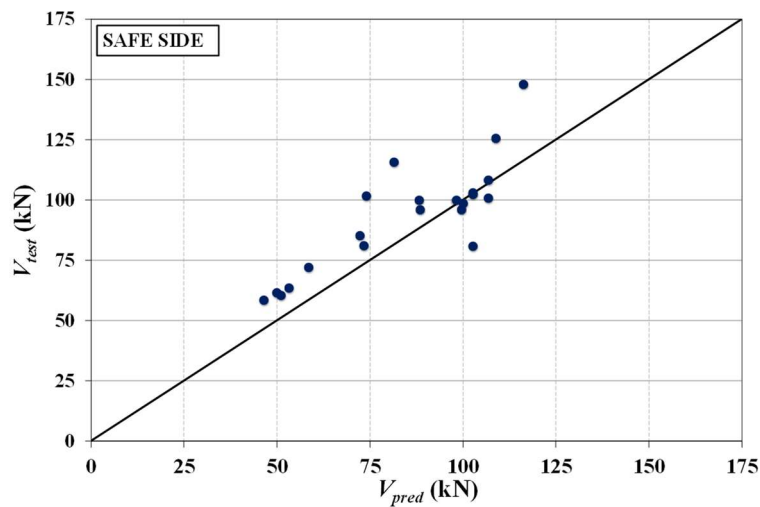
Figure 4-24 V_{test} vs. V_{pred} for Model 3 + ACI 318-14

Table 4-15. Values of AVG, STD, and COV_1 for Model 3+ ACI 318-14

MODEL	DB	N	AVG	STD	COV_1
Model 3 + ACI 318-14	3	21	1.12	0.15	0.19

4.5.4 Model 4 + EC2

V_{test} is plotted against V_{pred} for Model 4 + EC2-FA and Model 4 + EC2-VA in Figure 4-25a and Figure 4-25b, respectively. For Model 4 + EC2-FA, all points

fall above the $V_{test}/V_{pred}=1.0$ line, while for Model 4 + EC2-VA, four points out of 21 tests that comprised DB3 fall below this line. This implies that combining Model 4 with EC2 tends to underestimate (safe) the overall shear strength of the strengthened specimens, which is corroborated by the AVG values shown in Table 4-16. However, a better performance in terms of AVG is observed when Model 4 is combined with EC2-VA than when it is combined with EC2-FA. Combining Model 4 with EC2-VA also improves the performance of the model in terms of AVG and COV_1 when compared to the behavior of Model 4 alone (see Table 4-4).
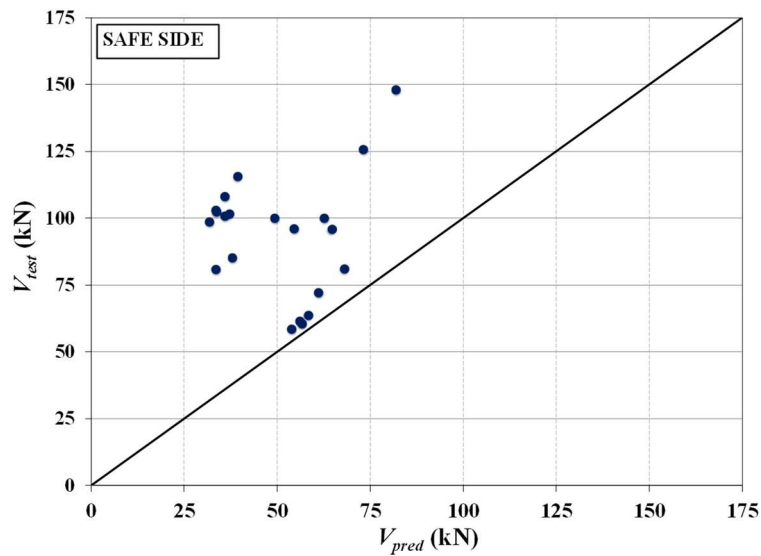
a)
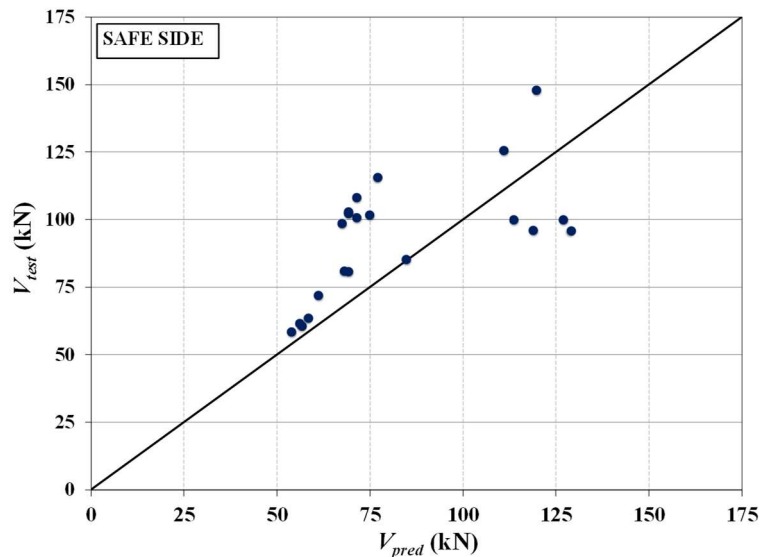
b)

Figure 4-25 V_{test} vs. V_{pred} for: a) Model 4 + EC2-FA; 2) Model 4 + EC2-VA

Table 4-16. Values of AVG, STD, and COV_1 for Model 4 + EC2

MODEL	DB	N	AVG	STD	COV_1
Model 4 + EC2-FA	3	21	2.02	0.77	1.27
Model 4 + EC2-VA			1.17	0.24	0.30

4.5.5 Comparison of the performance for Model 1 + EC2, Model 2 + EC2, Model 3 + ACI 318-14, and Model 4 + EC2

Table 4-17 summarizes values of AVG, STD, and COV_1 determined for the combination of models studied in this section. An improvement on the values of AVG and COV_1 is found when Models 1, 2, and 4 are combined with EC2-VA instead of EC2-FA. This result was anticipated considering that using a variable angle highly improves the performance of the Eurocode 2 model (see Section 4.4.3).

When the performance of Model 3 is assessed, results in Table xx and xxx show that better performance of the model in terms of AVG, and COV_1 is attained when it is combined with the ACI 318-14 instead of evaluated alone. However, it is worth noting that the assessment of this model is made based with a reduced subset of the experimental available experience (DB3). Model 1 + EC2-VA, on the other hand, has a lower variation of COV_1 for the three database subsets although values of AVG vary depending on the considered database.

Table 4-17. Values of AVG, STD, and COV_1 for all models with different databases: Overall shear strength

DB	MODEL	N	AVG	STD	COV1
1	1 + EC2-FA	79	1.14	0.77	0.78
	1 + EC2-VA		0.85	0.37	0.40
2	1 + EC2-FA	39	1.15	0.65	0.66
	2 + EC2-FA		1.36	0.56	0.66
	1 + EC2-VA		0.93	0.34	0.34
	2 + EC2-VA		1.13	0.30	0.32
3	1 + EC2-FA	21	0.74	0.35	0.44
	1 + EC2-VA		0.59	0.18	0.45
	3 + ACI 318-14		1.12	0.15	0.19
	4 + EC2-FA		2.02	0.77	1.27
	4 + EC2-VA		1.17	0.24	0.30

4.6   Conclusions

The database collected in Chapter 2 was used to evaluate the performance of four models for the prediction of the contribution of the shear strength of FRCM composites of RC beams. The performance evaluation was based both in terms of the additional shear strength provided by the FRCM system and the overall shear strength attained after the strengthening. The main conclusions drawn from this study are summarized as follows:

- Although Model 1 overestimates the additional shear strength provided by the FRCM composite, it presents a more consistent performance regarding values of COV_1 when compared with the other models. Models based on FRCM composite properties (Model 3 and 4) perform well for beams that failed by detachment, but they do not perform well for beams with no detachment.

- Although it was calibrated using a larger database, the AVG value obtained by Model 2 (1.43) is larger than the value obtained by Model 1 (1.12) considering a common dataset. In addition, the fact that Model 2 is only recommended for beams in which composite detachment is prevented limits its applicability.

- The use of the properties of the FRCM composite instead of the fiber mechanical characteristics in Models 3 and 4 does not result in a significant increase in accuracy of the models, measured in terms of COV_1. In fact, a simple formulation such as the one proposed by Model 1, based on fiber properties, is more accurate for beams with or without composite detachment.

- Results show that the performance of the models is highly influenced by the type of failure mode attained by the strengthened beams. Model 1 presents a more consistent behavior in terms of COV_1 with values that are in general lower than those obtained with the other models. However, values of AVG for this model highly vary according to the subset of points used to evaluate them.

- For Models 1, 2, and 4, a better performance in terms of both AVG and COV_1 is found when EC2-VA is used instead of EC2-FA. For DB3, the Model 3 + ACI 318-14 combination presents the value of AVG closer to 1.0 with the lowest value of COV_1. However, a more consistent behavior in terms of COV1 is found for Model 1 + EC2-VA, with similar values of this variable independently of the database considered, although a large variation of AVG is also observed.

- Predicted effective strains in the fibers computed using the truss analogy were considerably lower than the maximum strain measured by the strain gauges placed on the fibers.
- Comparison of fiber strains predicted by Model 1 and Model 2 and those measured by strain gauges showed that factors such as the stirrup spacing should be considered to develop more accurate and reliable design equations.

5. CONCRETE, STIRRUP, AND FRCM CONTRIBUTIONS TO THE SHEAR STRENGTH OF RC BEAMS

The main challenge in evaluating the contribution of the FRCM system to the overall strength of the beams is the assessment of the individual contributions of the concrete, and of the internal and externally bonded shear reinforcement. In this section, the quantification of each component is made based on the results of the tests on FRCM strengthened beams without anchors presented in Chapter 3 summarized in Table 5-1. It is highlighted that all the beams included in Table 5-1. failed in shear. Further information regarding the geometry and the mechanical properties of the beams as well as the fibers and cementitious matrix used and the procedure followed to strengthen the beams is described in detail in Section 3.

Table 5-1. Summary of test results for FRCM strengthened beams without anchors

Series	Beam	P_{max}	V_{max}	Increase over control		Δ_{Pmax}
		(kN)	(kN)	(kN)	(%)	(mm)
	S1-CONTROL	230.5	115.2	-	-	15.4
S1	S1-FRCM-F3-UN	284.8	142.4	27.2	23.6	17.8
	S1-FRCM-F4-UN	299.5	149.7	34.5	29.9	17.7
	S2-CONTROL	259.3	129.7	-	-	14.5
S2	S2-FRCM-F3-UN	307.9	154	24.3	18.7	17.1
	S2-FRCM-F4-UN	294.4	147.2	17.5	13.5	18.0

As discussed in sections 3.8, 4.1, 4.2, and 4.3, a simple approach that assumes that the overall shear strength of strengthened RC beams can be computed as the summation of the individual contributions of concrete, steel and the externally bonded composites has been used in the past to develop, calibrate, and evaluate models used for the design of RC beams strengthened in shear with both FRP and FRCM composites. However, the interaction between the different components of the shear strength, i.e., concrete, stirrups, and strengthening system, makes clear that design models need to focus on predicting the total strength of the beam instead of computing only the contribution of the strengthening system [29,33,53,54,84].

In this section, two different approaches, named approach 1 (AP1) and approach 2 (AP2), are followed to evaluate the individual shear strength components using

measurements obtained in the experimental campaign. It is worth highlighting that the approaches described in this section allow for computing not only the concrete, steel, and fiber contributions at the maximum strength reached by the beams but also for evaluating them at any point of the beam load history.

AP1 and AP2 rely on the values of strains in the stirrups and the composite within the studied shear span that were recorded with uniaxial electrical resistance strain gauges during testing, as described in Section 3.1.3. It is highlighted that since the strain readings from both the stirrups and the fibers come from discrete gauges, the values recorded and used in AP1 and AP2 are considered as average values of the strains along the shear span, as well as along the height of beam. It is also important to note that as the concrete crack pattern is unknown before testing, it was not possible to place the strain gauges exactly along the shear crack. Therefore, the contribution of the stirrups and the fibers is evaluated using mainly the measurements from strain gauges located along or near the shear crack, which are considered as average values of the actual strains in all the fibers along the shear crack, as expressed above.

5.1   Definition of Approach 1 (AP1) and 2 (AP2)

5.1.1   Approach 1 (AP1)

In AP1, the contribution of the stirrups (V_s) and the composite ($V_{f,AP1}$) to the shear strength are computed using the strains recorded during testing, and the concrete contribution ($V_{c,AP1}$) is computed as the shear strength of the strengthened specimen (V_{str}) minus the summation of V_s and $V_{f,AP1}$ as shown in Eq. (5-1):

$$V_{c,AP1} = V_{str} - \left(V_s + V_{f,AP1}\right) \qquad \text{5-1}$$

At any given point of the beam load history, V_s can be computed according to Eq. (5-2):

$$V_s = 2A_s \sum_{i=1}^{n} f_{si} \sin\alpha_s \text{ where } f_{si} = E_s\varepsilon_{si} \leq f_y \qquad \text{5-2}$$

In Eq. (5-2), E_s corresponds to the elastic modulus of the stirrups steel (200 GPa), ε_{si} is the strain recorded in stirrup i, and f_y is the measured yield stress of the stirrup (527 MPa). For the studied beams, the steel internal reinforcement inclination

angle (α_s) with respect to the longitudinal axis of the beams is equal to 90°, i.e., $\sin\alpha_s$ is equal to 1.0.

The values of $V_{f,AP1}$ are computed considering the width of the composite that is effectively crossed by the shear crack (w_{eff}) reflected in the composite jacket as shown schematically in Figure 5-1.
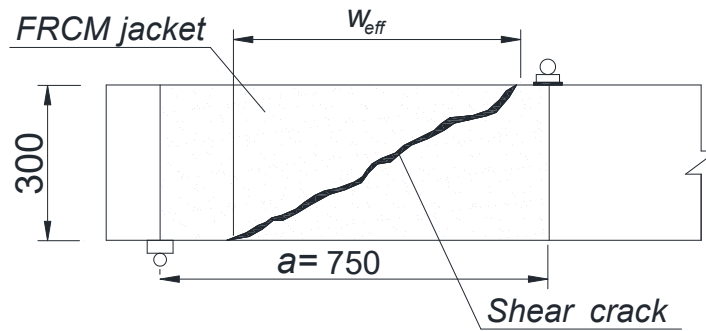
Figure 5-1 Evaluation of the composite width

Once w_{eff} is determined, $V_{f,AP1}$ is computed as:

$$V_{f,AP1} = 2t_f w_{eff} f_f \sin\alpha_f \qquad\qquad 5\text{-}3$$

$$f_f = E_f \varepsilon_f \qquad\qquad 5\text{-}4$$

where t_f corresponds to the equivalent nominal thickness of the fibers, f_f is stress in the fibers, E_f is the fiber elastic modulus, ε_f is the recorded fiber strain, and α_f is fiber inclination angle with respect to the beam longitudinal axis ($\alpha_f = 90°$ for the tested beams).

5.1.2 Approach 2 (AP2)

In AP1, the concrete contribution for each strengthened beam is computed from the fiber and stirrup contributions using the procedure described in Section 5.1.1. In the methodology proposed in AP2, the concrete contribution for each strengthened beam is determined using the behavior observed in the respective unstrengthened (control) beam. To do so, it is assumed that the concrete contribution to the beam shear strength reduces as a function of the shear crack width. It is also considered that the shear crack width is related to the level of strain in the stirrups. In fact, stirrups start to contribute only after they are crossed by the concrete cracks in the beam shear span, and values of strain, and consequently, of V_s, start increasing as the cracks widen. Therefore, it is possible to assume that

119

while larger shear crack widths imply an increase in the stirrup contribution, they cause a decrease in the concrete contribution to the shear strength.

In order to obtain a relationship between the stirrup strain and the concrete contribution to the shear strength, as a first step the concrete contribution to the unstrengthened beam, $V_{c,CONAP2}$, is computed as follows:

$$V_{c,CONAP2} = V_{CON} - V_{s,CON} \qquad 5\text{-}5$$

where $V_{s,CON}$ is the stirrup contribution to the unstrengthened beam, computed using Eq. (5-2) with the strains recorded in the stirrups in the control beam, and V_{CON} corresponds to the applied shear force in the control specimen. Figure 5-2 shows the locations of the stirrups and of the strain gauges mounted to the stirrups (ST#$_s$) for beams S1-CONTROL and S2-CONTROL, as well as the concrete crack pattern observed after testing the beams to failure. The applied load P versus stirrup strain ε_s relationships for beams S1-CONTROL and S2-CONTROL were presented in Figure 3-22.

a)   **b)**
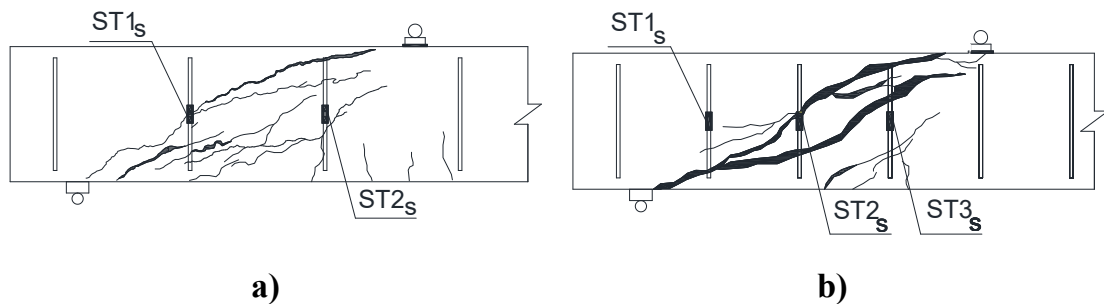
Figure 5-2 Cracking pattern and strain gauge location for beam: a) S1-CONTROL; b) S2-CONTROL

As observed in Figure 5-2b, the main shear crack of beam S2-CONTROL does not cross the stirrup on the left-hand side of the beam shear span (ST1$_s$), which implies a limited contribution of this stirrup to the beam shear strength. In fact, significant values of strain were not recorded by strain gauge ST1$_s$, and the contribution of this stirrup to the beam shear strength is neglected. As shown in Figure 3-22b, strain measurements recorded by strain gauge ST3$_s$ imply that the stirrup did not yield. However, strain gauge ST3$_s$ was not crossed directly by the shear cracks, and higher values of strain would be expected if the strain gauge had been located directly in the shear crack trajectory. Therefore, for the evaluation of $V_{s,CON}$ of beam S2-CONTROL, it is assumed that both stirrups yielded, and the readings from strain gauge ST2$_s$ are used to compute the contribution of the two stirrups

crossed by the shear crack, i.e., stirrups located in the right side of the shear span of the beam (Figure 5-2b).

Figure 5-3 shows the contributions of the concrete and steel stirrups ($V_{c,CONAP2}$ and $V_{s,CON}$, respectively) to the shear strength for beams S1-CONTROL and S2-CONTROL. It is highlighted that in Figure 5-3, values of applied shear force, V, are shown only up to the peak load.
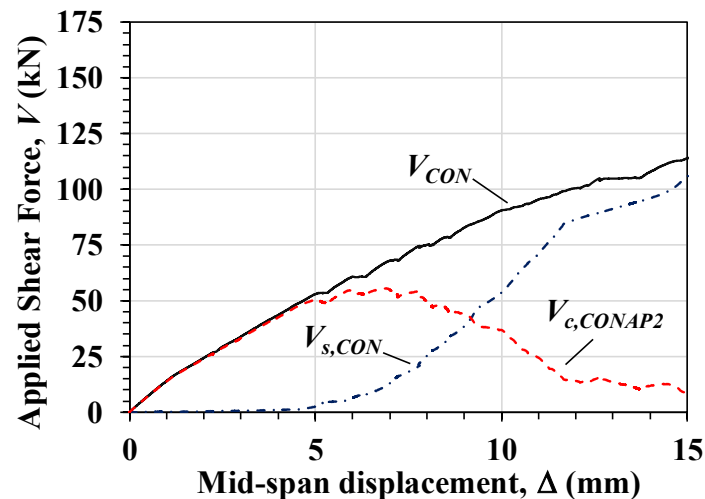
a)
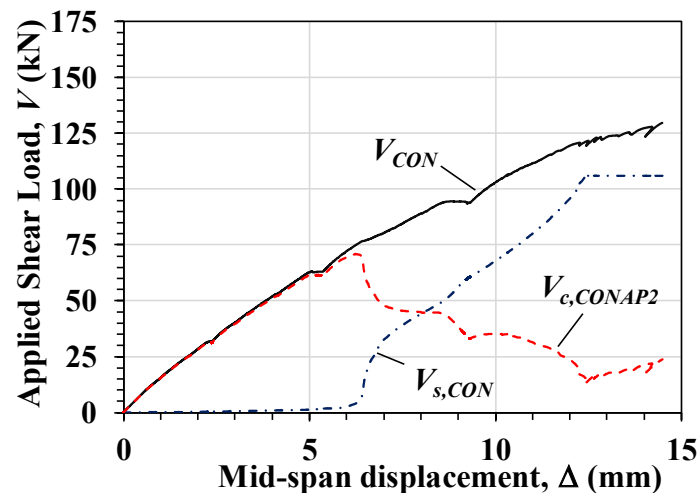
b)

Figure 5-3 Applied Shear Load V vs. Mid-span displacement Δ for beam: a) S1-CONTROL; b) S2-CONTROL

After the concrete contribution $V_{c,CONAP2}$ is computed, it is possible to evaluate the relationship between $V_{c,CONAP2}$ and the strains recorded in the stirrups. In Figure 5-4, values of $V_{c,CONAP2}$ are plotted against the strains measured by strain gauge $ST1_s$ for beam S1-CONTROL and strain gauge $ST2_s$ for beam S2-CONTROL, i.e.

the strain gauges that recorded the maximum values of strain (see Figure 3-22). As shown in Figure 5-4a, $V_{c,CONAP2}$ reaches a maximum value when the stirrup strains are roughly zero, i.e., before the shear cracks start to develop, for both beams S1-CONTROL and S2-CONTROL. After the stirrup strains start to increase, $V_{c,CONAP2}$ starts to decrease, and the mechanism contributing to the shear strength can be related to the aggregate interlock. As the shear force increases, the concrete cracks start to widen, which is reflected in the higher values of stirrup strain recorded. This increase in the crack width also diminishes the effect of the aggregate interlock, reducing the concrete contribution. Finally, $V_{c,CONAP2}$ reaches an approximately constant value that is not strictly related to the contribution of concrete but to additional strength mechanisms such as dowel action of the longitudinal reinforcement [9].

As shown in Figure 5-4a the behavior observed is similar for both control beams. In fact, when values of $V_{c,CONAP2}$ are normalized by the maximum value of the concrete contribution, $(V_{c,CONAP2})_{max}$ for the corresponding beam, the behavior of both beams can be idealized by a bilinear model, shown by the dashed line in Figure 5-4b. According to the model, the concrete contribution starts decreasing linearly after strains are measured in the stirrups and reaches a minimum for a value of ε_s approximately equal to the steel yield strain (ε_y=2650 $\mu\varepsilon$). After this point, the contribution of concrete to the shear strength becomes constant and is equal to approximately 0.25 of the maximum contribution $(V_{c,CONAP2})_{max}$. It is important to highlight that the analysis carried out in this section was made up to peak load. After this point, it is expected that concrete contribution is no longer constant and starts decreasing. In fact, as the steel contribution becomes constant due to yielding of the stirrups, the reduction in strength is associated with a decrease in the contribution of additional mechanisms that contribute to the overall shear strength.
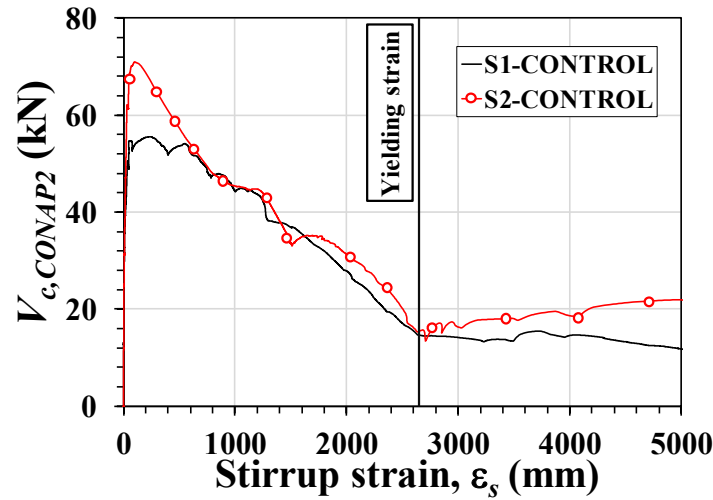
a)
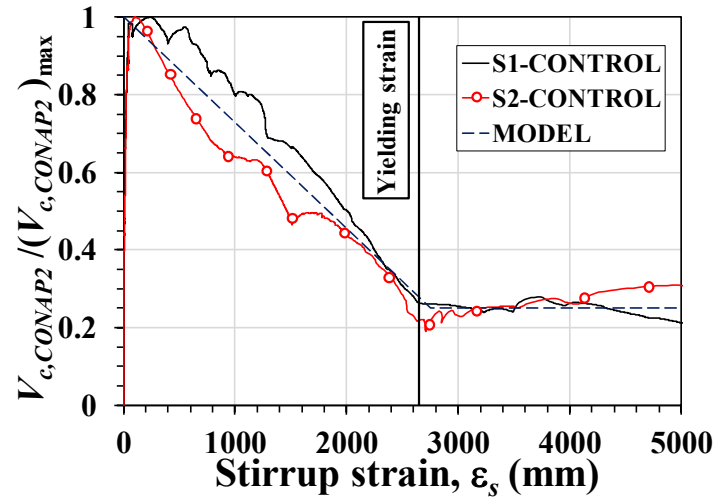
b)

Figure 5-4 Concrete contribution vs. Stirrup strain ε_s: a) $V_{c,CONAP2}$; b) $V_{c,CONAP2}$ relative to maximum value

The model described above is then used to compute the concrete contribution to the strengthened beams, $V_{c,AP2}$. To do so, the value of load in the strengthened beam at which strains in the stirrups start to be recorded is taken as the maximum value of the contribution of the concrete, $(V_{c,AP2})_{max}$. After $(V_{c,AP2})_{max}$ is attained, the concrete contribution $V_{c,AP2}$ is computed as a function of the stirrup strain following Eqs. (5-6) and (5-7) and the model described above (see Figure 5-4b):

$$V_{c,AP2} = \left(V_{c,AP2}\right)_{max} \left[1 - \frac{0.75}{\varepsilon_y}\right] \varepsilon_s \text{ for } 0 < \varepsilon_s \leq \varepsilon_y \qquad 5\text{-}6$$

$$V_{c,AP2} = 0.25 \left(V_{c,AP2} \right)_{max} \text{ for } \varepsilon_s > \varepsilon_y \qquad \text{5-7}$$

In AP2, the stirrup contribution V_s is computed using Eq. (5-2). The contribution of the FRCM jacket ($V_{f,AP2}$) is determined by subtracting V_s and $V_{c,AP2}$ from the shear load in the strengthened specimen, V_{str}, as shown in Eq. (5-8):

$$V_{f,AP2} = V_{str} - \left(V_s + V_{c,AP2} \right) \qquad \text{5-8}$$

5.2   Shear strength components for carbon FRCM-strengthened beams

5.2.1   Approach 1 (AP1)

Values of the width of the composite, w_{eff}, for beams S1-FRCM-F3-UN and S2-FRCM-F3-UN used to compute the fiber contribution $V_{f,AP1}$ according to AP1 are shown in Figure 5-5 . It is noted that the total width of the FRCM jacket was equal to the shear span (a=750 mm) as shown in Figure 5-5.
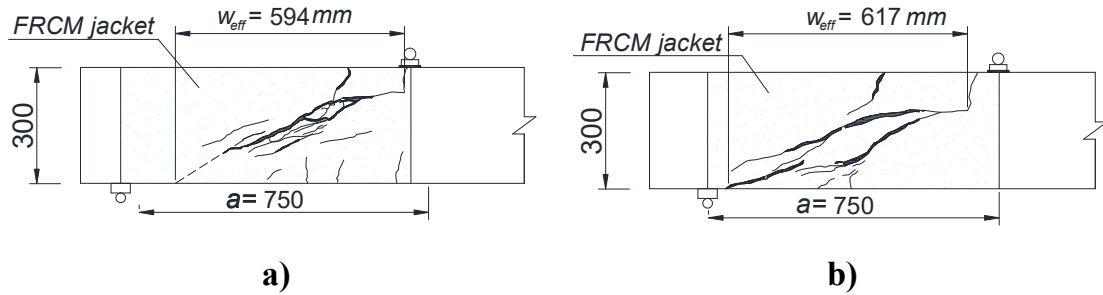
Figure 5-5 Evaluation of w_{eff} (dimensions in mm): a) S1-FRCM-F3-UN, b) S2-FRCM-F3-UN

It is worth noting that although the cracking pattern on the external face of the FRCM jacket for beam S1-FRCM-F3-UN did not extended to bottom of beam, it is assumed that the diagonal crack beneath the jacket, i.e., in the beam, does. Based on this assumption, w_{eff} for beam S1-FRCM-F3-UN was found projecting the main diagonal crack to the bottom of the beam (see dashed line in Figure 5-5).

The values of fiber strain used to compute the fiber contribution, $V_{f,AP1}$, are shown in Figure 3-28a and Figure 3-28b for beams S1-FRCM-F3-UN and S2-FRCM-F3-UN, respectively. Values of stirrup strain used for beams S1-FRCM-F3-UN and S2-FRCM-F3-UN are shown in Figure 3-24a and Figure 3-24b, respectively.

Figure 5-6 presents the values of $V_{c,AP1}$, V_s, and $V_{f,AP1}$ computed following the methodology proposed for AP1.
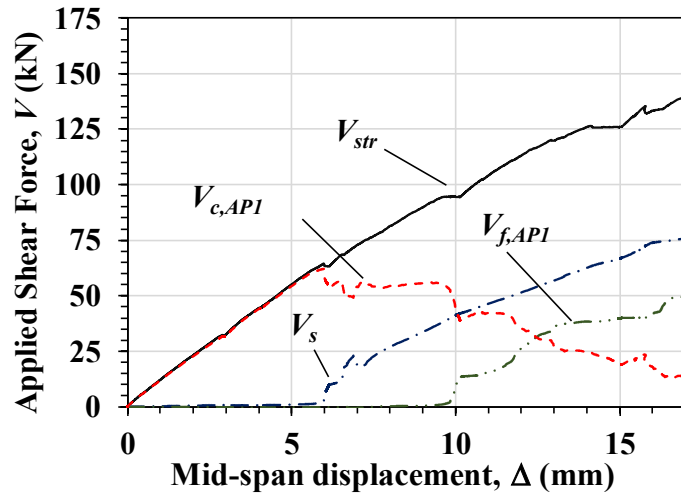
a)
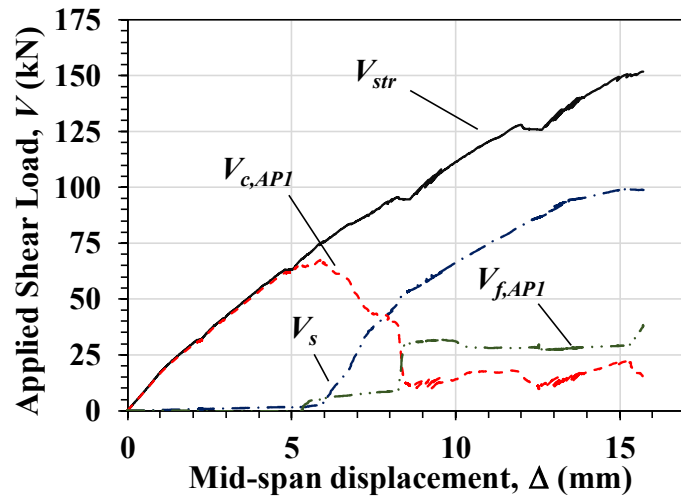
b)

Figure 5-6 Shear strength components computed according to AP1 for beam: a) S1-FRCM-F3-UN, b) S2-FRCM-F3-UN

It can be seen in Figure 5-6 that the evolution of $V_{c,AP1}$ computed by AP1 predicts a softer concrete degradation for beam S1-FRCM-F3-UN compared to beam S2-FRCM-F3-UN. In fact, for beam S2-FRCM-F3-UN, there is jump in $V_{c,AP1}$, and therefore in $V_{f,AP1}$, at a mid-span displacement, Δ, of approximately 8.3 mm that is not observed for beam S1-FRCM-F3-UN. This variation in the concrete and fiber contributions is attributed to an abrupt shear crack width increase, which results in a fast change in the fiber strain measurements. Figure 5-6a also shows that for beam S1-FRCM-F3-UN, the stirrup contribution starts when V is approximately 60 kN, which corresponds to a value of Δ equal to 5.5 mm. Although V_s starts increasing when V is equal to approximately 75 kN for beam S2-FRCM-F3-UN, the value of Δ is similar to that observed for beam S1-FRCM-F3-UN. It is also

125

noted that for beam S2-FRCM-F3-UN, V_s and $V_{f,AP1}$ start increasing almost simultaneously, while for beam S1-FRCM-F3-UN, $V_{f,AP1}$ is delayed and starts increasing for values of V and Δ of approximately 90 kN and 9.5 mm, respectively.

5.2.2 Approach 2 (AP2)

Figure 5-7 presents the values of $V_{c,AP2}$, V_s, and $V_{f,AP2}$ computed following the methodology proposed for AP2.

a)

b)
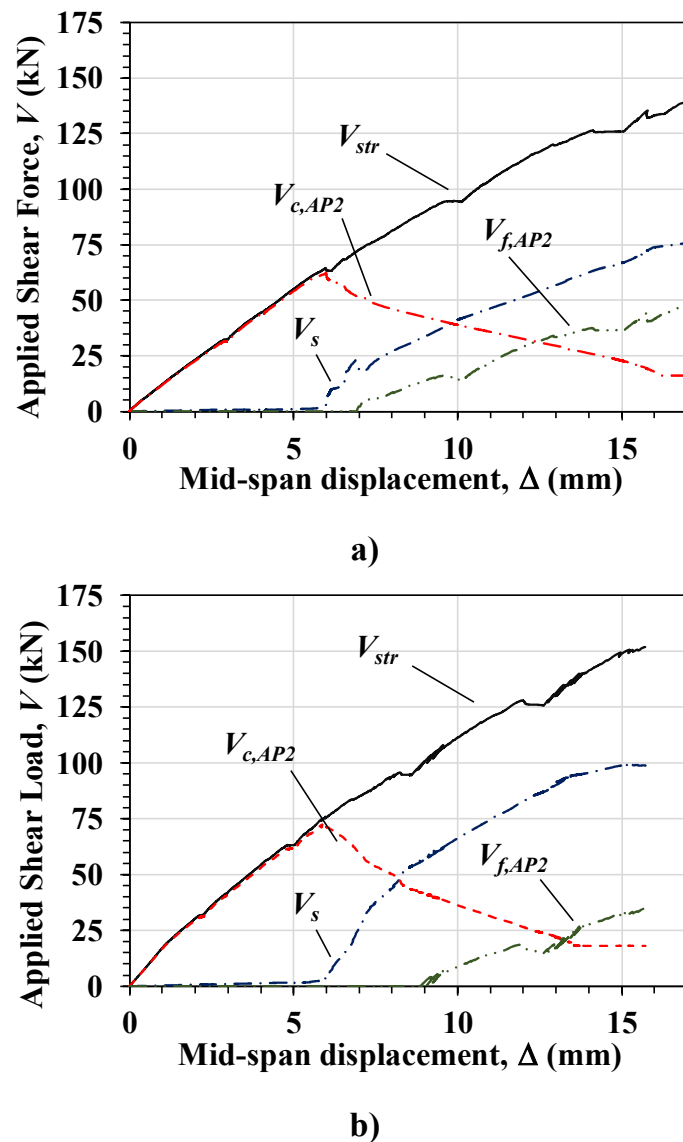
Figure 5-7 Shear strength components computed according to AP2 for beam: a) S1-FRCM-F3-UN; b) S2-FRCM-F3-UN

As observed in Figure 5-7, the use of the model described by Eqs. (5-6) and (5-7) predicts a linear decrease of the concrete contribution, $V_{c,AP2}$, for beam S1-FRCM-F3-UN after the value of $(V_{c,AP2})_{max}$. For the case of beam S2-FRCM-F3-UN, this

variation shows a bilinear behavior, explained by the change in slope of V_s at Δ=8.5 mm, which coincides with the point at which values of $V_{f,AP2}$ start to increase. It is also interesting to note that the value of mid-span displacement for which $V_{c,AP2}$ becomes constant is different for both beams. For beam S1-FRCM-F3-UN, the concrete contribution becomes constant for a value of Δ equal to 16.2 mm, while for beam S2-FRCM-F3-UN, this value is reached for Δ equal to 13.8 mm, approximately. It is also noted that the FRCM contribution starts for lower values of mid-span displacement and applied shear load for the case of beam S1-FRCM-F3-UN than for beam S2-FRCM-F3-UN.

5.2.3 Comparison of approaches

Figure 5-8 compares the concrete contribution computed according to AP1 and AP2 for beams S1-FRCM-F3-UN and S2-FRCM-F3-UN. Table 5-2 summarizes the values of V_c determined by AP1 and AP2 at the peak applied shear force for both beams.

For beam S1-FRCM-F3-UN, Figure 5-8a shows that there is a good agreement between the behaviors of V_c computed using the two approaches. However, a slightly higher concrete contribution at peak shear force is predicted by AP2. For beam S2-FRCM-F3-UN, higher values of V_c at the peak applied shear load are also predicted by AP2. For this beam, Figure 5-8a shows that AP2 is not able to predict the jump in the concrete contribution observed in AP1. This is explained by the fact that this jump is associated to a fast change in the fiber strains caused by a sudden increase in the shear crack width, as explained in Section 5.2.1. Since AP2 is based only on the internal transverse shear reinforcement strains and does not consider fiber strains, local phenomena as the one described above cannot be anticipated by this approach.
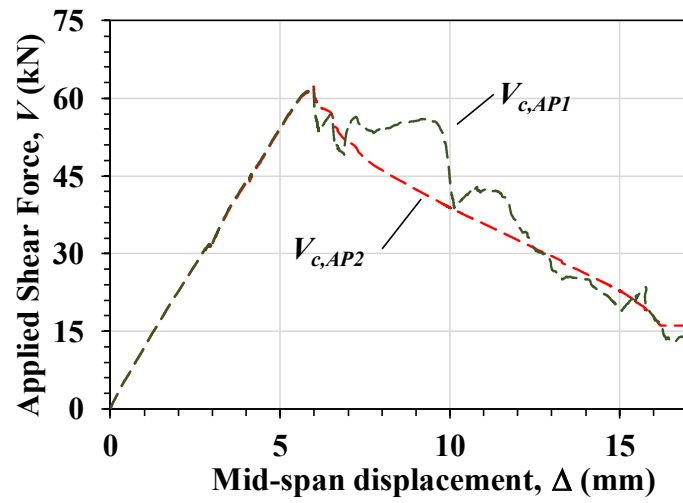
a)
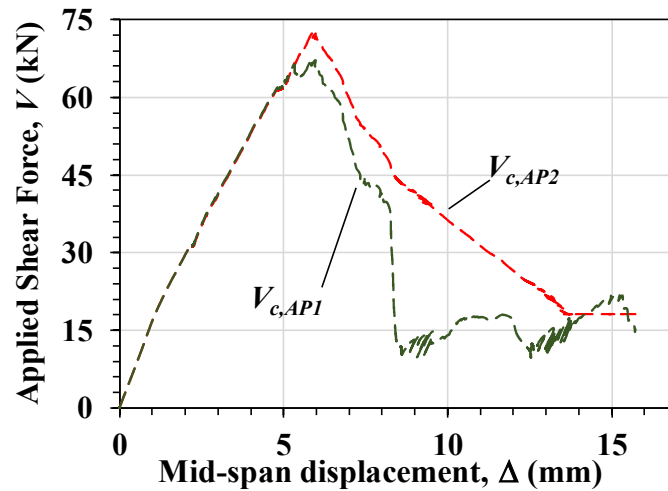
b)

Figure 5-8 Comparison of V_c computed according AP1 for beam: a) S1-FRCM-F3-UN, b) S2-FRCM-F3-UN

Table 5-2. Comparison of V_c computed with AP1 and AP2 for beams S1-FRCM-F3-UN and S2-FRCM-F3-UN

Beam	$V_{c,AP1}$ (kN)	$V_{c,AP2}$ (kN)
S1-FRCM-F3-UN	13.5	16.1
S2-FRCM-F3-UN	15.2	18.6

Figure 5-9 compares the fiber contribution computed according to AP1 and AP2 for beams S1-FRCM-F3-UN and S2-FRCM-F3-UN. Table 5-3 summarizes the

values of V_f determined by AP1 and AP2 at the peak applied shear force for both beams.
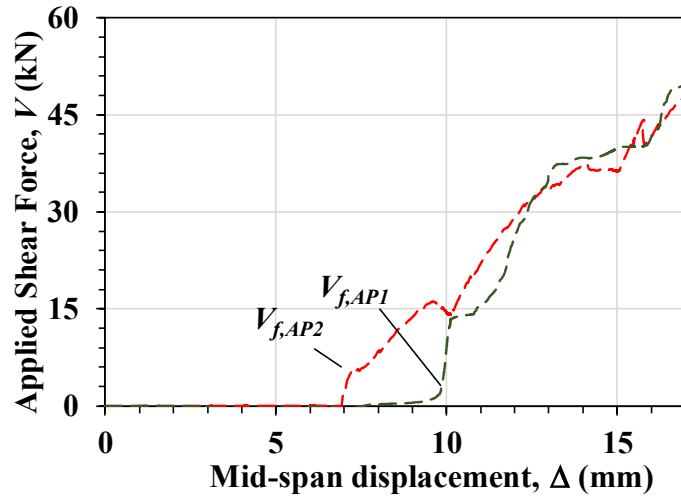
a)
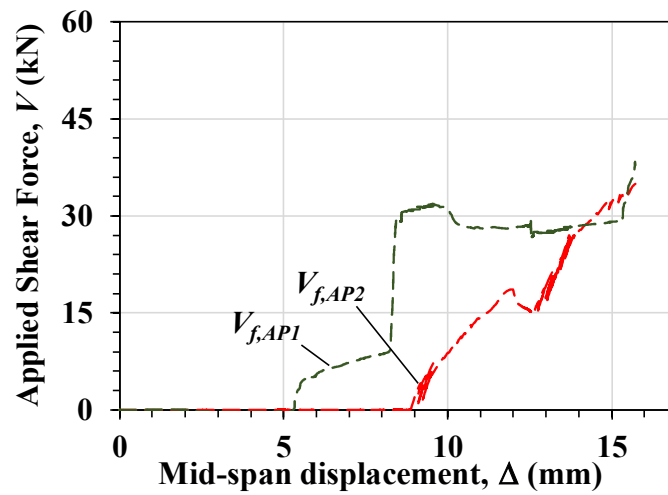
b)

Figure 5-9 Comparison of V_f computed according AP1 for beam: a) S1-FRCM-F3-UN, b) S2-FRCM-F3-UN

Table 5-3. Comparison of V_f computed with AP1 and AP2 for beams S1-FRCM-F3-UN and S2-FRCM-F3-UN

Beam	$V_{f,AP1}$ (kN)	$V_{f,AP2}$ (kN)
S1-FRCM-F3-UN	49.9	47.5
S2-FRCM-F3-UN	38.3	34.9

For beam S1-FRCM-F3-UN, Figure 5-9a shows that for values of V higher than 15 kN, the increase in V_f predicted by both approaches is similar. In fact, values of V_f at peak applied shear force, shown in Table 5-3, differ only by 4%. However, for values of V lower than 15 kN, the behavior predicted by both approaches is different. AP2 could not accurately predict the point at which the fibers start contributing to the shear strength, which is captured by the strain gauges measurements used in AP1.

Although values of V_f computed using AP1 and AP2 for beam S2-FRCM-F3-UN at the peak shear are similar, as shown in Table 5-3, in Figure 5-9b it can be seen that the evolution of the fiber contribution observed for both approaches does not have the agreement attained for beam S1-FRCM-F3-UN. As explained above, AP2 is not able to capture the rapid strain variation observed in the fiber strains for beam S2-FRCM-F4-UN (see Figure 3-28c).

5.3   Shear strength components for steel FRCM-strengthened beams

5.3.1   Approach 1 (AP1)

Values of the width of the composite, w_{eff}, for beams S1-FRCM-F4-UN and S2-FRCM-F4-UN used to compute the fiber contribution $V_{f,AP1}$ according to AP1 are shown in Figure 5-10.
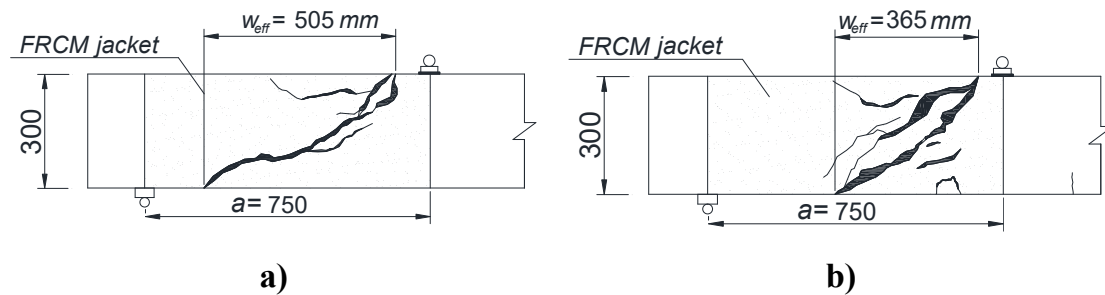
Figure 5-10 Evaluation of w_{eff} (dimensions in mm): a) S1-FRCM-F4-UN, b) S2-FRCM-F4-UN

The values of fiber strain used to compute the fiber contribution, $V_{f,AP1}$, are shown in Figure 3-29a and Figure 3-29b for beams S1-FRCM-F3-UN and S2-FRCM-F3-UN, respectively. Values of stirrup strain used for beams S1-FRCM-F3-UN and S2-FRCM-F3-UN are shown in Figure 3-25a and Figure 3-25b, respectively.

Figure 5-11 presents the values of $V_{c,AP1}$, V_s, and $V_{f,AP1}$ computed following the methodology proposed for AP1.
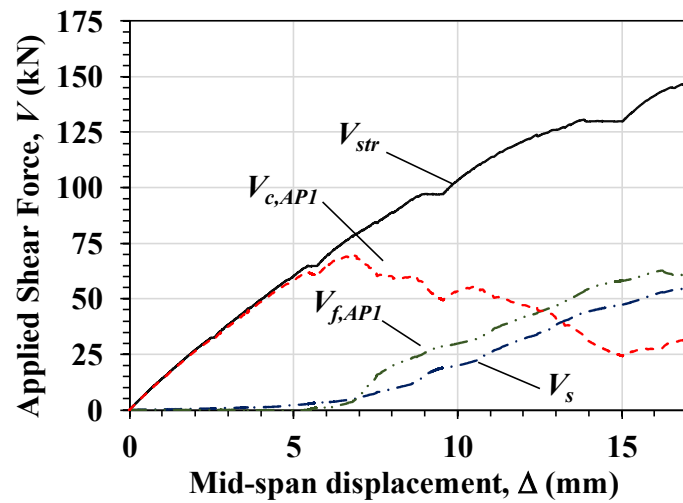
a)
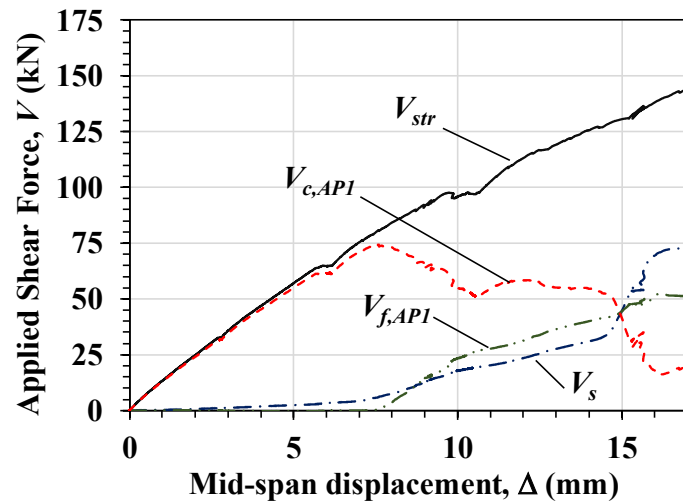
b)

Figure 5-11 Shear strength components computed according to AP1 for beam: a) S1-FRCM-F4-UN, b) S2-FRCM-F4-UN

Figure 5-11 shows that although maximum values of $V_{c,AP1}$ for beams S1-FRCM-F4-UN and S2-FRCM-F4-UN are similar (74 kN approximately), a higher value of $V_{c,AP1}$ is predicted by AP1 for beam S1-FRCM-F4-UN. It also worth noting that that for both beams, the concrete contribution reaches its minimum before the peak applied shear force is attained. The minimum values of $V_{c,AP1}$ are associated to the maximum values of fiber contribution, $V_{f,AP1}$, as observed in Figure 5-11a and Figure 5-11b. After $V_{f,AP1}$ reaches its maximum, a decrease in the fiber contribution is observed. This behavior is related to the presence of local debonding of the fibers (see Section 3.5.2), which results in a drop in the recorded fiber strains and therefore, in the fiber contribution. Considering that the stirrup contribution reaches its maximum at the peak shear applied force, an increase in the concrete

contribution with the decrease in the fiber contribution is predicted by Eq. (5-1), as observed Figure 5-11.

It is also noted that for beam S1-FRCM-F4-UN, V_s and $V_{f,AP1}$ start increasing almost simultaneously, while for beam S2-FRCM-F4-UN, $V_{f,AP1}$ is delayed and starts increasing for values of V and Δ of approximately 80 kN and 6.7 mm, respectively.

5.3.2 Approach 2 (AP2)

Figure 5-12 presents the values of $V_{c,AP2}$, V_s, and $V_{f,AP2}$ computed following the methodology proposed for AP2.
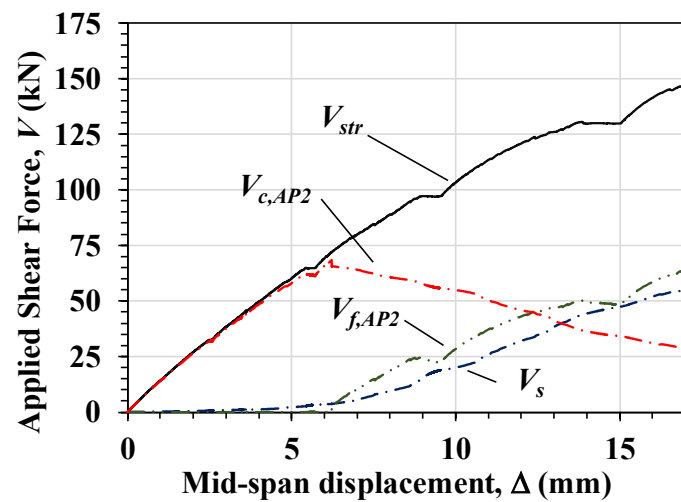
a)
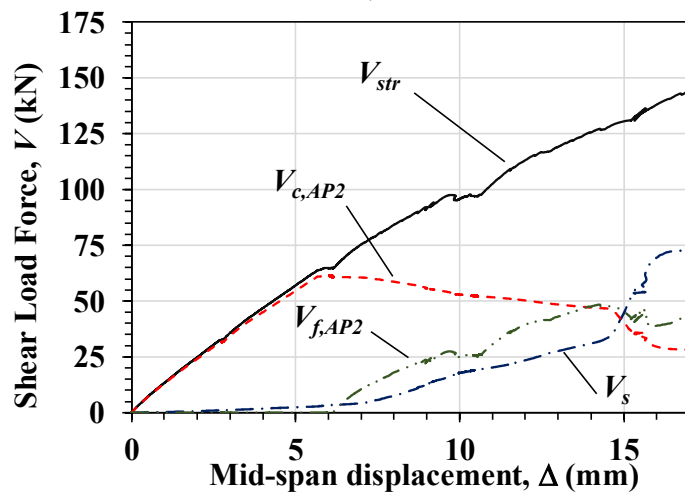
b)

Figure 5-12 Shear strength components computed according to AP2 for beam: a) S1-FRCM-F4-UN; b) S2-FRCM-F4-UN

As observed in Figure 5-12, for beam S1-FRCM-F4-UN after the value of $(V_{c,AP2})_{max}$ is reached, the use of the model described by Eqs. (5-6) and (5-7) predicts a linear decrease of the concrete contribution, $V_{c,AP2}$. For the case of beam S2-FRCM-F4-UN, a linear behavior is observed until a value of V=45kN and Δ=14.7 mm, approximately. After this point, there is a variation in the rate with which $V_{c,AP2}$ decreases. Considering that according to AP2, the variation of $V_{c,AP2}$ depends on the development of strains in the stirrups, this behavior is related with the higher increase rate for V_s observed after Δ=14.7 mm. It is also noted that the FRCM contribution starts for values of mid-span displacement that are similar for both beams (Δ=6.0 mm, approximately).

5.3.3 Comparison of approaches

Figure 5-13 compares the concrete contribution computed according to AP1 and AP2 for beams S1-FRCM-F4-UN and S2-FRCM-F4-UN. Table 5-4 summarizes the values of V_c determined by AP1 and AP2 at the peak applied shear force for both beams.

For beam S1-FRCM-F3-UN, Figure 5-13a shows that there is a good agreement between the behaviors of V_c computed using the two approaches up to a mid-span displacement Δ=13.0 mm. After this point, the concrete contribution decrease rate is higher for AP1. In addition, the minimum value of V_c for AP2 is attained at the peak applied shear force, which differs from the behavior observed for AP1, as discussed in Section 5.3.1. Higher values of V_c are obtained for AP1.

For beam S2-FRCM-F3-UN, values of $V_{c,AP1}$ and $V_{c,AP2}$ are the same until $(V_{c,AP2})_{max}$ is reached. After this point, the concrete contribution curve of AP1 predicts higher values of V_c than AP2 with a shape that differs from the linear behavior observed for AP2, up to a Δ=15.0 mm. For mid-span displacements higher than 15.0, values of $V_{c,AP1}$ are lower than values of $V_{c,AP2}$. In fact, results in Table 5-4 show that $V_{c,AP1}$ for beam S2-FRCM-F4-UN is approximately 19% lower than $V_{c,AP2}$.
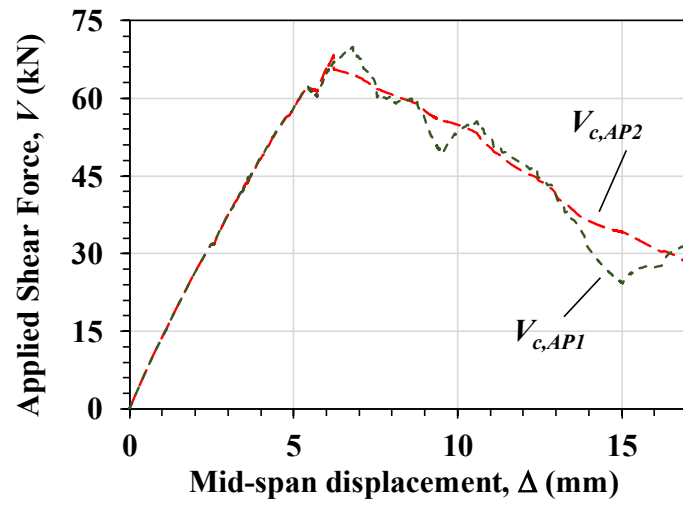
a)
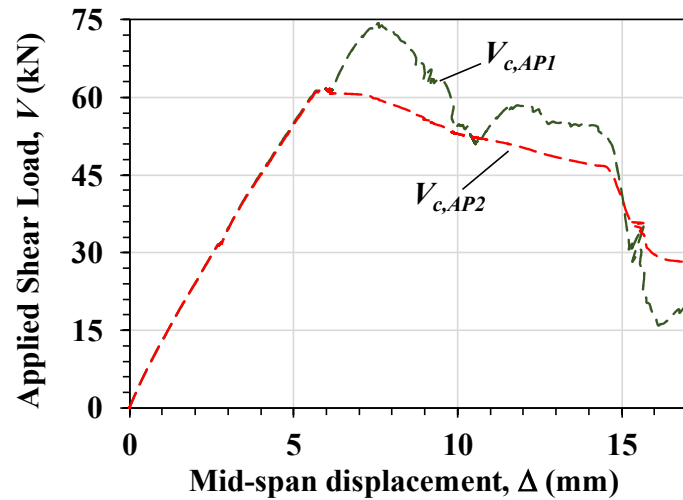
b)

Figure 5-13 Comparison of V_c computed according to AP1 and AP2 for beam: a) S1-FRCM-F4-UN, b) S2-FRCM-F4-UN

Table 5-4. Comparison of V_c computed with AP1 and AP2 for beams S1-FRCM-F4-UN and S2-FRCM-F4-UN

Beam	$V_{c,AP1}$ (kN)	$V_{c,AP2}$ (kN)
S1-FRCM-F4-UN	33.7	28.1
S2-FRCM-F4-UN	22.7	27.9

Figure 5-14 compares the fiber contribution computed according to AP1 and AP2 for beams S1-FRCM-F4-UN and S2-FRCM-F4-UN. Table 5-5 summarizes the

134

values of V_f determined by AP1 and AP2 at the peak applied shear force for both beams.
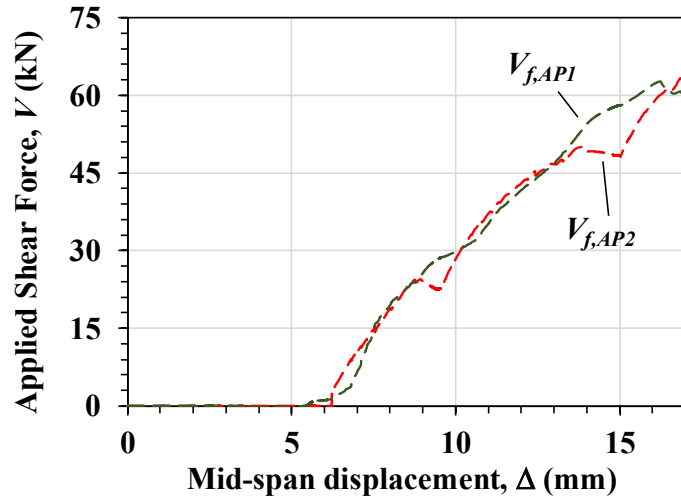
a)
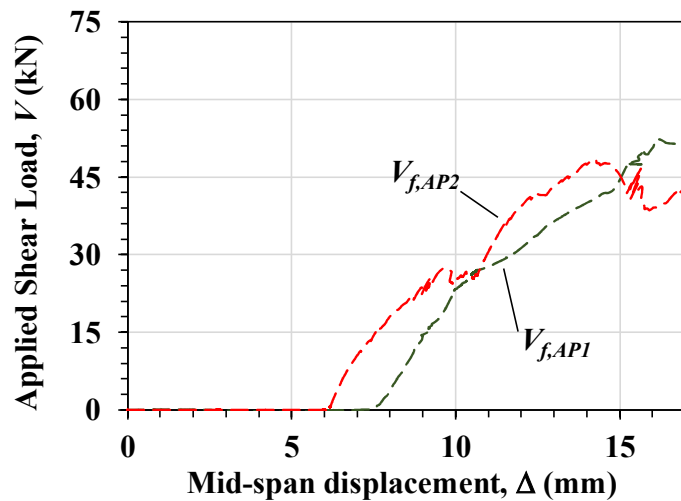
b)

Figure 5-14 Comparison of V_f computed according to AP1 and AP2 for beam: a) S1-FRCM-F4-UN, b) S2-FRCM-F4-UN

Table 5-5. Comparison of V_f computed with AP1 and AP2 for beams S1-FRCM-F4-UN and S2-FRCM-F4-UN

Beam	$V_{f,AP1}$ (kN)	$V_{f,AP2}$ (kN)
S1-FRCM-F4-UN	62.7	63.6
S2-FRCM-F4-UN	52.4	61.7

For beam S1-FRCM-F4-UN, Figure 5-14a shows that there is a good agreement between the values of V_f computed using AP1 and AP2, in terms of the curve shape, values at peak applied shear force (see Table 5-5), and value of mid-span displacement after which the fiber contribution starts to develop.

Values of V_f computed using AP2 at peak applied shear force are higher than those obtained using AP1 for beam S2-FRCM-F4-UN, as shown in Figure 5-14b. The value of Δ after which the fiber contribution starts to develop is lower for AP2 than for AP2. This makes that higher values of V_f are computed for AP2 than for AP1 for the same value of Δ, although the increase rate in the fiber contribution is similar for both approaches.

5.4   Conclusions

This chapter introduced two different approaches for the evaluation of the individual contributions of concrete, steel stirrups, and FRCM system to the overall shear strength of RC beams strengthened in shear. The methodologies proposed for these approaches were then applied using the experimental results of the FRCM-strengthened beams included in Chapter 2 of this thesis. The main conclusions drawn from this analysis can be summarized as follows:

- The contribution provided by the stirrups and the FRCM system is negligible for low values of mid-span displacement. In this region, the shear strength is equal to the concrete contribution.
- Results show that at peak applied load, although there is significant decrease in the concrete contribution, the overall shear strength of the beam is comprised of the concrete, stirrup, and fiber contributions. In fact, the contribution of concrete is lower than those of the stirrups and the fibers.
- After values of stirrup and fiber contributions start to increase, both approaches predict a decrease in the concrete contribution, regardless of the type of fiber or stirrup spacing of the beams.
- The contribution of the stirrups and fibers computed by both approaches generally agree. However, AP2 is not able to predict the point at which the FRCM system starts to contribute to the shear strength starts. In addition, AP2 is not able to capture the variation in the fiber contribution due to phenomena such as the sudden increase in crack width or the local debonding of the fibers.

6. ANALYTICAL DESIGN MODEL FOR DETERMINING THE FRCM CONTRIBUTION TO THE SHEAR STRENGTH OF RC BEAMS

In this section, an analytical design model for determining the contribution of the FRCM composite to the shear strength of strengthened RC beams is presented. The model is based on the bond behavior of the FRCM composite applied onto concrete substrates and assumes slippage of the fibers through the mortar matrix, which is a failure mode reported for FRCM-strengthened beams (see Section 2.4). The equations presented in this section are intended for U-wrapped beams, but the analysis carried out can be extended for the cases of side bonded and fully wrapped beams. For these two cases, the bonded length that contributes to the increase of the beam shear strength is different than in the case of U-wrapped beams and needs to be evaluated accordingly. In addition, the proposed equations need to be modified for the case of fracture of the fibers, which has been reported for the case of fully wrapped specimens (see Section 2.4).

6.1   FRCM bond behavior

Laboratory campaigns on bond behavior of FRP-concrete joints have shown that the debonding surface, in most of the cases, is located within a thin layer of concrete substrate or at the FRP/concrete interface [85], which implies that the overall performance of the strengthening system highly relies on the characteristics of the concrete substrate. In addition, the effective bond length, l_{eff}, plays a key role on the load-carrying capacity of the system. As defined by [68], the effective bond length (l_{eff}) for FRP composites is the length beyond which an extension of the bonded length cannot increase the bond strength. To avoid undesirable debonding failures, the assessment of the effective bond length is crucial for proper design of FRP strengthened structures and to determine the actual bond strength.

In Figure 6-1, taken from [86], the idealized applied load (P) vs. global slip (g) curve for FRP with bonded length longer than l_{eff} is shown. The global slip g is defined as the relative displacement between points on the composite strip and on the concrete substrate at the composite loaded end. For FRP composites, as shown in Figure 6-1, an initial linear phase develops until point A. After point A, which is associated with the onset of microcracking at the FRP-concrete interface, a nonlinear branch develops until point B. After B, the load remains constant until

point C. For bonded length shorter than l_{eff}, lower values of maximum load will be achieved. However, for bonded lengths longer than l_{eff}, the maximum attained load will not increase, and only a longer BC segment will be observed as a consequence of the shifting of the stress-transfer zone toward the free end [87].
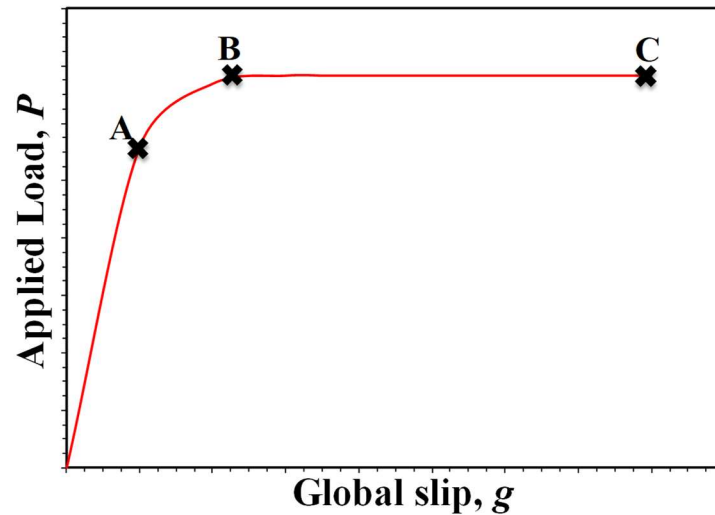
Figure 6-1. Idealized applied load (P) vs. global slip (g) response for FRP-concrete joints [86]

For FRCM-concrete joints, the behavior observed is different, and current models and equations for FRP composites cannot be directly employed. First of all, as pointed out by several authors [36,88], the debonding process generally occurs at the matrix-fiber interface, which implies a limited influence of the concrete substrate in the bond strength of the composite system. Furthermore, the idealized applied load (P) vs. global slip (g) curve shows important differences when compared to FRP-concrete joints [35], as shown in Figure 6-2.
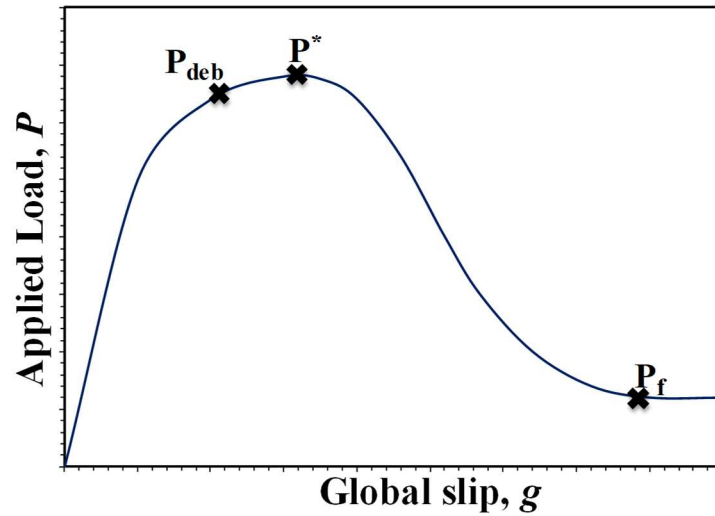
Figure 6-2. Idealized applied load (P) vs. global slip (g) response for FRCM-concrete joints [35]

As in the case of FRP-concrete joints, in FRCM-concrete joints after an initial linear increase the applied load becomes nonlinear until the debonding load P_{deb} is attained. However, due to the presence of friction (interlocking) between fiber filaments and between fibers and matrix, which is not observed in FRP-concrete joints, P increases further to P^*. For a bonded length longer than l_{eff}, the peak load, P^*, is attained when the stress transfer zone, which shifts toward the free end with increasing the global slip after the onset of debonding, reaches the free end. After this point, the applied load decreases with increasing global slip until the fibers are completely debonded and a constant applied load P_f, due only to friction, remains.

6.2   Analytical model for FRCM U-wrapped beams

For FRCM-concrete joints, the peak stress σ^* associated with the the peak load P^* can be computed as:

$$\sigma^* = \frac{P^*}{nt^*b^*} \qquad \qquad 6\text{-}1$$

where n is number of longitudinal fiber bundles, t^* is average thickness of a single longitudinal fiber bundle, and b^* is the nominal width of a single longitudinal fiber bundle. According to results of single-lap direct-shear tests, the relationship between the peak stress σ^* and the bonded length l provided by an FRCM-concrete joint can be expressed by a two-part function $\sigma^*(l)=(f(l), r(l))$, where $f(l)$ and $r(l)$ are functions that describe the peak stress behavior for bonded lengths less than (or equal to) and longer than (or equal to) the effective bond length l_{eff},

respectively. When $l=l_{eff}$, the peak stress provided by the FRCM-concrete joint is equal to the debonding stress σ_{deb}.

In general, $f(l)$ and $r(l)$ depend on the FRCM composite employed and, specifically, on the presence of a residual shear stress due to friction stress τ_f at the debonded interface. The frictional shear stress τ_f can be determined as:

$$\tau_f = \frac{P_f}{n_i n t^* l}$$
<div align="right">6-2</div>

where n_i is a coefficient that takes into account that the contact area between fibers and matrix is twice the bonded area of the fiber bundles (nt^*l) because the fibers slip with respect to both layers of matrix ($n_i=2$ for a single fiber layer that debonds from the embedding matrix).

As a first attempt, a quadratic and a cubic function are assumed for $f(l)$ in the case $\tau_f=0$ and $\tau_f \neq 0$, respectively, whereas $r(l)$ is assumed linear. The choice of a different function for the cases of $\tau_f=0$ and $\tau_f \neq 0$ is based on the assumption that composites that present a residual frictional shear stress would provide a higher peak load for bonded lengths less than or equal to the effective bonded length with respect to composites that do not show a residual frictional shear stress, even if the debonding load is assumed equal. For $\tau_f=0$, the slope m of the line $r(l)$ is equal to 0, whereas $m \neq 0$ for $\tau_f \neq 0$ (see Figure 6-3). In general, according to the results by [35] on PBO FRCM-concrete joints, m can be computed as:
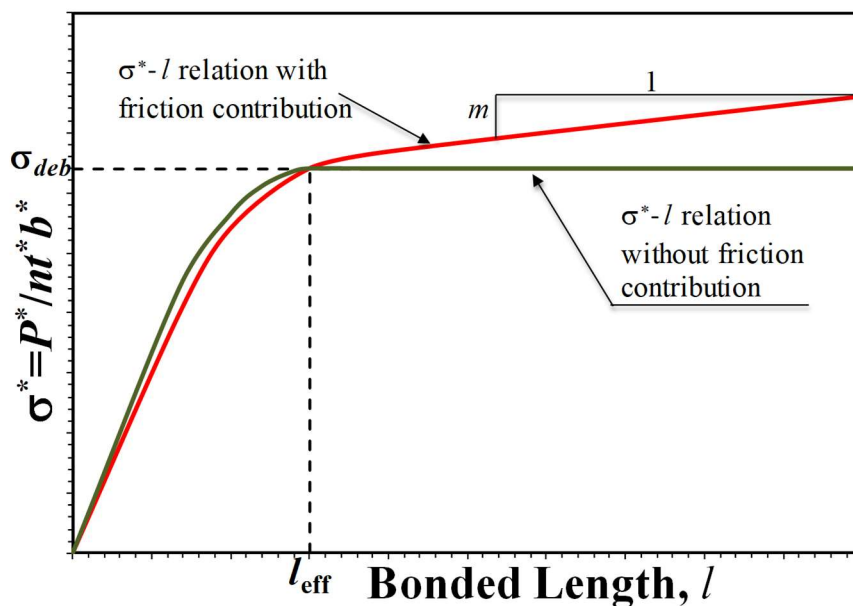
$$m = \frac{n_i \tau_f}{t^*} \qquad \text{6-3}$$

If $\tau_f=0$, the peak stress $\sigma^*(l)$ is:

$$\sigma^*(l) = \begin{cases} f(l) = \sigma_{deb} \dfrac{l}{l_{eff}} \left(2 - \dfrac{l}{l_{eff}} \right) \; if \; l \le l_{eff} \\ r(l) = \sigma_{deb} \; if \; l \le l_{eff} \end{cases} \qquad \text{6-4}$$

When a frictional shear stress is present, $\sigma^*(l)$ is:

$$\sigma^*(l) = \begin{cases} f(l) = \dfrac{l_{eff}(c + m) - 2\sigma_{deb}}{l_{eff}^3} l^3 + \dfrac{3\sigma_{deb} - l_{eff}(2c + m)}{l_{eff}^2} l^2 + cl \; if \; l \le l_{eff} \\ r(l) = m(l - l_{eff}) + \sigma_{deb} \; if \; l \le l_{eff} \end{cases} \qquad \text{6-5}$$

where c is a coefficient that should be calibrated on direct-shear test experimental results.

It should be noted that Eq. (6-4) is equal to the equation adopted by the Italian guideline CNR DT 200/R1 2013 [38] for FRP composites applied to concrete substrates, which has been shown to provide accurate estimations of the flexural and shear strength of FRP strengthened RC beams compared to other design guidelines [41].

For an FRCM-strengthened beam with fibers inclined at angle β with respect to the beam longitudinal axis, and a main diagonal shear crack inclined at angle θ with respect to the beam longitudinal axis, it can be assumed that the shear crack width $w(\psi)$ increases linearly with increasing the coordinate of the shear crack axis ψ (see Figure 6-4), as shown in Eq. (6-6):

$$w(\psi) = \alpha\psi \qquad \text{6-6}$$
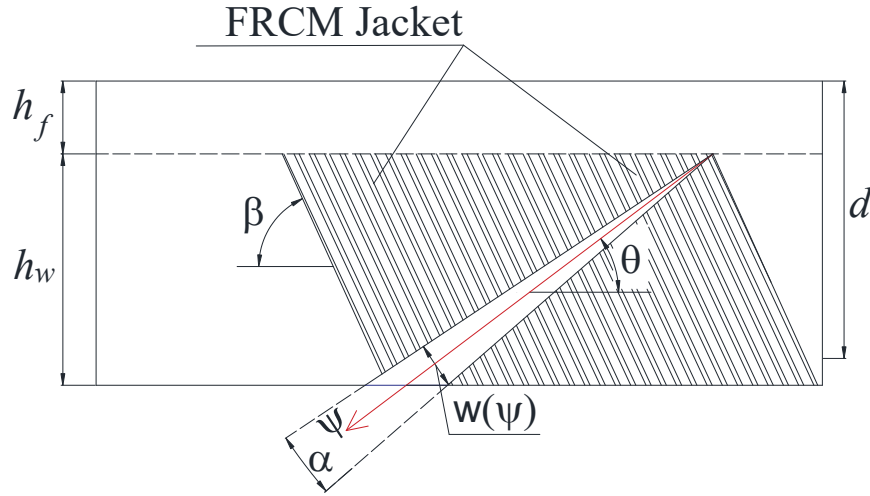
Figure 6-4 Idealized RC beam strengthened in shear with FRCM composite.

If $\tau_f=0$, according to Eq. (6-4), and using Figure 6-5, the average stress along the shear crack, $\bar{\sigma}_f$, on a U-wrapped FRCM composite crossing the shear crack is:

$$
\bar{\sigma}_f = \begin{cases} \sigma_{deb}\left(1 - \dfrac{1}{3}\dfrac{\psi_{eff}}{\psi}\right) & if\ \psi \geq \psi_{eff} \\[2em] \sigma_{deb}\dfrac{\psi}{\psi_{eff}}\left(1 - \dfrac{1}{3}\dfrac{\psi}{\psi_{eff}}\right) & if\ \psi < \psi_{eff} \end{cases}
\qquad 6\text{-}7
$$

If $\tau_f \neq 0$, Eq. (6-5) applies and $\bar{\sigma}_f$ becomes:

$$
\bar{\sigma}_f = \begin{cases} \dfrac{1}{\psi}\left\{ \begin{aligned} &(\psi - \psi_{eff})\left[\sigma_{deb} + \dfrac{sin\theta}{sin\beta}\dfrac{m}{2}(\psi - \psi_{eff})\right] + \\ &\psi_{eff}^2\dfrac{sin\theta}{sin\beta}\left[\dfrac{\psi_{eff}^2}{4}\dfrac{sin\theta}{sin\beta}\dfrac{l_{eff}(c+m) - 2\sigma_{deb}}{l_{eff}^3}\right] + \\ &\dfrac{\psi_{eff}}{3}\dfrac{sin\theta}{sin\beta}\dfrac{3\sigma_{deb} - l_{eff}(2c+m)}{l_{eff}^2} + \dfrac{c}{2} \end{aligned}\right\} & if\ \psi \geq \psi_{eff} \\[4em] \psi\dfrac{sin\theta}{sin\beta}\left[\begin{aligned} &\dfrac{\psi^2}{4}\left(\dfrac{sin\theta}{sin\beta}\right)^2\dfrac{l_{eff}(c+m) - 2\sigma_{deb}}{l_{eff}^3} + \\ &\dfrac{\psi}{3}\dfrac{sin\theta}{sin\beta}\dfrac{3\sigma_{deb} - l_{eff}(2c+m)}{l_{eff}^2} + \dfrac{c}{2} \end{aligned}\right] & if\ \psi < \psi_{eff} \end{cases}
\qquad 6\text{-}8
$$

For design purposes, it can be assumed that the shear crack has a length ψ equal to:

$$\psi = \frac{\min\{h_w, z\}}{sin(\theta)} \qquad\qquad 6\text{-}9$$

where h_w is the height of the web of a T-beam, and $z=0.9d$ is the beam inner lever arm. For rectangular sections, the flange thickness (h_f) is equal to zero, and ψ $=0.9d/sin\theta$.

It can be proven that the maximum average stress, and $\overline{\sigma_{f,max}}$, is obtained when (see Figure 6-5):

$$\psi_{eff} = l_{eff}\frac{sin(\beta)}{sin(\theta)} \qquad\qquad 6\text{-}10$$
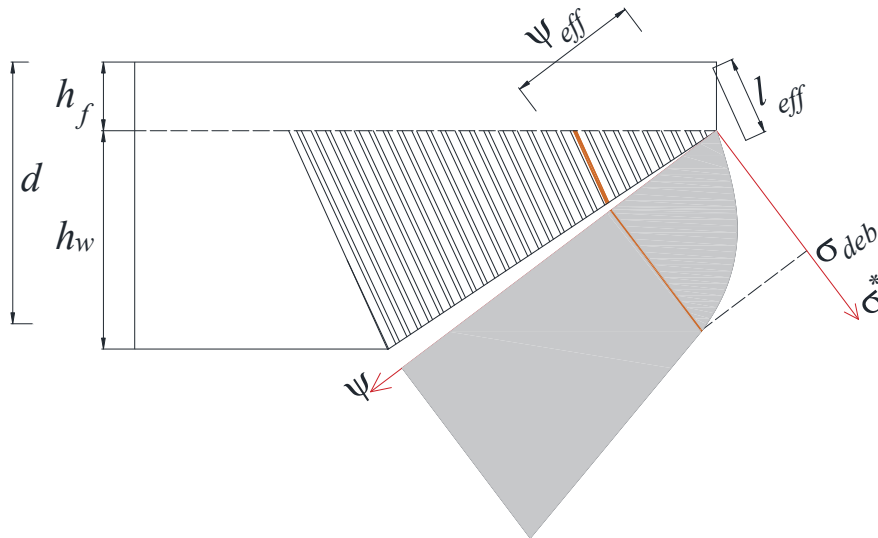
Figure 6-5 Variation of bond stress in the FRCM composite with respect to the crack length.

For the case of $\tau_f=0$, $\overline{\sigma_{f,max}}$ is:

$$\overline{\sigma_{f,max}} = \begin{cases} \sigma_{deb}\left(1 - \frac{1}{3}\frac{l_{eff}}{\min\{h_w,z\}}\right)sin(\beta) & if\ l_{eff} \geq \frac{\min\{h_w,z\}}{sin(\beta)} \\ \sigma_{deb}\frac{\min\{h_w,z\}}{l_{eff}}\frac{sin(\theta)}{sin(\beta)}. \\ \left(1 - \frac{1}{3}\frac{\min\{h_w,z\}}{l_{eff}}\frac{sin(\theta)}{sin(\beta)}\right)sin(\theta) & if\ l_{eff} < \frac{\min\{h_w,z\}}{sin(\beta)} \end{cases} \qquad 6\text{-}11$$

If $\tau_f \neq 0$, $\overline{\sigma_{f,max}}$ becomes:

$$\overline{\sigma_{f,max}} = \begin{cases} \dfrac{1}{\min\{h_w,z\}} \left\{ \begin{array}{l} \left[\sigma_{deb} + \dfrac{m}{2}\left(\dfrac{h_w}{\sin\beta} - l_{eff}\right)\right](h_w - l_{eff}\sin\beta) + \\[2mm] l_{eff}\sin\beta \dfrac{6\sigma_{deb} + l_{eff}(c-m)}{12} \end{array} \right\} & if\ l_{eff} \geq \dfrac{\min\{h_w,z\}}{\sin(\beta)} \\[10mm] \dfrac{\min\{h_w,z\}}{\sin(\beta)} \left[\begin{array}{l} \left(\dfrac{\min\{h_w,z\}}{2\sin\beta}\right)^2 \dfrac{l_{eff}(c+m) - 2\sigma_{deb}}{l_{eff}^3} + \\[2mm] \dfrac{\min\{h_w,z\}}{3\sin(\beta)} \dfrac{3\sigma_{deb} + l_{eff}(2c-m)}{l_{eff}^2} + \dfrac{c}{2} \end{array} \right] & if\ l_{eff} < \dfrac{\min\{h_w,z\}}{\sin(\beta)} \end{cases}$$

6-12

6.3 Experimental investigation of carbon FRCM composite materials applied onto concrete support

In this section, the bond behavior of carbon FRCM composites applied to concrete supports are investigated using a single-lap direct-shear test. The aim of this study is to verify if the assumptions made in the development of the model (see previous section) hold for the case of the carbon FRCM composites used during the experimental campaign discussed in Chapter 3.

6.3.1 Test set-up

The bond behaviour of carbon FRCM-concrete joints was investigated by means of the classical push-pull single-lap direct-shear test configuration [36]. Concrete blocks (prisms) with 125 mm x 125 mm cross-section and 500 mm length, restrained to the machine base using a steel frame (Figure 6-6), were employed. A strip of FRCM composite, comprised of one layer of fiber net embedded within two 4 mm thick matrix layers, was applied onto the concrete substrate. Different bonded lengths l were tested (Figure 6-6).
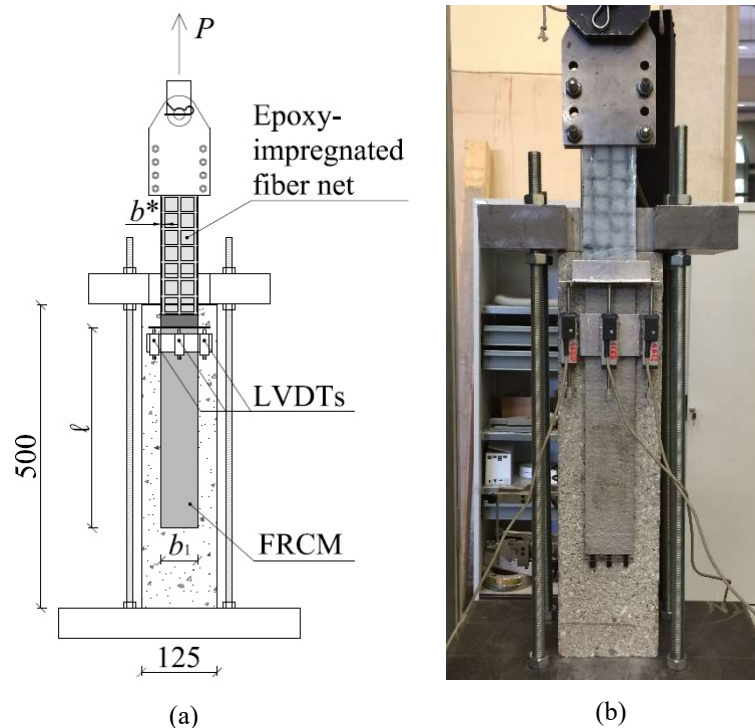
Figure 6-6 a) Single-lap direct-shear test set-up (measures in mm). b) Photo of specimen DS_CS170BL_330_60_2.

The fiber net was embedded within the matrix only in the bonded region whereas it was impregnated with epoxy resin outside the bonded region in an attempt to distribute the load and avoid premature failure [37]. Two aluminium plates were bonded to the end of the epoxy-impregnated fiber net to improve gripping by the testing machine. Two through-bolted steel plates connected to the testing machine through a hinge joint were used to clamp the aluminium plates. An Ω–shaped aluminium plate was bonded to the concrete block near (approximately 20 mm from) the loaded end of the composite. Two LVDTs were mounted on the sides and one LVDT was mounted on the middle of the Ω–shaped plate to measure the displacement of the fibers with respect to the concrete support. The LVDTs reacted off of a thin aluminium L–shaped plate bonded to the epoxy-impregnated fibers at the loaded end (Figure 6-6). The displacement measured by the central LVDT was used to control the test and was increased at a constant rate equal to 0.008 mm/s. It should be noted that the average displacement measured by the two LVDTs on the sides of the composite corresponds to the global slip g if the substrate is considered rigid.

6.3.1 Materials employed

The FRCM materials employed were commercially available from a single manufacturer and are the same used during the experimental campaign presented in Chapter 3(see Section3.1.1). The carbon fiber net was comprised of fiber bundles spaced at 20 mm in the longitudinal and transversal directions with an overall area weight of 170 g/m^2. The area A_b of a single bundle of carbon fibers is 0.94 mm^2, as reported by the manufacturer.

Compressive tests according to UNI EN 12390-3 [49] were carried out on six 150 mm cubes cast from the same batch used to cast the concrete blocks. The average cubic compressive strength was 59.3 MPa (CoV=0.150). Three batches of the same matrix, named matrix S, were used at different times to cast the FRCM composite. Although each batch was prepared in the same manner and the specimens were cured in the same way, the matrix mechanical properties obtained are slightly different. A minimum of three 40 mm x 40 mm x 160 mm samples were cast from each batch of matrix used to prepare the FRCM. The matrix samples were tested according to UNI EN 1015-11 [89] on the same day the corresponding direct-shear tests were carried out. The first batch, named batch A, had an average flexural strength, f_{flex}, and average compressive strength, r_{cm}, equal to 3.60 MPa and 16.70 MPa, respectively. The second batch, named batch B, had f_{flex}=5.59 MPa and r_{cm}=16.98 MPa.

6.3.1 Experimental results

The results of 14 single-lap direct-shear tests conducted on carbon FRCM-concrete joints are presented. Four different bonded lengths l were adopted, namely 100 mm, 200 mm, 330 mm, and 450 mm. The bonded width of the carbon FRCM composite, b_1=60 mm, was designed to include three longitudinal fiber bundles and to leave a distance of half the net spacing between the matrix edge and the external fiber bundle edge. Specimens were named following the notation DS_FMK_X_Y_Z, where F=fiber employed (C=carbon), M=matrix employed (matrix S), K indicates the area weight of the fiber net in g/m^2, X=bonded length (ℓ) in mm, Y=bonded width (b_1) in mm, and Z=specimen number. The peak load P^* and the corresponding peak stress σ^*, are reported in Table 6-1 for each specimen tested.

Table 6-1. Results of single-lap direct-shear tests

SPECIMEN NAME	P^* [kN]	Average P^* [kN]	σ^* [MPa]	Average σ^* [MPa]	MATRIX BATCH
DS_CS170BL_100_60_1	0.75		270		A
DS_CS170BL_100_60_2	0.57	0.54	200	166.7	A
DS_CS170BL_100_60_3	0.42		150		A
DS_CS170BL_100_60_4	0.42		150		C
DS_CS170BL_200_60_1	0.87		310		A
DS_CS170BL_200_60_2	0.96	0.86	340	306.7	A
DS_CS170BL_200_60_3	0.76		270		A
DS_CS170BL_330_60_1	1.57		560		A
DS_CS170BL_330_60_2	1.58	1.51	560	535.0	A
DS_CS170BL_330_60_3	1.23		440		A
DS_CS170BL_330_60_4	1.64		580		C
DS_CS170BL_450_60_1	1.71		610		A
DS_CS170BL_450_60_2	1.85	1.70	660	605.0	A
DS_CS170BL_450_60_3	1.54		550		A

The load responses of specimens with carbon FRCM composites are reported in Figure 6-7. The failure was characterized by debonding of the fiber net from the embedding matrix. Specimens DS-CS170BL-100-60-1, DS_CS170BL-330-60-3, and DS_CS170BL_450_60_3 presented a peak load significantly different than other specimens with the same bonded length (see Table 6-1). This may be due to the different bond behaviour of some of the longitudinal fiber bundles in these specimens.

On the other hand, it appears that the different mechanical properties of the matrix batches employed did not affect the load responses. This evidence suggests that the inherent bond between matrix and fiber, rather than the mechanical properties of the matrix, plays the fundamental role in determining the load-carrying capacity of FRCM-concrete joints [37].
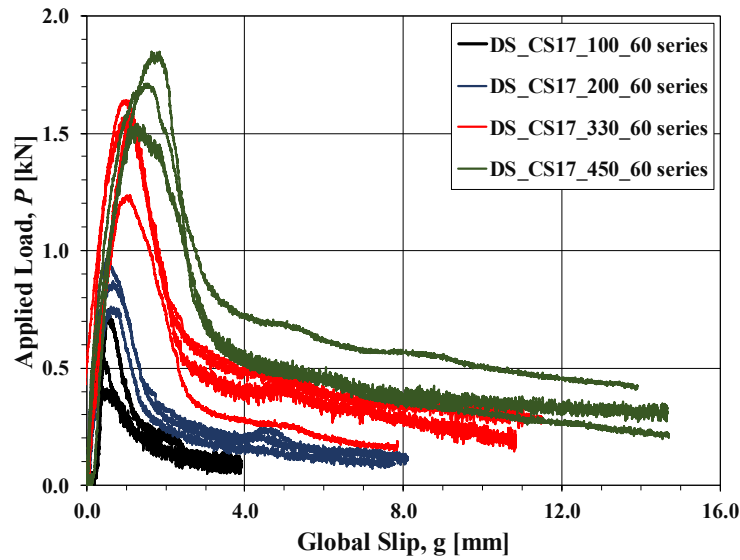
Figure 6-7 Applied load P vs. Global slip g curve for carbon FRCM-concrete joints

Results in Figure 6-8 and Table 6-1 indicate that the peak stress σ^* increases with bonded length l, with lower increases rates for values of l larger or equal to 330 mm. In fact, σ^* for specimens with bonded length l=450 mm is only slightly larger than the peak load for specimens with l=330 mm (average increase = 11.5%). This suggests that the length needed to fully establish the stress transfer mechanism (i.e. the effective bond length) is less than 330 mm. However, further test of FRCM-concrete joints with bonded length between 200 and 330 mm are needed to determine the exact value of the l_{eff}. These results are also required to calibrate the equation that describes the relationship between the peak stress σ^* and the bonded length l for values of l lower than l_{eff} ($f(l)$, see Eq. (6-5)).
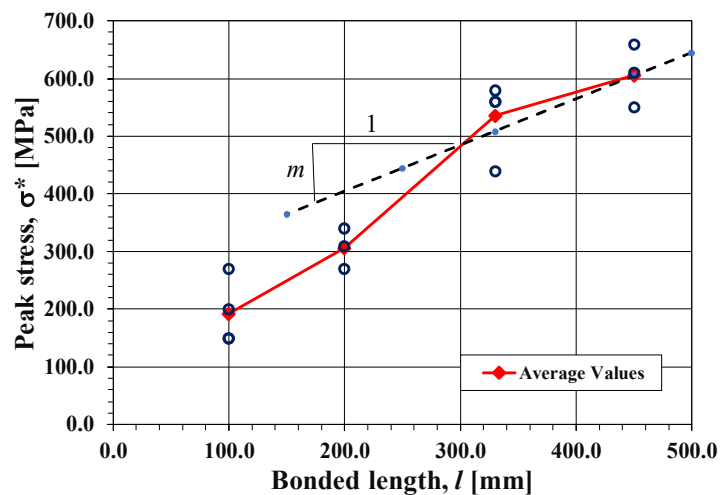
Figure 6-8 Peak stress σ* vs. Bonded length l for carbon FRCM-concrete joints

148

In Table 6-2, values of P_f and the friction stress τ_f computed according to Eq. (6-2) for the specimens tested are shown. Results show with the exception of the specimens with l=100 mm, average values of τ_f are similar indistinctely of the composite bonded length. When the average value of τ_f for all the specimens testes is used, a value of m=0.80 kN/m, computed according to Eq. (6-3) is found.

Table 6-2. Values of P_f and τ_f

SPECIMEN NAME	P_f [kN]	Average P_f [kN]	τ_f [MPa]	Average τ_f [MPa]
DS_CS170BL_100_60_1	0.11		0.111	
DS_CS170BL_100_60_2	0.10	0.09	0.101	0.093
DS_CS170BL_100_60_3	0.08		0.084	
DS_CS170BL_100_60_4	0.08		0.075	
DS_CS170BL_200_60_1	0.11		0.056	
DS_CS170BL_200_60_2	0.12	0.11	0.061	0.072
DS_CS170BL_200_60_3	0.09		0.047	
DS_CS170BL_330_60_1	0.28		0.084	
DS_CS170BL_330_60_2	0.21	0.25	0.064	0.067
DS_CS170BL_330_60_3	0.19		0.057	
DS_CS170BL_330_60_4	0.32		0.098	
DS_CS170BL_450_60_1	0.21		0.047	
DS_CS170BL_450_60_2	0.42	0.31	0.093	0.070
DS_CS170BL_450_60_3	0.31		0.069	
		AVG		0.075

In Figure 6-8, a straight line with a slope equal to m is drawn (dashed line in Figure 6-8), using as fixed point the value of σ^* found for l=450 mm. It can be seen that this line agrees with the line that connects the average values of σ^* for the joints with l=330 mm and 450 mm. This result corroborates the assumption that for values of bonded length longer than l_{eff}, the bonded stress behavior of the FRCM-concrete joints can be described with a linear function, r(l), with slope equal to m (see Sections 6.2, Eq. (6-5)).

6.4 Final remarks

In this section, a new model for the evaluation of the FRCM contribution to the shear strength of FRCM U-wrapped specimens, that considers the bond behavior of the composite when it is applied onto concrete substrates, was discussed. The model is based on the equations proposed by [38] for the case of FRP strengthened

specimens and modifies them to take into account the presence of the friction between the fibers and the cementitious matrix.

The model evaluates the stress in the FRCM composite along the shear crack considering an idealized peak stress vs. bonded length relationship that was developed using the behaviour observed for PBO FRCM-concrete joints tested using a tradional push-pull single-lap direct-shear test.

However, the peak stress vs. bonded length relationship evaluated for carbon FRCM-concrete joints showed a similar behavior to that observed for PBO FRCM-concrete joints. Although it was not possible to find the actual value of l_{eff}, results show that for the carbon FRCM composite employed in this thesis, l_{eff} was longer than 200 mm and less than 330 mm. Additional tests are required in order to determine the actual value of l_{eff} and calibrate the peak stress vs. bonded length response for l less than l_{eff}. For values of l larger than 330 mm, i.e., larger than l_{eff}, the experimental results allowed to verify that the increase in the peak stress can be idealized by a linear relationship that depends on the frictional shear stress. These results suggest that the assumptions used during the development of the model are appropiate, but additional tests are needed in order to determine the required peak stress vs. bonded length relationship.

7.   CONCLUSIONS

The behavior of RC beams strengthened in shear with fiber reinforced cementitious matrix (FRCM) composites was investigated in this thesis.

In Chapter 2, a review of the scientific literature available regarding the shear strengthening of RC beams with FRCM composites was carried out. This review included the development of a database of experimental tests performed on shear strengthened RC beams with the FRCM system. The information collected in the database was used to investigate the data distribution of main geometrical and mechanical properties of the beams and the FRCM composites. It was also employed to analyze the influence of selected parameters on the response of RC beams strengthened in shear with FRCM composites. The results obtained showed that FRCM composites can increase the shear strength of RC beams, and, for some limited cases, the strengthening was able to modify a brittle shear failure in unstrengthened specimens to a more ductile flexure failure in strengthened beams. The effectiveness of the strengthening system appears to be influenced by parameters including the wrapping configuration, number of layers, matrix compressive strength relative to the concrete compressive strength, and axial rigidity of the fibers. In addition, the interaction between the internal transverse steel reinforcement and the strengthening system, already reported for FRP composites, was also observed for the beams included in the database.

In Chapter 3, the results of an experimental campaign conducted on RC beams strengthened in shear with FRP and FRCM composites were presented. Besides the type of composite, variables studied included the internal transverse reinforcement ratio, type of fiber, and the presence of anchors. The behavior of the beams was discussed in terms of additional shear strength provided by the strengthening system, failure mode, and values of measured strains in the stirrups and the fibers. Results show that the gain in the shear strength of strengthened beams increases with increasing axial stiffness of the composite. Internal-external shear reinforcement interaction, i.e. reduction of the stirrup strain due to the presence of the composite, was observed for both FRP and FRCM strengthened beams, but the interaction was less pronounced for those with FRCM composites. The anchors employed in this study did not affect the shear strength of the beams, but changes in the concrete crack pattern, mid-span displacement, and failure mode were observed. For FRCM strengthened beams, strains measured in the fibers

showed higher exploitation ratios, i.e. the ratio between the maximum measured fiber strain and the rupture strain, for beams with carbon FRCM than those with steel FRCM.

In Chapter 4, four design models proposed to predict the contribution of the FRCM composite to the shear strength of RC beams were assessed using the database developed. Results show that the use of the properties of the FRCM composite instead of the fiber mechanical characteristics does not significantly increase the accuracy of the models. A simple formulation based on a constant value of effective fiber strain, based on the bare fiber properties, was found to be more accurate for beams with or without composite detachment. In general, combining the models for predicting the contribution of the FRCM system to the shear strength of the beams with the requirements established by available guidelines for predicting the shear strength of the unstrengthened beams improves the performance of the models in terms of both safety and accuracy.

Chapter 5 was devoted to estimate the individual contributions of the concrete, stirrups, and fibers to the overall shear strength of FRCM strengthened RC beams. In order to do so, two different approaches, based on the measured strains in the stirrups and fibers, were presented. Results showed that for low values of load, the shear strength of the beams was due exclusively to the concrete contribution. After the concrete starts cracking, the contribution of the stirrups and the fibers start to increase, and the concrete contribution decreases. When the peak shear strength of the beams is attained, the stirrup and fiber contributions reached their maximum contribution while the concrete contribution is at its minimum.

In Chapter 6, a model for predicting the contribution of the FRCM system to the shear strength of RC beams, based on the bond behavior of the composite, is discussed. In this chapter, the equations to obtain the average stress and maximum average stress attained in the FRCM composite for a U-wrapped beam are introduced. Although further experimental evidence is required to calibrate and validate the model, the results obtained from single-lap direct-shear tests showed that the assumptions made to develop the model are appropriate.

8. FUTURE WORK

The results presented in this thesis are aimed to improve the knowledge regarding the shear strengthening of RC beams with FRCM composites. However, considering the limited available information in the subject, it is considered that the above conclusions will need to be validated when more experimental data become available. It is also hoped that the evaluation of the database and distribution of data carried out in this thesis will help researchers to plan future experimental tests that focus on variables with scarce data, such as strains in internal transverse shear reinforcement, the influence of the ratio between the compressive strength of the cementitious matrix and the concrete, the study of different types of fibers, and how the use of anchors help mitigate detachment and other forms of FRCM composite debonding.

Additional experimental evidence is required to calibrate and validate the design model presented in this work. In particular, tests should focus on evaluating peak stress vs. bonded length for different type of fibers and cementitious matrix, and number of composite layers.

Furthermore, the interaction between the internal and external shear reinforcement requires special attention in the development of future design models aimed to compute the final total shear capacity of a strengthened element, as the simple addition of concrete, steel, and FRCM composite contributions might not provide accurate results. In addition, the inclusion of variable shear crack angle in the design models needs to be studied to evaluate the influence and potential to improve the available models. Design models such as the modified compression field theory and its simplified version, which have shown an appropriate performance for predicting the shear strength of unstrengthened beams, might be studied in the future to analyze their applicability for the case of FRCM-strengthened beams.

154

9. REFERENCES

[1] Triantafillou TC, Papanicolaou CG. Shear strengthening of reinforced concrete members with textile reinforced mortar (TRM) jackets. Mater Struct Constr 2006;39:93–103.

[2] Pellegrino C, D'Antino T. Experimental behaviour of existing precast prestressed reinforced concrete elements strengthened with cementitious composites. Compos Part B Eng 2013;55:31–40.

[3] Gonzalez-Libreros JH, Sneed LH, D'Antino T, Pellegrino C. Behavior of RC beams strengthened in shear with FRP and FRCM composites. Eng Struct 2017;150:830–42. doi:10.1016/j.engstruct.2017.07.084.

[4] Alabdulhady M, Sneed LH, Carloni C. Torsional behavior of RC beams strengthened with PBO-FRCM composite – An experimental study. Eng Struct 2017;136:393–405. doi:DOI: 10.1016/j.engstruct.2017.01.044.

[5] Ombres L. Concrete confinement with a cement based high strength composite material. Compos Struct 2014;109:294–304. doi:10.1016/j.compstruct.2013.10.037.

[6] Tetta ZC, Bournas DA. TRM vs FRP jacketing in shear strengthening of concrete members subjected to high temperatures. Compos Part B Eng 2016;106:190–205.

[7] Blanksvärd T, Täljsten B, Carolin A. Shear strengthening of concrete structures with the use of mineral-based composites. J Compos Constr 2009;13:25–34.

[8] Sneed L, Verre S, Carloni C, Ombres L. Flexural behavior of RC beams strengthened with steel-FRCM composite. Eng Struct 2016;127:686–99.

[9] Joint ACI-ASCE Committee 445. Recent Approaches to Shear Design of Structural Concrete. J Struct Div ASCE 1999;124:1375–417.

[10] Brückner A, Ortlepp R, Curbach M. Textile reinforced concrete for strengthening in bending and shear. Mater Struct 2006;39:741–8. doi:10.1617/s11527-005-9027-2.

[11] Brückner A, Ortlepp R, Curbach M. Anchoring of shear strengthening for T-beams made of textile reinforced concrete (TRC). Mater Struct 2008;41:407–18. doi:10.1617/s11527-007-9254-9.

[12] Al-Salloum Y, Elsanadedy HM, Alsayed SH, Iqbal RA. Experimental and numerical study for the shear strengthening of reinforced concrete beams using textile-reinforced mortar. J Compos Constr 2012;16:74–90.

[13] Contamine R, Si Larbi A, Hamelin P. Identifying the contributing mechanisms of textile reinforced concrete (TRC) in the case of shear repairing damaged and reinforced concrete beams. Eng Struct 2013;46:447–58. doi:10.1016/j.engstruct.2012.07.024.

[14] Azam R, Soudki K. FRCM Strengthening of Shear-Critical RC Beams. J Compos Constr 2014;18:1–9. doi:10.1061/(ASCE)CC.1943-5614.0000464.

[15] Baggio D, Soudki K, Noël M. Strengthening of shear critical RC beams with various FRP systems. Constr Build Mater 2014;66:634–44. doi:10.1016/j.conbuildmat.2014.05.097.

[16] Tzoura E, Triantafillou TC. Shear strengthening of reinforced concrete T-beams under cyclic loading with TRM or FRP jackets. Mater Struct 2014:14–6.

[17] Escrig C, Gil L, Bernat-Maso E, Puigvert F. Experimental and analytical study of RC beams shear strengthened with different types of textile-reinforced mortar. Constr Build Mater 2015;83:248–60.

[18] Jung K, Hong K, Han S, Park J, Kim J. Shear Strengthening Performance of Hybrid FRP-FRCM. Adv Mater Sci Eng 2015;2015. doi:10.1155/2015/564876.

[19] Ombres L. Structural performances of reinforced concrete beams strengthened in shear with a cement based fiber composite material. Compos Struct 2015;122:316–29.

[20] Tetta ZC, Koutas LN, Bournas DA. Textile-reinforced mortar (TRM) versus fiber-reinforced polymers (FRP) in shear strengthening of concrete beams. Compos Part B Eng 2015;77:338–48.

[21] Trapko T, Urbańska D, Kamiński M. Shear strengthening of reinforced concrete beams with PBO-FRCM composites. Compos Part B Eng 2015;80:63–72. doi:10.1016/j.compositesb.2015.05.024.

[22] Loreto G, Babaeidarabad S, Leardini L, Nanni A. RC beams shear-strengthened with fabric-reinforced-cementitious-matrix (FRCM) composite. Int J Adv Struct Eng 2015;7:341–52. doi:10.1007/s40091-015-0102-9.

[23] Awani O, El-maaddawy T, Refai A El. Numerical Simulation and Experimental Testing of Concrete Beams Strengthened in Shear with Fabric-Reinforced Cementitious Matrix. J Compos Constr 2016;20:1–11. doi:10.1061/(ASCE)CC.1943-5614.0000711.

[24] Tetta ZC, Koutas LN, Bournas DA. Shear strengthening of full-scale RC T-beams using textile-reinforced mortar and textile-based anchors. Compos Part B Eng 2016;95:225–39.

[25] Sneed LH, Ramirez JA. Influence of Effective Depth on Shear Strength of Concrete Beams — Experimental Study. ACI Struct J 2010;107:554–511.

[26] Bousselham A, Chaallal O. Shear Strengthening Reinforced Concrete Beams with Fiber-Reinforced Polymer: Assessment of Influencing Parameters and Required Research. ACI Struct J 2004;101:219–27. doi:10.14359/13019.

[27] Leung CKY, Chen Z, Lee S, Ng M, Xu M, Tang J. Effect of Size on the Failure of Geometrically Similar Concrete Beams Strengthened in Shear with FRP Strips. J Compos Constr 2007;11:487–96. doi:10.1061/(ASCE)1090-0268(2007)11:5(487).

[28] Kani GNJ. Kani G.N.J. (1967). How Safe Are Our Large Reinforced Concrete Beams? ACI J 1967;64:128–41.

[29] Pellegrino C, Modena C. Fiber-Reinforced Polymer shear strengthening of reinforced concrete beams: experimental study and analytical modeling. ACI Struct J 2007;103:720–8.

[30] Pellegrino C, Modena C. An experimentally based analytical model for the shear capacity of FRP-strengthened reinforced concrete beams. Mech Compos Mater 2008;44:231–44.

[31] Chen JF, Teng JG. Shear Capacity of FRP-Strengthened RC Beams: FRP debonding. Constr Build Mater 2003;17:27–41.

[32] Pellegrino C, Vasic M. Assessment of design procedures for the use of externally bonded FRP composites in shear strengthening of reinforced concrete beams. Compos Part B Eng 2013;45:727–41.

[33] Chen GM, Teng JG, Chen JF, Rosenboom O. Interaction between Steel Stirrups and Shear-Strengthening FRP Strips in RC Beams. J Compos Constr 2010;14:498–509.

[34] Khalifa A, Gold WJ, Nanni A, M.I. AA. Contribution of Externally Bonded FRP to Shear Capacity of RC Flexural Members. J Compos Constr 1998;2:195–202. doi:10.1061/(ASCE)1090-0268(1998)2:4(195).

[35] D'Antino T, Carloni C, Sneed LH, Pellegrino C. Matrix-fiber bond behavior in PBO FRCM composites: A fracture mechanics approach. Eng Fract Mech 2014;117:94–111. doi:10.1016/j.engfracmech.2014.01.011.

[36] Sneed LH, D'Antino T, Carloni C. Investigation of bond behavior of polyparaphenylene benzobisoxazole fiber-reinforced cementitious matrix composite-concrete interface. ACI Mater J 2014;111:569–80. doi:10.14359/51686604.

[37] D'Antino T, Pellegrino C, Carloni C, Sneed LH, Giacomin G. Experimental Analysis of the Bond Behavior of Glass, Carbon, and Steel FRCM

Composites. Key Eng Mater 2014;624:371–8. doi:10.4028/www.scientific.net/KEM.624.371.

[38] National Research Council (CNR). Guide for the design and construction of externally bonded FRP systems for strengthening existing structures. CNR-DT 200. Rome, Italy: 2013.

[39] ACI Committee 440. Guide for the design and construction of externally bonded FRP systems for strengthening concrete structures. ACI 440.2R. Farmington Hills, MI.: 2008.

[40] Fédération Internationale du Béton (fib). Externally bonded FRP reinforcement for RC structures, Task Group 9.3, Bulletin No. 14. Lausanne, Switzerland: 2001.

[41] D'Antino T, Triantafillou TC. Accuracy of design-oriented formulations for evaluating the flexural and shear capacities of FRP-strengthened RC beams. Struct Concr 2016;17:425–42. doi:10.1002/suco.201500066.

[42] Triantafillou TC, Antonopoulos CP. Design of Concrete Flexural Members Strengthened in Shear with FRP. J Compos Constr 2000;4:198–205.

[43] D'Antino T, Sneed LH, Carloni C, Pellegrino C. Influence of the substrate characteristics on the bond behavior of PBO FRCM-concrete joints. Constr Build Mater 2015;101:838–50. doi:10.1016/j.conbuildmat.2015.10.045.

[44] ACI Committee 549. Guide to design and construction of externally bonded Fabric-Reinforced Cementitious Matrix (FRCM) systems for Repair and Strengthening Concrete and Masonry Structures. ACI549R-13. Farmington Hills, MI.: 2013.

[45] Sas G, Täljsten B, Barros J, Lima J, Carolin A. Are available models reliable for predicting the FRP contribution to the shear resistance of RC beams? J Compos Constr 2009;13:514–34.

[46] Grelle S, Sneed LH. Review of anchorage systems for externally bonded FRP laminates. Int J Concr Struct Mater 2013;7:17–33.

[47] Trapko T. The effect of high temperature on the performance of CFRP and FRCM confined concrete elements. Compos Part B Eng 2013;54:138–45. doi:10.1016/j.compositesb.2013.05.016.

[48] Barton B, Wobbe E, Dharani LR, Silva P, Birman V, Nanni A, et al. Characterization of reinforced concrete beams strengthened by steel reinforced polymer and grout (SRP and SRG) composites. Mater Sci Eng A 2005;412:129–36.

[49] EN-12390-3. Testing hardened concrete-Part 3: Compressive strength of test specimens. Brussels, Belgium: EUROPEAN COMMITTEE FOR STANDARDIZATION; 2009.

[50] G&PIntech. C-SHEET. Tech Datasheets 2016. www.gpintech.com (accessed September 1, 2016).

[51] EN-12390-5. Testing hardened concrete - Part 5: Flexural strength of test specimens. Brussels, Belgium: EUROPEAN COMMITTEE FOR STANDARDIZATION; 2009.

[52] Bousselham A, Chaallal O. Effect of transverse steel and shear span on the performance of RC beams strengthened in shear with CFRP. Compos Part B Eng 2006;37:37–46.

[53] Grande E, Imbimbo M, Rasulo A. Effect of transverse steel on the response of RC beams strengthened in shear by FRP: experimental study. J Compos Constr 2009;13:405–14.

[54] Pellegrino C, Modena C. FRP Shear Strengthening of RC Beams with Transverse Steel Reinforcement. J Compos Constr 2002;6:1–8.

[55] Koutas LN, Triantafillou TC. Use of anchors in shear strengthening of reinforced concrete T-Beams with FRP. J Compos Constr 2013;17:101–7.

[56] Comité Européen de Normalisation (CEN). Eurocode 2: Design of concrete structures-part 1-1: general rules and rules for buildings. EN 1992-1-. Brussels, Belgium: 2004.

[57] Lu XZ, Chen JF, Ye LP, Teng JG, Rotter JM. RC beams shear-strengthened with FRP: Stress distributions in the FRP reinforcement. Constr Build Mater 2009;23:1544–54.

[58] The Concrete Society. TR55 - Design guidance for strengthening concrete structures using fibre composite materials. Third Edit. UK: 2012.

[59] Teng JG, Chen GM, Chen JF, Rosenboom OA, Lam L. Behavior of RC beams shear strengthened with bonded or unbonded FRP wraps. J Compos Constr 2009;13:394–404. doi:10.1061/(ASCE)CC.1943-5614.0000040.

[60] Denton S, Shave J, Porter A. Shear strengthening of reinforced concrete structures using FRP composite. In: Hollaway, LC, Chryssanthopoulos, MK and Moy S, editor. Adv. Polym. Compos. Struct. Appl. Constr., Abington, Cambridge: Woodhead Publishing Limited,; 2004, p. 134–43.

[61] Chen JF, Teng JG. Shear Capacity of Fiber-Reinforced Polymer-Strengthened Reinforced Concrete Beams : Fiber Reinforced Polymer Rupture 2003;129:615–25.

[62] D'Antino T, Pellegrino C, Salomoni V, Mazzuco G. Shear behavior of RC structural members strengthened with FRP materials : A three dimensional numerical approach. ACI Spec Publ 2012:69–84.

[63] Maeda T, Asano Y, Sato Y, Ueda T, Kakuta Y. A study on bond mechanism of carbon fiber sheet. Non-Metallic Reinf. Concr. Struct. Proc. 3rd Symp,

Tokyo, Japan: 1997, p. 279–86.

[64] J.F.Chen & J.G.Teng. Anchorage Strength Models for FRP and Steel Plates. J Struct Eng 2001;127:784–91.

[65] D'Antino T, Pellegrino C. Bond between FRP composites and concrete: Assessment of design procedures and analytical models. Compos Part B Eng 2014;60:440–56. doi:10.1016/j.compositesb.2013.12.075.

[66] Grace C, Yang Y, Sneed L. Fracture Mechanics Approaches to Predicting the Behavior of Reinforced Concrete Members with Externally-bonded Fiber Reinforced Polymer Laminates. A Fract Approach FRP-Concrete Struct ACI Spec Publ 2012:1–20.

[67] Triantafillou TC. Fracture mechanics approaches to concrete strengthening using FRP materials. Fract. Mech. Concr. Struct. Proc. Fram., Gifu (Japan): AEDIFICATIO Publishers, D-79104; 1998, p. 1761–70.

[68] J.F.Chen & J.G.Teng. Anchorage strength mdels for FRP and steel plates. J Struct Eng 2001;127:784–91.

[69] Comité Européen de Normalisation (CEN): Eurocode 8: Design of structures for earthquake reistance – Part 3: Assessment and retrofitting of buildings. EN 1998-3. Brussels, Belgium: 2005.

[70] Neubauer U, Rostasy F. Design aspects of concrete structures strengthened with externally bonded CFRP plates. In: Publications E, editor. Proc. 7th Int. Conf. Struct. Faults Repair, Vol. 2, 1997, p. 109–18.

[71] Jirawattanasomkul T, Dai J, Zhang D, Senda M, Ueda T. Experimental Study on Shear Behavior of Reinforced-Concrete Members Fully Wrapped with Large Rupture-Strain FRP Composites. J Compos Constr 2014;18:1–12. doi:10.1061/(ASCE)CC.1943-5614.0000442.

[72] Bousselham A, Chaallal O. Maximum Shear Strength of RC Beams Retrofitted in Shear with FRP Composites. J Compos Constr 2009;13:302–14. doi:10.1061/(ASCE)1090-0268(2009)13:4(302).

[73] Mofidi A, Chaallal O. Shear strengthening of RC beams with EB FRP: Influencing factors and conceptual debonding model. J Compos Constr 2011;15:62–74. doi:10.1061/(ASCE)CC.1943-5614.0000153.

[74] Carolin A, Täljsten B. Theoretical Study of Strengthening for Increased Shear Bearing Capacity. J Compos Constr 2005;9:497–506. doi:10.1061/(ASCE)1090-0268(2005)9:6(497).

[75] Sabau C, Gonzalez-Libreros JH, Sneed LH, Sas G, Pellegrino C, Täljsten B. Use of image correlation system to study the bond behavior of FRCM-concrete joints. Mater Struct 2017;50:172. doi:10.1617/s11527-017-1036-4.

[76] D'Antino T, Papanicolaou C. Mechanical characterization of textile

reinforced inorganic-matrix composites. Compos Part B Eng 2017. doi:10.1016/j.compositesb.2017.02.034.

[77] Si Larbi A, Contamine R, Ferrier E, Hamelin P. Shear strengthening of RC beams with textile reinforced concrete (TRC) plate. Constr Build Mater 2010;24:1928–36. doi:10.1016/j.conbuildmat.2010.04.008.

[78] National Research Council (CNR). Guide for the design and construction of externally bonded FRP systems for strengthening existing structures. CNR-DT 200. Rome, Italy: 2004.

[79] Cladera A, Marı AR. Shear strength in the new Eurocode 2 . A step forward ? Struct Concr 2007;8:57–66.

[80] Vecchio FJ, Collins MP. The Modified Compression-Field Theory for reinforced concrete elements subjected to shear. ACI J 1986;83:219–31.

[81] Park S-Y. Prediction of shear strength of R/C beams using Modified Compression Field Theory and ACI Code. KCI Concr J 1999;11:5–17.

[82] Bentz EC, Vecchio FJ, Collins MP. Simplified Modified Compression Field Theory for Calculating Shear Strength of Reinforced Concrete Elements. ACI Struct J 2006;103:614.-624.

[83] ACI Committee 318. Building Code Requirements for Structural Concrete and Commentary (ACI 318-14). Farmington Hills, MI.: 2014.

[84] Chen GM, Teng JG, Chen JF. Shear strength model for FRP-strengthened RC beams with adverse FRP-steel interaction. J Compos Constr 2013;17:50–66.

[85] Carloni C, Subramaniam KV. Application of fracture mechanics to debonding of FRP from RC members. Am Concr Institute, ACI Spec Publ 2012:1–16.

[86] D'Antino T. Bond Behavior in Fiber Reinforced Polymer Composites and Fiber Reinforced Cementitious Matrix Composites. University of Padua, 2014.

[87] Subramaniam K V., Carloni C, Nobile L. Width effect in the interface fracture during shear debonding of FRP sheets from concrete. Eng Fract Mech 2007;74:578–94. doi:10.1016/j.engfracmech.2006.09.002.

[88] D'Ambrisi A, Feo L, Focacci F. Experimental analysis on bond between PBO-FRCM strengthening materials and concrete. Compos Part B Eng 2013;44:524–32. doi:10.1016/j.compositesb.2012.03.011.

[89] EN UNI 1015-11. Methods of test for mortar for masonry – Part 11: determination of flexural and compressive strength of hardened mortar. Brussels, Belgium: EUROPEAN COMMITTEE FOR STANDARDIZATION; 2007.

APPENDIX A. EXPERIMENTAL DATABASE (STRENGTHENED BEAMS)

164

Ref.	Name	Shape	b_w [mm]	d [mm]	a/d	f_c [MPa]	ρ_l	ρ_w	SC	Fiber	Anchors	s_f [mm]	w_f [mm]	E_f [GPa]	f_f [MPa]	n	ρ_f	f_{cm} [MPa]	E_{FRCM} [GPa]	ρ_{cm}	V_{FRCM} [kN]	Failure mode	V_{FRCM}/V_{CON}
[1]	M2	R	150	272	2.85	25.3	0.015	0.0014	W	C	N	1	1	225	3350	2	0.0013	30.6	NR	0.070	63.7	F	1.09
	M2-s	R	150	272	2.85	25.3	0.015	0.0014	W	C	N	1	1	225	3350	2	0.0012	30.6	NR	0.070	60.6	F	1.04
	M1	R	150	272	2.85	25.3	0.015	0.0014	W	C	N	1	1	225	3350	1	0.0006	30.6	NR	0.047	41.8	S	0.72
[10]	R2	R	150	256	3.91	23.2	0.032	0.0000	W	G	N	1	1	75	574	2	0.0015	77.2	NR	0.080	25.5	S	0.44
	R3	R	150	256	3.91	23.2	0.032	0.0000	W	G	N	1	1	75	574	3	0.0022	77.2	NR	0.053	43.5	S	0.74
[11]	PB-1/1	T	120	372	2.69	25.5	0.042	0.0042	U	G	N	1	1	75	574	2	0.0018	82.8	NR	0.100	44.7	S	0.19
	PB-1/2	T	120	372	2.69	26.3	0.042	0.0042	U	G	N	1	1	75	574	4	0.0037	85.3	NR	0.167	41.5	S	0.18
	PB-1/3	T	120	372	2.69	28.6	0.042	0.0042	U	G	N	1	1	75	574	6	0.0055	79.3	NR	0.233	46.8	S	0.19
	PB-2/1	T	120	372	2.69	27.1	0.042	0.0042	U	G	Y	1	1	75	574	2	0.0018	70.6	NR	0.100	51.3	S	0.21
	PB-2/2	T	120	372	2.69	25.6	0.042	0.0042	U	G	Y	1	1	75	574	4	0.0037	86.7	NR	0.167	67.4	S	0.29
	PB-2/3	T	120	372	2.69	28.7	0.042	0.0042	U	G	Y	1	1	75	574	6	0.0055	75.4	NR	0.233	72.4	S	0.29
	PB-3/1	T	120	372	2.69	28.0	0.042	0.0042	U	G	Y	1	1	75	574	3	0.0027	72.0	NR	0.133	34.1	S	0.14
	PB-3/2	T	120	372	2.69	34.0	0.042	0.0042	U	G	Y	1	1	75	574	3	0.0027	79.1	NR	0.133	42.1	S	0.16
	PB-3/3	T	120	372	2.69	32.0	0.042	0.0042	U	G	Y	1	1	75	574	4	0.0037	63.3	NR	0.167	56.9	S	0.22
[7]	C40s0-M2-G2a	R	180	419	2.98	46.2	0.032	0.0000	SB	C	N	1	1	253	3800	1	0.0002	45.0	NR	0.222	59.9	S	0.96
	C40s0-M2-G2b	R	180	419	2.98	46.2	0.032	0.0000	SB	C	N	1	1	253	3800	1	0.0002	45.0	NR	0.222	58.4	S	0.93
	C40s0-M3-G2	R	180	419	2.98	46.2	0.032	0.0000	SB	C	N	1	1	201	3800	1	0.0002	77.0	NR	0.222	55.0	S	0.88
	C40s0-M2-G1	R	180	419	2.98	46.2	0.032	0.0000	SB	C	N	1	1	253	3800	1	0.0002	45.0	NR	0.222	41.5	S	0.66
	C40s0-M2-G2	R	180	419	2.98	46.2	0.032	0.0000	SB	C	N	1	1	253	3800	1	0.0002	45.0	NR	0.222	63.4	S	1.01
	C40s0-M2-G3	R	180	419	2.98	46.2	0.032	0.0000	SB	C	N	1	1	253	3800	1	0.0002	45.0	NR	0.222	40.7	S	0.65
	C40s0-M1-G3	R	180	419	2.98	46.2	0.032	0.0000	SB	C	N	1	1	262	2950	1	0.0002	22.0	NR	0.222	27.5	S	0.44
[12]	BS2	R	150	159	2.52	20.0	0.013	0.0000	SB	B	N	1	1	31.9	623	2	0.0017	23.9	NR	0.080	10.9	S	0.36
	BS3	R	150	159	2.52	20.0	0.013	0.0000	SB	B	N	1	1	31.9	623	2	0.0012	23.9	NR	0.080	11.3	S	0.37
	BS4	R	150	159	2.52	20.0	0.013	0.0000	SB	B	N	1	1	31.9	623	4	0.0034	23.9	NR	0.133	14.0	S	0.46
	BS5	R	150	159	2.52	20.0	0.013	0.0000	SB	B	N	1	1	31.9	623	4	0.0024	23.9	NR	0.133	15.8	S	0.52
	BS6	R	150	159	2.52	20.0	0.013	0.0000	SB	B	N	1	1	31.9	623	2	0.0017	56.4	NR	0.080	11.3	S	0.37
	BS7	R	150	159	2.52	20.0	0.013	0.0000	SB	B	N	1	1	31.9	623	2	0.0012	56.4	NR	0.080	11.3	S	0.37
	BS8	R	150	159	2.52	20.0	0.013	0.0000	SB	B	N	1	1	31.9	623	4	0.0034	56.4	NR	0.133	17.7	S	0.58
	BS9	R	150	159	2.52	20.0	0.013	0.0000	SB	B	N	1	1	31.9	623	4	0.0024	56.4	NR	0.133	26.6	S	0.88
[13]	R30-C-UJ-Hl-TRC(5)	R	120	204	3.18	25.6	0.026	0.0000	U	G	N	1	1	74	1102	1	0.0012	42.0	2.72	0.083	30.3	F	0.38
	R30-S-SB-P-TRC(10)	R	120	204	3.18	25.6	0.026	0.0000	SB	G	N	120	100	74	1102	1	0.0010	42.0	2.72	0.139	28.3	F	0.36

Ref.	Name	Shape	b_w [mm]	d [mm]	a/d	f_c [MPa]	ρ_l	ρ_w	SC	Fiber	Anchors	s_f [mm]	w_f [mm]	E_f [GPa]	f_f [MPa]	n	ρ_f	f_{cm} [MPa]	E_{FRCM} [GPa]	ρ_{cm}	V_{FRCM} [kN]	Failure mode	V_{FRCM}/V_{CON}
	R30-S-SB-P-TRC(5)	R	120	204	3.18	25.6	0.026	0.0000	SB	G	N	120	100	74	1102	1	0.0010	42.0	2.72	0.069	25.3	S	0.32
	R30-S-UJ-Hl-TRC(5)	R	120	204	3.18	25.6	0.026	0.0000	U	G	N	200	40	74	1102	1	0.0002	42.0	2.72	0.017	5.8	S	0.07
	R40-S-UJ-Hl-TRC(5)	R	120	204	3.18	35.2	0.026	0.0000	U	G	N	200	100	74	1102	1	0.0006	42.0	2.72	0.042	11.0	S	0.10
	R40-C-UJ-Hl-TRC(2)	R	120	204	3.18	35.2	0.026	0.0000	U	G	N	1	1	74	1102	1	0.0012	42.0	2.72	0.033	3.0	S	0.03
[14]	SB-GT	R	150	308	3.25	31.1	0.021	0.0000	SB	G	N	1	1	75	2300	1	0.0006	58.0	NR	0.093	11.4	S	0.18
	UW-GT	R	150	308	3.25	31.1	0.021	0.0000	U	G	N	1	1	75	2300	1	0.0006	58.0	NR	0.093	28.4	S	0.46
	SB-CT1	R	150	308	3.25	31.1	0.021	0.0000	SB	C	N	1	1	230	3800	1	0.0005	58.0	NR	0.093	16.0	S	0.26
	UW-CT1	R	150	308	3.25	31.1	0.021	0.0000	U	C	N	1	1	230	3800	1	0.0005	58.0	NR	0.093	14.2	S	0.23
	SB-CT2	R	150	308	3.25	31.1	0.021	0.0000	SB	C	N	1	1	230	3800	1	0.0012	58.0	NR	0.093	61.0	S	0.99
	UW-CT2	R	150	308	3.25	31.1	0.021	0.0000	U	C	N	1	1	230	3800	1	0.0012	58.0	NR	0.093	65.0	S	1.05
[15]	Beam 4	R	150	310	2.90	41.6	0.030	0.0021	U	G	N	275	200	75	2300	1	0.0010	40.0	NR	0.058	35.5	S	0.32
	Beam 5	R	150	310	2.90	41.6	0.030	0.0021	U	G	Y	275	200	75	2300	1	0.0010	40.0	NR	0.058	38.5	S	0.35
[16]	L1	T	150	320	2.50	16.7	0.016	0.0000	U	C	N	1	1	225	3375	1	0.0006	21.8	NR	0.053	9.6	S	0.17
	L2	T	150	320	2.50	18.0	0.016	0.0000	U	C	N	1	1	225	3375	2	0.0013	21.8	NR	0.080	11.4	S	0.19
	H1	T	150	320	2.50	19.4	0.016	0.0000	U	C	N	1	1	225	3375	1	0.0013	21.8	NR	0.053	19.9	S	0.32
	H2	T	150	320	2.50	19.2	0.016	0.0000	U	C	N	1	1	225	3375	2	0.0026	21.8	NR	0.080	33.1	S	0.54
	L2A15	T	150	320	2.50	20.1	0.016	0.0000	U	C	Y	1	1	225	3375	2	0.0013	21.8	NR	0.080	51.8	S	0.83
	L2A15ha	T	150	320	2.50	19.2	0.016	0.0000	U	C	Y	1	1	225	3375	2	0.0013	21.8	NR	0.080	55.6	S	0.91
	L2A10	T	150	320	2.50	10.1	0.016	0.0000	U	C	Y	1	1	225	3375	2	0.0013	21.8	NR	0.080	84.3	S	1.87
	H1A15	T	150	320	2.50	10.7	0.016	0.0000	U	C	Y	1	1	225	3375	1	0.0013	21.8	NR	0.053	51.9	S	1.12
	H2A15	T	150	320	2.50	11.1	0.016	0.0000	U	C	Y	1	1	225	3375	2	0.0026	21.8	NR	0.080	48.0	S	1.01
	H2A10	T	150	320	2.50	20.8	0.016	0.0000	U	C	Y	1	1	225	3375	2	0.0026	21.8	NR	0.080	45.6	S	0.72
[17]	V-BR3-01	R	300	254	2.76	28.0	0.008	0.0007	U	B	N	1	1	95	2990	1	0.0004	24.6	48	0.067	29.9	S	0.44
	V-CXM25-01	R	300	254	2.76	28.0	0.008	0.0007	U	C	N	1	1	240	4320	1	0.0003	25.0	80	0.067	34.3	S	0.50
	V-CXM25-02	R	300	254	2.76	28.3	0.008	0.0007	U	C	N	1	1	240	4320	1	0.0003	25.0	80	0.067	11.9	S	0.17
	V-PXM750-01	R	300	254	2.76	28.3	0.008	0.0007	U	PBO	N	1	1	270	5800	1	0.0003	30.0	128	0.067	31.9	S	0.46
	V-PXM750-02	R	300	254	2.76	28.3	0.008	0.0007	U	PBO	N	1	1	270	5800	1	0.0003	30.0	128	0.067	39.2	S	0.57
	V-GPHDM-02	R	300	254	2.76	28.3	0.008	0.0007	U	G	N	1	1	90	2610	1	0.0003	35.4	90	0.067	33.4	S	0.48
[18]	W600-L1	R	150	270	2.22	28.0	0.015	0.0000	SB	C	N	1	1	240	4300	1	0.0014	45.0	160	0.067	19.0	S	0.36
	W600-L2	R	150	270	2.22	28.0	0.015	0.0000	SB	C	N	1	1	240	4300	2	0.0029	45.0	160	0.100	23.5	S	0.45
	W50-N4	R	150	270	2.22	28.0	0.015	0.0000	U	C	N	183	50	240	4300	1	0.0004	45.0	160	0.018	6.0	S	0.11

Ref.	Name	Shape	Geometry				Int. Reinf.		FRCM Composite									f_{cm}	E_{FRCM}	ρ_{cm}	Results		V_{FRCM}/V_{CON}
			b_w	d	a/d	f_c	ρ_l	ρ_w	SC	Fiber	Anchors	s_f	w_f	E_f	f_f	n	ρ_f				V_{FRCM}	Failure	
			[mm]	[mm]		[MPa]						[mm]	[mm]	[GPa]	[MPa]			[MPa]	[GPa]		[kN]	mode	
	W50-N5	R	150	270	2.22	28.0	0.015	0.0000	U	C	N	138	50	240	4300	1	0.0005	45.0	160	0.024	9.0	S	0.17
	W50-N6	R	150	270	2.22	28.0	0.015	0.0000	U	C	N	110	50	240	4300	1	0.0006	45.0	160	0.030	11.0	S	0.21
	W100-N3	R	150	270	2.22	28.0	0.015	0.0000	U	C	N	250	100	240	4300	1	0.0006	45.0	160	0.027	8.0	S	0.15
	W100-N4	R	150	270	2.22	28.0	0.015	0.0000	U	C	N	167	100	240	4300	1	0.0009	45.0	160	0.040	19.5	S	0.37
	W600-N1	R	150	270	2.22	28.0	0.015	0.0000	U	C	N	1	1	240	4300	1	0.0014	45.0	160	0.067	28.5	S	0.54
	TRA1	R	150	225	3.00	30.8	0.019	0.0023	U	PBO	N	1	1	270	5800	1	0.0006	30.4	128	0.107	19.0	F	0.25
	TRA2	R	150	225	3.00	30.8	0.019	0.0023	U	PBO	N	260	150	270	5800	1	0.0004	30.4	128	0.062	9.9	S	0.13
	TRB1	R	150	225	2.78	45.0	0.028	0.0032	U	PBO	N	1	1	270	5800	1	0.0006	30.4	128	0.107	34.2	F	0.32
[19]	TRB2	R	150	225	2.78	29.2	0.028	0.0032	U	PBO	N	1	1	270	5800	2	0.0012	30.4	128	0.160	27.4	S	0.40
	TRB3	R	150	225	2.78	29.2	0.028	0.0032	U	PBO	N	210	100	270	5800	2	0.0006	30.4	128	0.076	27.5	S	0.40
	TRB4	R	150	225	2.78	38.3	0.028	0.0032	U	PBO	N	210	100	270	5800	1	0.0003	30.4	128	0.051	10.2	S	0.11
	TRB5	R	150	225	2.78	38.3	0.028	0.0032	U	PBO	N	210	100	270	5800	3	0.0009	30.4	128	0.102	10.2	S	0.11
	SB_M1	R	102	177	2.60	21.6	0.022	0.0000	SB	C	N	1	1	225	3800	1	0.0019	31.1	NR	0.078	2.7	S	0.09
	SB_M2	R	102	177	2.60	22.6	0.022	0.0000	SB	C	N	1	1	225	3800	2	0.0037	28.2	NR	0.118	15.1	S	0.51
	SB_M3	R	102	177	2.60	22.6	0.022	0.0000	SB	C	N	1	1	225	3800	3	0.0056	26.9	NR	0.157	34.0	S	1.14
[20]	UW_M1	R	102	177	2.60	23.8	0.022	0.0000	U	C	N	1	1	225	3800	1	0.0019	31.1	NR	0.078	21.1	S	0.71
	UW_M2	R	102	177	2.60	23.8	0.022	0.0000	U	C	N	1	1	225	3800	2	0.0037	31.1	NR	0.118	39.1	S	1.32
	UW_M3	R	102	177	2.60	22.6	0.022	0.0000	U	C	N	1	1	225	3800	3	0.0056	26.9	NR	0.157	57.8	S	1.95
	FW_M1	R	102	177	2.60	21.6	0.022	0.0000	W	C	N	1	1	225	3800	1	0.0019	31.1	NR	0.078	32.7	S	1.10
	FW_M2	R	102	177	2.60	21.6	0.022	0.0000	W	C	N	1	1	225	3800	2	0.0037	28.2	NR	0.118	45.4	F	1.53
[21]	B1	R	150	204	4.90	42.9	0.051	0.0013	W	PBO	N	200	100	270	5270	1	0.0003	29.0	NR	0.040	70.1	S	1.19
	S0-FRCM-1	R	150	250	3.00	36.0	0.050	0.0000	SB	C	N	1	1	230	3800	1	0.0004	74.0	NR	0.160	66.8	S	1.11
	S0-FRCM-2	R	150	250	3.00	36.0	0.050	0.0000	SB	C	N	1	1	230	3800	2	0.0008	74.0	NR	0.240	87.5	S	1.46
[23]	S1-FRCM-1	R	150	250	3.00	36.0	0.050	0.0025	SB	C	N	1	1	230	3800	1	0.0004	74.0	NR	0.160	68.4	S	0.64
	S1-FRCM-2	R	150	250	3.00	36.0	0.050	0.0025	SB	C	N	1	1	230	3800	2	0.0008	74.0	NR	0.240	72.1	S	0.67
	S2-FRCM-1	R	150	250	3.00	36.0	0.050	0.0050	SB	C	N	1	1	230	3800	1	0.0004	74.0	NR	0.160	67.7	S	0.51
	S2-FRCM-2	R	150	250	3.00	36.0	0.050	0.0050	SB	C	N	1	1	230	3800	2	0.0008	74.0	NR	0.240	73.6	S	0.55
	L_1	R	152	248	3.07	29.1	0.030	0.0027	U	PBO	N	1	1	270	1664	1	0.0001	35.0	127	0.046	18.1	S	0.22
[22]	L_4	R	152	248	3.07	29.1	0.030	0.0027	U	PBO	N	1	1	270	1664	4	0.0006	35.0	127	0.115	42.2	S	0.51
	H_1	R	152	248	3.07	42.9	0.030	0.0027	U	PBO	N	1	1	270	1664	1	0.0001	35.0	127	0.046	24.0	S	0.26
	H_4	R	152	248	3.07	42.9	0.030	0.0027	U	PBO	N	1	1	270	1664	4	0.0006	35.0	127	0.115	56.2	S	0.61
[24]	CH2	T	200	385	2.29	15.2	0.033	-	U	C	N	1	1	225	3800	2	0.0019	37.4	NR	0.060	30.0	S	0.37
	CL3	T	200	385	2.29	13.8	0.033	-	U	C	N	1	1	225	4800	3	0.0019	35.8	NR	0.080	37.0	S	0.45

Ref.	Name	Shape	Geometry			Concrete	Int. Reinf.		FRCM Composite												Results		V_{FRCM}/V_{CON}
			b_w	d	a/d	f_c	ρ_l	ρ_w	SC	Fiber	Anchors	s_f	w_f	E_f	f_f	n	ρ_f	f_{cm}	E_{FRCM}	ρ_{cm}	V_{FRCM}	Failure	
			[mm]	[mm]		[MPa]						[mm]	[mm]	[GPa]	[MPa]			[MPa]	[GPa]		[kN]	mode	
	CH4	T	200	385	2.29	14.0	0.033	-	U	C	N	1	1	225	3800	4	0.0038	36.1	NR	0.100	62.5	S	0.77
	G7	T	200	385	2.29	13.8	0.033	-	U	G	N	1	1	74	1400	7	0.0031	33.7	NR	0.160	61.0	S	0.75
	CH2_A100	T	200	385	2.29	15.2	0.033	-	U	C	Y	1	1	225	3800	2	0.0019	34.5	NR	0.060	73.0	S	0.90
	CL3_A100	T	200	385	2.29	14.9	0.033	-	U	C	Y	1	1	225	4800	3	0.0019	37.9	NR	0.080	74.0	S	0.91
	CH4_A50	T	200	385	2.29	14.9	0.033	-	U	C	Y	1	1	225	3800	4	0.0038	36.6	NR	0.100	96.0	S	1.18
	CH4_A100	T	200	385	2.29	14.5	0.033	-	U	C	Y	1	1	225	3800	4	0.0038	33.4	NR	0.100	155.0	S	1.90
	G7_A100	T	200	385	2.29	14.5	0.033	-	U	G	Y	1	1	74	1400	7	0.0031	37.4	NR	0.160	69.5	S	0.85
[6]	UW_MCL3_20	R	102	177	2.60	20.8	0.022	-	U	C	N	1	1	225	4800	3	0.0036	38.7	NR	0.157	33.0	S	1.27
	UW_MG7_20	R	102	177	2.60	20.0	0.022	-	U	G	N	1	1	74	1400	7	0.0060	35.5	NR	0.314	46.0	S	1.77

Fiber: C= Carbon, G = Glass, B = Basalt. SC. Strengthening configuration, see Table 2-1. Failure mode: F = Flexure, S = Shear. NR= Not reported.

APPENDIX B. EXPERIMENTAL DATABASE (CONTROL BEAMS)

170

Ref.	Name	Shape	Geometry			Concrete	Reinforcement		Results	
			b_w [mm]	d [mm]	a/d	$f_{c,cyl}$ [MPa]	ρ_l	ρ_w	V_c [kN]	$(V_c + V_s)_{exp}$ [kN]
[1]	C	R	150	272	2.85	25.315	0.015	0.0014	-	58.3
[10]	C	R	150	256	3.91	23.2	0.032	-	58.5	-
[11]	PB-0	T	120	372	2.69	26.8	0.042	0.0042	-	238.0
[7]	C40s0	R	180	419	2.98	46.2	0.032	0.0000	62.6	-
[12]	BS1-1	R	150	159	2.52	20.0	0.013	0.0000	29.5	-
	BS1-2	R	150	159	2.52	20.0	0.013	0.0000	31.4	-
[13]	R30	R	120	204.2	3.18	25.6	0.026	0.0000	79.3	-
	R40	R	120	204.2	3.18	35.2	0.026	0.0000	114.5	-
[14]	C-N	R	150	307.5	3.25	37.5	0.021	0.0000	61.8	-
[15]	Control	R	150	310	2.90	41.6	0.030	0.0021	-	111.5
[16]	C	T	150	320	2.50	16.2	0.016	0.0000	57.1	-
[17]	V-CONTROL	R	300	254	2.76	33.9	0.008	0.0007	75.4	-
[18]	Control	R	150	270	2.22	28.0	0.015	-	52.5	-
	S300	R	150	270	2.22	28.0	0.015	0.0048	52.5	86.0
	S200	R	150	270	2.22	28.0	0.015	0.0032	52.5	84.0
[19]	TRA0	R	150	225	3.00	30.8	0.019	0.0023	-	75.4
	TRB0	R	150	225	2.78	45.0	0.028	0.0032	-	105.7
[21]	Control	R	150	204	4.90	42.9	0.051	0.0013	-	58.7
[20]	CON	R	102	177	2.60	21.6	0.022	0.0000	29.7	-
[23]	S0-NS	R	150	250	3.00	36	0.050	0.0000	60.0	-
	S1-NS	R	150	250	3.00	36	0.050	0.0025	-	107.6
	S2-NS	R	150	250	3.00	36	0.050	0.0050	-	133.3

171